FILM FORMATION ON STAINLESS STEEL IN ACIDIFIED DICHROMATE SOLUTIONS

Thesis submitted to the University of Newcastle upon Tyne for the degree of Doctor of Philosophy

by

R.O. ANSELL, B.Sc. A.R.C.S.

March 1977

ABSTRACT

A process for producing decorative coatings on stainless steel, by immersion in a solution of chromic and sulphuric acids, has been studied. The composition of the film produced has been investigated using a number of spectroscopic techniques. Both alternating and direct current methods have been used to investigate the conduction properties of the film.

The formation of the film in the dichromate solution results from a combination of the anodic process of steel oxidation and the cathodic process of dichromate reduction. The rates of these processes have been found to increase with time during the formation of the film, as does the rate of film formation. A qualitative mechanism, which explains most of the experimental results, is proposed.

CONTENTS

CHAPTER 1

INTRODUCTION

1.1. THE COLOURING PROCESS

When stainless steel is immersed in a solution containing sulphuric and chromic acid a coloured film is formed on the surface of the steel[1,2]. The colour of the film produced depends on the length of time the specimen is immersed in the solution, the concentration of sulphuric and chromic acids and the temperature of the solution. The most favourable conditions for the formation of the film are to use a solution 2.5M in chromic acid and 5M in sulphuric acid at $70^{o}C$[1]. Coloured films are usually produced in this solution after a time of immersion of between 10 and 30 minutes. If the specimen is removed from the solution too soon the surface of the steel will be apparently unchanged, if it is removed too late a powdery deposit is obtained on the surface. Between these limits a lustrous coloured film is produced on the steel surface.

Although the length of time of immersion of the steel in the solution can be used as a method of producing a particular coloured film it is not always a reliable method[2]. Better control over the colour produced can be achieved by monitoring the potential of the stainless steel with respect to a reference electrode[3,4]. As shown in Figure 1.1 the potential of the steel increases rapidly in the induction period, it then stabilises in the plateau region and then increases almost linearly with time during the colouring region until it finally stabilises. The linear increase in potential with time during the colouring region can be used to monitor the colour of the surface film produced, since the potential which the steel attains above the plateau ΔV is related to the specimen colour[3]. The

relationship between Δ V and the colour is maintained even when the time scale of the process changes. The colours of films produced for potentials ΔV above the plateau is shown in Table 1.

This Thesis describes work designed to further the understanding of the colouring process. The remainder of this introduction describes the anodic behaviour of metals and the phenomena of corrosion, which form a background to the understanding of the process. In subsequent chapters the composition and properties of the film formed on the surface of the steel are discussed. Finally the processes which occur during the formation of the film are considered.

1.2. THE ANODIC BEHAVIOUR OF METALS IN AQUEOUS SOLUTIONS

The overall current-potential curve for a metal in an aqueous solution is generally of the form shown in Fig. 1.2. Hydrogen evolution occurs at sufficiently negative potentials. Normally if an electrode is held in this region for a sufficient length of time any pre-existing film on the metal surface will be reduced. On making the potential more positive, an anodic current which increases approximately logarithmically is seen, corresponding to the region of active metal dissolution. At the more negative potentials in this region, the active dissolution of the metal may be controlled by crystallographic features of the metal lattice[5,6]. Thus the rate controlling step can be, for example, the nucleation and growth of holes in the metal. The dissolving metal ion leaves the lattice as a solvated species since this leads to a greater free energy change[7].

$$M + xH_2O \longrightarrow M^{z+}xH_2O + 2e$$

At more positive potentials, however, dissolution is normally

controlled by the rate of charge transfer, often to an anion which forms a surface "complex" with the metal. The mechanism of active dissolution may also involve the formation of intermediate valence states during dissolution or the participation of anion catalysts[8].

Anodic dissolution does not increase indefinitely with increase in potential. Above a certain potential (V) the current increases less rapidly with potential, than the logarithmic relation would predict. At more positive potentials the current falls markedly with increase in potential, the potential at which the current starts to fall being termed the passivation potential V_p. Eventually the current becomes independent of potential and the electrode is said to be passivated. The potential at which this occurs is termed the potential of complete passivity (V_{pp}).

The processes which cause the decrease in dissolution current have been the subject of considerable research effort. Two principle explanations have been put forward:

1) adsorption of oxygen, favoured by an increase in potential, results in a decrease in the number of sites from which metal ions can dissolve

2) the formation of a protective film leads to a decrease in the dissolution current.

1.2.1. THEORIES FOR THE PASSIVATION OF METALS

1.2.1.1. ADSORPTION THEORY

Kolotyrkin[9] argued that the passivation process and the passive region are associated with the adsorption of oxygen. Increasing adsorption of oxygen with potential decreases the area of metal surface available to react. In the region from the passivation potential to complete passivation

a logarithmic decrease of available metal surface with potential was assumed. This would explain the approximately exponential fall in the observed current. In the passive region, where the current is independent of potential, the rates of adsorption and dissolution are equal.

Kolotyrkin based his theory on; the polarisation curves he obtained for iron, chromium, nickel and stainless steel, their steady state behaviour in the passive region, and a differential capacitance against potential curve which he argued did not show sufficient change to be consistent with oxide film formation.

Whilst this theory may be valid in the region between the passivation potential and the potential of complete passivity, the isolation of film from the surface of passivated metals contradicts his views about the passive region.

Uhlig[10] argued that the processes which occur during the passivation of transition metals are the physical adsorption of oxygen molecules followed by dissociation and chemisorption of oxygen atoms. Further adsorption of oxygen molecules on to the original chemisorbed layer is necessary to allow the nucleation of the oxide, this grows laterally (more quickly than vertically) to form a continuous oxide. The growth of this oxide is controlled by electron transfer from metal to oxide.

These conclusions were based on a variety of experimental evidence, but the experiments of Germer and Macrae[11] are probably of most importance. They found, by LEED studies of nickel surfaces, that both chemisorbed oxygen as well as nickel oxide could be identified. Heating the specimens to near the melting point eliminated the nickel oxide diffraction pattern but that of chemisorbed oxygen remained. The chemisorbed layer, therefore, is apparently more stable than nickel oxide and consequently its formation more likely.

Uhlig pointed out that a layer of chemisorbed oxygen atoms plus a layer of oxygen molecules corresponds to the amount of oxygen present in the passive layer determined coulometrically by Arnold and Vetter[12]. This is also true for the layers present on 18:8 stainless steel, iron and titanium. Moreover the calculated equilibrium potential for the adsorbed film corresponds better with the potential immediately preceding the breakdown of passivity than does that of any known oxide. The stability of adsorbed oxygen and hence of thin passivating layers on transition metals is attributed to bonding via their unfilled d energy levels.

Frankenthal[13] measured the quantity of electricity needed to reduce the layers produced by anodic polarisation of iron in borate buffer solutions. He considered that up to the potential of complete passivity (V_{pp}) his data fitted a preferential dissolution adsorption mechanism. In this mechanism dissolution occurs by direct activated transfer of metal ions into solution, the rate of dissolution depending on the type of site from which the metal ion dissolves. Adsorption at these various sites leads to passivation and complete passivation (V_{pp}) can occur with less than monolayer coverage of the surface. When steady state conditions have been achieved in the passive region, dissolution occurs by ionic transport through films whose thicknesses are considerably greater than a monolayer.

1.2.1.2. OXIDE FILM THEORY

Bockris and coworkers[14] studied the films formed on an iron electrode in a borate buffer solution, using ellipsometric techniques. On the basis of their results, they proposed the following mechanism.

A 2-dimensional oxide forms before the passivation potential V_p. The coverage with this oxide increases with potential until at V_p the coverage is almost complete. Dissolution of iron occurs at areas of the metal surface

not covered with film via an intermediate hydroxide species

$$Fe + OH^- \rightleftharpoons FeOH + e$$

$$FeOH \xrightarrow{\text{r.d.s.}} FeOH^+ + e$$

$$FeOH^+ \rightleftharpoons Fe^{2+} + OH^-$$

A 3-dimensional oxide layer is formed from the 2-dimensional layer by a place exchange mechanism followed by discharge of hydroxyl ion,

$$\begin{array}{c} OH \\ | \\ Fe \end{array} \xrightarrow{\text{place exchange}} \begin{array}{c} Fe \\ | \\ OH \end{array}$$

$$\begin{array}{c} Fe \\ | \\ OH \end{array} + OH^- \xrightarrow{\text{r.d.s.}} \begin{array}{c} OH \\ | \\ Fe \\ | \\ OH \end{array} + e$$

After the passivation potential V_p the fall in current is due to increasing coverage with the $Fe(OH)_2$ layer. In the passive region the $Fe(OH)_2$ is gradually converted to Fe_2O_3.

Fleischmannand Thirsk[15] investigated the current-time transients that would be observed in situations of nucleation and growth of thin passivating layers on metal surfaces at constant potential. They showed theoretically that maxima would be observed and that it is possible to distinguish between curves for adsorption and nucleation. They concluded that the kinetics of the initial stages of passivation are consistent with the formation of an ordered 2-dimensional film of definite chemical phase.

Armstrong and Thirsk[16] studied mercury and mercury amalgams, using alternating current techniques. They found separate potential regions where

adsorbed, 2-dimensional, and 3-dimensional films were present. They concluded that,

1) On anodic polarisation metals generally show specific anion adsorption followed by the formation of a two dimensional film in turn followed by a three dimensional film.

2) In regions where specific anion adsorption begins no sharp decrease in metal dissolution was found, thus anion adsorption appeared unlikely to cause the passivity of metals.

3) 2-dimensional films generally produce a sharp decrease in the rate of metal dissolution but in a number of cases they do not. The potential range over which a two dimensional film may be stable can vary considerably from millivolts up to almost one volt.

4) 3-dimensional non-porous films on metal surfaces generally inhibit metal dissolution considerably.

1.2.1.3. OXIDE FILM-ADSORPTION THEORY

As well as the proponents of the more extreme views on passivity there are a number who take an intermediate stand. Hoar[7] has proposed a combined oxide film-adsorption theory.

According to Hoar in the region of active dissolution the process

$$M + H_2O \longrightarrow M^{2+}_{(aq)} + 2e$$

is possible, however with increase in potential the process

$$M + H_2O \longrightarrow MO_{(solid)} + 2H^{+} + 2e$$

becomes thermodynamically feasible. Hoar suggests that this process is

also kinetically easier. The water molecules will be orientated with their oxygen atoms next to the metal surface. The adsorbed water molecules could lose protons to water molecules in a layer further out and simultaneously metal cations can move into positions between the negative ions OH^- or O^{2-} (the spaces will be produced by repulsion between the anions). The cations can now move into position in the film, anywhere on the surface rather than just at energetic sites. The process will thus be limited only by the rate of proton transfer between molecules and consequently an oxide monolayer firmly attached to the surface (adsorbed) will rapidly form.

CONCLUSION

The problems associated with the interpretation of the changes which occur in the region of the active-passive transition, result from the difficulty in obtaining experimental information about the state of the interface between the electrode and the solution, in this region. Techniques which require removal of the electrode from solution cannot resolve the argument, and the unambiguous interpretation of the results obtained by in situ techniques is difficult.

Consideration of the principle theories of the nature of passivating layers leads to the conclusion that whilst partial passivation can result from an adsorbed layer of oxygen or a 2-dimensional layer of oxide, the true passive state is only attained when a definite phase oxide is present on the metal.

1.2.1.4. THE MECHANISM OF FORMATION OF PHASE OXIDE

There are two principle mechanisms for the formation of passive films on metal surfaces:

a) The dissolution-precipitation mechanism, where the film is formed

by the products of the metal dissolution reaction precipitating onto the electrode surface.

b) The solid state mechanism. Here anions, which derive from the solvent, react directly with the metal to form a passivating film.

In the dissolution-precipitation case the film must be assumed to be formed at a distance from the electrode which is greater than the thickness of the double layer, otherwise the two mechanisms are indistinguishable.

Armstrong and Harrison[17] treated the dissolution-precipitation mechanism at the rotating disc electrode theoretically. They showed that when this mechanism applies the maximum current obtainable should be increased by increasing the rotation speed of the electrode.

1.2.2. THEORIES TO ACCOUNT FOR THE BEHAVIOUR OBSERVED IN THE PASSIVE STATE

Vetter[18] considered the thermodynamic equilibria which are present at the phase boundaries on an electrode covered with a passive film. The potential difference ($_o\varepsilon_{1,2}$) at the metal/oxide boundary is obtained by equating the electrochemical potentials of metal ions in the oxide and the metal.

$$_o\varepsilon_{1,2} = (_2\mu_{me^+} - {}_1\mu_{me^+})/zF \qquad (1)$$

where μ = chemical potential

z = charge on the ion

F = Faraday constant

The potential difference at the oxide/solution boundary is

regulated by the oxide ion equilibrium

$$H_2O(aq) \rightleftharpoons O^{2-}(aq) + 2H^+(aq)$$

$$_o\varepsilon_{2,3} = \frac{1}{2F}(\mu_{O^{2-}} + 2\mu_{H^+} - \mu_{H_2O}) \quad (2)$$

$$_o\varepsilon_{2,3} = \frac{1}{2F}(\mu_{O^{2-}} + 2\mu^o_{H^+} + \mu_{H_2O}) + 2RT \ln a_{H^+}) \quad (3)$$

where a_{H^+} activity of hydrogen ions.

If the oxide composition is constant $\mu_{O^{2-}}$ is constant and for a dilute solution μ_{H_2O} is constant so that

$$_o\varepsilon_{2,3} = d - 2.303\frac{RT}{F}\ pH \quad (4)$$

where d = constant.

The anodic dissolution current will be given by

$$i = i_o \exp(\alpha 3F\ _o\varepsilon_{2,3}/RT)$$

$$i = i_o \exp\frac{3\alpha F}{RT}(d - 2.303\frac{RT}{F}\ pH)$$

$$i = i_o \exp\frac{3\alpha F}{RT} \exp(-2.303\frac{RT}{F}\ pH)$$

Plots of log i against pH were found to be linear and allowed the determination of α as 0.3 which provides experimental justification for this theory[19].

The total current which flows through the passive layer is comprised of the component for metal ion dissolution and that for layer

growth or removal (when the electrode is in equilibrium at a particular potential the latter current will be zero). Vetter considers that a high field must be present in the passive layer to account for the ionic current and this is given by a relationship of the form (Section 1.2.3.)

$$i = i_o \exp(\beta E) \qquad (5)$$

There is, however, no electronic current in the passive layer but the electrons are in equilibrium. That is the Fermi level for the electrons is constant throughout the layer

$$\eta_e = \mu_e - F\varphi \qquad (6)$$

where η_e = Fermi potential

φ = potential of the electron

μ_e = chemical potential of the electrons

The variation in chemical potential of the electrons balances the effect of the electric field. The change in chemical potential of the electrons arises as a result of a change in composition of the oxide. The oxide composition at various positions in the layer is consequently solely a function of the potential. For a semiconductor a small change in composition would result in a large change in the chemical potential of the electron particularly if the Fermi level of the semiconductor is within the band gap. Vetter thus envisages the passive layer as having a continuously variable composition from the metal surface to the outer layer of the oxide.

When the ionic current flows through the passive layer the potential difference between the oxide and the solution will be given by the sum of the equilibrium oxide/solution potential difference and an overvoltage.

$$\varepsilon_{2,3} = {}_{o}\varepsilon_{2,3} + \eta_{2,3} \qquad (7)$$

The potential difference ${}_{o}\varepsilon_{23}$ is a function only of the oxide composition (equation 4).

The experimental electrode potential

$$\varepsilon_{n} = (\varphi_{1} - \varphi_{s}) + \varepsilon_{23} \qquad (8)$$

is equal to the potential difference between the metal and the outer surface of the oxide plus the potential between the oxide and solution.

If a defined potential is applied to the passive electrode which is more positive than it's equilibrium potential the electric field in the oxide will increase as a result of an increase in $(\varphi_{1} - \varphi_{s})$ and so will the potential difference at the oxide solution boundary. A current will flow and oxide will be produced until the electric field in the oxide and the potential difference at the oxide/solution interphase reach new equilibrium values.

In the case of the iron electrode[20] the composition of the oxide does not need to change greatly to maintain electronic equilibrium since the Fermi level is within the band gap. In this case the oxide-solution potential difference will also not change greatly. As a consequence of this the new equilibrium layer will have the same electric field as the initial layer since the dissolution current is the same and is related to the field strength by equation (5). Change in the potential will therefore cause an increase in the current flowing which corresponds to layer formation. Once the layer has reached the required thickness so that the electric field is restored to its original value the layer will not thicken further. Thus, Vetter's theory gives an explanation of the lack of dependence of the current on potential in the passive region and the increase in layer thickness with potential.

1.2.3. IONIC TRANSPORT THROUGH THE OXIDE FILMS

Two principle theories have been advanced for ionic transport through oxide films, the high-field assisted migration theory of Mott and Cabrera[21] and Verwey[22] and the place exchange mechanism of Sato and Cohen[23].

1.2.3.1. HIGH FIELD ASSISTED IONIC MIGRATION

Ionic conductivity arises as the result of the movement of lattice defects which may be either vacant cation or anion sites, or interstitial anions or cations. A mobile metal ion is considered to move through an immobile lattice and no allowance is made for the fact that one ion may block the path of another. The ions are considered to overcome an energy barrier between lattice sites as a result of their thermal energy and the effect of the applied field. The proportion of ions with sufficient energy to overcome an energy barrier W is given by exp(- W/kT). The effect of the electric field will reduce the height of the energy barrier between two successive sites by qaE where q is the charge on the ion, E is the field strength and a is half the distance between successive sites (for a symmetrical barrier). The current resulting from ions moving with the field is given by

$$i = 2anvq \exp(-(W - qaE)/kT) \qquad (1)$$

where v = number of chances per second that a given ion may jump the barrier if it has sufficient energy

k = Boltzmans constant

T = Absolute temperature

n = number of mobile ions per unit volume

q = charge on ion

In general the field strength E is sufficiently high that the

current due to ions moving against the applied field will be negligible. (High field approximation).

Verwey applied this theory to the case of γ Al_2O_3 for which Gunterschultze and Betz[24] had found an experimental relationship

$$i = A \exp B E$$

The value of "a" calculated using their results along with equation 1 was much larger than that expected from the size of the γAl_2O_3 unit cell.

Mott and Carbrera[21] considered that the change in field across a thin film would be small. The current is therefore controlled by the rate of entry of ions into the oxide rather than by their progress through the oxide. Using similar arguments to those described above, this model leads to the equation

$$i = n'v'q \exp -((W' - qa'E)/kT) \qquad (2)$$

where n' concentration of ions on the surface

v' number of chances per second that a given ion may jump the barrier if it has sufficient energy

W' height of the energy barrier metal to oxide

q charge on the ion

a half the jump, distance from metal to oxide

The concentration of ions n' in the oxide is not fixed and in the steady state can be obtained by equating the current in the oxide (equation 1) to that of ions over the energy barrier (equation 2).

Young[25] regards the viewpoints of Mott and Cabrera and Verwey as limiting cases. He applied Poisson's equation to the mobile and non-mobile species to obtain the field strength in the oxide. He then used equation 1 and the assumption that, in the steady state only n and E vary with thickness of the oxide, to obtain an equation for the current. Young's equation reduces to that of Mott and Cabrera as the thickness tends to zero and to that of Verwey as the thickness tends to large values.

1.2.3.2. PLACE EXCHANGE MECHANISM

Sato and Cohen[23] proposed their place exchange mechanism on the basis of experimental work of Nagamaya and Cohen. The latter workers found that with iron in neutral solution the current in the passive region obeyed an equation of the form $\log i = A - Q_T/B$, where Q_T is the film thickness and A and B are constants at constant potential. This does not agree with that predicted by the Mott-Cabrera or Verwey theories i.e. $\log i = C + D/Q_T$. Sato and Cohen showed that a place exchange mechanism predicted the current to depend on film thickness according to the equation

$$i = k \exp (bE - Q_T/B)$$

where k, b, B, are constants

E = potential

In their mechanism, an oxygen atom is adsorbed and exchanges places with a metal atom. A second atom of oxygen is then adsorbed on the metal atom and both first and second metal-oxygen pairs exchange places simultaneously. Further adsorption follows with simultaneous rotation of

all the pairs after adsorption. This mechanism results in a linear increase in activation energy for the process with film thickness and leads to a theoretical equation of the same form as the empirical equation.

1.2.4. TRANSPASSIVE DISSOLUTION

When the potential of the electrode is made sufficiently anodic the anodic current for some metals increases, as a result principally of metal dissolution. This phenomenonis associated with those metals that can form higher valency oxides which are soluble in the solution. Chromium, molybdenum and tungsten exemplify this behaviour. The region of transpassive dissolution is important in this study, since the potentials at which the film is produced on coloured stainless steel lie in the transpassive region.

Transpassive dissolution is observed for steels in which the chromium content is greater than 12% to 16%[26,27,28,29](there is some variation in this value in the literature) and is attributed[30,31] to the oxidation of insoluble chromium III present in the passive layer to soluble chromium VI. Whilst the behaviour of stainless steel in the early transpassive region is similar to that of chromium, the current in the transpassive region does not always increase continuously with potential. Above a certain potential the current falls with further increase in potential and secondary passivity is observed. Prazak, Prazak and Cihal[26] observed secondary passivity only for alloys with chromium contents between 18% and 30%. They suggested that the effect of alloy composition on transpassive dissolution could be understood in terms of stoichiometric changes in a spinel oxide on the transpassive steel which can theoretically occur at alloy compositions of 15.5% and 30.7% chromium in the alloy. Epelboin and coworkers[27,32], however suggest that the behaviour of stainless steels in

the transpassive region can be profoundly affected by the carbon or silicon content of the steel. They believe that secondary passivity arises as a result of the presence of carbon or silicon in the oxide layer on the transpassive electrode which limits the diffusion of reaction products. Whilst no recent studies of the behaviour of steel in the transpassive region have been found, more detailed studies have been made of the transpassive behaviour of chromium.

In the transpassive region chromium dissolves as chromium VI. This was shown in the early work of Roberts and Shutt[33] who studied the behaviour of chromium galvanostatically and determined the nature of the chromium dissolving in the transpassive region by both coulometric and titration methods. More recently the dissolution of chromium as chromium VI has been shown directly by a ring-disc technique[34].

Whilst the chromium species dissolving in the transpassive region is in no doubt, differing views exist as to the nature of the chromium surface in the transpassive region. Heumann and coworkers[35,36] suggested that in the transpassive region a layer of CrOOH which is present on the passive electrode is oxidised to the hexavalent state.

$$CrOOH + 2OH^- \longrightarrow H_2CrO_4 + H^+ + 3e$$

Plieth and Vetter[37] suggest that the layer present on transpassive chromium is a chromium oxide of continuously variable oxidation state and that in acid solution the rate determining step of the dissolution is

$$CrO_3 ox. \longrightarrow CrO_3 \text{ aq.}$$

Knoedler and Heusler[38], however propose on the basis of a.c. impedance

methods that the transpassive surface is covered with a monolayer of adsorbed species rather than a film. Armstrong and Henderson[34,39] who used both ring-disc and a.c. impedance techniques support the views of Vetter.

It may be concluded that in the transpassive region chromium is covered with a film whose composition is a function of potential and that dissolution of this film occurs as chromium VI.

1.3. CORROSION

The behaviour of metals in aqueous environments was discussed in Section 1.2 . It was shown that under potentiostatic conditions, the process which occurred depends on the potential. In many practical situations there is no external control of the potential and the behaviour of the metal depends on spontaneous reactions.

Perhaps the most important principle to be considered under these conditions is that the nett current flow is zero, that is the anodic current for the reaction of the metal is balanced by cathodic currents due to species in solution. The cathodic reactions which most frequently occur are the evolution of hydrogen and the reduction of oxygen;

$$2H_3O^+ + 2e \longrightarrow 2H_2O + H_2$$

$$O_2 + 4H^+ + 4e \longrightarrow 2H_2O \qquad \text{acid solution}$$

$$O_2 + 2H_2O + 4e \longrightarrow 4OH^- \qquad \text{alkaline solution}$$

Often the metal surface is heterogeneous, consisting of areas which undergo dissolution readily and areas which allow reduction to occur

readily. Such situations are frequently described in terms of the local cell theory of corrosion. The anodic process occurs in one specific area and the cathodic process in another. Since these two areas are in electrical contact, the system behaves as if it were a short circuited cell; the "local current" flowing between the anodic and cathodic areas.

Pure homogeneous metals, however, also corrode and the basis of a more general theory was supplied by Wagner and Traud[40]. They considered that the anodic and cathodic processes could occur simultaneously at the metal solution interphase. They also proposed that all partial processes are additive and that the potential which the electrode attains will be that at which the algebraic sum of the partial processes is zero.

This theory is probably best understood using what have come to be known as Evans diagrams[41,42], in which the magnitudes of the anodic and cathodic currents are plotted against potential. Vetter[43] gives an example of the application of this approach to the corrosion of a chemically heterogeneous surface. If we consider an alloy consisting of a base metal and a noble metal, the respective areas of each being A_1 and A_2, then the current-potential curves will be as shown in Fig. 1.3.

Initially we will consider the behaviour of the alloy as if it were two separate pieces of metal. The base metal would attain a potential V, where the rates of metal dissolution and hydrogen evolution are equal

$$(i_{m_1}^{diss})_{A_1} = (i_{m_1}^{H_2})_{A_1}$$

Since the noble metal will not undergo anodic dissolution, hydrogen evolution on it is not possible. The equilibrium potential for this metal will therefore be more positive than that of the base metal.

When the two metals are connected, however, hydrogen evolution can

occur on both metals and a new potential V' will be attained such that the rate of hydrogen evolution is equal to the rate of base metal dissolution.

$$i_{corr} = (i_{m_1}^{diss})_{2} A_1 = (i_{m_1}^{H_2})_{2} A_1 + i_{m_2}^{H_2} A_2$$

The local current flowing between the base metal and the noble metal would be

$$i_L = (i_{m_1}^{diss})_{2} A_1 - (i_{m_1}^{H_2})_{2} A_1 = i_{m_2}^{H_2} A_2$$

This approach can, thus, explain both the decrease in corrosion rate of an impure metal as its purity is increased as well as the fact that the pure metal can corrode at an appreciable rate.

This type of approach has also been applied to the behaviour of metals in solutions of oxidising agents which can often be used in low concentrations to inhibit corrosion.

1.3.1. THE BEHAVIOUR OF METALS IN SOLUTIONS OF OXIDISING AGENTS

The effect of oxidising agents on metals has been discussed by Stern[44] and by Kolotyrkin[45]. Their conclusions with regard to selecting suitable passivating inhibitors are that;

a) inhibitors that create passivity, function primarily by producing a mixed potential which is more positive than the potential for complete passivation

b) to achieve this, the redox potential of the oxidising agent must be more positive than the potential for complete passivation and at the potential corresponding to the maximum current density for dissolution the

current density for the redox reaction must be higher than the former current density.

Kolotyrkin[45] obtained a potentiostatic polarisation curve for nickel in 0.5M sulphuric acid solution. He then measured the open-circuit potential and the dissolution rate of a nickel electrode immersed in a 0.5M sulphuric acid solution containing various concentrations of oxidising agents. He found that the potentials and dissolution currents obtained in this manner, agreed closely with the polarisation curve for nickel.

Piotrowski and Lebet[46] studied the passivation of stainless steel in the presence of oxidising agents. They determined the anodic polarisation curves for stainless steel and cathodic reduction curves for the ferrous/ferric, quinone/hydroquinone and ceric/cerous couples on passivated steel electrodes. They showed that the open-circuit potentials attained by the steel in these solutions corresponded to those predicted by the intersection of the anodic and cathodic curves. They identified situations in which the steel would passivate (ferric/ferrous) would not passivate (quinone/hydroquinone) and a situation where the cathodic reduction curve was diffusion limited in the region of the active-passive transition, so that the electrode could be passivated by vigorous stirring. (Ceric/cerrous.)

Stern and Makrides[47] used a rotating disc electrode to study the inhibition of iron-chromium alloys in sulphuric acid solution by ferric sulphate. They suggested that if the inhibitor has no specific effect on the electrode, such as adsorption, then the critical current density for passivation i_p and the passivation potential V_p, for the partial anodic process will not differ from those found in the absence of inhibitor. In the presence of ferric sulphate the anodic current for metal ion dissolution is equal to the rate of ferric iron reduction . The latter process is

diffusion limited in the region of the active-passive transition and so the behaviour observed depends on the concentration of ferric sulphate and the rotation speed. Knowing the concentration, rotation speed, and the hydrodynamic rate constant, the diffusion limited current for ferric ion reduction and hence the metal dissolution current was calculated. This current was plotted against the potentials measured with various ferric iron concentrations and rotation speeds. The resulting curve was the same as that obtained by galvanostatic polarisation in the absence of ferric sulphate. Moreover the passivation potential V_p and the critical current density for passivity were found to be constant for various concentrations of inhibitor, and agreed with those obtained in the galvanostatic experiments. Thus, they concluded that the presence of ferric iron does not alter the anodic behaviour of stainless steel and that it functions as an inhibitor by supplying the necessary current to allow passivation to occur.

Cartledge[48] expressed the view that some anions cause inhibition by a specific non-cathodic action. He polarised iron electrodes in the presence of labelled pertechnetate ions ($TcO_4^{=}$), at potentials which were more positive than the equilibrium potentials for their reduction. He found that the current densities and charges necessary for the passivation of iron, in the presence of pertechnetate ions were less than those in sulphate solutions. Moreover by measuring the beta-activity of such passivated electrodes he found that there were no technetium species present on the surface.

In a summary of his views[49] on the action of inorganic inhibitors, Cartledge made the following observations;

a) whereas some source of oxidation is necessary for passivation, it need not come from the inhibitor

b) passivating inhibitors produce the same kind of surface film as that resulting from anodic polarisation

c) the inhibitor greatly reduces both the charge and the minimum current for anodic passivation without itself necessarily being reduced

d) there is an antagonistic action between inhibiting and non-inhibiting anions in the electrolyte

e) under the most favourable conditions for passivation, the residual corrosion current may be low enough for the thermodynamically reversible potential of the inhibitor to be established.

A number of workers have presented evidence supporting the view that specific adsorption of anions can be important in the passivation process. Thus, Hackerman and Powers[50] studied the behaviour of chromium in radioactive solutions and found that there was selective adsorption of anions by the chromium surface.

Posey and Sympson[51] studied the effects of sulphate, thiocyanate, chloride and hydroxide ions on the reduction of cupric ion on passive stainless steel electrodes. They concluded that specific adsorption of anions catalyses the rate of the reduction reaction and that the adsorption follows a potential-dependent Langmuir isotherm.

Brasher and Mercer[52] investigated the influence of pH and concentration of dissolved oxygen on the uptake of radioactive chromium by mild steel. At pH values below 5.5 the uptake of radioactive chromium was independent of the presence of oxygen and diminished with decreasing pH. With increase of pH above 5.5, in oxygenated solutions, the amount of radioactive chromium in the film gradually decreases until at pH 13 no radioactive chromium is present on the surface of the steel. In the absence of oxygen the uptake of radioactive chromium falls from pH 5.5 to pH 9 but then remains roughly constant to pH 13.

These results show that when mild steel is immersed in chromate solutions it is passivated over the pH range from 1.6 to 13 and in almost all situations an adsorbed (or ion-exchanged) chromium containing layer is found. The mixed ferric chromic oxide layer that is formed, grows logarithmically with time and its composition varies with pH and oxygen content of the solution. The proportions of the two oxides are determined by

a) the predominating oxidising species in solution, oxygen (predominant at high pH values) or chromate

and b) the relative stabilities of the oxides.

In a later paper[53], they investigated the passivity of commercially pure iron in chromic acid solution. They measured both the uptake of labelled chromium on iron and the dissolution of labelled iron in chromic acid over the pH range 7.5 to 0.4. The chromium uptake was found to be linearly dependent on the logarithm of time down to pH 1.0. At pH 0.4 the chromium uptake was erratic. In chromic acid solutions the weight of labelled iron in solution was found to be proportional to $(\text{time})^{\frac{1}{2}}$. The logarithm of the dissolution current at a particular time varied linearly with pH and these lines had slopes parallel to those obtained by Vetter[19] for the stationary current with passive iron.

Using Heusler's theory[54] for the formation of passive films on iron, they showed that a logarithmic relationship can be predicted theoretically for the rate of film growth, if the rate determining step is the formation of oxide ions in the oxide at the oxide-solution interphase. They concluded that chromium is taken into the passive film, but the processes which occur can be treated in the same way as those which normally occur in sulphuric acid.

It may be said in conclusion that in some cases oxidising inhibitors

function by producing a mixed potential in the passive region but that there are also cases in which the specific effect of the anion can be identified. It would, therefore, be rash to suggest that the mode of action of oxidising inhibitors is governed solely by one or other of these factors .

1.4. OUTLINE OF THE PRESENT WORK

The work described in this thesis is divided into two main areas, the first concerns the characterisation and properties of the film material and the second the processes which occur during the formation of the film material. The nature of the film present on the surface of the steel and the techniques used to elucidate it are described in Chapter 2. The conduction properties of the film material and their dependence on the film thickness are described in Chapters 3 and 4. The general electrochemical theory which underlies the formation of the film material is described in Chapter 5 and the electrochemical techniques used to investigate it in Chapter 6.

One of the principal difficulties in obtaining kinetic information about the colouring process is that of separating the anodic and cathodic partial currents, during the formation of the film. The possible methods which have been considered in the attempt to overcome this problem are,

a) Ring disc studies, which allow the dissolution current to be measured

b) Measurement of dissolution rates of the steel through the film in the absence of dichromate

c) Measurement of the weight loss of the steel during film formation.

It was not possible to perform suitable ring disc studies and the reasons for this are discussed in Appendix A. The measurements of

dissolution rates through film is discussed in Chapter 7 and the determination of the dissolution rate by weight loss measurement in Chapter 9. The investigation of the cathodic process, that is, dichromate reduction is described in Chapter 8. In the final chapter, existing views of the film formation reactions are discussed and a qualitative explanation of the colouring process put forward.

TABLE 1.1

Relation between the potential above the plateau and the colour produced, for stainless steel specimens.

Potential above the plateau ΔV (mV)	Colour
4	hardly visible brown
6	bronze blue
8	blue
10	pale blue
12	gold/blue
14	pale gold
16	gold
18	red
21	blue green
23	green

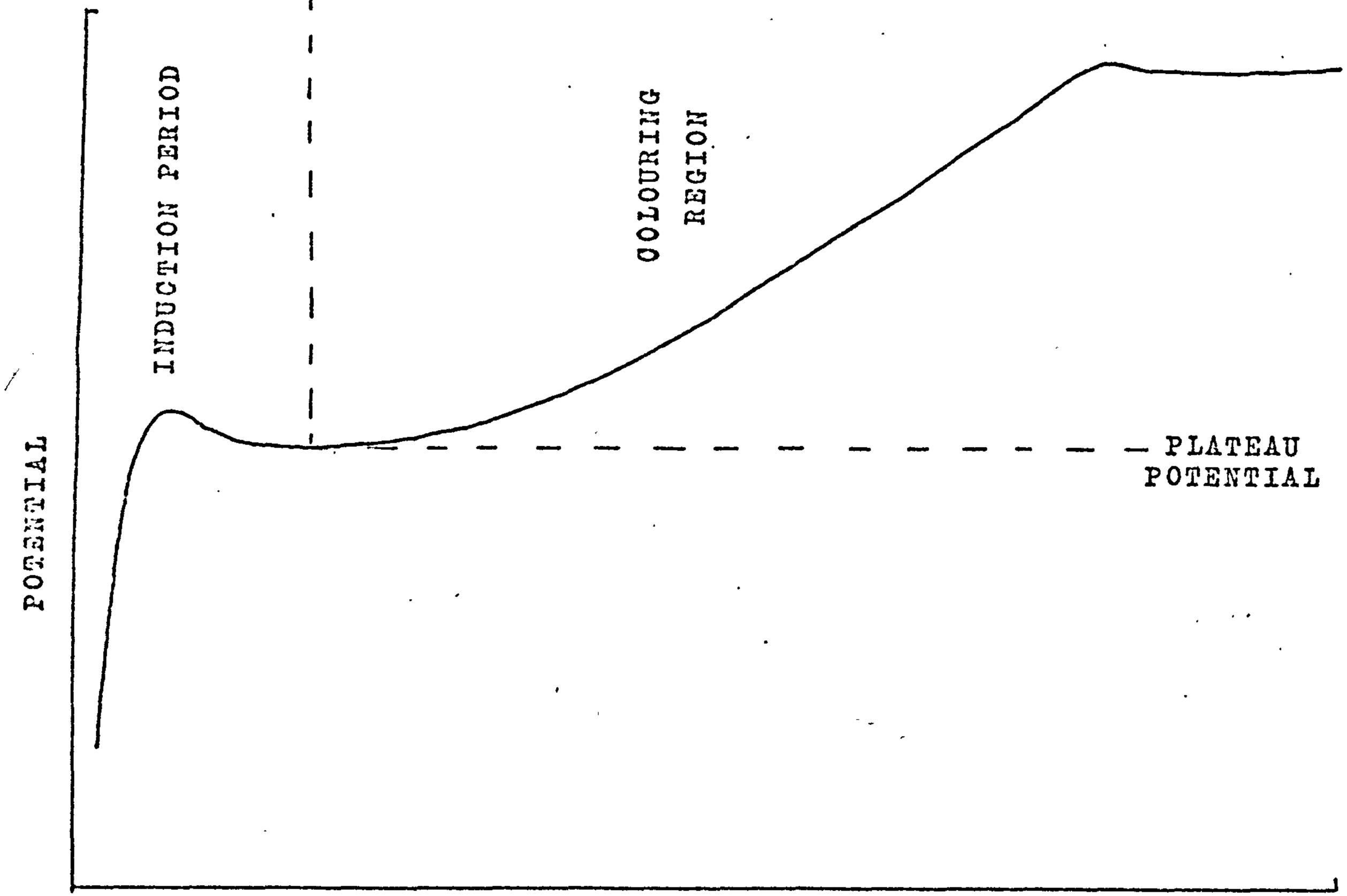

FIG.1.1 SCHEMATIC POTENTIAL-TIME CURVE FOR STAINLESS STEEL IN THE COLOURING BATH.

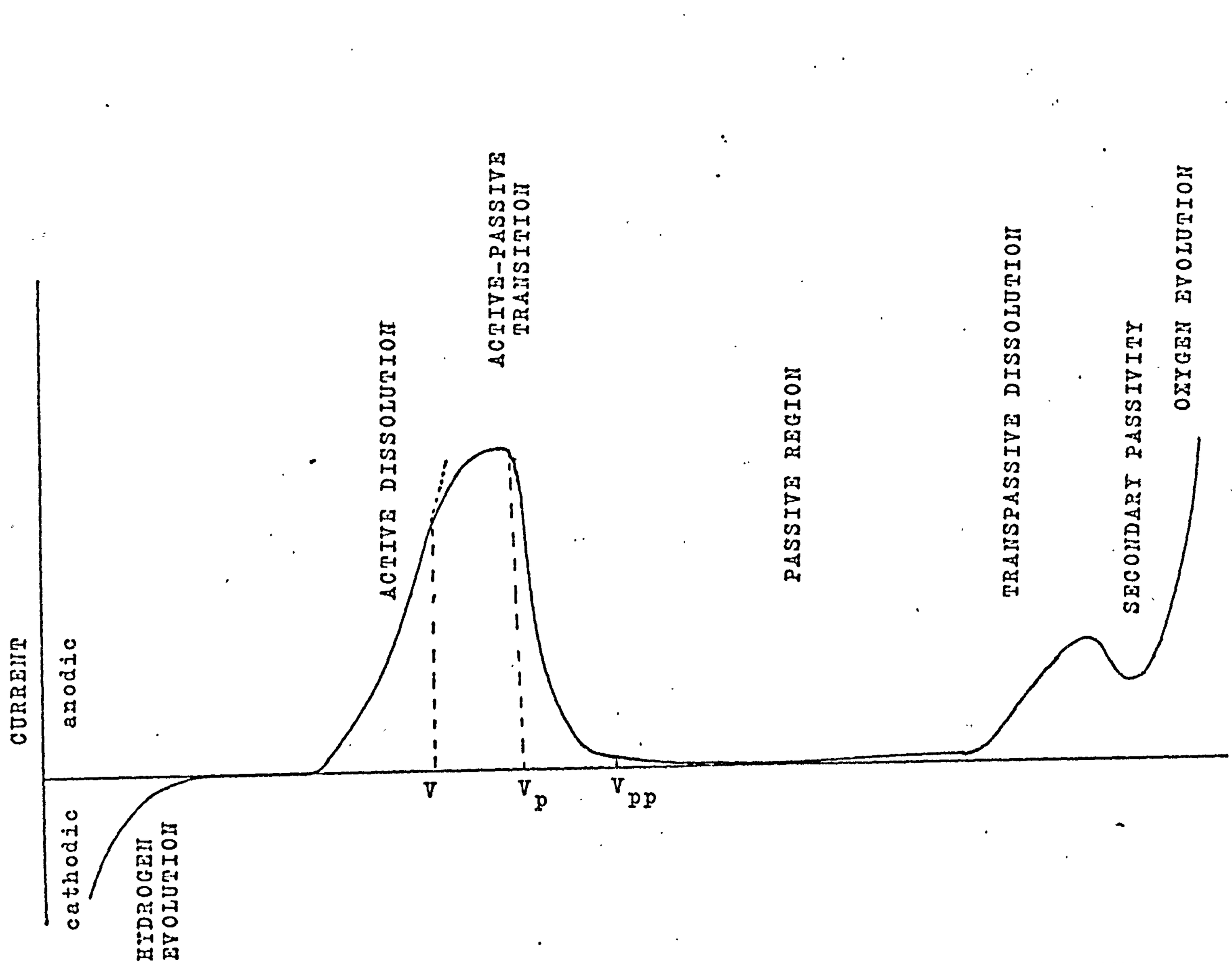

FIG.1.2. OVERALL CURRENT-POTENTIAL CURVE FOR A METAL IN AN AQUEOUS SOLUTION.

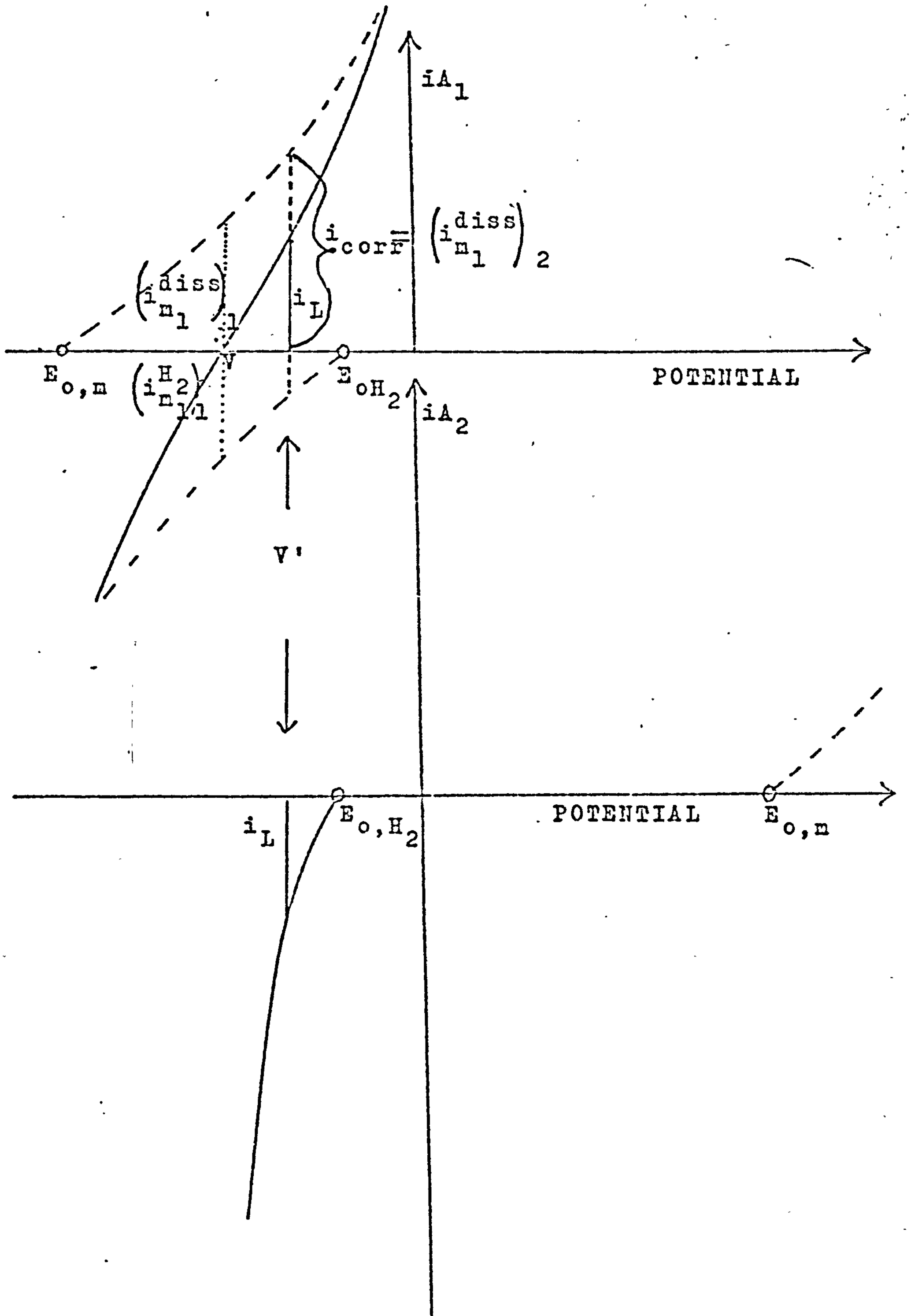

FIG.1.3 THE CORROSION OF A CHEMICALLY HETEROGENEOUS SURFACE

CHAPTER 2

THE NATURE OF THE FILM ON COLOURED STAINLESS STEEL

2.1. INTRODUCTION

Before an understanding of the processes involved in the formation of the coloured film produced on stainless steel in the sulphuric acid, chromic acid solution can be reached, several questions about the nature of the film must be resolved. Information is required about the composition, structure, and thickness of the film. Moreover it is necessary to know how these properties vary as the steel progresses through the sequence of colours.

Previous workers[2,3] have measured the optical properties of the film and have come to the conclusion that the colours produced on the steel surface result from interference effects. The colour produced on the steel surface changes with increasing thickness of the film material. From the positions of reflectance maxima and minima in the near infra-red, visible and near ultra-violet regions of the spectrum, optical thicknesses of the film were calculated. By assuming values of the refractive index and density of the film material, film thicknesses lying between 0.1 μm and 0.3 μm and film weights lying between 0.04 and 0.10 mg cm^{-2} have been calculated.

Films on the steel surface have been analysed[3] by electron probe microanalysis yielding a composition of 21.3% Cr, 11.5% Fe and 6.3% Ni. A film stripped[3] from the surface of the steel, by anodic etching in 50% water, 50% ethanol containing 100g l^{-1} succinic acid has been analysed by atomic absorption analysis and found to contain 19.6% Cr 11.7% Fe and 2.1% Ni.

Electron diffraction patterns of the stripped material gave broadened rings implying a small crystallite size and the patterns were found to be consistent with a cubic structure of a spinel type. Infra-red analysis of the stripped film material showed bands which could be assigned to vibrations associated with lattice or co-ordinated water in the film. The infra-red spectrum showed more similarity with that of Fe_3O_4, a spinel oxide than that of Cr_2O_3 or $Cr_2O_3.x\ H_2O$.

On the basis of these results the authors[3] suggested that the film has a spinel structure and is hydrated with a probable composition; $(Cr\ Fe)_2\ O_3$ $(Fe\ Ni)O \times H_2O$. The authors further suggested, on the basis of transmission electron micrographs of stripped film material, that the film is porous.

In this chapter, further attempts to characterize the film material are described. The information that is required can be split into three different categories; the composition of the film, its thickness and its structure. Two basic techniques have been used, involving respectively; studies of the film on the surface of the substrate steel, and studies of film material which has been removed from the substrate.

Toward the end of the studies reported in this thesis, workers[55] at International Nickel Ltd. found that coloured films could be produced on the surface of a nickel-iron alloy 'Nilomag' * alloy 771. The potential-time curve obtained during the formation of these films was similar to that of stainless steel. These films also showed a progressive change of colour with potential and/or length of time of immersion in 5M sulphuric acid 2.5M chromic acid.

* 'Nilomag' alloy 771 is a registered trademark of Henry Wiggin Ltd.

These films showed a variation in apparent colour with change in angle of incidence indicating that the colour results from interference effects. This fact and the similar potential-time curve observed during their formation suggests that the mechanism of their formation might be similar to that of the films on stainless steel. Since the nickel-iron alloy does not contain chromium, any chromium species in the film formed on it must have originated from the solution. A knowledge of the presence and nature of such species in the coloured film on the alloy, should therefore help to clarify the role of dichromate in the formation of the coloured film on stainless steel.

2.2. INVESTIGATION OF THE FILM MATERIAL ON THE SUBSTRATE STEEL

2.2.1. COMPOSITION

These methods are easier and quicker to apply than those which require film removal. They are in general spectroscopic techniques. Serious problems are caused however by the presence of the substrate metal because the analytical 'probe' (e.g. electrons) may penetrate through the film to the substrate. The analytical results will then include some contribution from the substrate and the problem becomes particularly acute if the same elements are present in the film and substrate. Moreover the effective depth of penetration of the analytical 'probe' may be unknown so that the contribution from the substrate cannot be determined.

The methods applied were; X-ray fluorescence analysis, scanning electron microscopy with energy dispersive analysis, electron microprobe analysis and photo-electron spectroscopy. Only with the last method was penetration of the coloured film unimportant.

2.2.1.1. SAMPLE PREPARATION

Preliminary experiments were carried out with specimens coloured using the simple immersion procedure described in Section 1.1. Stainless steel specimens (EN 58E) were degreased in acetone and thoroughly rinsed in doubly distilled water prior to immersion in 2.5M chromic acid 5M sulphuric acid at 70°C. The specimens were immersed for various times to produce the coloured films. After immersion the specimens were washed in distilled water and dried by draining onto a filter paper. The sample size was determined by the particular spectroscopic technique to be employed. In the case of X-ray fluorescence analysis, electron microprobe analysis and scanning electron microscopy it was not possible to obtain quantitative information about the composition of the film because of penetration effects. Consequently the preparation of further samples with better control of sample preparation was not carried out. Sample preparation for X-ray photoelectron spectroscopy is discussed in Section 2.2.1.5.

2.2.1.2. X-RAY FLUORESCENCE ANALYSIS

In this technique an X-ray photon source is used to excite a sample to emit its own characteristic X-rays. The X-ray source produces photons of sufficient energy to eject an electron from an inner energy level of the atom. This vacancy is filled by an electron from an outer energy level resulting in the emission of an X-ray characteristic of the particular atom being studied. The wavelength, or energy of the X-ray is used to determine which elements are present in the sample and the intensity to measure how much of each element is present.

RESULTS AND DISCUSSION

The results obtained with X-ray fluorescence analysis on the

uncoloured steel and progressively coloured films are reported in Table 2.1. Although penetration of the substrate has occurred, it can be seen that the film material contains more chromium and silicon but less iron than the substrate. The changes in the proportions of the other elements are too small to be significant.

2.2.1.3. SCANNING ELECTRON MICROSCOPY (S.E.M.) WITH ENERGY DISPERSIVE ANALYSIS (E.D.A.X.)

In S.E.M. an electron beam, incident on the sample causes the emission of X-rays characteristic of the elements present. These can be analysed using an energy dispersive analysis which allows the separation of the X-rays emitted on the basis of their energies. A qualitative analysis of the elements present can be achieved. The penetration depth of the beam is of the order of 1 μm; since the films are appreciably less thick than this (Section 2.2.3) some contribution from the substrate is again obtained.

RESULTS AND DISCUSSION

The results obtained by energy dispersive analysis are shown in Figures 2.1, 2.2 for the stainless steel substrate and films at two stages of the colouring process. Signals were obtained from iron, chromium and nickel when excitation energies of both 10 kV (Fig. 2.1) and 20 kV (Fig. 2.2) were used. There was an increase in the ratio of the chromium peak to the iron peak on going from the untreated steel to the early stage of colouring and from the early to the later stage of colouring, for both excitation energies. The changes in the ratios of the chromium peaks to the iron peaks with progressive colouring are also greater than those obtained with X-ray fluorescence analysis.

These results again show that the film material contains more chromium than the substrate steel and suggest that penetration of the steel is occurring at 20 kV excitation energy.

2.2.1.4. ELECTRON PROBE MICROANALYSIS

In this technique the specimen is bombarded with electrons causing the emission of an X-ray spectrum characteristic of the elements present. The X-rays are analysed according to their wavelength and intensity. In conjunction with reference spectra from the pure elements, this allows a quantitative analysis of the substrate. The depth of specimen analysed is 1 μm.

RESULTS AND DISCUSSION

The results of this analysis, in Table 2.2, show that the film material contains more chromium and less iron than the substrate steel in agreement with the results obtained by X-ray fluorescence analysis. The fall in the proportion of nickel in the coloured specimens suggests that there is less nickel in the film than the substrate steel. As with E.D.A.X. analysis the changes in composition shown by electron probe micro-analysis are greater than those obtained with X-ray fluorescence analysis as a result of the greater sampling depth of the latter technique.

2.2.1.5. X-RAY PHOTOELECTRON SPECTROSCOPY

This is a comparatively new technique which has distinct advantages for studying surfaces. The sample is irradiated with X-rays usually of energy 1253.6 eV (Mg $K\alpha_1$, $K\alpha_2$). Instead of collecting the X-rays emitted from the specimen, as with X-ray fluorescence analysis, the electrons which are emitted are studied. These electrons are analysed according to

the kinetic energy which they possess. The spectra obtained are plots of electron energy against number of electrons emitted. A schematic diagram of the AEI ES 200A spectrometer used in this work is shown in Fig. 2.3 and a typical narrow kinetic energy scan in Fig. 2.5.

Using the kinetic energy of the emergent electrons and the energy of the incident radiation the binding energy of the ejected electrons can be calculated from the expression:

$$h\nu = KE + BE$$

The binding energy of the electron is characteristic of the core energy level from which it was emitted. Since this depends, upon the particular element present, its effective oxidation state and its chemical environment, information on all of these is obtained. Moreover the number of electrons of a given kinetic energy is proportional to the number of atoms of which they are characteristic. Consequently quantitative analysis is also possible.

The peculiar advantage of the technique for studying surfaces is that although the penetration depth of the incident X-rays may be several thousand Angstroms the escape depth of the electrons is only 10 to 30 Å. Previous X-ray photoelectron spectroscopy (XPS) studies[56,57,58,59], of films electrochemically produced on metal surfaces, have shown that much information can be gained from these studies.

SAMPLE PREPARATION

Stainless steel foil specimens (EN 58E Goodfellow Metals Ltd.) were immersed in 2.5M chromic acid, 5M sulphuric acid solution at 70°C and their potentials monitored with respect to a commercial (E.I.L.) saturated

calomel electrode (SCE). The specimens were removed at various stages of the colouring process (Fig. 2.4) washed in distilled water, dried by draining onto filter paper and transported to the spectrometer in a desiccator.

The specimens were mounted on a copper sample holder to provide good electrical and thermal contact and examined using an AEI ES 200A spectrometer. The pressure in the sample chamber was typically 10^{-7} Torr. Calibration was with respect to the carbon 1s electron peak due to a thin layer of hydrocarbon pump oil in the spectrometer. The spectra were analysed by comparison with spectra of known species. When necessary, overlapping peaks were resolved using a Du Pont model 301 curve resolver with a Gaussian-Lorentzian peak shape.

RESULTS

Typical spectra for various specimens are shown in Figs. 2.5, 2.6 and 2.7. Iron, chromium and oxygen could be detected in the untreated and treated steel, in addition; manganese and sulphur could be detected for specimens removed in both the induction period and colouring region. Nickel could not be detected at any stage.

For some elements, the shapes of the peaks obtained suggest the presence of more than one oxidation state. In such cases the peaks were resolved by comparison with previous work[59,60] and the spectra obtained from appropriate compounds, Table 2.3. The proportions of these different species are given in Table 2.4. The peaks may be assigned as follows; chromium 3p electron peaks at 48.4 eV, 46.4 eV and 44.1 eV to chromium VI, chromium IV/V and chromium III respectively, iron 3p electron peak at 53.4 eV to elemental iron metal, the sulphur 2p3/2, 2p½ doublet at 169.9 eV, 168.5 eV to sulphate incorporation. The oxygen 1s electron peak is, in

all cases, a composite peak due to the presence of various oxides, hydroxides and water of hydration on the specimen surface. As a first approximation the overall peak envelope may be resolved into peaks at 532.7 eV, 531.4 eV and 530.0 eV due to water of hydration, hydroxide and oxide species respectively. The Mn 2p3/2 peak had a binding energy of 641.1 eV and cannot be assigned at present. The foregoing assignations and those of the remaining Fe 3p electron peaks will be discussed later.

The intensity ratios given in Table 2.5 suggest that the proportions of chromium and manganese in the layer increase with respect to that of iron in the induction period, but do not vary significantly throughout the colouring region.

The presence of peaks due to metal in the elemental state suggest that the oxide layer in these cases is less than 20 Å thick. Thus the layer present on the steel surface is of this order in the induction period but not in the untreated or coloured state.

ASSIGNMENT OF THE PEAKS

The assignment of the chromium 3p electron peaks is based on a comparison with previous work[59] on the reduction of Cr (VI) at a gold electrode. The peaks at 44.1 eV and 48.6 eV are partially resolved in the spectra but they cannot account for the total peak area. The third peak cannot be assigned absolutely but could be tentatively assigned to an intermediate in the reduction of Cr (VI) to Cr (III).

The iron 3p electron spectra are difficult to analyse because of the extremely sloping background. The results suggest a different environment for the iron with coloured stainless steel as opposed to the untreated steel. The binding energies correspond closely to those obtained with Fe_3O_4 and Fe_2O_3 respectively.

The oxygen 1s electron and sulphur 2p electron spectra are assigned on the basis of previous results[60]. Only one manganese species is detected and cannot be reasonably assigned to a particular oxidation state.

PROPORTIONS AND INTENSITIES OF THE PEAKS

The untreated steel shows only one chromium 3p electron peak which is assigned to chromium III. The presence of two other species is established even after the shortest period of immersion and thereafter they remain very constant, until the powdery stage is reached (Table 2.4). The original film present on the stainless steel surface is at least partially removed initially since specimens removed in the induction period show a peak due to iron metal in the substrate steel. However in the colouring region the film has become sufficiently thick to obscure the iron metal peak.

DISCUSSION

On the basis of this evidence it can be seen that the original film present on the untreated steel is modified, to some extent, by dissolution on immersion in the colouring solution. The film present in the induction period thickens and the ratio of chromium to iron in it increases. The ratio of the amounts of iron and chromium and the relative amounts of the different chromium species present in the film remain constant throughout the colouring region and differ from those in the induction period. Hence the composition of at least the surface of the film formed in the colouring region does not change with increase in thickness. These changes will be shown later to be consistent with the formation of an initial passivating type of film on the steel surface followed by a change in properties to form a transpassive type of film in

the colouring region.

CONCLUSIONS

1) The film present on coloured stainless steel contains nine different species. These species are present on all specimens studied in the colouring region.
2) The proportion of chromium to iron remains constant throughout the colouring region.
3) Chromium is present in the film in at least two valency states.
4) The film is hydrated.
5) There is a change in composition between films found in the initial stages of the process and those found in the colouring region.

2.2.2. STRUCTURE

2.2.2.1. SCANNING ELECTRON MICROSCOPY

A fine beam of electrons from a filament is focussed on the specimen surface by means of magnetic lenses. Current is passed through scanning coils situated between the last magnetic lens and a cathode ray tube, in such a way that the electron beam scans a square raster on the specimen surface and a larger raster is produced simultaneously on the cathode ray tube. The electron beam produces various types of emission from the specimen surface, the most important of which, from the S.E.M. point of view, is the emission of secondary electrons. The emitted electrons are detected and the resulting signal after amplification is used to modulate the brightness of the display on the cathode ray tube. The brightness of a particular point on the cathode ray tube is related to the number of secondary electrons produced at the corresponding point on the specimen surface so that an enlarged image of the specimen surface is

progressively built up on the C.R.T. The magnification produced is determined by the ratio of the area of the cathode ray tube to the area of specimen which is scanned.

RESULTS AND DISCUSSION

S.E.M. images of the surface of stainless steel did not exhibit a great deal of surface structure, Fig.2.8. Indeed there appears to be little change in surface structure between the stainless steel substrate and the film material.

2.2.3. THICKNESS

A green coloured specimen was set in a cold setting resin so that the plane of the specimen was at an angle of 30^{o} to the surface of the resin. The resin and the steel were polished to expose the edge of the steel which was then examined in the S.E.M. The S.E.M. image of the specimen is shown in Fig. 2.9. The area marked on the figure most probably corresponds to the film on the steel surface and from the magnification used and the angle of the specimen an approximate thickness of 0.5μm was calculated.

This thickness is in reasonable agreement with those obtained by previous workers[3] using optical techniques, who found thickness lying between 0.1 and 0.3μm. It is also consistent with the fact that energy dispersive analysis or electron probe microanalysis of the film included a contribution from the substrate steel.

2.2.4. WORK WITH A NICKEL-IRON ALLOY

For the reasons given in Section 2.1 samples of coloured nickel-iron alloy were prepared and the species present on their surfaces

investigated using X-ray photoelectron specroscopy.

Sample preparation and potential measurements were carried out using 'Nilomag' alloy 771 foil in the manner described for stainless steel in Section 2.2.1.5. The composition of the foil was determined by X-ray fluorescence analysis as 14.2% Fe, 4.6% Cu and 3.68% Mo, the balance being substantially Ni and the chromium content less than 0.05%. The potential-time curve obtained is shown in Fig. 2.10. Specimens removed at different stages on the potential-time curve (indicated in Fig. 2.10) were examined using X-ray photoelectron spectroscopy, as described in Section 2.2.1.5.

RESULTS

Iron, nickel, molybdenum and oxygen could be detected in the untreated and treated Nilomag. Chromium and sulphur were also found throughout the induction period and colouring region. Copper could not be detected at any stage of the treatment. Typical XPS spectra for these elements are shown in Figs. 2.11, 2.12, 2.13 and 2.14. The assignment of the electron peaks for chromium, oxygen and sulphur was made on the basis of comparison with the previously described work on stainless steel (Section 2.2.1.5.). Nickel 2p3/2 electron peaks at 851.8 eV, 853.7 eV and 855.8 eV were assigned to nickel metal, nickel oxide (NiO) and nickel oxide (multiplet splitting) respectively and the molybdenum 3d5/2 electron peaks at 227.7 eV and 232.2 eV were assigned to molybdenum metal and molybdenum VI respectively. The proportions of these different species are given in Table 2.6.

The absolute intensities of the metallic species detected on the Nilomag surface are included in Table 2.7. Both nickel metal and molybdenum metal are detectable in the untreated foil and after 20 secs. immersion in the colouring bath.

DISCUSSION

ASSIGNMENT OF THE PEAKS

The nickel 2p3/2 electron peaks can be assigned on the basis of previous work[60], on the nature of the surface oxide formed on a nickel electrode in 0.5M sulphuric acid in the passive and transpassive regions. The peak at 855.1 eV could be assigned to $Ni(OH)_2$ or a nickel (III) oxy hydroxide. It is probably due to the former material on the untreated Nilomag, but in view of the highly oxidising nature of the electrolyte the latter material is probably present on the coloured specimens.

The assignment of the molybdenum species present was made on the basis of previous work[61], the binding energy of the molybdenum species corresponding with that of molybdic acid and sodium molybdate which suggests that it is a Mo (VI) species.

As with stainless steel, the iron 3p electron spectra are difficult to analyse because of the extremely sloping background. As with stainless steel, the iron 3p electron spectra are difficult to analyse because of the extremely sloping background. The situation for Nilomag is, however, more complicated. The spectrum of specimen 5 suggests the presence of two peaks and an analysis of all the spectra on this basis yields the results in Table 2.6, but no attempt at assignment of these species is made.

THE INTENSITIES OF THE PEAKS

There is no chromium present on the surface of the untreated Nilomag. After 20s immersion, when the specimen had reached a potential of +990 mV (S.C.E.) chromium species were present on its surface (Sample 1). As shown in Table 2.7, the proportion of chromium species on the surface

increases during the induction period (specimens 1 and 2) but remains constant in the colouring region. The presence of chromium in this film shows that the chromic acid must be taking part in the film formation reactions. The absolute intensities of the iron nickel and molybdenum species detected on the Nilomag specimens (Table 2.7) suggest that the proportion of iron in the film shows little variation, that the nickel content increases slightly at the later stage of colouring and that the proportion of molybdenum increases during the induction period and remains constant in the colouring region.

The proportions of the different iron, nickel and oxygen species present on the coloured specimens (3, 4, 5)(Table 2.6) remains nearly constant for the coloured specimens, there is, however, some variation in chromium content between specimens 3, 4. These observations suggest that there is little change in the composition of the film present on Nilomag in the colouring region.

CONCLUSIONS

The results obtained above show that the Nilomag is covered with a film that thickens during the initial stages of the induction period since nickel and molybdenum metal can be detected on specimen 1 after 20s immersion but not on specimen 2. This is consistent with the change in potential of the specimen with time during the induction period since progressively thicker films are produced with increase in potential in the passive region.

The presence of chromium species on the surface of the Nilomag, even after a short period of immersion in the film forming solution, shows that the reduction products of dichromate are incorporated into the surface film. The surface composition of the film remains constant throughout the colouring region and there is evidence for the presence of Cr (VI) in this

film at the later stages of colouring. It would thus appear reasonable, on the basis of the similarities between the behaviour of the Nilomag and stainless steel, that chromium species are also incorporated in the case of stainless steel.

2.3. INVESTIGATION OF THE FILM AFTER REMOVAL FROM THE SUBSTRATE STEEL

Several workers[63-66] have isolated oxide films from stainless steel, using techniques which dissolve the steel and leave the oxide film.

The technique recommended by workers at the National Physical Laboratory was to dissolve the substrate in a saturated solution of iodine in methanol under anaerobic conditions. The principle difficulty with the method was to ensure that the film obtained was representative of the material originally present on the steel surface.

2.3.1. THE IODINE-METHANOL METHOD OF OXIDE FILM REMOVAL

METHANOL PURIFICATION

Analar methanol (1 litre) was poured into the delivery flask (Fig. 2.15) containing a molecular sieve (Linde type 4A). A stream of dry nitrogen was introduced into the flask via tap 14, tap 13 being open and protected by a trap containing the molecular sieve. The nitrogen was allowed to deaerate the solution overnight; the agitation provided by the nitrogen hastening the drying process.

FILM STRIPPING PROCEDURE

Stainless steel foil specimens (Goodfellow Metals Ltd. type EN 58E) 0.025 mm thick and 1 cm^2 in area were coloured on one side by immersion in 5M sulphuric acid, 2.5M chromic acid held at 70°C One side of the stainless steel foil was protected by Lacomit acid resistant lacquer which

was peeled off the sample after colouring, residual traces of Lacomit were removed using acetone.

The coloured film produced was coated with a layer of transparent plastic film (Alloprene, I.C.I. Ltd.). The Alloprene was applied as a 1% (w/v) solution in chloroform. The samples were then placed, plastic side downwards, on the sintered glass disc in the film stripping chambers (Figs. 2.16 and 2.17). The chambers were then attached to the cones on the film stripping apparatus and held in place by springs. The apparatus was then partially evacuated and subsequently purged with dry nitrogen.

The delivery flask (Fig. 2.15) was connected by means of socket 1 to flask A (Fig. 2.17). The latter flask was evacuated through tap 1, tap 14 on the delivery vessel being open and tap 13 connected to a stream of dry nitrogen. In this manner the methanol was transferred to flask A. A similar procedure was adopted for filling flask B which contained sufficient iodine to saturate the added methanol.

The iodine-methanol solution was transferred to the film stripping apparatus from flask B by attaching a pump to tap 7, 8, 9, 10 in turn and allowing nitrogen to enter the apparatus via tap 12, tap 11 and taps 3, 4, 5, 6 respectively being open.

The iodine-methanol solution was left in contact with the steel for four days. The samples were washed with methanol, using the method described above but evacuating through taps 7 to 10. After washing with methanol the specimens of the film material on their plastic supports were taken out of the apparatus for examination.

2.3.2. COMPOSITION OF THE STRIPPED FILMS

It was originally intended that the stripped film material should be weighed, dissolved in a suitable solution and analysed by atomic

absorption analysis. Several difficulties were encountered in attempting to weigh the stripped film. In the first approach, the weights of the coloured steel, the coloured steel coated with Alloprene and the stripped film supported on the Alloprene were measured. In principle, the weight of the film can be obtained from these weights. Unfortunately, this method gave film weights which were predominantly negative. This resulted partly from the fact that the weight of the film (c.a. 100 μg) was much smaller than the weights of the Alloprene and the coloured steel (about 1 and 17 mg respectively). The cumulative inaccuracy involved in three weighings was comparable with the weight of the film. Errors in film weight could also arise as a result of changes in weight of the Alloprene layer caused by immersion in the film stripping solution, or incomplete removal of solvent during the application of the Alloprene layer.

An alternative method of obtaining the film weight was to transfer the film from its Alloprene backing to a light support of accurately known weight and weigh the film on the support. This was not found to be possible, however, partly due to disintegration of the film material on removal of the Alloprene and partly due to the lack of a support which would allow the complete removal of the Alloprene, by washing with chloroform, and be sufficiently light to allow an accurate determination of the film weight.

Problems were also encountered in dissolving the film material to carry out the atomic absorption analysis. The film material did dissolve in an aqueous solution of hydrofluoric acid but this solvent was unsuitable for use in the atomic absorption apparatus because the solution comes into contact with a glass nebuliser.

As a result of these difficulties optical and spectroscopic methods of analysis were used. The latter included, X-ray fluorescence, energy dispersive analysis and transmission electron microscopy.

OPTICAL EXAMINATION OF THE STRIPPED FILM

Optical examination of the stripped film material, with the aid of a microscope providing magnifications of up to 600X, showed no visible traces of residual steel, providing the specimen had been left in contact with the iodine-methanol solution for at least 96 hours. There were areas of the film which appeared brown, areas which exhibited interference colours and occasional brown crystals on the film surface.

X-RAY FLUORESCENCE ANALYSIS

Material from the stainless steel which was either uncoloured or covered with a blue film was analysed using the X-ray fluorescence technique. The ratios of the elements found are reported in Table 2.8. This data appears consistent with the X.P.E.S. data described in Section 2.2.1.5.

ENERGY DISPERSIVE ANALYSIS

Material stripped from blue coloured steel was mounted on a copper grid using a technique which will be described in Section 2.3.3.1. The E.D.A.X. analysis of the specimen (Fig. 2.18) shows peaks for iron, chromium, nickel, silicon and sulphur from the film material as well as peaks for copper, from the grid and chlorine and titanium resulting from incomplete removal of the Alloprene.

The presence of nickel in the stripped film is not in accord with the X.P.E.S. of the film on the substrate steel or the X-ray fluorescence analysis of stripped film material. This suggests that the specimens used for E.D.A.X. analysis suffered some contamination from either the substrate steel or its hydrolysis products. Even in the presence of some substrate contamination, the ratio of the height of the

chromium peak to the iron peak in the E.D.A.X. analysis indicates that the film contains more chromium than the substrate steel.

2.3.3. STRUCTURE OF THE STRIPPED FILMS

TRANSMISSION ELECTRON MICROSCOPY

In this technique a collimated beam of electrons impinge on the specimen resulting in some scattering of the electron beam. The transmitted and scattered beams are focussed, using an objective electron lens, at different positions in the focal plane of the lens. An objective aperture situated in this focal plane allows either the direct beam to form an image in the projection lens system of the microscope (bright field image) or if the aperture is laterally displaced, the scattered beam forms the image (dark field image). The details of the image observed are determined by the extent to which each has occurred.

If the distribution of intensities in the focal plane of the aperture is studied, diffraction patterns are obtained. In the case of monocrystalline substances this is a spot pattern. However, if the substance is amorphous the diffraction pattern usually consists of hazy rings.

RESULTS

Stripped film material, from blue coloured stainless steel, was placed on a copper grid and the plastic backing removed by leaving the specimen in contact with a chloroform liquid-vapour interface. The film, supported on the copper grid, was then examined using the transmission electron microscope.

Fig. 2.19 shows transmission electron micrographs of the stripped film. The best indication of the nature of this material is probably

obtained from Fig. 2.19(b) which corresponds to a region where the film is very thin. The micrograph suggests that the film is composed of small crystallites.

A representative electron diffraction pattern obtained from the stripped material is shown schematically in Fig. 2.20(a). The ring pattern obtained was hazy and although unambiguous identification of the film material is impossible there are similarities between the diffraction pattern for the stripped film and FeO. Cr_2O_3 (Fig. 2.20(b)).

SUMMARY

1) From the S.E.M. thickness data (Section 2.2.3.) and because of the penetration effects of energy dispersive and X-ray fluorescence analysis (Sections 2.2.1.3. and 2.2.1.2.) respectively the thickest films found most probably do not exceed 0.5 μm.

2) On the basis of X-ray fluorescence analysis (Sections 2.2.1.2. and 2.3.2.2.) and electron probe microanalysis (Section 2.2.1.4.) the film material has a higher content of chromium and silicon and a lower content of iron than the steel itself.

3) The ratio of Cr/Fe on the outer surface of the film appears to increase during the induction period but then remains essentially constant as the film thickens (Section 2.2.1.5.).

4) The cationic species present in the film include iron, chromium and manganese on the basis of X.P.E.S. (Section 2.2.1.5.) and X-ray fluorescence analysis (of stripped film material Section 2.3.2.).

5) X.P.E.S. studies (Section 2.2.1.5.) suggest that sulphur is present as the sulphate due probably to incorporation, oxygen is present as oxide, hydroxide and water. Chromium is present in the film as Cr III, Cr VI and

probably Cr V or Cr VI.

6) The T.E.M. electron diffraction pattern shows similarities with that of $FeO.Cr_2O_3$ (Fig. 2.20(b)) which is a spinel structure. The X.P.S. evidence for iron in the film in a form similar to Fe_3O_4 (Section 2.2.1.5.) also suggests that the film has a spinel structure.

7) Although chromium species are found to be present on the surface of steel, both during the induction and colouring regions, this cannot be taken as unambiguous evidence that dichromate from the solution is incorporated into the film. Similar chromium species would be expected to be present on the surface of the stainless steel undergoing transpassive dissolution.

8) The presence of chromium species on the surface of coloured Nilomag (Section 2.2.4.) suggests, however, that the reduction products of dichromate and Cr VI are incorporated into the film formed on the surface of the stainless steel.

TABLE 2.1

X-RAY FLUORESCENCE ANALYSIS OF COLOURED STAINLESS STEEL

Specimen No.*	Cr	Co	Mo	Ti	Al	Si	Mn	Fe	Ca	Ni	Nb	Zr	V
Untreated steel	18.61	0.24	0.48	0.01	0.17	0.50	1.56	68.16	0.17	10.64	0.01	0.01	0.05
1	18.75	0.24	0.48	"	0.18	0.54	1.60	67.91	0.17	10.65	"	"	"
2	18.89	0.24	0.47	"	0.17	0.56	1.59	67.69	0.17	10.68	"	"	"
3	19.00	0.24	0.51	"	0.16	0.59	1.57	67.56	0.17	10.65	"	"	"
4	19.22	0.24	0.50	"	0.15	0.62	1.60	67.49	0.16	10.59	"	"	"

* Increasing specimen number corresponds to increase in immersion time

TABLE 2.2

ELECTRON PROBE MICROANALYSIS

	Fe	Cr	Ni
early film	63%	21%	10%
late film	49%	25%	8%
late film	48%	26%	7%

TABLE 2.3

Sample	Physical State†	Binding Energy* (eV)
Fe_2O_3	Powder	55.8 (Fe 3p)
Fe_3O_4	Powder	56.6 (Fe 3p)
Fe	Sheet	55.7, 53.1 (Fe 3p)
MnO_2	Powder	642.6 (Mn $2p\frac{3}{2}$)
Mn_3O_4	Powder	641.7 (Mn $2p\frac{3}{2}$)
Mn	Sheet	640.7 (Mn $2p\frac{3}{2}$)**

† All powders were mounted on double-sided sellotape.

* All binding energies are with respect to C 1s = 284.6 eV.

** See Ref. 62

Table 2.4 THE PROPORTIONS OF THE PEAKS PRESENT ON THE SURFACE

Sample	Sample number	Cr 3p			Ni $2p^{3}/2$			Fe 3p				O 1s		
		44.1	46.4	48.4	851.8	853.7 +855.8	855.1	53.4	55.6	56.4	57.5	530.0	531.4	532.7
Stainless steel	0	>95	–	–	–	–	–	–	>95	–	–	32	36	32
Stainless steel	1	60	15	25	–	–	–	22	–	78	–	32	57	11
Stainless steel	2	60	15	25	–	–	–	13	–	87	–	43	39	18
Stainless steel	3	56	16	28	–	–	–	–	–	>95	–	42	36	22
Stainless steel	4	56	16	28	–	–	–	–	–	>95	–	42	40	18
Stainless steel	5	56	16	28	–	–	–	–	–	>95	–	45	36	19
Stainless steel	6	61	20	19	–	–	–	–	–	>95	–	40	45	15

– = *Species not detected*

TABLE 2.5

INTENSITY RATIOS FOR THE STAINLESS STEEL SAMPLES

Sample No.	V/mV	Stage reached	Intensity Ratios	
			$\frac{Fe(ox)}{Cr(ox)}$	$\frac{Fe(ox)}{Mn(ox)}$
0	-	untreated	4.1	---
1	-	induction period	2.2	4.6
2	0	induction period	1.1	2.3
3	7	colouring region	0.86	1.2
4	13	"	0.77	0.92
5	23	"	0.63	0.84
6	31	"	0.69	---

--- in these cases no manganese was detected

Table 2.6 THE PROPORTIONS OF THE PEAKS PRESENT ON THE SURFACE

Sample	Sample number	Cr 3p			Ni $2p^{3}/2$			Fe 3p				O 1s			Mo $3d^{5}/2$	
		44.1	46.4	48.4	851.8	853.7 +855.8	855.1	53.4	55.6	56.4	57.5	530.0	531.4	532.7	227.7	232.3
Nilomag 771	0	–	–	–	18	44	38	24	–	76	–	13	74	13	43	57
Nilomag 771	1	~90	⊁	⊁	26	45	29	24	–	76	–	15	69	16	30	70
Nilomag 771	2	~90	⊁	⊁	–	69	31	–	–	60	40	10	69	21	–	>95
Nilomag 771	3	~90	⊁	⊁	–	75	25	–	–	60	40	11	67	22	–	>95
Nilomag 771	4	56	18	26	–	75	25	–	–	46	54	9	71	20	–	>95
Nilomag 771	5	62	15	23	–	74	26	–	–	56	44	15	65	20	–	>95

– = *Species not detected*

⊁ = *The sloping background makes the presence/absence of these species difficult to determine*

TABLE 2.7

Absolute intensities for the 'Nilomag' alloy 771.

Sample No.	ΔV/mV	Stage reached	(Total) Fe	(Total) Cr	(Total) Ni	(Total) Mo
0	-	untreated	44	0	70	30
1	-	induction period	52	15	73	56
2	-	induction period	43	23	67	132
3	8	colouring region	34	37	63	134
4	20	"	37	36	87	131
5	21	"	36	33	87	141

TABLE 2.8

X-RAY FLUORESCENCE ANALYSIS OF STRIPPED FILM MATERIAL

SAMPLE	Fe	Cr	Mn
blue	65%	32%	3.6%
coloured	41%	45%	14%
steel	42%	43%	15%
Stainless steel substrate	70%	20%	4%

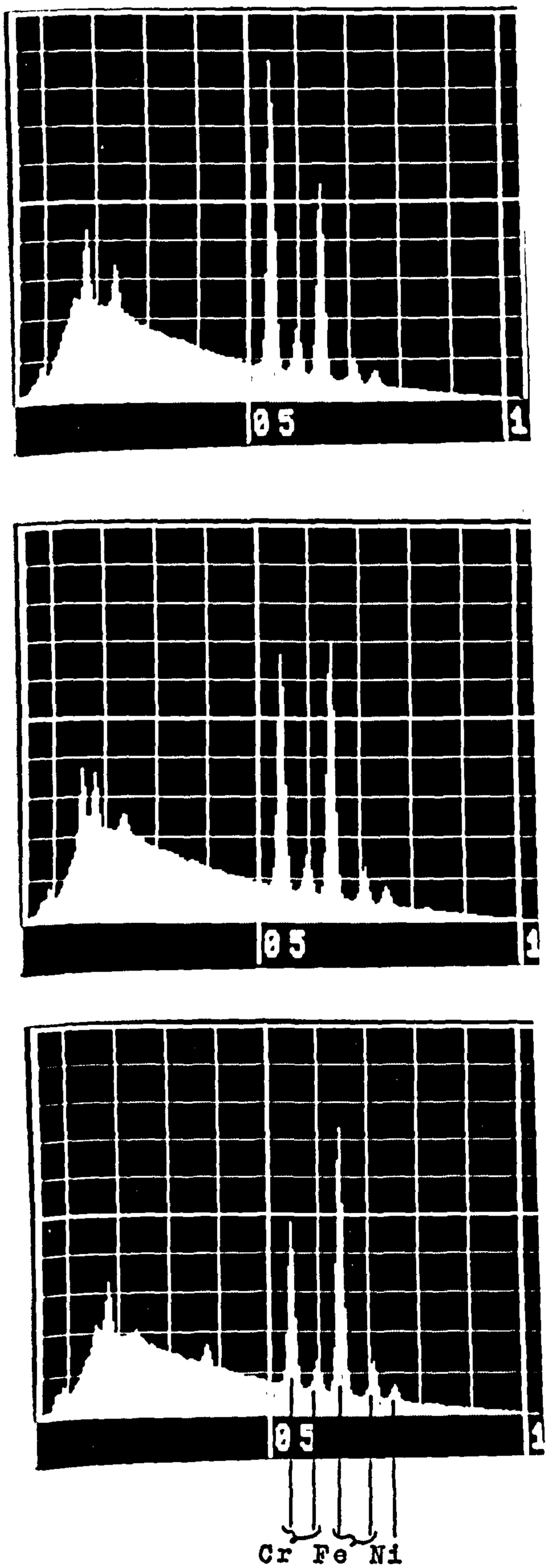

a) Late coloured steel

b) Early coloured steel

c) Untreated steel

10kV excitation

FIG.2.1 EDAX ANALYSIS OF COLOURED STAINLESS STEEL.

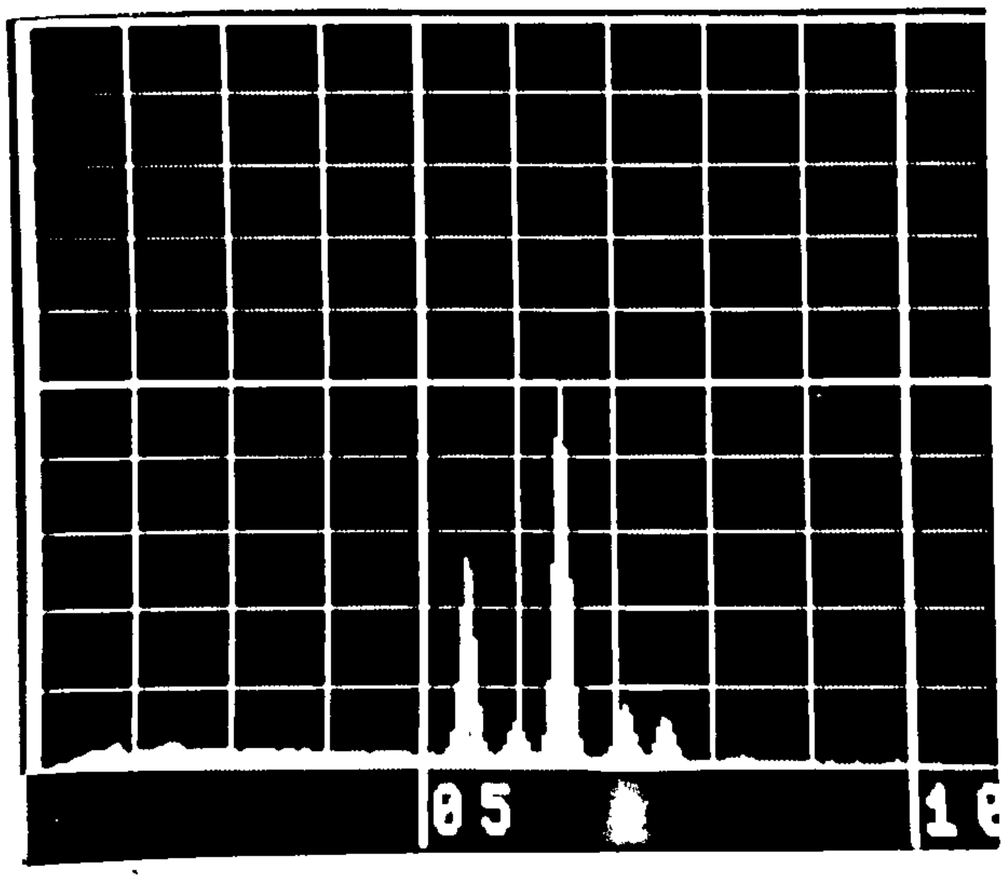

a) Late coloured steel

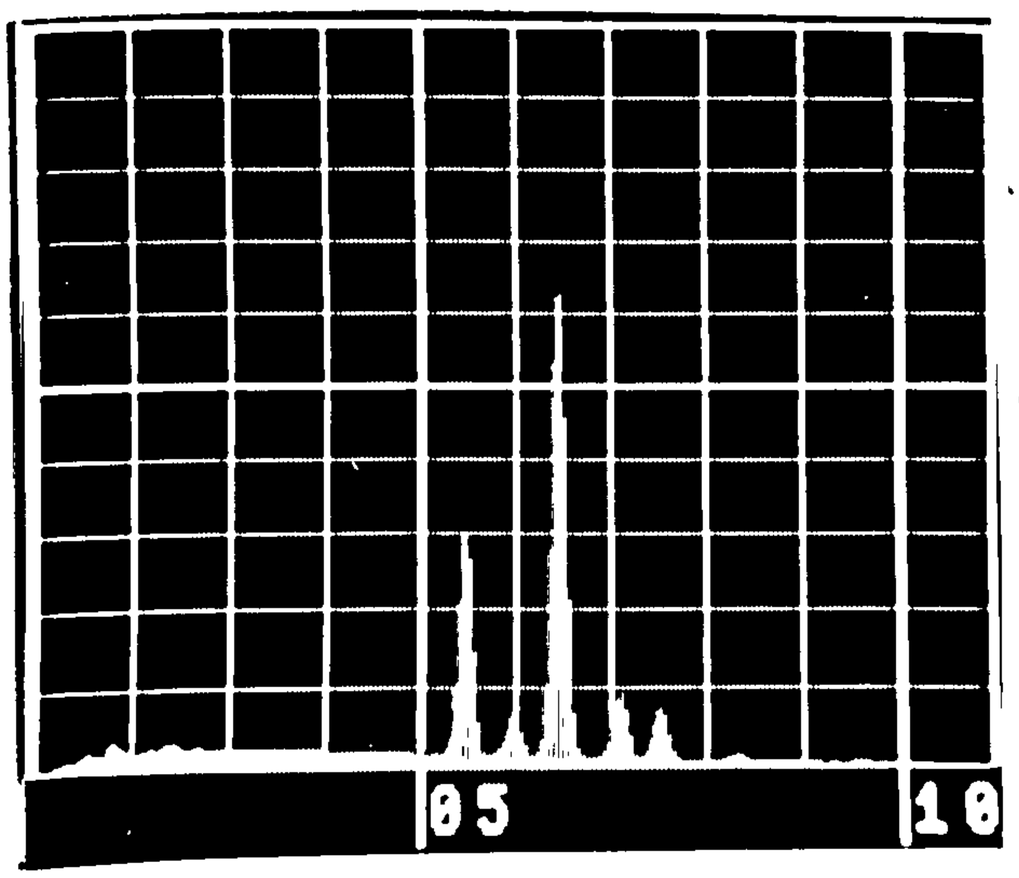

b) Early coloured steel

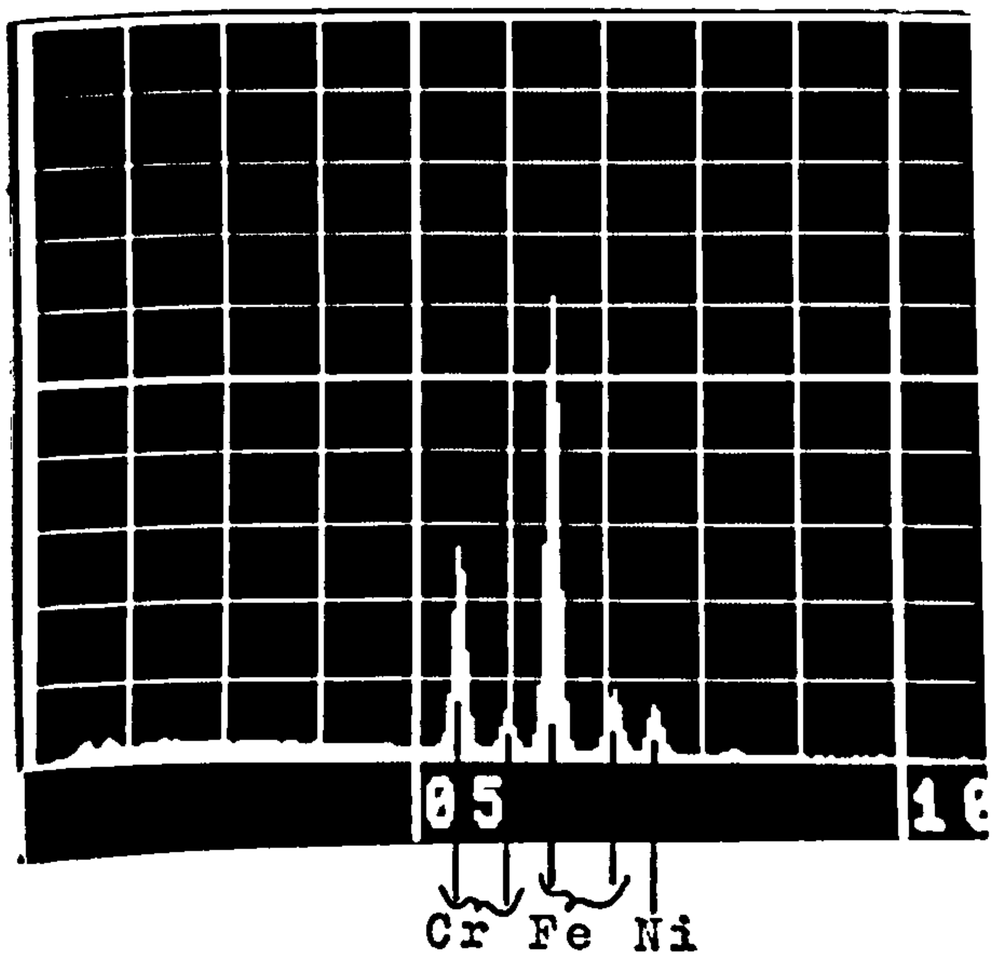

c) Untreated stool

20kv excitation

FIG.2.2. EDAX ANALYSIS OF COLOURED STAINLESS STEEL

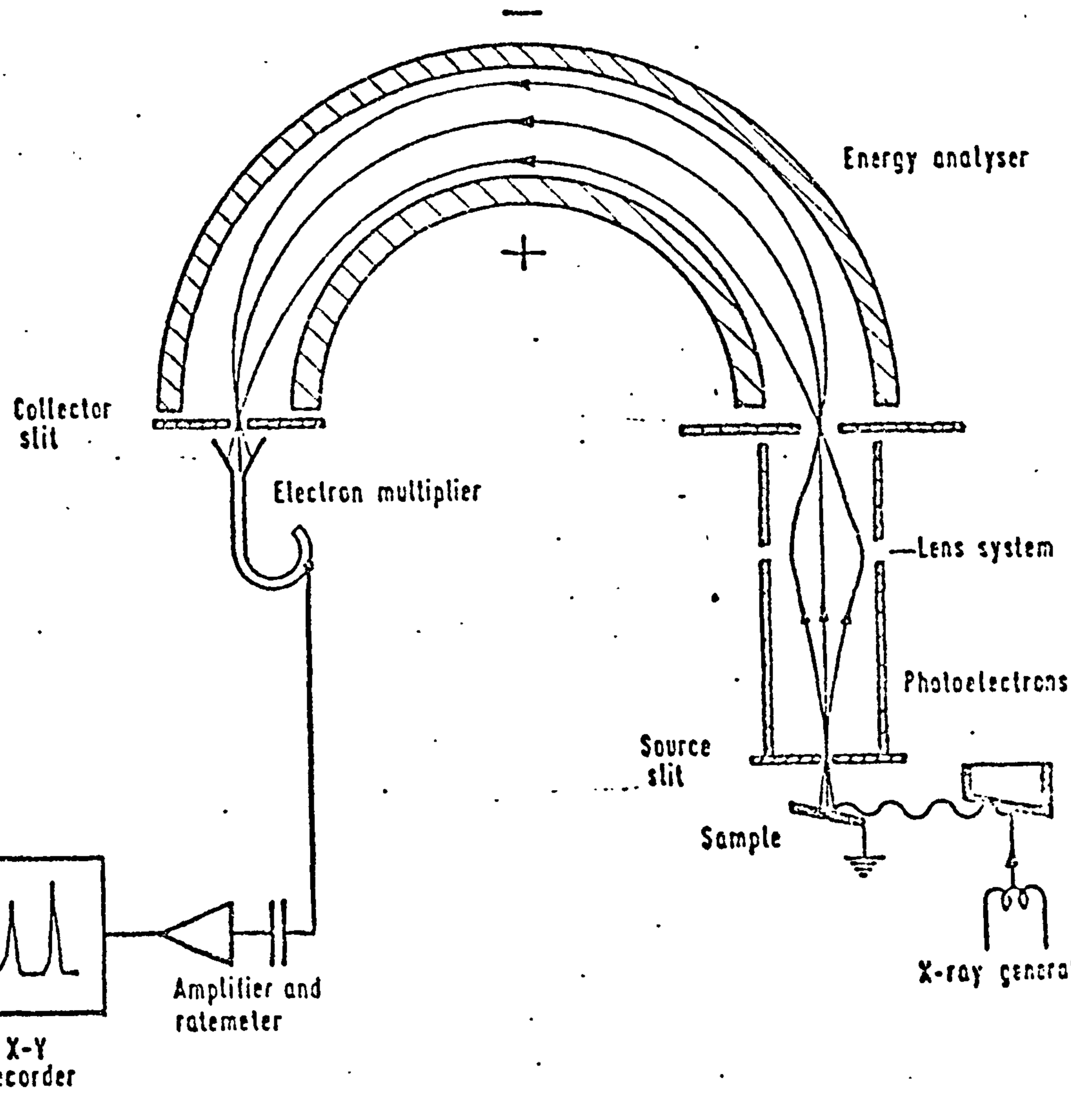

FIG.2.3 SCHEMATIC DIAGRAM OF THE
A.E.I. ES 200 A SPECTROMETER.

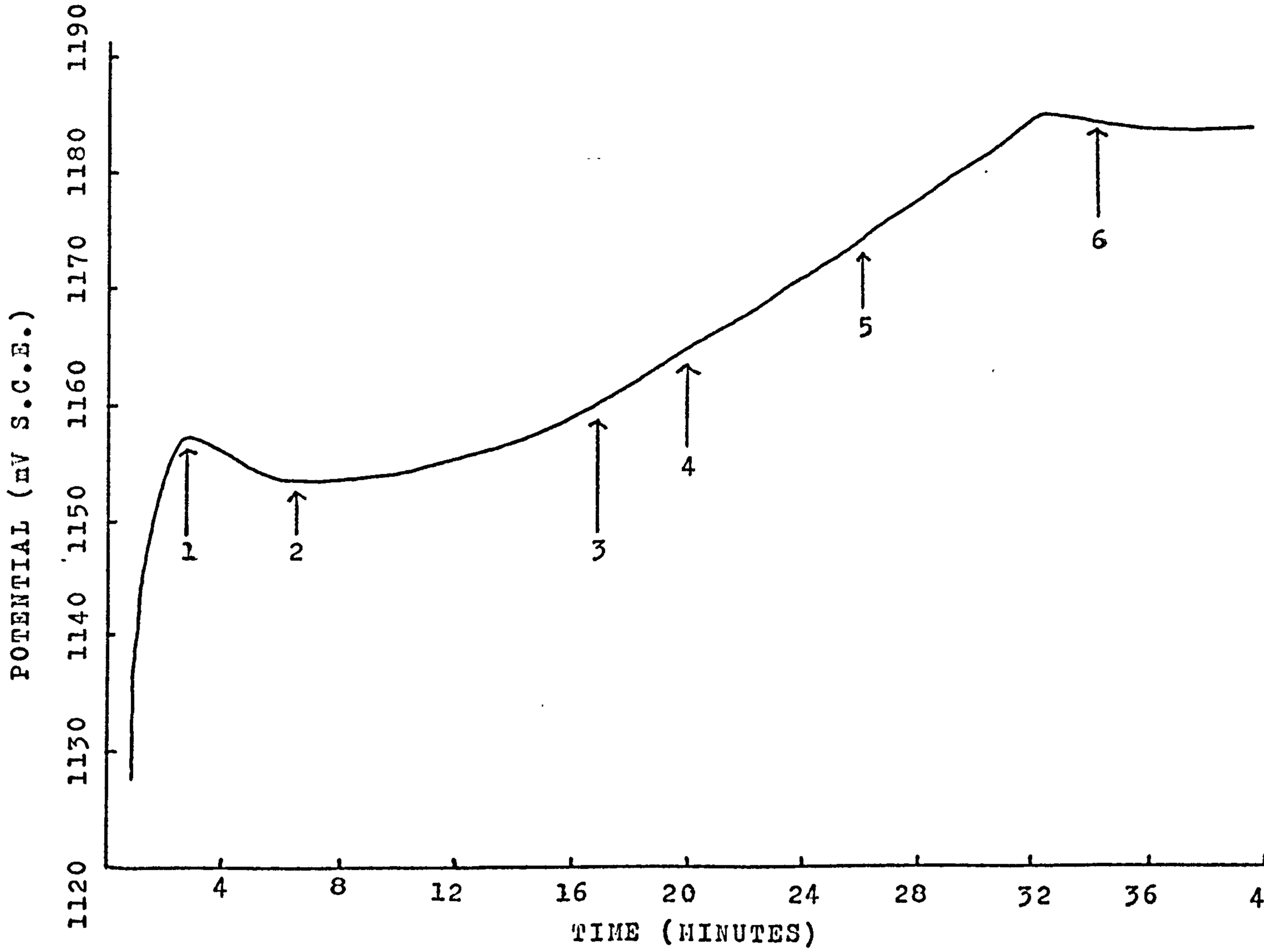

FIG.2.4. POTENTIAL TIME CURVE FOR STAINLESS STEEL SAMPLES USED FOR X.P.E.S.

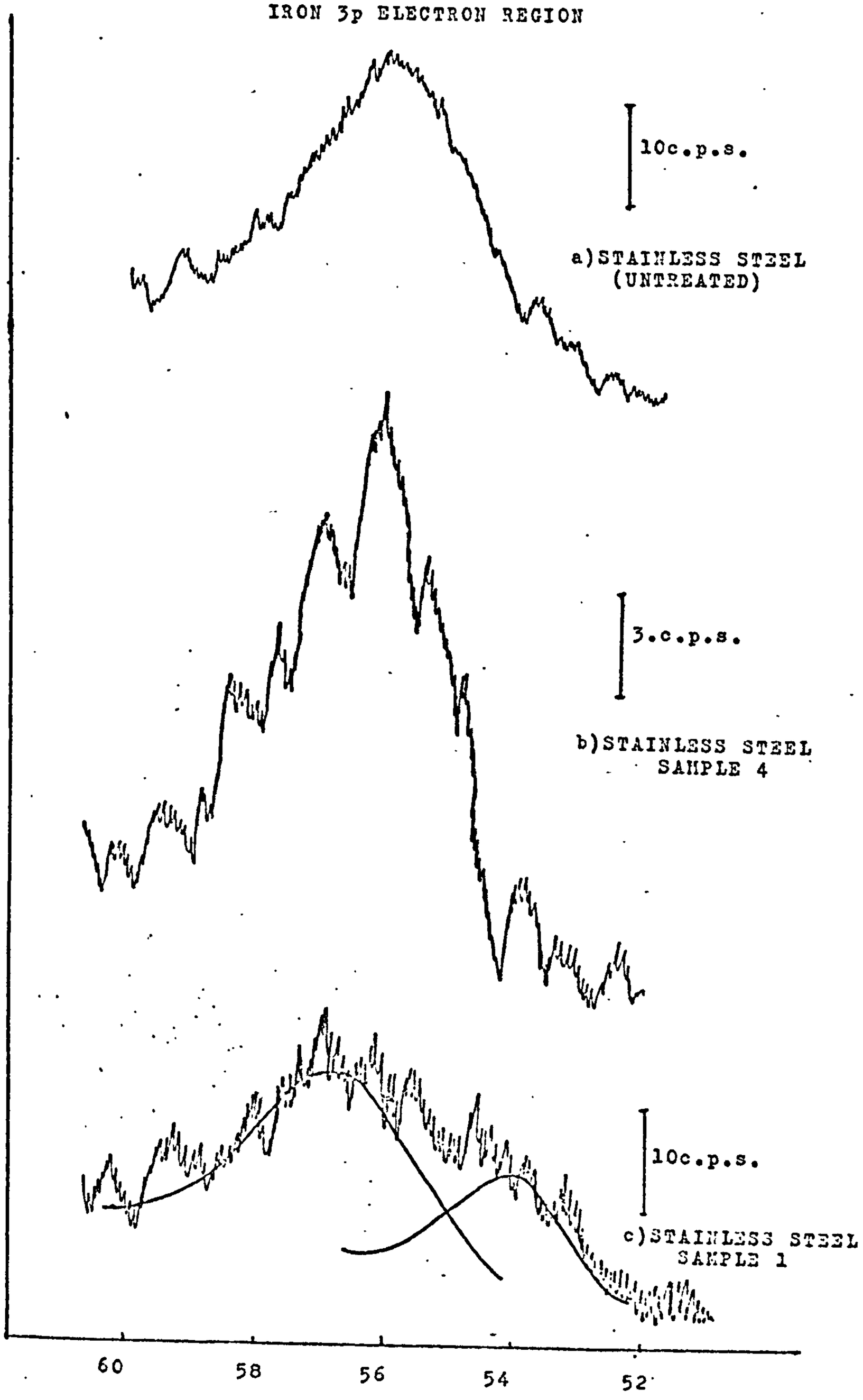

FIG.2.5 IRON 3p ELECTRON REGION

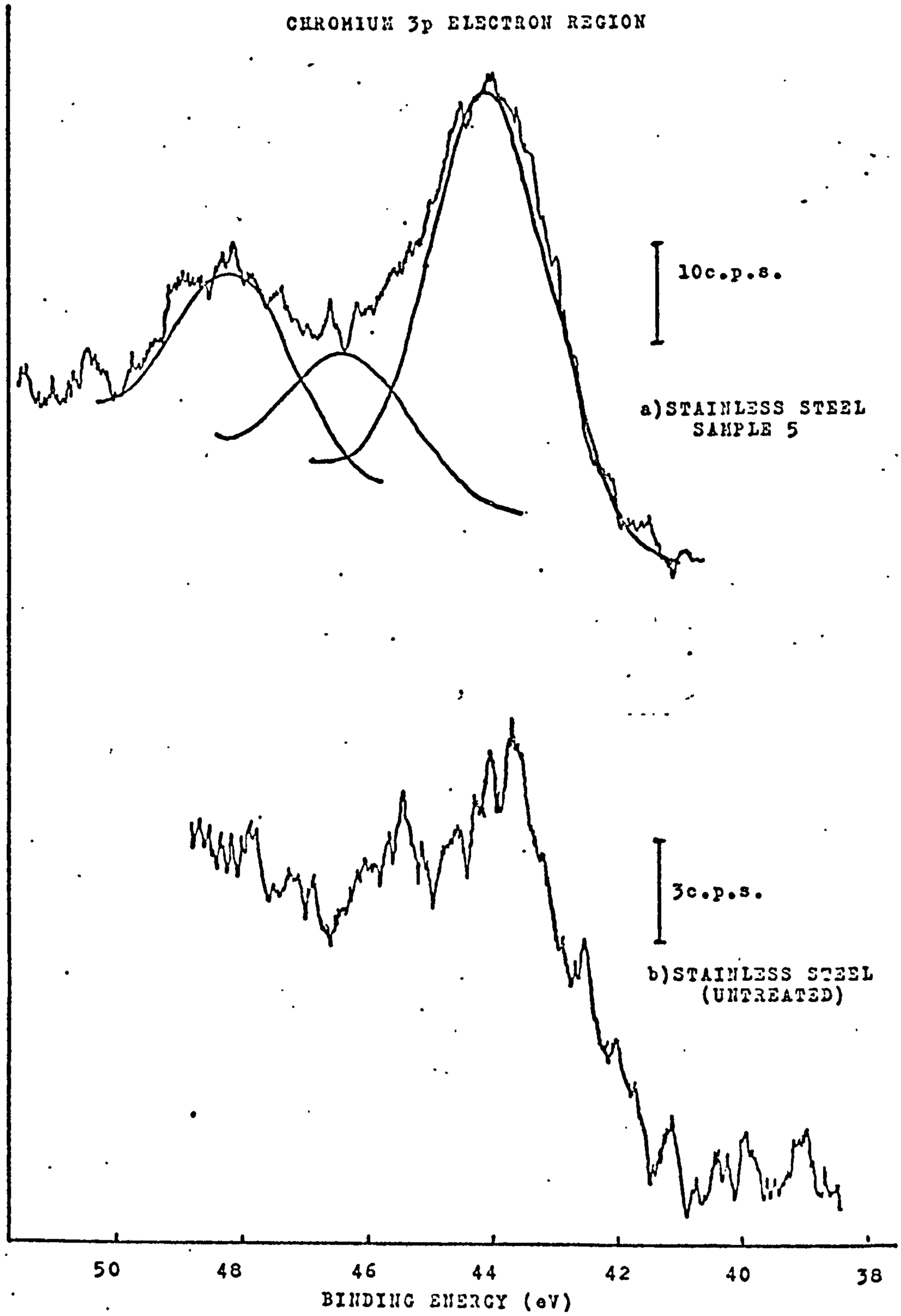

FIG.2.6 CHROMIUM 3p ELECTRON REGION

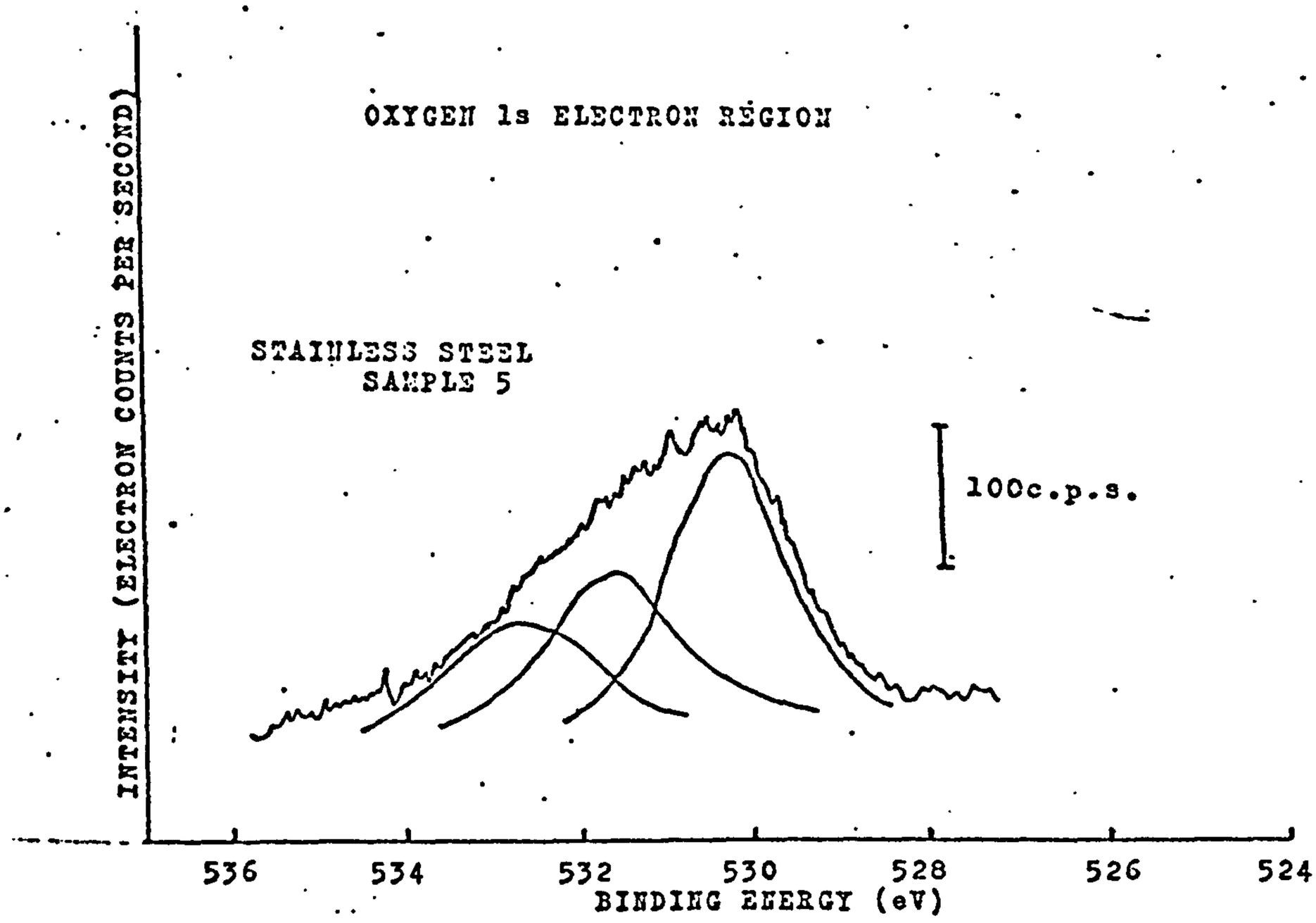

FIG.2.7 OXYGEN 1s ELECTRON REGION

FIG. 2.8. S.E.M. IMAGE OF STAINLESS STEEL SURFACE

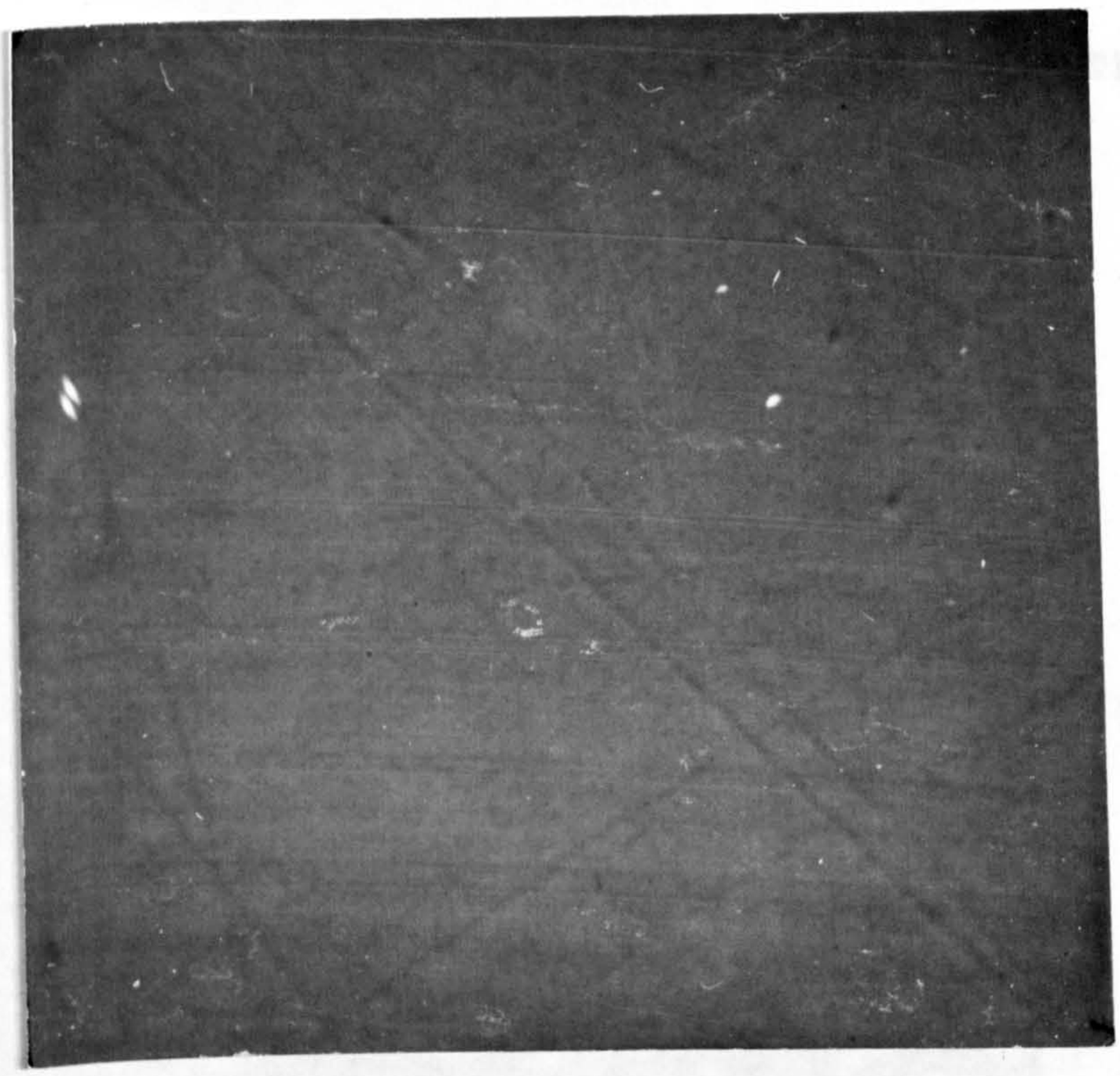

a) Coloured stainless steel (mag. 10,600)

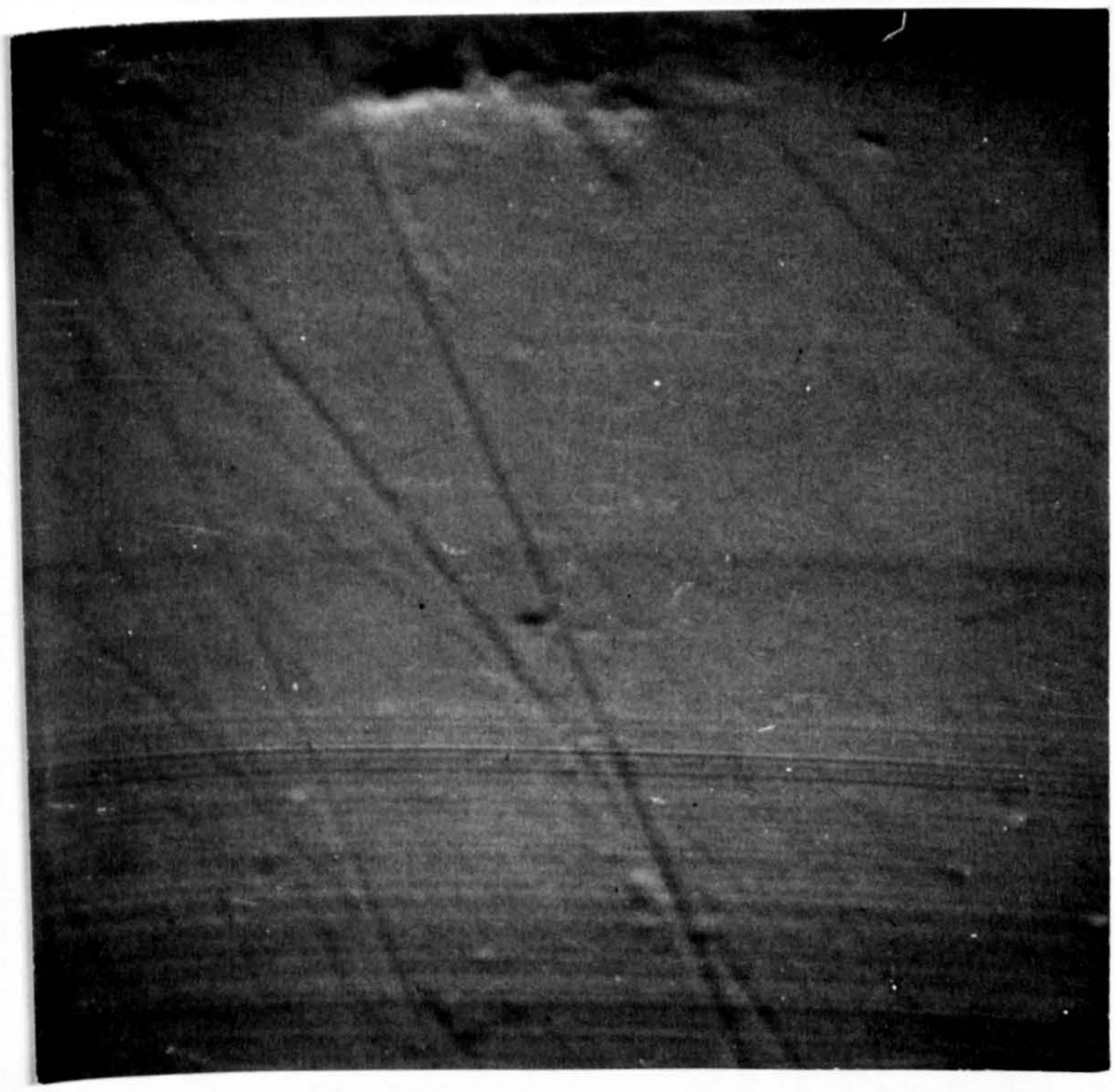

b) Untreated stainless steel (mag. 10,600)

FIG 2.9. S.E.M. IMAGE OF A SECTION THROUGH THE FILM ON THE SURFACE OF COLOURED STAINLESS STEEL.

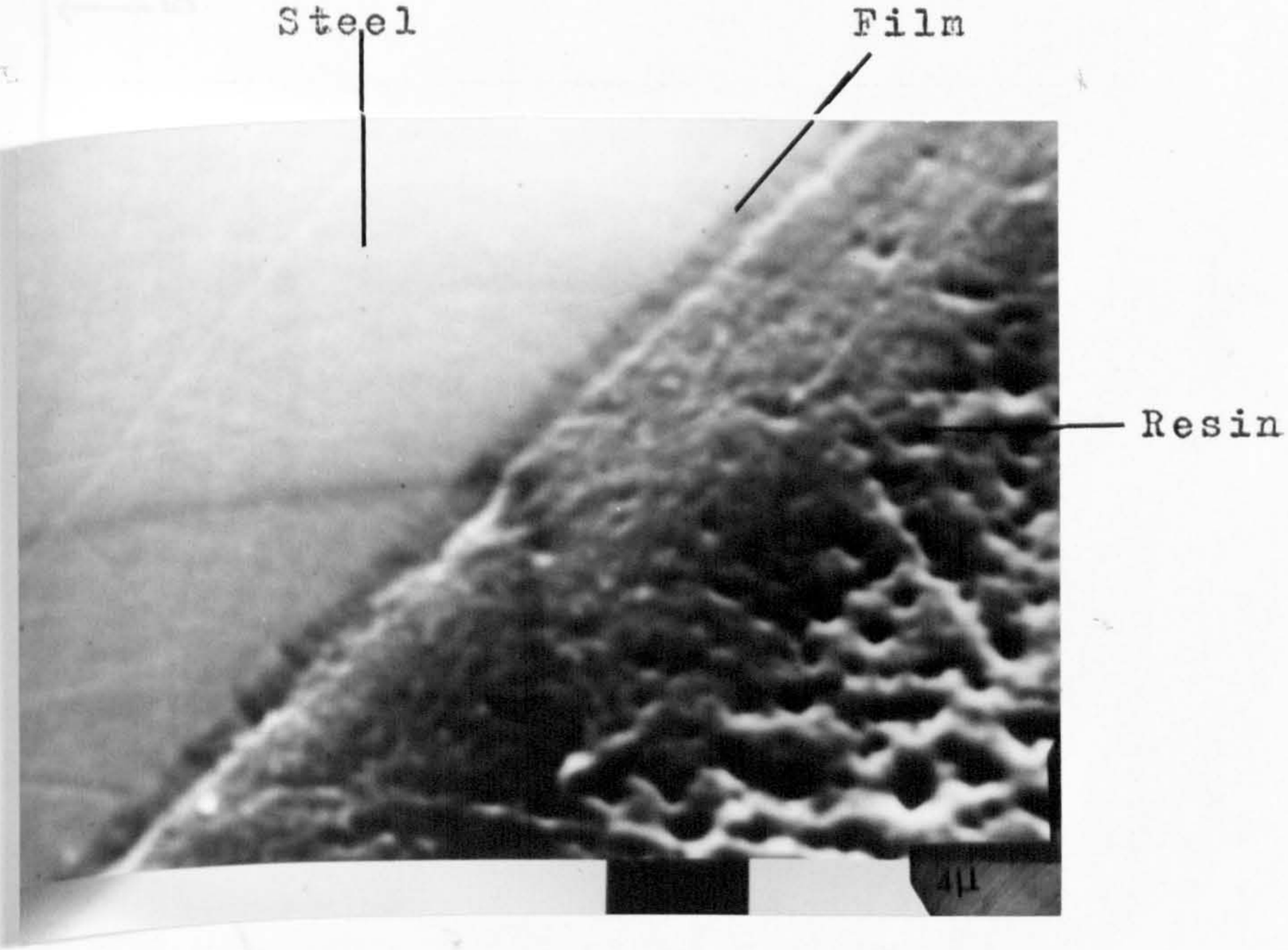

(Angle of section 30°)

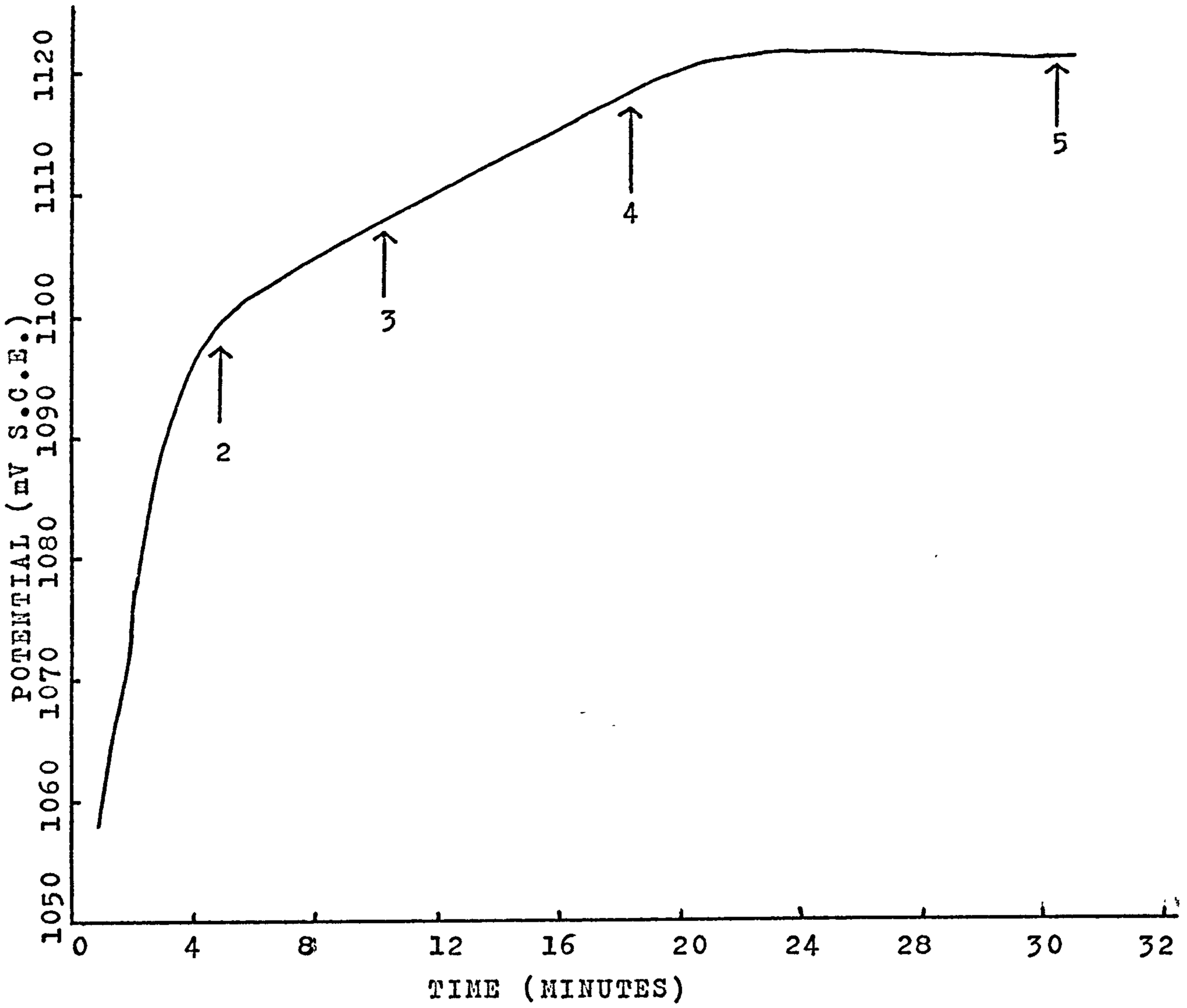

FIG. 2. 10 POTENTIAL TIME CURVE FOR NILOMAG SAMPLES USED FOR X.P.E.M.

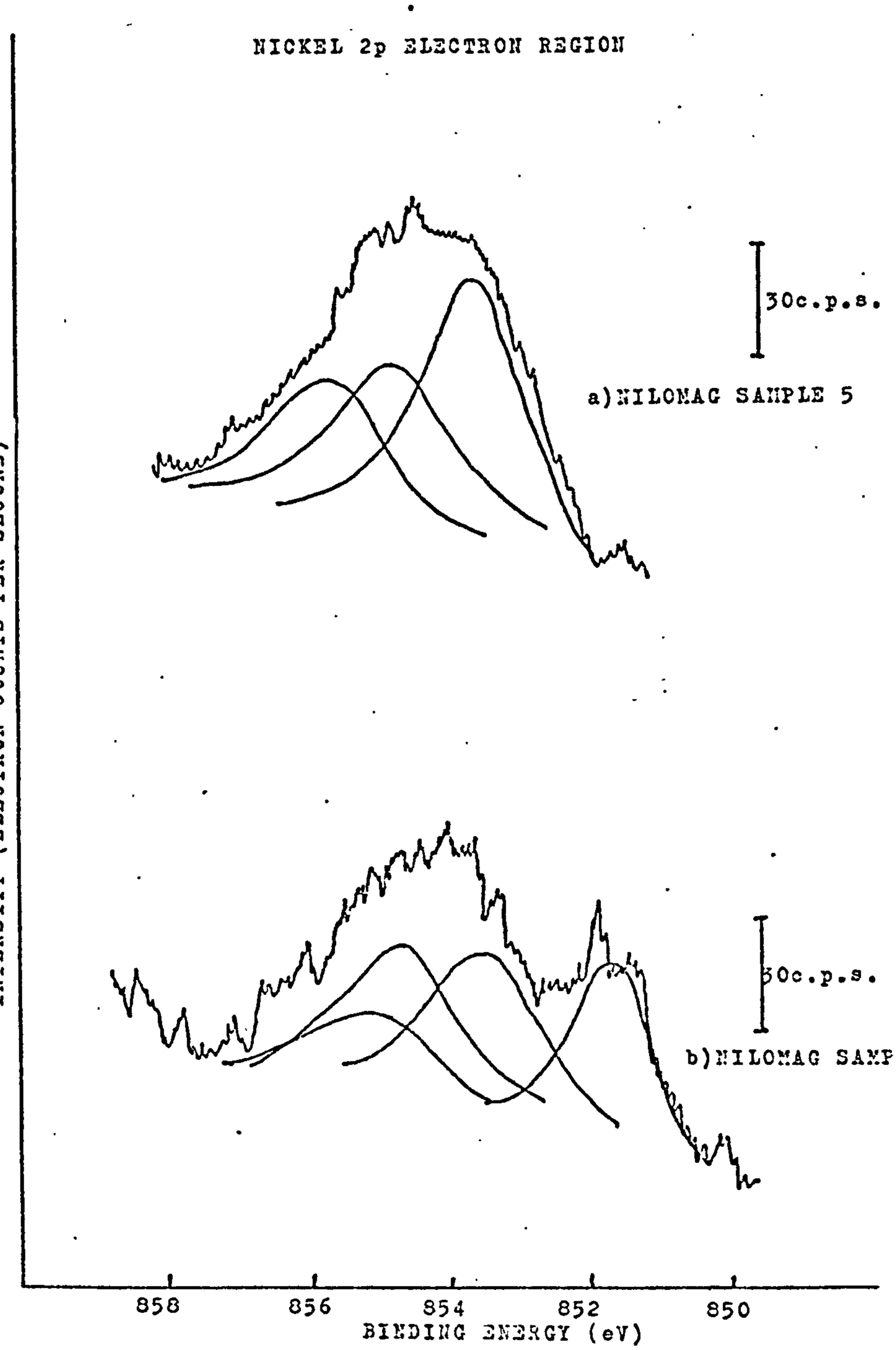

FIG.2.11 NICKEL 2p ELECTRON REGION

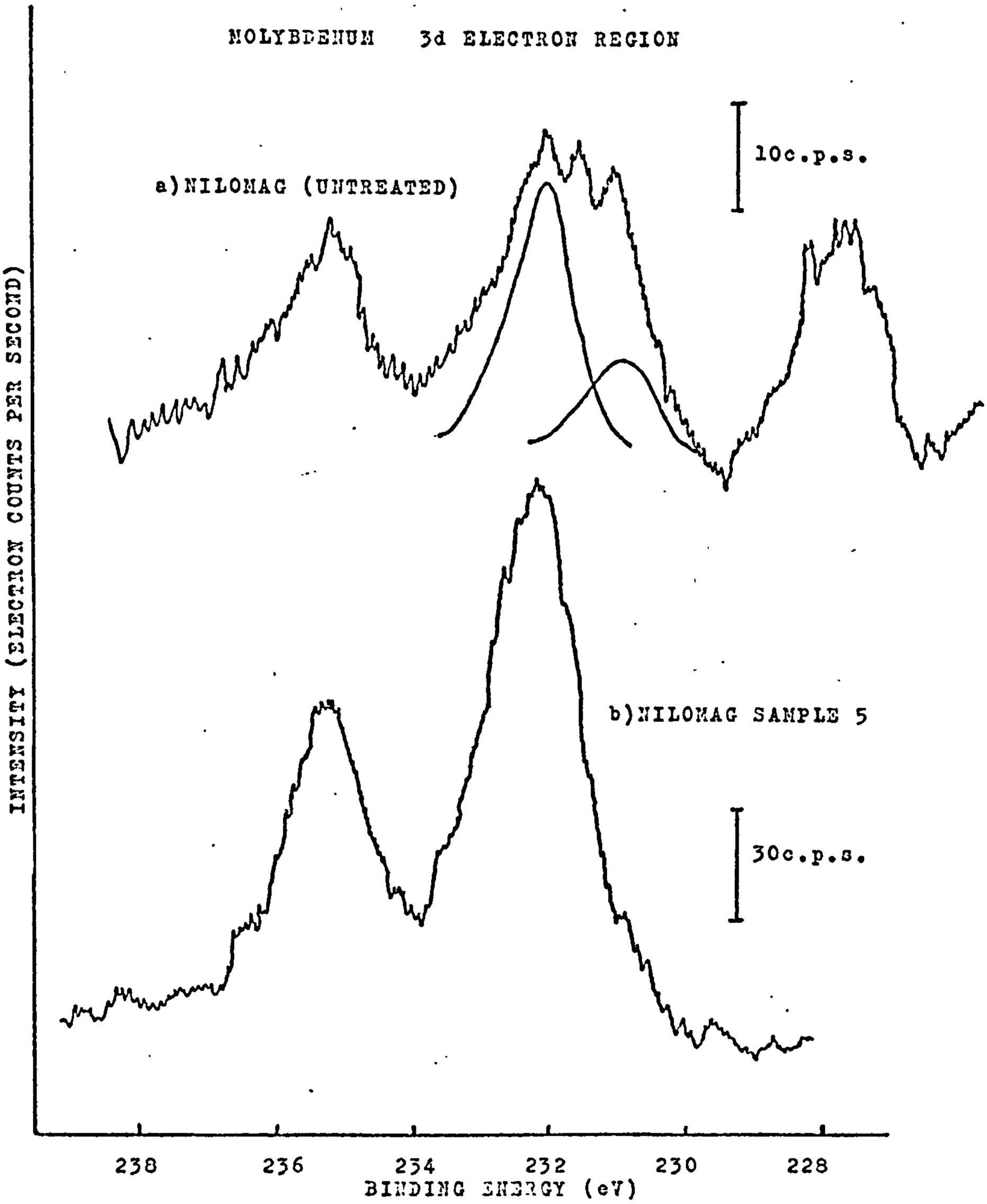

FIG.2.12 MOLYBDENUM 3d ELECTRON REGION

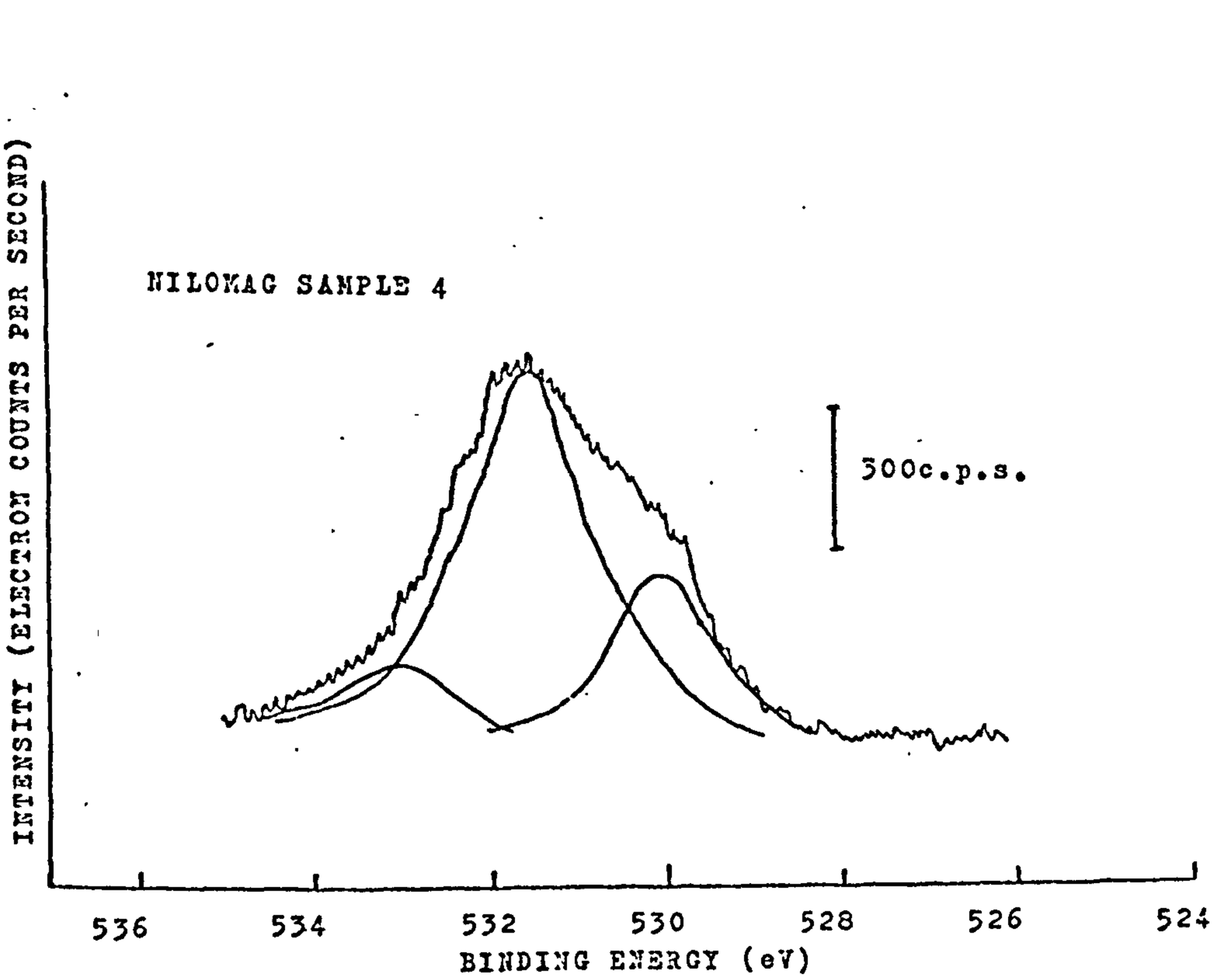

FIG. 2.13 OXYGEN 1s ELECTRON REGION

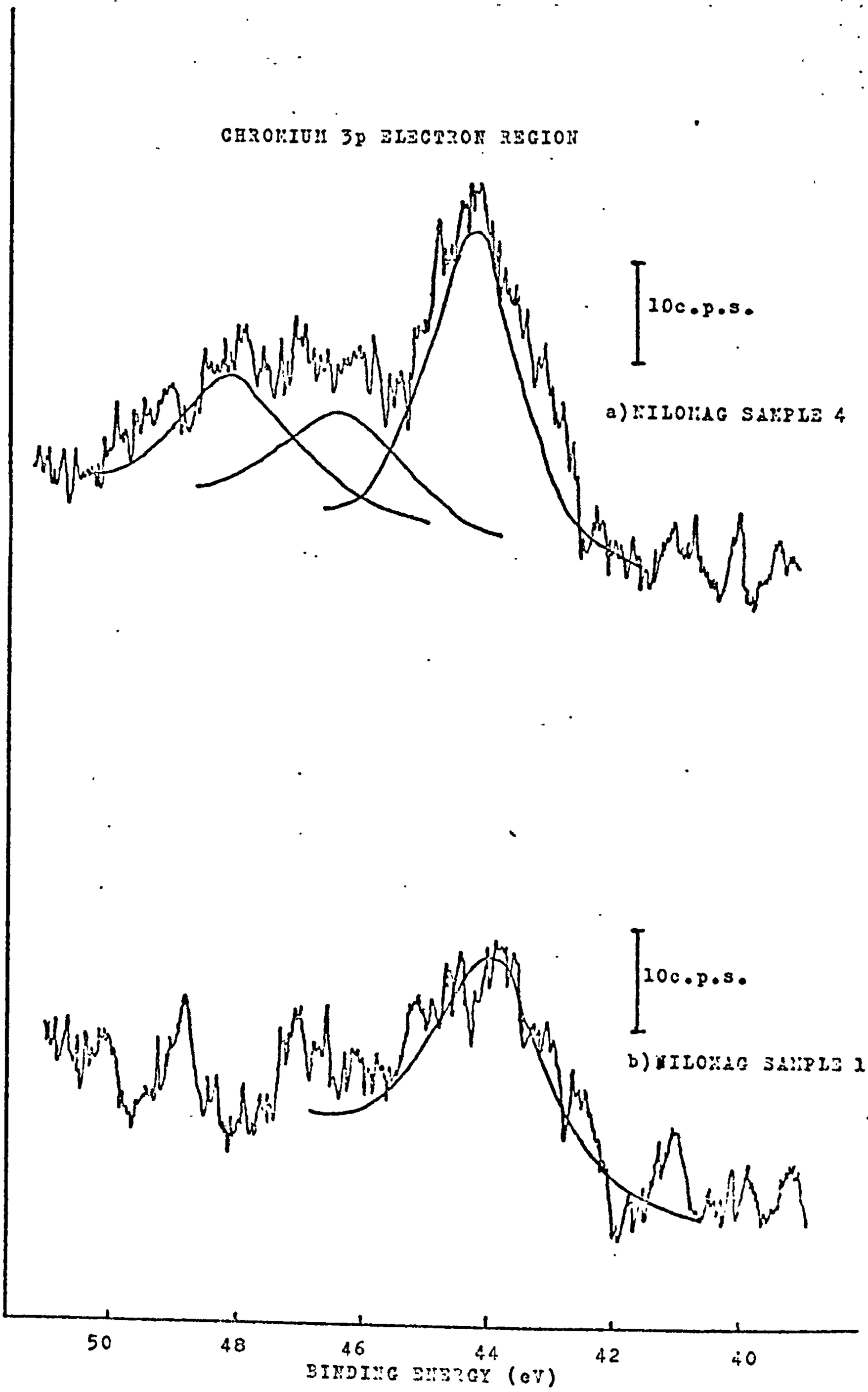

FIG.2.14 CHROMIUM 3p ELECTRON REGION

FIG2.15METHANOL PURIFICATION AND DELIVERY APPARATUS

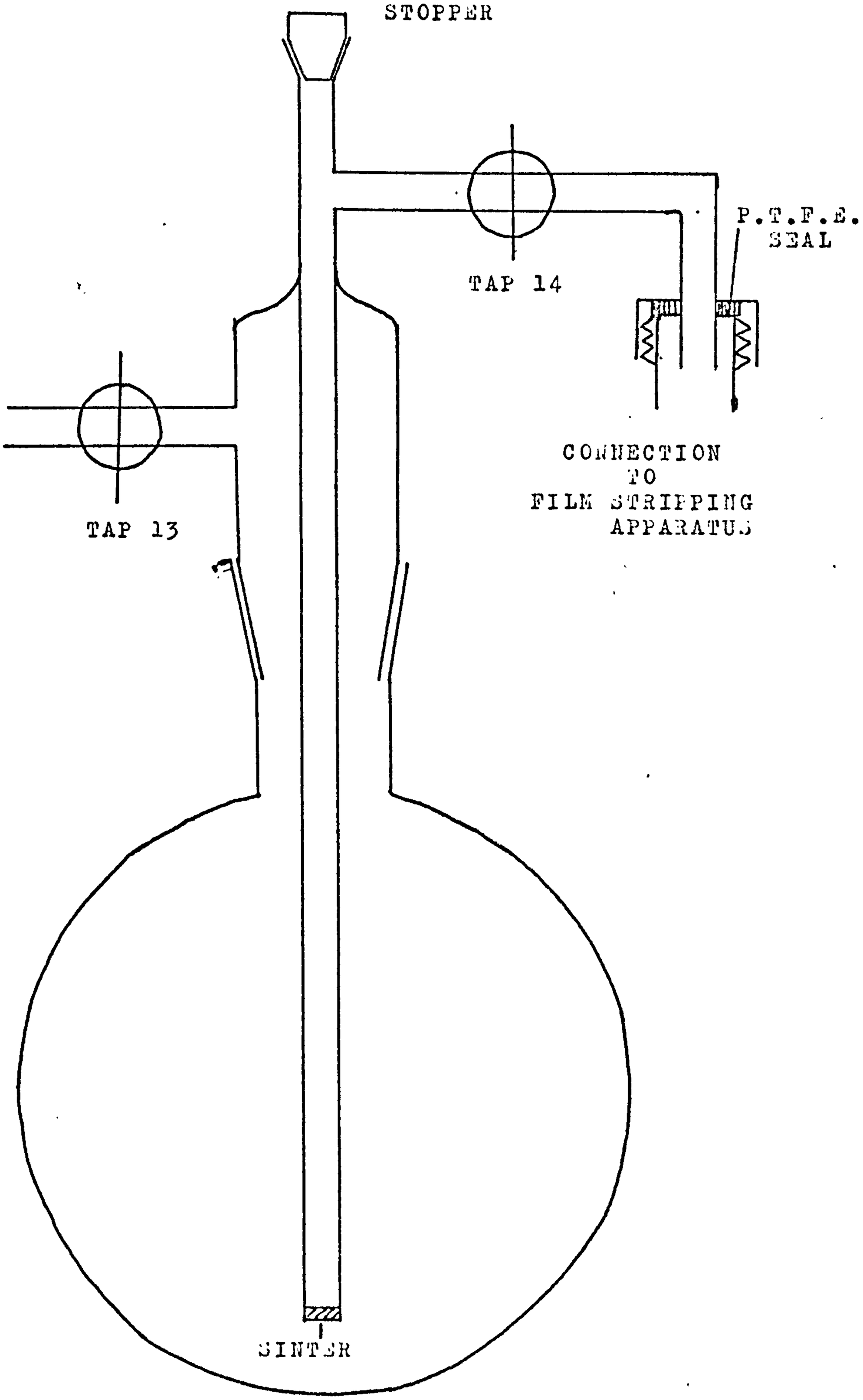

FIG.2.16 FILM STRIPPING CHAMBER

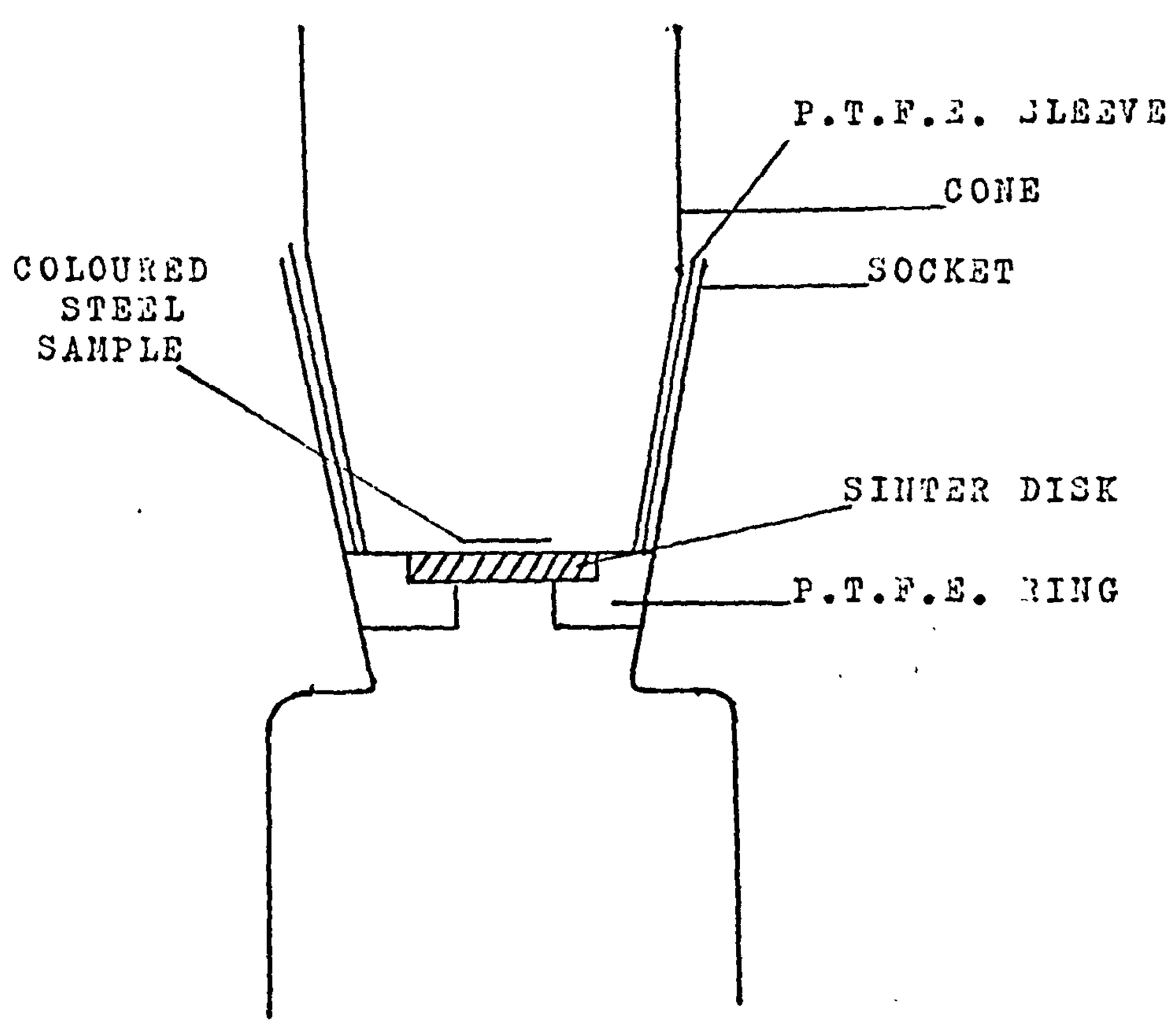

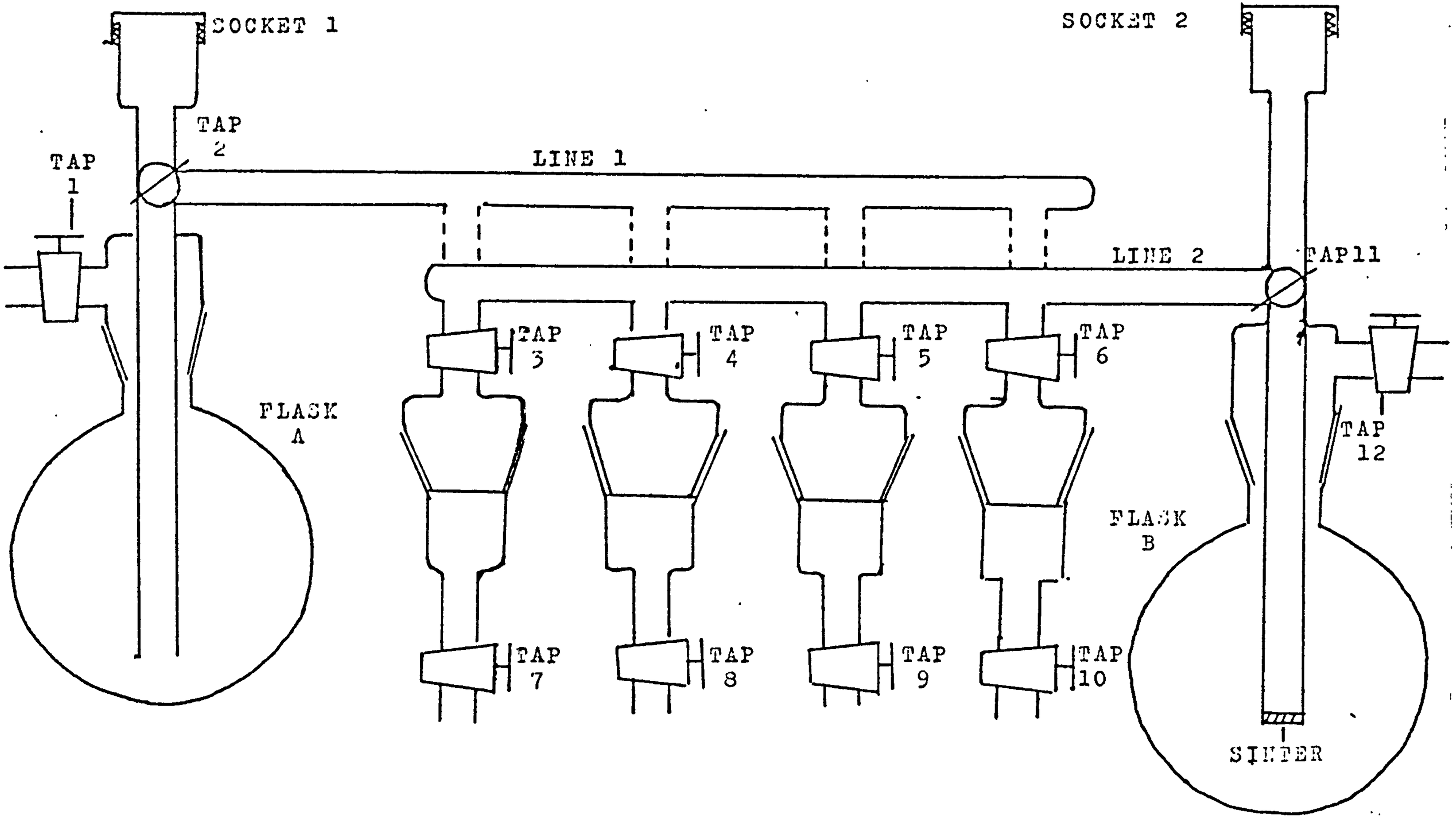

FIG.2.17 FILM STRIPPING APPARATUS

FIG. 2.18 EDAX ANALYSIS OF STRIPPED FILM MATERIAL

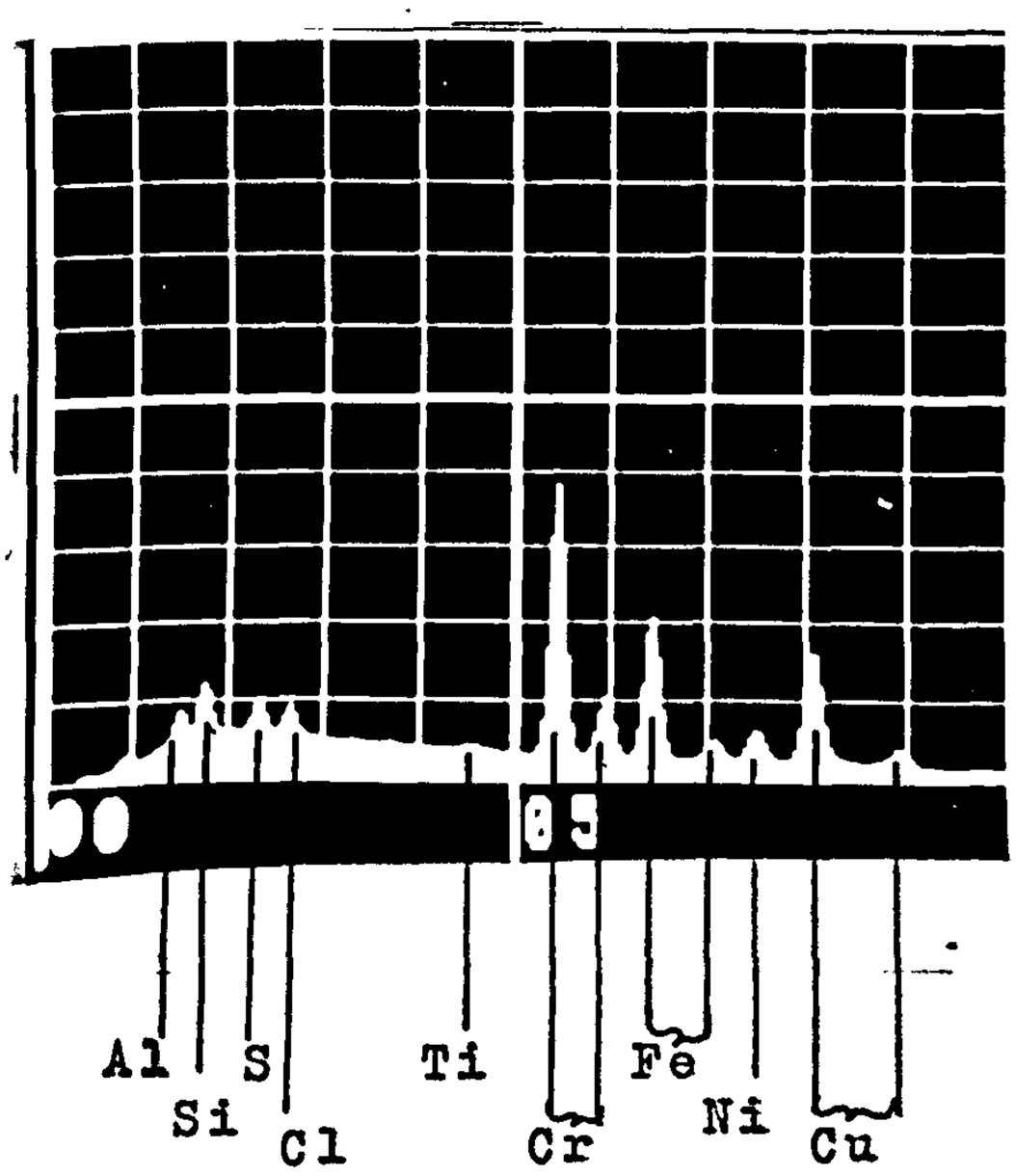

FIG 2.19 TRANSMISSION ELECTRON MICROGRAPHS

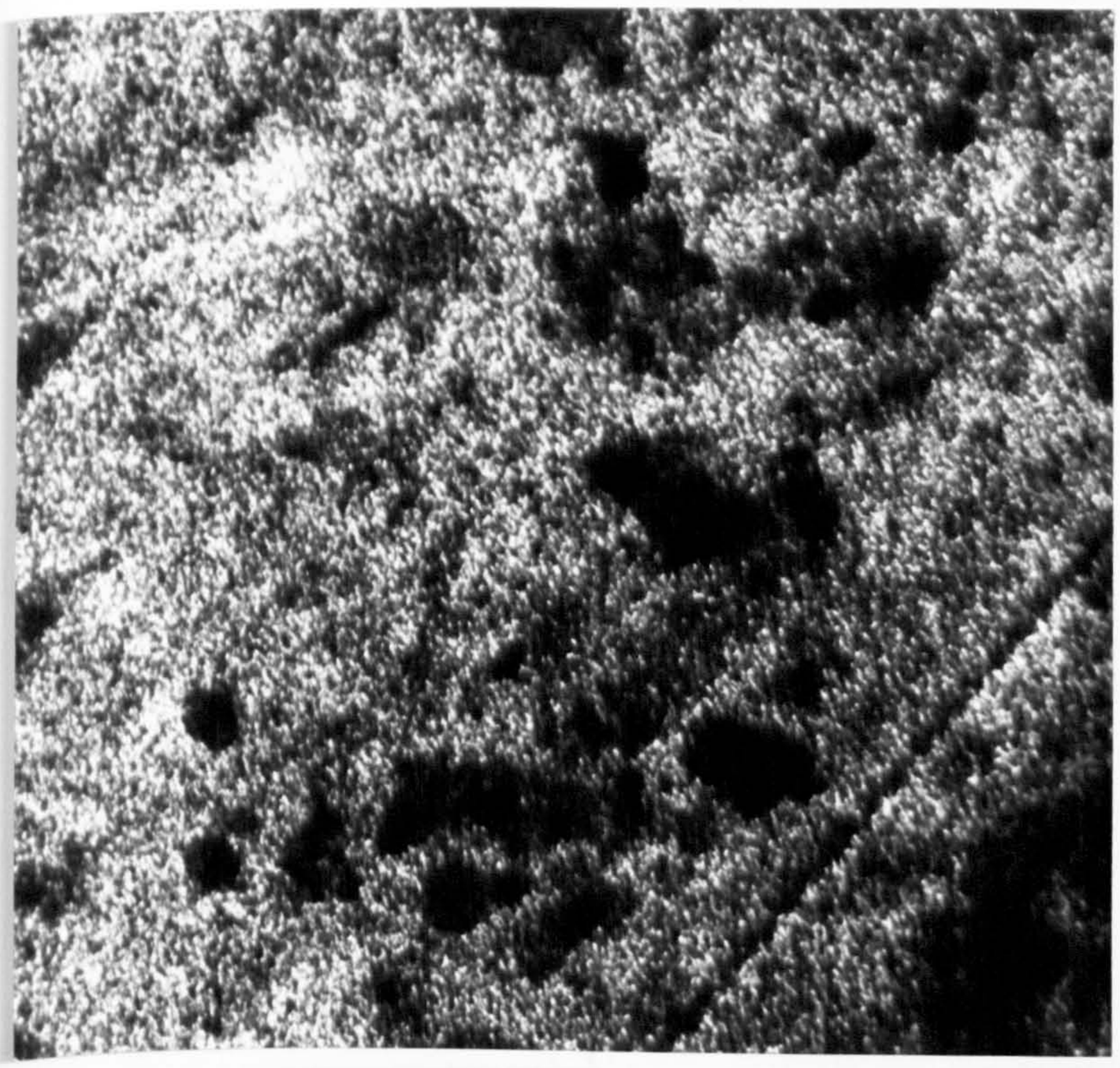

a) Stripped film (mag. 40,500)

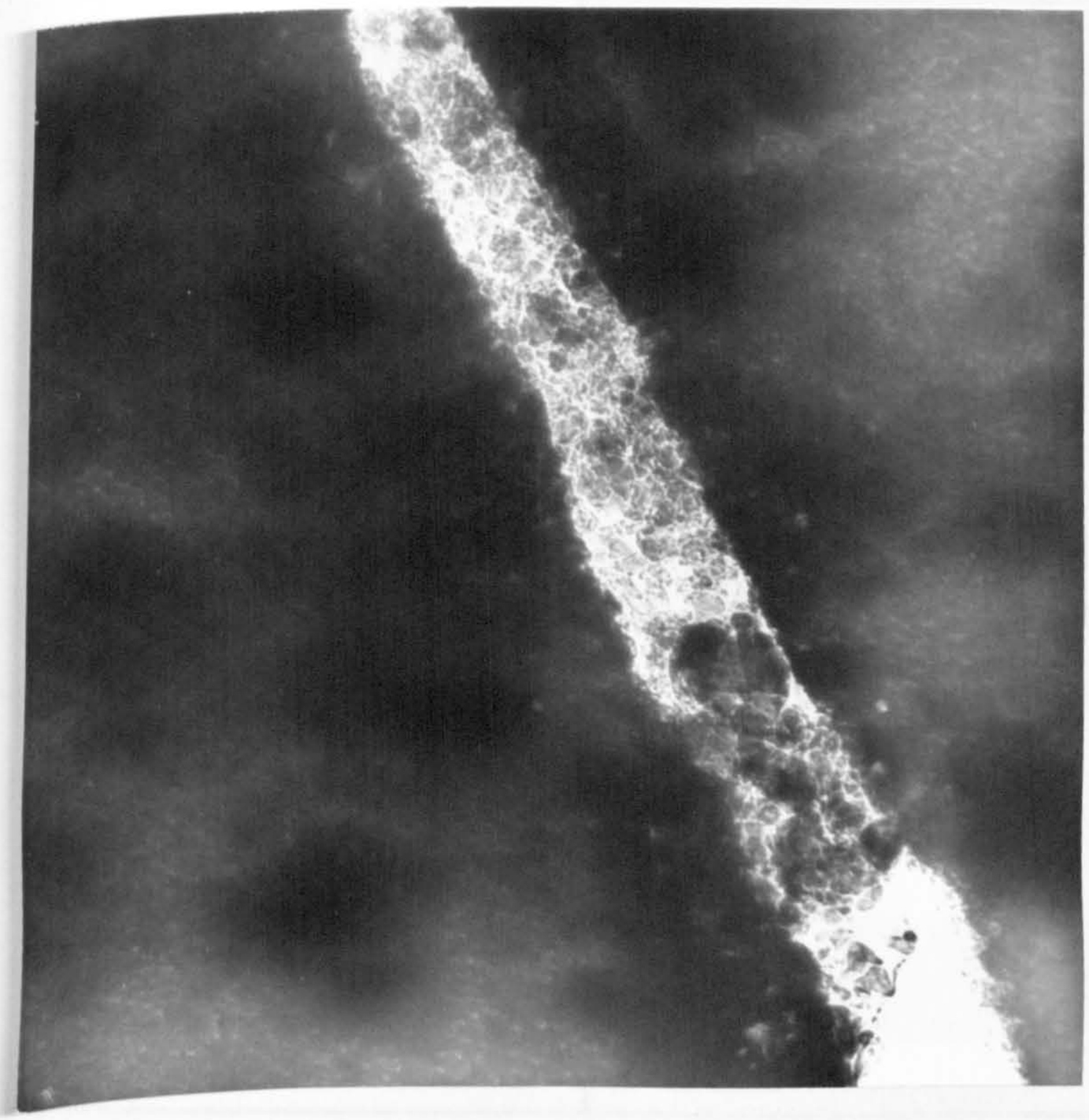

b) Stripped film (mag. 87,600)

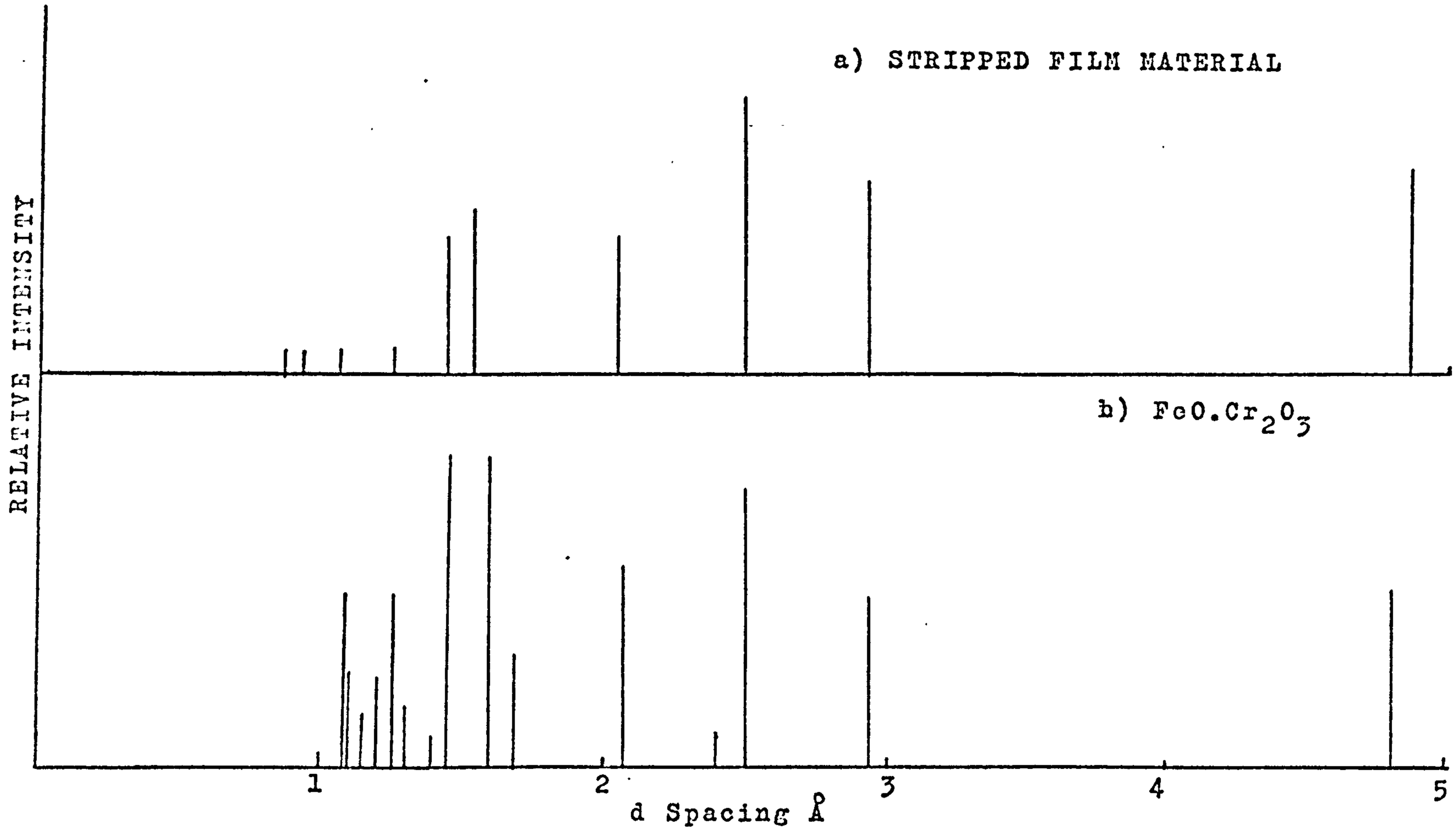

FIG.2.20 ELECTRON DIFFRACTION PATTERNS.

CHAPTER 3

THE RESISTANCE OF FILMS ON COLOURED STAINLESS STEEL

3.1. INTRODUCTION

This work was undertaken to determine the magnitude of the resistance of the film present on stainless steel and its variation with thickness of the film material. In the first part of the chapter the work carried out using D.C. methods to find a suitable ohmic contact to the film surface is described. In the second part of the chapter the use of A.C. techniques at fixed frequency, to establish that the resistance values obtained were not due to either short circuiting through the film material or surface conduction, is described. The correlation between resistance of the film and the film thickness is discussed in the subsequent chapter.

3.2. EXPERIMENTAL

3.2.1. CONTACTS

Preliminary measurements were made using a mercury contact to the film material and a crocodile clip contact to the stainless steel substrate. Initially glass tubes, attached to the surface of the film using Araldite, were used to contain the mercury (Fig. 3.1). A platinum wire was used to connect the mercury to the measuring apparatus. An easier method, which was less likely to affect the film surface, was to contain the mercury in a neoprene ring on the surface of the film (Fig. 3.1).

Subsequent measurements were made with evaporated nickel or vapour deposited carbon contacts. In these cases the surface of the specimen was masked by a glass plate with a circular hole in it during the deposition of

the contact. The nickel and carbon contacts were evaporated onto the surface using an Edwards 12E 6 coating unit operated at a pressure of 10^{-4} - 10^{-5} Torr. Contact was made to the deposited carbon or nickel layer using mercury and a neoprene ring as described above.

3.2.2. D.C. MEASUREMENTS

For convenience, the stainless steel/film/contact system is called the film in this section.

The resistance was originally measured using a potentiometer to supply the potential difference across the film and a resistor in series with it. The potential difference across the film was determined by using a digital voltmeter and the current flowing through the film measured as the voltage drop across the resistor, again using a digital voltmeter.

The variation in current as the potential difference across the film increased and then decreased linearly, was determined using a saw-tooth voltage generator in conjunction with a potentiostat. (Fig. 3.2). The film was connected between the working and reference electrode terminals of the potentiostat and a resistor which was large compared with the film resistance was connected between the reference and secondary electrode terminals of the potentiostat. This resistor was necessary to provide a satisfactory feedback ratio to the potentiostat. The current-voltage curves were recorded on a Bryans 2400 XY recorder by feeding the output from the voltage generator into the X amplifier of the recorder, and the voltage drop across a current measuring resistor, in series with the film, into the Y axis of the recorder.

Current-time curves were obtained by holding the potential at +25 mV or -25 mV using the potentiostat, in a similar manner to that described above, and recording the current, as the potential drop across a

suitable resistor, on a Y-t recorder.

3.2.3. A.C. MEASUREMENTS

A.C. measurements of the film resistance and capacitance at a fixed frequency of 1592 Hz were made using a Wayne Kerr B221 Mark III Universal Bridge and a low impedance adaptor (Q221 Mark III).

3.3. D.C. MEASUREMENTS

3.3.1. MERCURY CONTACTS

Seven pieces of EN 58E stainless steel (specimen Nos. 1-7) were each coloured blue. Glass tubes were attached to specimens 1-3, using Araldite. No special precautions were taken in handling the films. Five glass tubes were attached to specimen 4 with Araldite. This specimen was kept in a desiccator over silica gel. With specimens 5, 6 and 7 a neoprene ring used to contain the mercury contact. The results obtained from these samples are summarized in Table 3.1 and Figs. 3.3 and 3.4.

Specimens 1, 4, 5, 6 and 7 had low resistances and gave linear current-voltage curves over a 50 mV potential sweep. Steady state measurements also gave linear current-voltage curves in agreement with the sweep data. The variation in resistance values of specimen 4, to which five tubes were attached in different places on the film, is probably due in part to resistive path length variations through the substrate steel.

Specimens 2 and 3 gave exponential current-voltage curves (Fig. 3.4) indicative of a high resistance. Measurements on each particular specimen were not reproducible and attempts to increase the reproducibility, by leaching the specimens in water followed by desiccation, were unsuccessful. Some reduction in the resistance was observed after washing the specimen in chloroform.

The possibility that the low resistance behaviour was due to mechanical damage to the surface, caused by attaching the glass tube, is discounted by the fact that specimens 5, 6 and 7 which were measured with the mercury contact contained in a neoprene ring, also showed low resistance behaviour. It appeared more likely therefore that the high resistance behaviour was caused by contamination of the surface by grease.

When mercury contacts were made to thicker films the resistance varied with time (Figs. 3.5 and 3.6). To avoid this unsatisfactory behaviour, alternative contacts were investigated.

3.3.2. CARBON CONTACT

The current-potential curve obtained with a carbon contact did not vary with time but was exponential in form (Fig. 3.7). The current at constant applied voltage was also independent of time and almost independent of the polarity of the applied voltage, being slightly larger when carbon was positive with respect to the steel. The non-ohmic behaviour of the carbon contact made it unsuitable for measuring the resistance of the film material.

3.3.3. NICKEL CONTACT

With a nickel contact on a gold coloured film (specimen 11) the current, at constant potential, was independent of time and polarity of the applied potential. This behaviour was in contrast to that of the mercury contact to the same gold film which was markedly time dependent (Section 3.3.1.). Similar time independent behaviour was obtained with another gold coloured film (specimen 14). With both these films current voltage curves were linear and reproducible (Fig. 3.8).

When aluminium was evaporated on top of the nickel contact in an

attempt to reproduce measurements made by previous workers[67], the behaviour of the specimen 7' was similar to that obtained in the absence of the aluminium layer.

The results of these experiments are collected in Table 3.2.

3.3.4. DISCUSSION

The cause of the time-dependent behaviour, observed with mercury contacts, is not clear but such contacts are clearly unsatisfactory. The high, non-ohmic resistance measured with a carbon contact suggests that the film is a semi-conductor.

Nickel contacts to the coloured film appeared to be the most satisfactory, giving linear current-voltage curves and thus acting as ohmic contacts. The resistance values obtained, however, were much lower (c.a. 500 x) than those reported previously. This gave rise to fears that the film might have suffered mechanical damage which would allow a short circuit through the film material. Moreover it was not certain that the conduction path was actually through the film to the substrate; conduction could have occurred across the surface of the film.

In order to clarify this situation an alternating current method of measuring the film resistance and capacitance was used. If the nickel contact system possessed appreciable capacitance then the possibility of a short circuit through the film to the substrate steel would be ruled out. Surface conduction could be tested for and eliminated if necessary by the use of a guard ring on the surface of the film. Measurements of the resistance and capacitance of the film were initially made at fixed frequency using a Wayne Kerr Bridge. These are described in the next section.

3.4. A.C. MEASUREMENTS

3.4.1. FILM PENETRATION

The resistance and capacitance of a number of films with nickel contacts were measured at 1592 Hz. The D.C. resistances of the films were measured using a potentiostat as described previously.

In addition to specimen 7' (blue), specimen 11 (gold) used in previous measurements, a red film (specimen 16) and a "hardened" blue film (specimen 9) were also studied. The "hardened" film was prepared by cathodic polarisation of the blue coloured steel at a current density of 1 - 2 mA cm^{-2} for five minutes in a solution containing 250g litre CrO_3 and 2.5g litre H_3PO_4 at room temperature. This procedure developed by International Nickel Ltd.[68] results in the deposition of chromium oxide on the film surface thus blocking any imperfections in the film material and hence gives the film a greater resistance to mechanical damage. Evaporated nickel contacts were used for all the films except specimen 7' which had aluminium evaporated on top of the nickel.

The results of these experiments, expressed as the resistance and capacitance for a parallel combination, are reported in Table 3.3

3.4.2. SURFACE CONDUCTION

A coloured specimen had a concentric ring of nickel (20 mm I.D. and 30 mm O.D.) evaporated around a central nickel coating of 11 mm diameter. With suitable neoprene masks, mercury contacts were made to both the central nickel film and the guard ring. The conductivity was then measured using the Wayne Kerr bridge in both the two and three terminal configurations. In the latter arrangement only the resistance between the connections made to the central nickel film and the steel plate is

measured. No difference was observed between the two measurements, indicating that surface conduction was not important. The resistance between the central film and the steel substrate was 2.52 ohm.

In a second experiment the measuring leads from the Wayne-Kerr bridge were connected to the central mercury pool and the pool in contact with the guard ring, the third terminal being connected to the stainless steel substrate. The resistance between the central and outer nickel contacts was 667 Ω. The surface conductivity of the film was calculated from the value and the dimensions of the assembly in the following manner.

If the resistance of the film = ρ ohm per square then the resistance of an annulus of material of thickness dr is,

$$\text{resistance} = 2\pi\rho r\, dr$$

$$\therefore \text{ total resistance between disc and ring} = \int_{r_1}^{r_2} 2\pi\rho r\, dr$$

$$= \left[\pi\rho r^2\right]_{r_1}^{r_2}$$

Substituting the measured values in this equation gives a value of 304 ohm per square for the conductivity.

3.4.3. DISCUSSION

All the specimens exhibited appreciable capacitance.

Since deliberately scratching the specimen surface caused the capacitance to fall to zero it must be concluded that the evaporated nickel does not make contact with the substrate steel. Possible supporting evidence for this conclusion is provided by the measurements with the "hardened" film. The resistance of this film was only about five times that of the unhardened film. This change could have resulted from a change

in the electrical properties of the film material resulting from cathodic polarisation.

TABLE 3.1

SAMPLE (blue films)	RESISTANCE ohm
1	0.10
4	0.7 - 0.24[1]
5	0.08
6	0.08
7	0.12

[1] Represents variation in resistance over the five tubes attached.

TABLE 3.2

SAMPLE No.	Colour	CONTACT	CURRENT TIME CURVE	R/ohm Initial	Final	CURRENT POTENTIAL CURVE	R/ohm Initial	Final
8	gold	Hg	-	-	-	resistance increasing with time	0.5	10
11	gold	Hg	time dependent resistance increasing with time	0.12	12.5	resistance increasing with time	0.4	0.7
11	gold	Ni	time independent	2.5	-	-	-	-
7'	blue	Ni + Al	time independent	0.73	-	linear	0.7	-
14	gold	Ni	time independent	-	-	linear	2.4	-
14	gold	C	time independent slight polarity dependence	10^4	-	linear over 50 mV non-linear over 500 mV	16×10^3	-

TABLE 3.3

SAMPLE	COLOUR	VAPOUR DEPOSIT	Rp ohm	Cp F	Rdc ohm
11	gold	Ni	2.46	0.165	2.5
7'	blue	Ni + Al	0.768	0.679	0.89
9	hardened blue	Ni	3.57	2.04	3.33
16	red	Ni	5.74	1.5	not measured

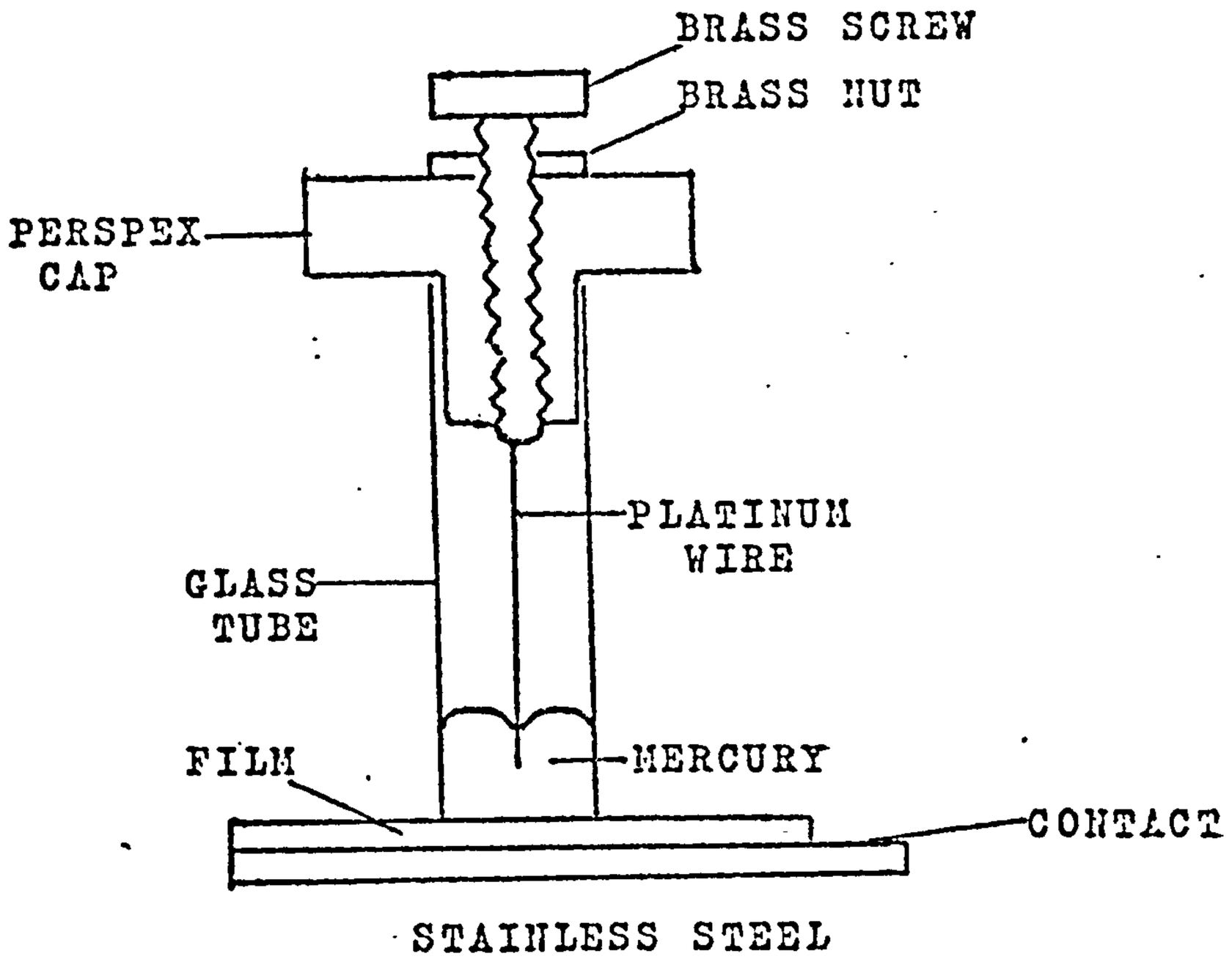

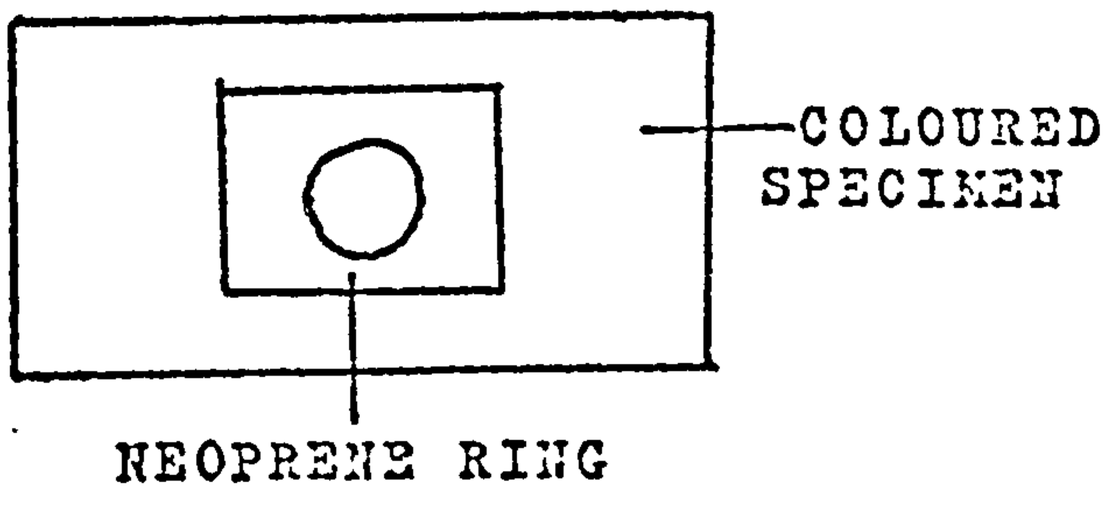

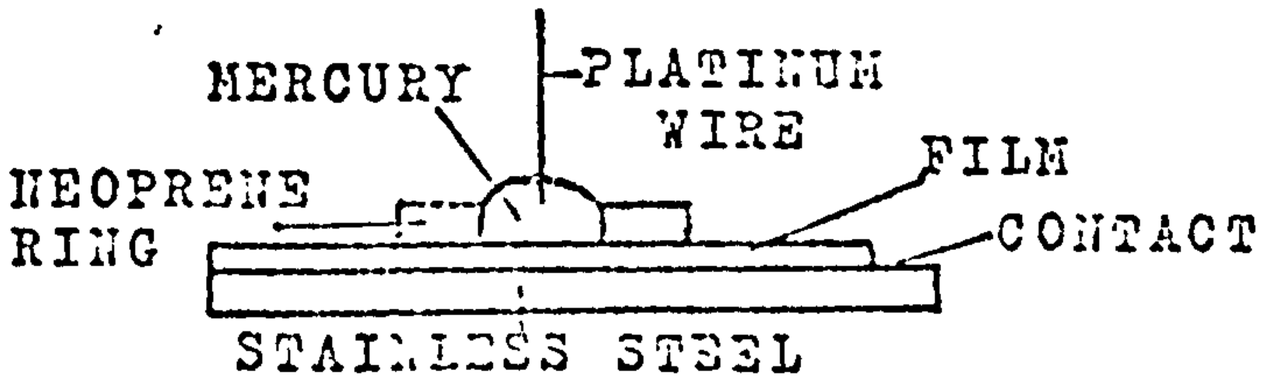

FIG. 3.1 METHOD OF MAKING CONTACT TO THE FILM

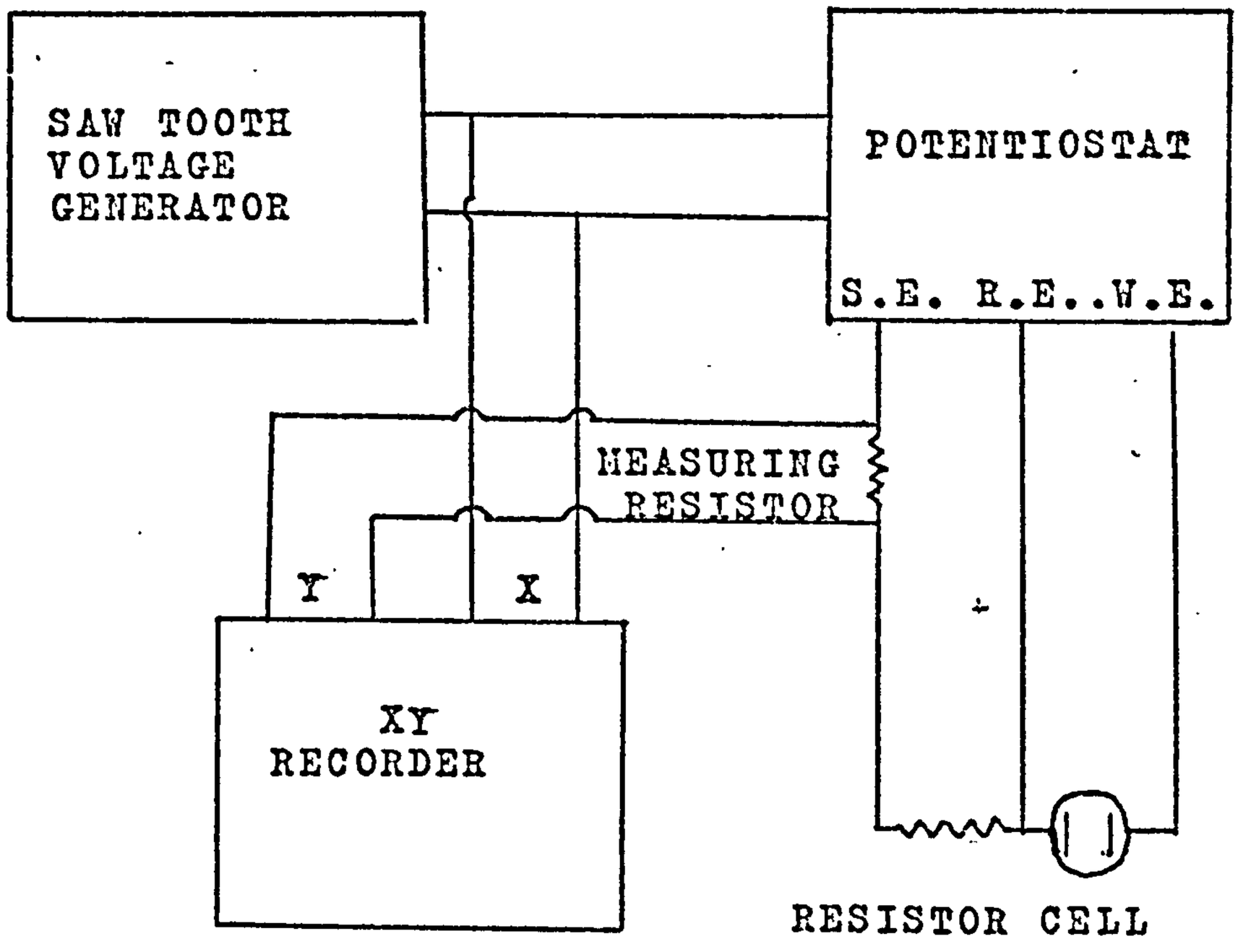

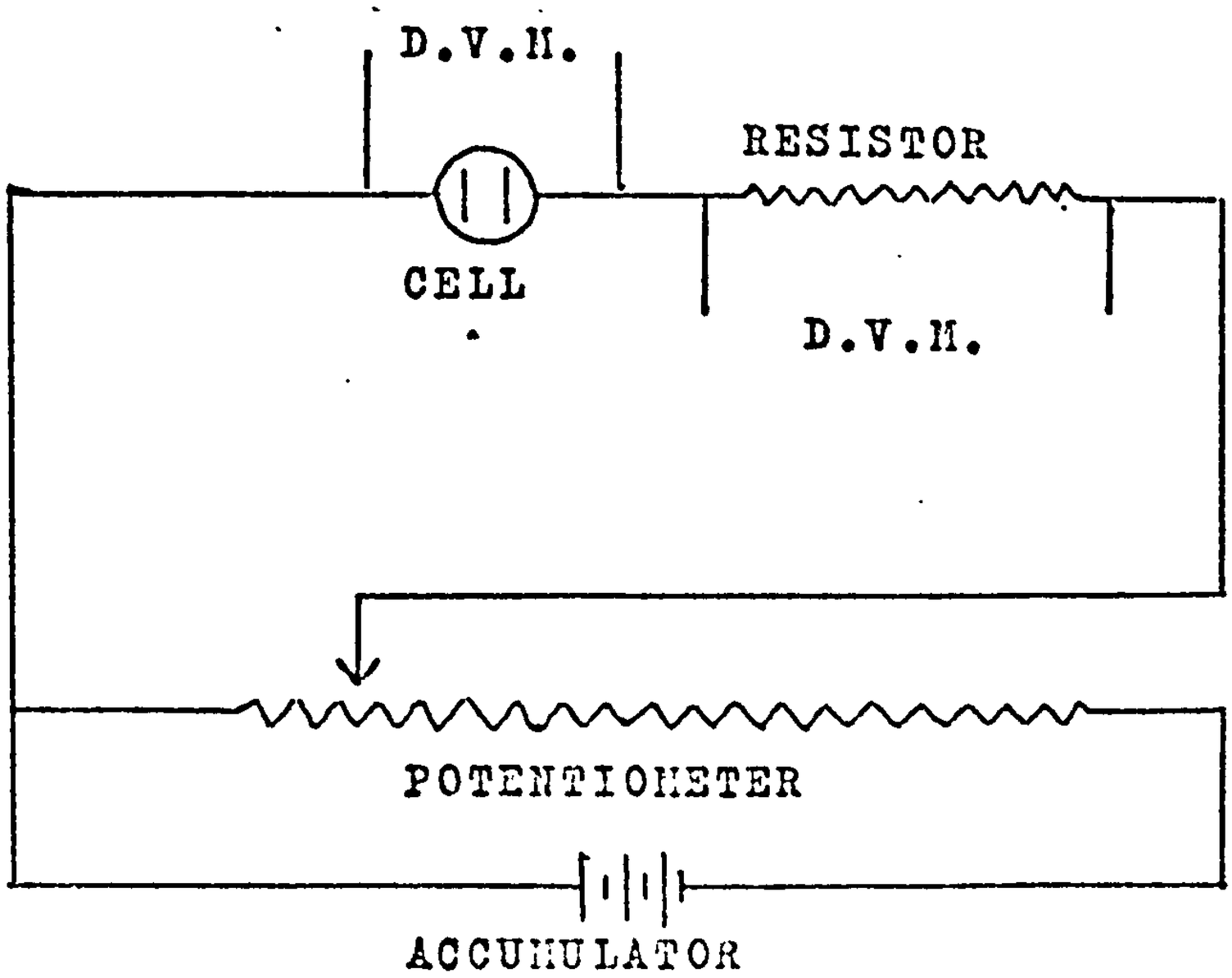

FIG.3.2 CIRCUITS FOR RESISTANCE MEASUREMENTS

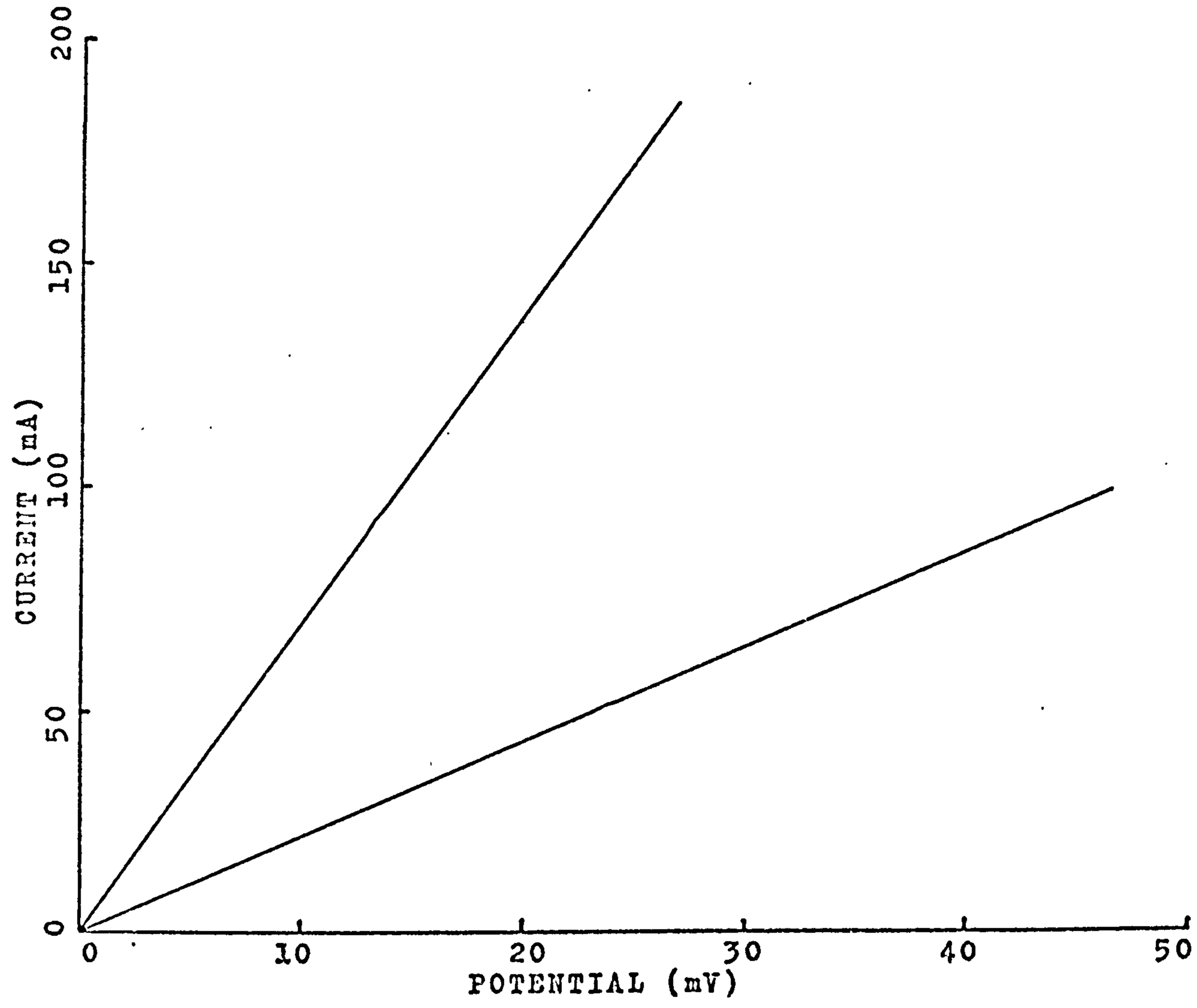

FIG. 3.3 CURRENT–POTENTIAL CURVE FOR MERCURY CONTACT TO A BLUE COLOURED FILM (LOW RESISTANCE BEHAVIOUR EXTREME CASES FOR SPECIMEN 4)

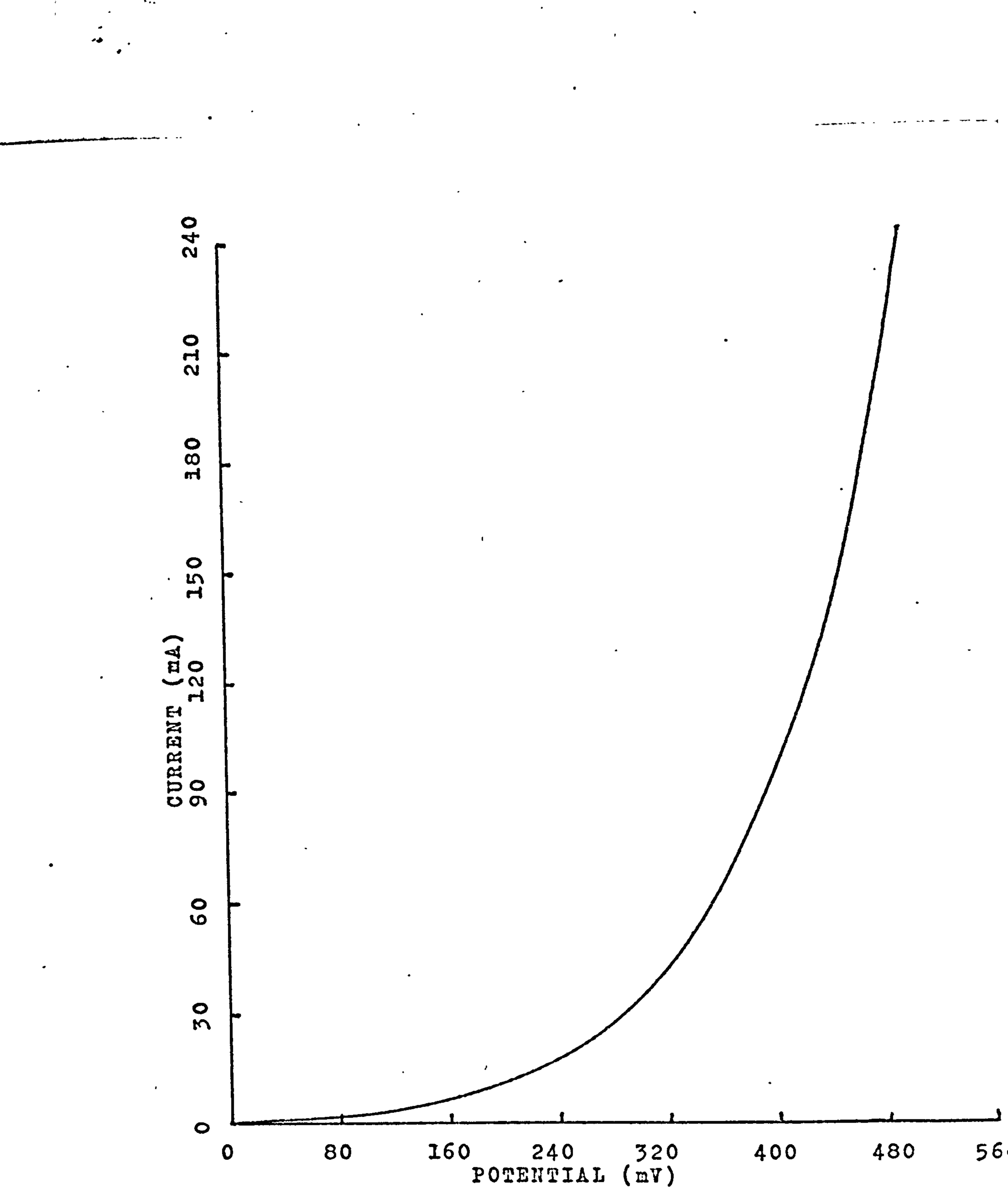

FIG 3.4 CURRENT-POTENTIAL CURVE FOR MERCURY CONTACT TO A BLUE COLOURED FILM (HIGH RESISTANCE)

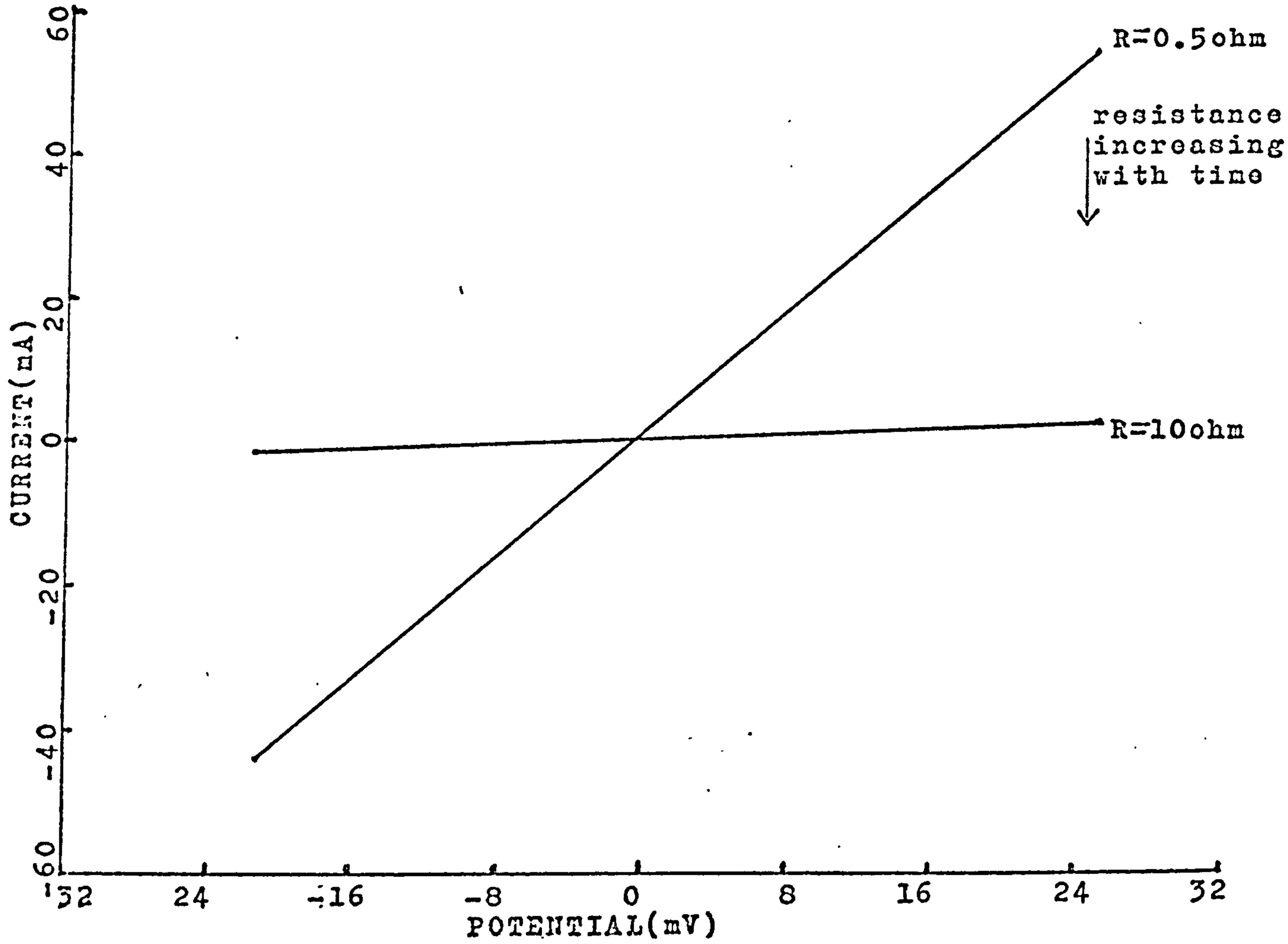

FIG. 3.5 VARIATION IN CURRENT POTENTIAL CURVE WITH TIME FOR MERCURY CONTACTS TO A GOLD COLOURED FILM.

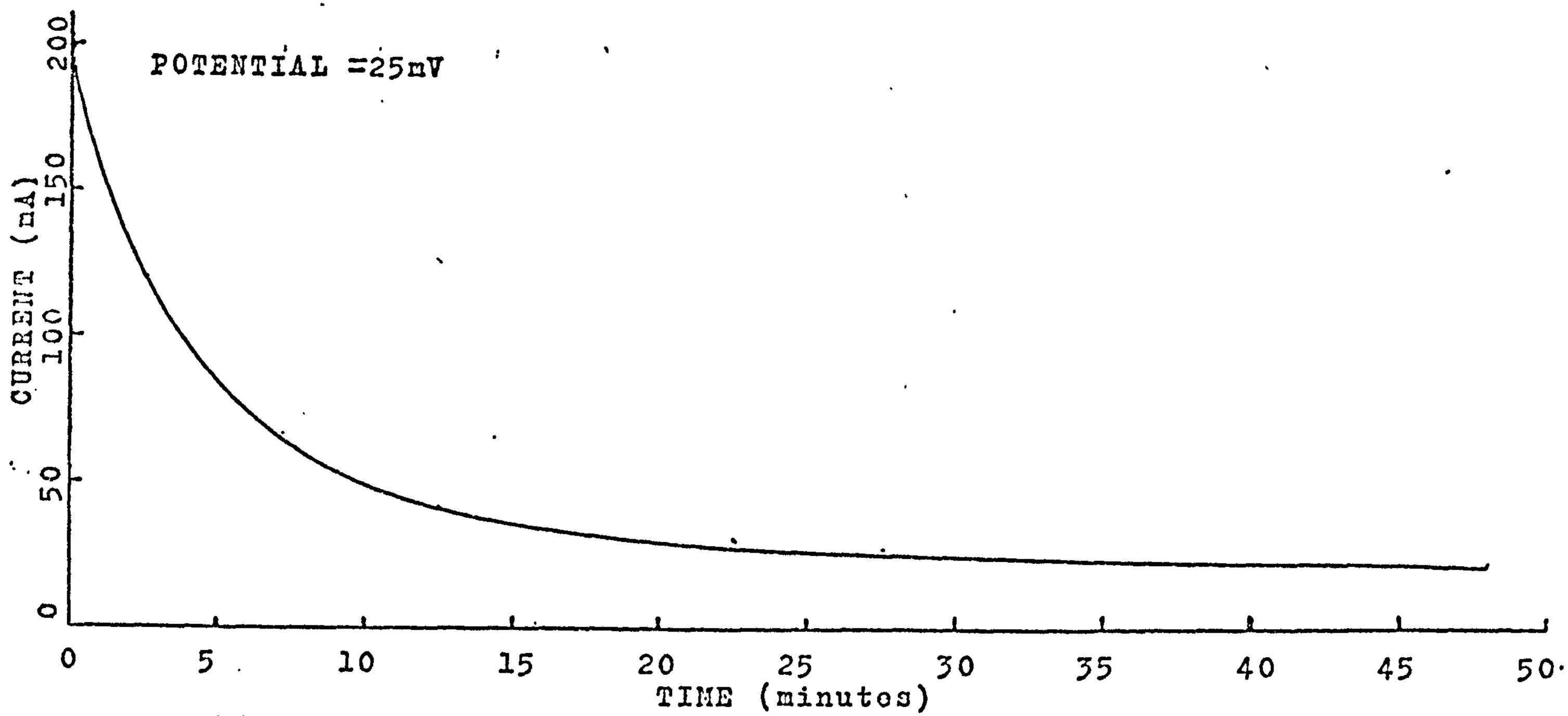

FIG. 3.6 VARIATION OF CURRENT WITH TIME FOR A MERCURY CONTACT TO A GOLD COLOURED FILM

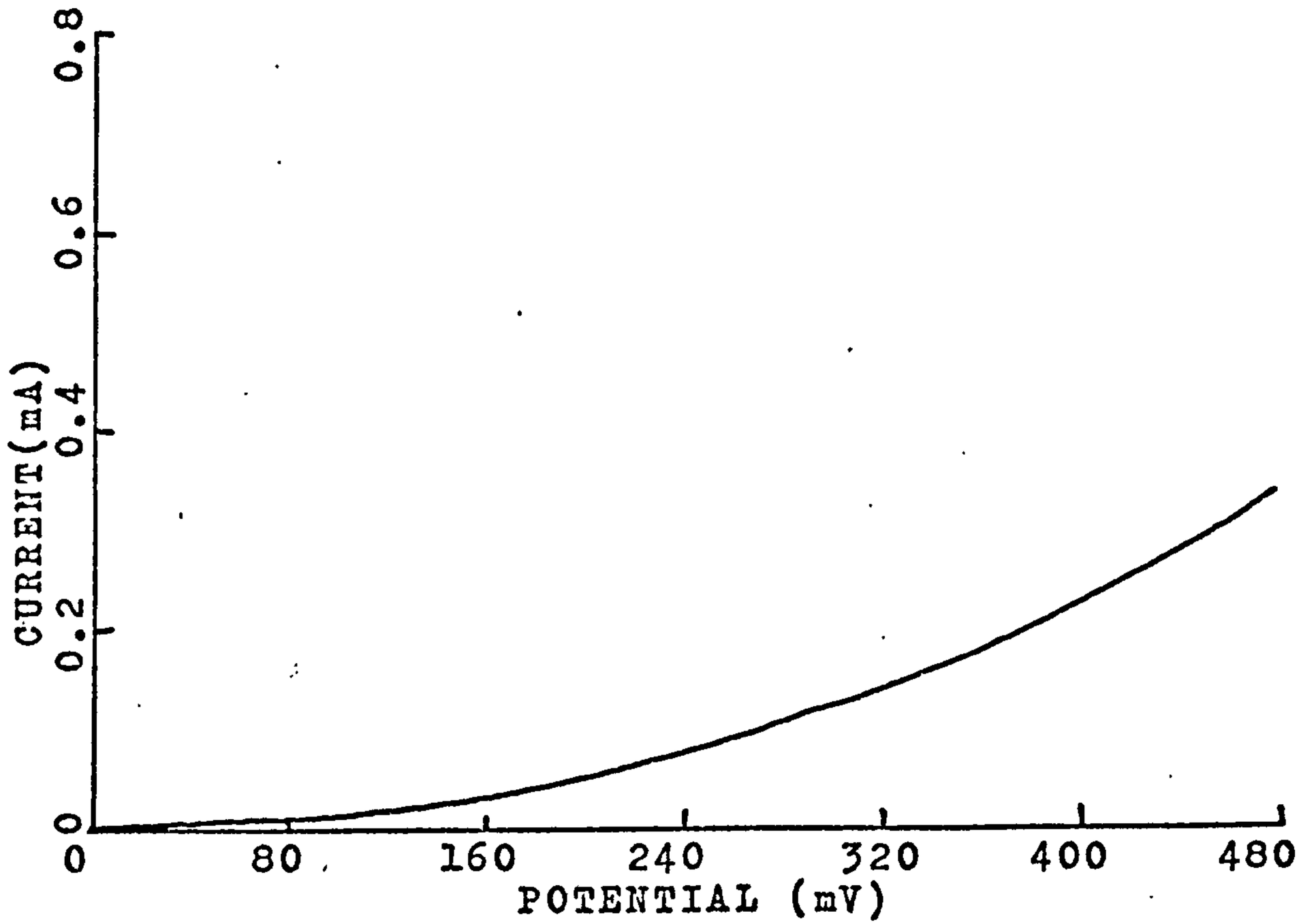

FIG. 3.7 CURRENT-POTENTIAL CURVE FOR EVAPORATED CARBON CONTACT TO A GOLD COLOURED FILM

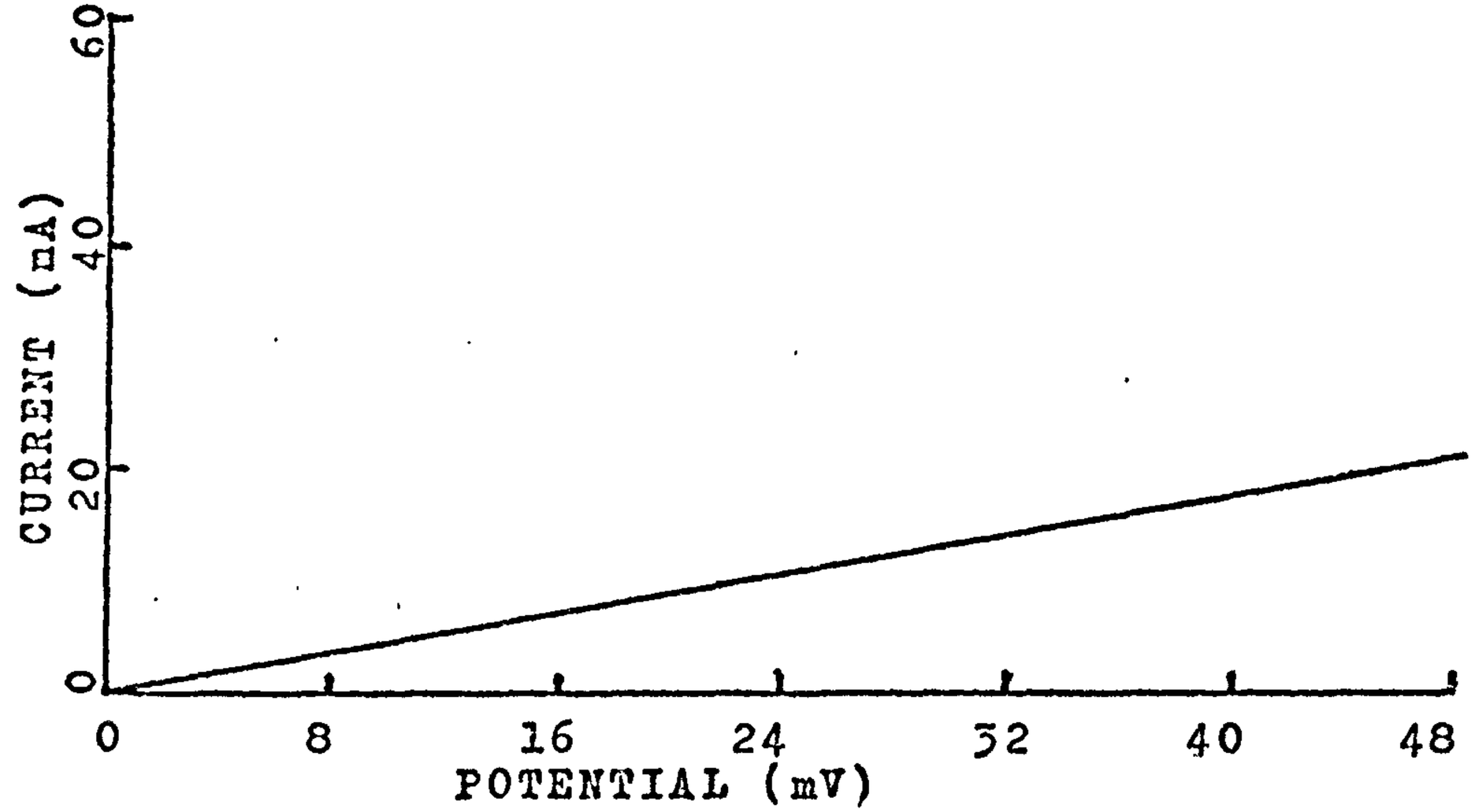

FIG. 3.8 CURRENT-POTENTIAL CURVE FOR EVAPORATED NICKEL CONTACT TO A GOLD COLOURED FILM.

CHAPTER 4

IMPEDANCE MEASUREMENTS ON FILMS ON COLOURED STAINLESS STEEL

4.1. INTRODUCTION

Of the contacts used to measure the resistance of the coloured film described previously, the evaporated nickel contact appeared the most satisfactory. Even with this contact, however, films of nominally the same colour showed considerable variations in resistance. This section describes how this variability was traced to contamination of the specimen surface by grease, and how a criterion for judging whether the specimen was clean or not was derived.

The measurements reported here were made using the D.C. method described previously and a method which allowed the frequency dependence of the impedance of the system to be determined. The latter type of measurement can be used to obtain a greater insight into the properties of the system than simply measuring the resistance and capacitance at a fixed frequency. Perhaps one of the most direct ways of using the frequency dependence of the impedance is to plot the real part of the impedance of the system against the imaginary part for each frequency used. Such a plot is known as a complex plane impedance plot and these have been used by a great number of workers in both aqueous and non aqueous systems[69-71].

4.2. THEORY

A sinusoidally varying potential can be represented by,

$$V = V_o \exp(j\omega t)$$

If this potential is applied across a pure resistance

$$V = i R \quad \text{(instantaneously)}$$

$$i = \frac{V_o}{R} \exp(j\omega t)$$

The current flowing is also sinusoidally varying at the same frequency as the applied potential and in phase with it. The impedance z of the resistor may be defined;

$$i = \frac{V}{z}$$

hence $$z = R + j(0) \qquad (1)$$

If the potential is applied across a pure capacitor

$$q = CV$$

$$\frac{dq}{dt} = C\frac{dV}{dt}$$

$$i = Cj\omega V_o \exp(j\omega t)$$

The current flowing is of the same frequency as the applied potential but 90^o ahead of it. The impedance of the capacitance is defined by;

$$i = \frac{V}{z}$$

$$z = 0 - \frac{j}{\omega C} \qquad (2)$$

For more complicated circuits the impedance values defined above

can be used along with Kirchoff's laws to calculate the impedance of the circuit.

4.2.1. RESISTANCE AND CAPACITANCE IN PARALLEL

For a resistance in parallel with a capacitance Fig. 4.1(a)

$$V = i_1 z_R$$

$$V = i_2 z_c$$

$$i = i_1 + i_2$$

$$i = \frac{V}{z_R} + \frac{V}{z_c}$$

$$i = V\left(\frac{1}{z_R} + \frac{1}{z_c}\right) \qquad (3)$$

but the impedance is defined as,

$$V = i z \qquad (4)$$

Combining equations (3) and (4) gives the impedance of the circuit as;

$$z = \frac{z_R z_c}{z_R + z_c}$$

Substituting for z_R and z_c from equations (1) and (2) gives the impedance of the circuit as;

$$z = \frac{R_p / j\omega C_p}{R_p + 1/j\omega C_p}$$

$$= \frac{R_p}{1 + j\omega C_p R_p}$$

Separating the real and imaginary parts;

$$z = \frac{R_p}{1 + j\omega C_p R_p} \times \frac{1 - j\omega C_p R_p}{1 - j\omega C_p R_p}$$

$$= \frac{R_p - j\omega C_p R_p^2}{1 + \omega^2 C_p^2 R_p^2}$$

$$z = \frac{R_p}{1 + \omega^2 C_p^2 R_p^2} - \frac{j\omega C_p R_p^2}{1 + \omega^2 C_p^2 R_p^2} \qquad (5)$$

Comparison of equation (5) with the general expression for the impedance

$$z = z' - jz''$$

yields

$$z' = \frac{R_p}{1 + \omega^2 C_p^2 R_p^2} \qquad (6)$$

and $$z'' = \frac{\omega C_p R_p^2}{1 + \omega^2 C_p^2 R_p^2} \qquad (7)$$

It can be shown that z' and z'' obey the equation;

$$(z' - \frac{R_p}{2})^2 + (z'')^2 = (\frac{R_p}{2})^2$$

which is the equation of a semicircle (if z', z'' are positive) having a centre at $(\frac{R_p}{2}, 0)$. (Fig. 4.1.a)

4.2.2. RESISTANCE IN SERIES WITH A PARALLEL COMBINATION OF RESISTANCE AND CAPACITANCE

For this circuit (Fig. 4.1.b)

$$V = I(Z_p + Z_R)$$

and consequently the impedance of the system is

$$z = (Z_p + Z_R) \qquad 1.$$

Substituting for Z_p from equation (5) gives

$$z = \frac{R_p}{1 + \omega^2 C_p^2 R_p^2} - \frac{j\omega C_p R_p^2}{1 + \omega^2 C_p^2 R_p^2} + R_3$$

$$= \frac{R_p}{1 + \omega^2 C_p^2 R_p^2} + R_3 - \frac{j \omega C_p R_p^2}{1 + \omega^2 C_p^2 R_p^2} \qquad (8)$$

$$\therefore \quad z' = \frac{R_p}{1 + \omega^2 C_p^2 R_p^2} + R_3, \quad z'' = \frac{\omega C_p R_p^2}{1 + \omega^2 C_p^2 R_p^2}$$

where R_3 is the value of the series resistance.

The complex plane plot for this system (Fig. 4.1.b) is a semicircle of radius $R_p/2$ centred on the z' axis at $(R_3 + R_p/2, 0)$.

The parallel resistance R_p can be obtained from the difference between the low and high frequency intercepts on the z' axis and the parallel capacitance C_p from

$$\frac{z''}{z' - R_3} = \omega C_p R_p$$

4.2.3. TWO PARALLEL RESISTANCE-CAPACITANCE COMBINATIONS IN SERIES

If the system investigated has an equivalent circuit consisting of two parallel resistance-capacitance combinations in series (Fig. 4.1.c) then the form of the complex plane plot will depend on the relative magnitudes of the time constants $R_1 C_1$ and $R_2 C_2$. When the time constants are different, but, not markedly so, the complex plane impedance plot is a semicircle whose

centre lies beneath the real axis[72]. In the case of dielectric loss measurements, Cole and Cole[73] obtained similar graphs in plots of the real part of the complex dielectric constant, against its imaginary part.

A method of obtaining the individual values of the resistances and capacitances in the equivalent circuit shown in Fig. 4.1.c. from the frequency dependence of the impedance of the system is outlined below.

$$V = i z_1 + i z_2$$

Hence the impedance $z = \frac{V}{i} = z_1 + z_2$

$$\therefore \quad z = z_1' - j z_1'' + z_2' - j z_2''$$

$$z = z_1' + z_2' - j(z_1'' + z_2'')$$

The individual impedance of each parallel combination is given by equations (6) and (7) as

$$z_1' = \frac{R_1}{1 + \omega^2 C_1^2 R_1^2}, \quad z_1'' = \frac{\omega C_1 R_1^2}{1 + \omega^2 C_1^2 R_1^2}$$

$$z_2' = \frac{R_2}{1 + \omega^2 C_2^2 R_2^2}, \quad z_2'' = \frac{\omega C_2 R_2^2}{1 + \omega^2 C_2^2 R_2^2}$$

It can be seen from these equations that

$$z_1'' = \omega C_1 R_1 z_1'$$

$$z_2'' = \omega C_2 R_2 z_2'$$

if we let $x = C_1 R_1$ and $y = C_2 R_2$

then $z_1'' = \omega \times z_1'$

$z_2'' = \omega \; y \; z_2'$

$\therefore \quad z'' = z_1'' + z_2'' = \omega (x \; z_1' + y \; z_2')$ (9)

$z' = z_1' + z_2'$

Substituting in equation (9) gives

$$z'' = \omega (x \; z_1' + y(z' - z_1'))$$

$$z_1' (x - y) = (\frac{z''}{\omega} - y \; z')$$

Substituting for z_1' from equation (6)

$$\frac{R_1}{1 + \omega^2 x^2} (x - y) = (\frac{z''}{\omega} - y \; z')$$

$$R_1(x - y) = (\frac{z''}{\omega} - y \; z')(1 + \omega^2 x^2)$$

$$R_1(x - y) = \frac{z''}{\omega} - y \; z' + z'' \omega \; x^2 - z' \omega^2 x^2 y \qquad (10)$$

Similarly $z_1' = z' - z_2'$

$$z'' = \omega (x(z' - z_2') + y \; z_2')$$

$$z_2'(y - x) = (\frac{z''}{\omega} - x \; z')$$

$$\frac{R_2}{1 + \omega^2 y^2} (y - x) = (\frac{z''}{\omega} - x \; z')$$

$$R_2(y - x) = (\frac{z''}{\omega} - x \; z')(1 + \omega^2 y^2)$$

$$R_2(y - x) = \frac{z''}{\omega} - x z' + z''\omega y^2 - z'\omega^2 x y^2 \qquad (11)$$

Subtracting (11) from (10) gives,

$$R_1(x - y) - R_2(y - x) = 0 + (x - y)z' + z''\omega(x^2 - y^2) - z'\omega^2 x y (x - y)$$

Dividing by (x - y)

$$R_1 + R_2 = z' + z''\omega(x + y) - z'\omega^2 x y$$

Since R_o the d.c. value (low frequency intercept on the z' axis) must equal $R_1 + R_2$ (equivalent circuit Fig. 4.1.c.)

$$R_o - z' = z''\omega(x + y) - z'\omega^2 x y \qquad (12)$$

$$\therefore \quad \frac{R_o - z'}{z''\omega} = (x + y) - \frac{z'\omega}{z''} x y$$

A plot of $(\frac{R_o - z'}{z''\omega})$ against $\frac{z'\omega}{z''}$ will be a straight line with a slope equal to - x y and an intercept (x + y). If we consider the numerical value of x y is b and of (x + y) is a

then $(x + y) = a$

$$(x y) = b$$

$$x(a - x) = b$$

$$\therefore \quad x^2 - a x + b = 0 \qquad (13)$$

The values of x and y are the roots of this equation and so $x = R_1 C_1$ and $y = R_2 C_2$ can be evaluated. If these values are substituted back into the

equation for the real part of the impedance,

$$z' = \frac{R_1}{1 + \omega^2 C_1^2 R_1^2} + \frac{R_2}{1 + \omega^2 C_2^2 R_2^2}$$

$$z'(1 + \omega^2 x^2) = R_1 + R_2\left(\frac{1 + \omega^2 x^2}{1 + \omega^2 y^2}\right)$$

A plot of $z'(1 + \omega^2 x^2)$ against $\left(\frac{1 + \omega^2 x^2}{1 + \omega^2 y^2}\right)$ allows the determination of R_1 and R_2 and their sum must, of course, equal R_o. Hence C_1 and C_2 can be obtained from the products $C_1 R_1$ and $C_2 R_2$.

4.2.4. TWO PARALLEL RESISTANCE-CAPACITANCE COMBINATIONS AND A RESISTANCE IN SERIES

The total impedance of the two parallel combinations was treated in the last section. It can be seen that for two parallel resistance-capacitance combinations and a series resistance (equivalent circuit Fig. 4.1.d.)

$$V = i z_{Rc} + i R_3$$

The impedance $z = \frac{V}{i} = z_{Rc} + R_3$

From the previous treatment

$$z = z_1' + z_2' - j(z_1'' + z_2'') + R_3$$

The real part of the impedance of the system is

$$z' = z_1' + z_2' + R_3$$

and the imaginary part is

$$z'' = z_1'' + z_2'' \qquad 1.$$

The effect of the series resistance R_3 will thus be to displace all the points on the impedance plot at distance R_3 along the real axis. The plot will thus be a semicircle with its centre below the real axis and a high frequency intercept equal to R_3 (Fig. 4.1.d.)

Since $(z' - R_3) = z_1' + z_2'$

and $z'' = z_1'' + z_2''$

The equations from the previous treatment may be used if $(z' - R_3)$ is substituted for z' in the appropriate equations.

4.3. MEASUREMENT OF THE IMPEDANCE

The real and imaginary parts of the impedance were measured using a system (Fig. 4.2) incorporating a phase sensitive detector. A sinusoidally varying voltage was applied across the cell and an accurately known carbon resistor connected in series. A high impedance differential amplifier was connected first across the cell and then across the resistor, the output being fed into a phase sensitive detector. The gate on the latter unit was operated by a square wave produced by a reference unit driven from the signal source. This square wave could be either in phase with the applied sine wave or 90^{o} out of phase. Consequently the integrated output voltage of the phase sensitive detector was proportional to either the in-phase or out-of-phase voltages across the cell and the resistor. The real and imaginary components of the cell impedance can then be derived.

The measured quantities are

$$V_1 = k V_R^{o}$$

$$V_2 = k\, V_R^{90}$$

$$V_3 = k\, V_c^{o}$$

$$V_4 = k\, V_c^{90}$$

1.

The constant k depends on the instrumental settings but remains constant if these are not varied during the measurement.

The voltage drop across the cell is given by,

$$V = V' + j\, V''$$

$$= V_c^{o} + j\, V_c^{90}$$

Since the resistor is in series with the cell and its impedance $z = R$ the current flowing through the cell is given by,

$$i = \frac{V_R^{o} + j\, V_R^{90}}{R}$$

which gives, in terms of the measured voltages

$$z = R\frac{(V_3/k + j\, V_4/k)}{(V_1/k + j\, V_2/k)}$$

$$= R\left(\frac{V_3 + j\, V_4}{V_1 + j\, V_2}\right)$$

Separating real and imaginary parts

$$z = R\left(\frac{V_3 + j\, V_4}{V_1 + j\, V_2}\right) \times \left(\frac{V_1 - j\, V_2}{V_1 - j\, V_2}\right)$$

$$= R\left(\frac{V_1V_3 + V_2V_4 + j(V_4V_1 - V_2V_3)}{V_1^2 + V_2^2}\right)$$

$$= R\left(\frac{V_3V_1 + V_2V_4}{V_1^2 + V_2^2}\right) + j\,R\left(\frac{V_4V_1 - V_2V_3}{V_1^2 + V_2^2}\right)$$

The real part of the impedance is obtained from the real values using

$$z' = R\left(\frac{V_3V_1 + V_2V_4}{V_1^2 + V_2^2}\right)$$

and the imaginary part

$$z'' = R\left(\frac{V_2V_3 - V_4V_1}{V_1^2 + V_2^2}\right)$$

4.4. EXPERIMENTAL

As will be apparent from the reported results, the resistance values obtained from the first series of specimens were irregular and very high. This was eventually found to result from contamination caused principally by the presence of silicone grease, used as a lubricant in a commercial 'sterile' syringe employed to transfer mercury to the specimen surface. When it was realised that such contamination might have occurred specimens were washed in petroleum ether and mercury transferred to the specimen surface using a glass dropper. As a consequence of the decrease in the resistance with these specimens the experimental procedure used with the second series of specimens was designed to ensure, as far as possible, that contamination did not occur.

4.4.1. FIRST SERIES

The stainless steel specimens, 1½" by 2½", were coloured in 2.5M chromic acid and 5M H_2SO_4 at 70°C. They were then well washed with distilled water and left to dry in a desiccator. The specimens were

attached to a glass plate using double sided Sellotape and covered with a second glass plate, with a circular hole in it, which acted as a mask (Fig. 4.3). The masked specimen was placed in an evaporation chamber and ¾" of 0.028" nickel wire placed in a tungsten filament 3" above the specimen. The pressure on the chamber was reduced to 10^{-4} to 10^{-5} torr and the nickel was evaporated onto the exposed area of the specimen surface.

The specimens were removed from the evaporation chamber and attached to the base of a perspex box (Fig. 4.3) by two clamps one of which was brass so that contact could be made to the stainless steel substrate. The lid was fitted to the box, the position of the platinum wire probe adjusted and the lid removed.

The base of the box was placed in a dessicator, a neoprene ring positioned over the nickel coated area of the specimen and mercury introduced into the neoprene ring with a 'sterile' plastic syringe. The lid was then fixed to the base of the box and connection made to the platinum wire probe and brass clamp by means of wires which passed through the top of the desiccator.

The resistance of the film was measured using either the phase sensitive detector for A.C. values or the potentiostat for D.C. values, as described previously.

4.4.2. SECOND SERIES

The procedure described above was modified in the following ways. Prior to colouring the specimens were immersed in petroleum spirit (B.pt 60-80°C) and degreased by wiping with tissue paper. They were left in petroleum spirit until required, being withdrawn and dried immediately prior to colouring. During colouring their potentials were monitored against a hydrogen electrode. The coloured specimens were washed in

distilled water and allowed to dry, then stored in a covered container. The remainder of the experimental procedure was as described in Section 4.4.1. except that the mercury was transferred using a glass dropper which had been cleaned in a mixture of concentrated sulphuric acid and nitric acid. A further modification was to dispense with the use of a desiccator to prevent the possibility of contamination from the grease on the flange of the desiccator.

4.5. RESULTS

4.5.1. FIRST SERIES

A typical complex plane plot for a 'contaminated' specimen is shown in Fig. 4.4. The behaviour observed with the same specimen after it had been degreased by immersion in petroleum ether is shown in Fig. 4.5. The D.C. resistance values obtained with such specimens before and after washing with petroleum ether are reported in Table 4.1.

The fall in resistance resulting from washing with petroleum ether strongly suggested that the initial resistance arose from contamination by grease. This was confirmed by the much lower resistances obtained with the second series of specimens.

4.5.2. SECOND SERIES

In some cases the measured resistance increased slowly with time (Fig. 4.6). Specimens showing this behaviour were rejected.

The complex impedance plane plots obtained could all be fitted by a semicircle. In some cases, however, the centre of the semicircle lay below the real axis. Examples of the extremes of behaviour encountered are shown in Fig. 4.7 and Fig. 4.8.

When the centre of the semicircle lay on the real axis the values of R_p, R_3 and C_p were obtained as described in Section 2.2. When this was not the case, the procedure described in Section 2.4. was employed. Typical plots of $Z'(1 + w^2 C_1^2 R_1^2)$ versus $(1 + w^2 C_1^2 R_1^2)/(1 + w^2 C_2^2 R_2^2)$ are shown in Figs. 4.9 and 4.10.

The values of resistance and capacitance obtained, along with the equivalent circuits used, are shown in Table 4.2. Fig. 4.11 is a plot of the resistance against the reciprocal of the capacitance while Figs. 4.12 and 4.13 are plots of the resistance and reciprocal of the capacitance against the potential above the plateau attained during colouring.

4.6. DISCUSSION

4.6.1. COMPLEX PLANE IMPEDANCE PLOTS

The specimens in series 1 which initially exhibited very high resistances gave complex plane plots which were semicircles with their centres lying well below the real axis (see Fig. 4.4). The marked reduction in resistance and movement of the origin of the semicircle toward the real axis, which was observed after washing the specimens with petroleum ether, strongly suggests that these specimens were initially contaminated by grease. The distortion of the semicircle produced by contamination will be discussed later in connection with the equivalent circuits for these systems.

When further precautions were taken to prevent surface contamination, the complex plane plots were semicircles with their origins either on or close to the real axis (Figs. 4.7 and 4.8).

The appropriate equivalent circuits for these various situations are discussed below.

4.6.2. EQUIVALENT CIRCUITS

The appropriate equivalent circuit for the system steel, film, nickel contact can be deduced by comparing the shape of the observed complex plane plot with that predicted for a given equivalent circuit.

If the film were an ionic conductor and dissolution/deposition reactions could occur at the steel and nickel electrodes, the equivalent circuit should be that shown in Fig. 4.14.a. In this circuit, R_e represents the resistance of the electrolyte, C_g the geometric capacitance across the electrolyte, C_{dl} the capacitances associated with the electrode-electrolyte interfaces and R_{ct} the charge-transfer (or faradaic) resistances. Because the time constants $R_e C_g$ and $R_{ct} C_{dl}$ are normally very different, such an equivalent circuit would yield at least two semicircles in the complex plane plot. Moreover, since R_{ct} is not an ohmic resistance the D.C. behaviour of the system should not obey Ohm's law. Neither of these predictions were observed. This could not be because one or both of the electrodes was a 'blocking' electrode, i.e. one at which no faradaic process can occur. If this were the case, no D.C. current could be passed and the equivalent circuit and complex plane plot would be those shown in Fig. 4.1.4.b. It may be concluded therefore that the film is not a predominantly ionic conductor.

For an electronically conducting film, which is probably a semi-conductor, the equivalent circuit and D.C. behaviour would depend on whether the electrodes made ohmic or non-ohmic contacts. In the latter case non-linear current-potential relations should be observed in D.C. experiments. Since this was not the case it may be concluded that ohmic contacts were established. Space-charge capacitances may exist at the interfaces between metals and semi-conductors. Under these circumstances the equivalent circuit would be that shown in Fig. 4.14.c. Unless the time constants

R_i C_g and R_o C_{sc} were identical, the equivalent circuit should consist of two semicircles or one semicircle with its origin below the real axis. Since with a number of films of differing resistance the complex plane plots were semicircles with their origin accurately on the real axis it must be concluded that C_{sc} is negligibly small. The displacement of the high frequency intercept of these semicircles from the origin indicates that a resistance in series with R_i is present. This may be associated with the electrode-electrolyte interfaces or the leads. The appropriate equivalent circuit is that shown in Fig. 4.14.d. in which the film can be regarded as behaving like a leaky condensor.

The initial complex plane plots obtained with series 1 specimens appear to be associated with the presence of a layer of grease, probably between the nickel and mercury. The simplest equivalent circuit applicable to this situation would be that shown in Fig. 4.14.e, in which the grease gives rise to a second parallel combination of resistance and capacitance. As shown in Section 2.3. such a circuit could give rise to impedance plots of the type observed. It is noteworthy that with 'uncontaminated' specimens (Figs. 4.7 and 4.8) the impedance is virtually frequency independent below 5 kHz, and the highest resistance was only 19.2 ohm. By contrast the impedance of contaminated speciments was markedly frequency dependent below 5 kHz and their resistances normally exceeded 100 ohm. The behaviour of these specimens is therefore dominated by the impedance of the grease. In accord with this, after washing in petroleum ether, the resistance was reduced and the impedance was frequency dependent at higher frequencies.

These results with contaminated specimens suggest that small amounts of surface contamination could account for the depressed semicircles obtained with some of the specimens in series 2. Such contamination could well arise from pump-oil during the evaporation procedure. With these

specimens an equivalent circuit such as that shown in Fig. 4.14.e could again be applicable. If this is so the values of R_p and C_p obtained after analysing these results by the procedure outlined in Section4.2.4., should again be those corresponding to the film behaving as a leaky condenser.

4.6.3. LEAKY CONDENSER MODEL

If the film behaves as a leaky condenser, its capacitance should be that of a parallel plate condenser and given by

$$C_g = \frac{\varepsilon \varepsilon_o l}{A}$$

C_g = geometric capacitance

ε = dielectric constant (relative permittivity)

l = thickness of film material

A = common area of contacts

ε_o = permittivity of a vacuum

The resistance of the film material would be given by

$$R_f = \rho \frac{l}{A}$$

R_f = film resistance

ρ = resistivity of film material.

The measured capacitance should be inversely proportional to the film thickness and the measured resistance directly proportional to the film thickness. A correlation between the resistance, or the reciprocal of the capacitance and ΔV which is related to the film thickness would thus be expected. Since as shown in Figs. 4.12 and 4.13 such a correlation is

obtained this confirms that the resistance and capacitance values do correspond to those of the film.

Since measurements of film resistance and capacitance are made on the same specimen at the same time the thickness l and the area A would be the same for a particular film. Thus if the dielectric constant and specific resistivity of the film material are constant throughout the range of film thickness a plot of R_f against $1/C_g$ is a test of the leaky condenser model. As shown in Fig. 4.11 this graph is indeed linear. Moreover since the slope of this plot is the product of the permittivity and resistivity of the film ($\varepsilon \varepsilon_o \rho$) it is unlikely that either of these quantities changes with film thickness. This suggests that the composition of the material does not vary with its thickness.

Accepting that the composition of the film remains constant, the variation of R_p or $1/C_p$ with Δ V reflects the variation of film thickness with Δ V. As shown in Figs. 4.15 and 4.16 it appears that the film thickness increases logarithmically with increase in Δ V.

4.7. CONCLUSIONS

In the preceding section, the use of alternating current methods to obtain the resistance and capacitance of the film material has been discussed. It has been shown, that care must be exercised to ensure that the specimen is free of contamination. The way in which impedance plots can be used to isolate the film impedance, if gross contamination is not present, has been demonstrated.

The linearity of the resistance against the reciprocal of the capacitance plot gave a value for the product of resistivity and dielectric constant of the film material ($\varepsilon \rho$) equal to 1.06×10^7 ohm cm.

If a film thickness of 0.5×10^{-4} cm (Section 2.2.3.) is taken for a green film ($\Delta V = 21$ mV) the resistivity of the film material is 5.9×10^{5} ohm cm. Evans et al[3] found that the resistivity increases with film thickness from 2×10^{5} to 2.5×10^{6} ohm cm. Whilst the value obtained in the present work is similar in magnitude to that of Evans the linearity of the R_p, $1/C_p$ plot strongly suggests that the resistivity does not vary with film thickness.

Taking the value 5.9×10^{5} ohm cm and the relationship between the logarithm of resistance and potential above the plateau (Fig. 4.15) the relationship between film thickness and potential may be evaluated as

$$l = 3.1 \times 10^{-8} \exp (0.355 \Delta V)$$

The dielectric constant of the film material evaluated using the thickness data is 18.3. Evans et al[3] found that the dielectric constant of the film material decreased with increase in film thickness from 50 to 20. A dielectric constant of 15.6 has been found for the passive film present on the surface of stainless steel by Okamoto and Shibata[74].

TABLE 4.1

D.C. RESISTANCE VALUES FOR FIRST SERIES SPECIMENS

Specimen number	Plateau potential mV	Final potential mV	Potential above plateau mV	Colour	Resistance (d.c.) ohm	Resistance after washing in petroleum spirit 1st wash	2nd wash	3rd wash
46	1304	1320	16	GOLD	150	15.2	14.7	
47	1290	1304	14	GOLD	10,000*	325		
49	1294	1310	16	GOLD	10^6			
51	1289	1301	12	BLUE	800*	274	1	
52	1291	1304	13	BLUE	10			
55	1298	1312	14	BLUE/GOLD	1200	55.4	18.6	4.1
56	1300	1313	13	BLUE/GOLD	100*	17	3.5	5.4

(1) Resistance values with an asterisk were obtained from the low frequency intercept of the complex plane impedance plot.

(2) Area of nickel contact 1.54 cm^2.

TABLE 4.2

RESISTANCE AND CAPACITANCE VALUES FOR SECOND SERIES SPECIMENS AND THE EQUIVALENT CIRCUITS USED IN THEIR CALCULATION

Specimen number	Equivalent circuit	V mV	R_p Ω	$1/C_p$ $(\mu F)^{-1}$
94	2RC + R	12	1.18	0.67
119	RC + R	13	0.9	0.35
105	RC + R	14	1.6	1.6
102	2RC + R	16	4.14	5.18
117	2RC + R	17	6.87	7.72
121	2RC + R	18	6.45	7.45
108	2RC + R	19	9.13	9.93
122	2RC + R	21	19.2	20.11
17	RC + R	-	9.57	11.20
21	RC + R	-	7.2	7.89
124	2RC + R	-	13.69	14.49

(1) Area of nickel contact 1.54 cm^2

CIRCUIT

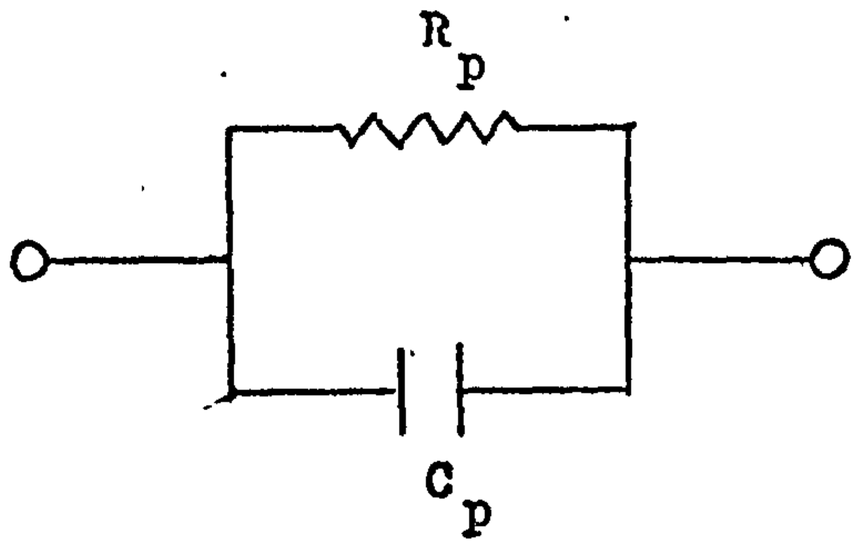

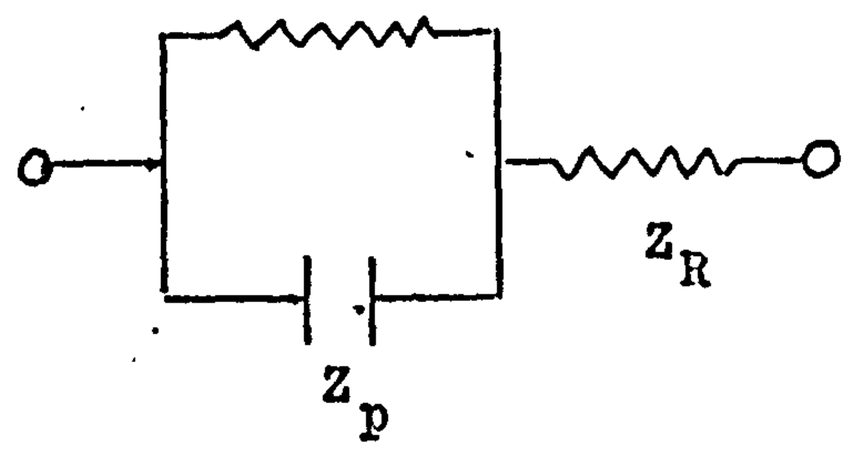

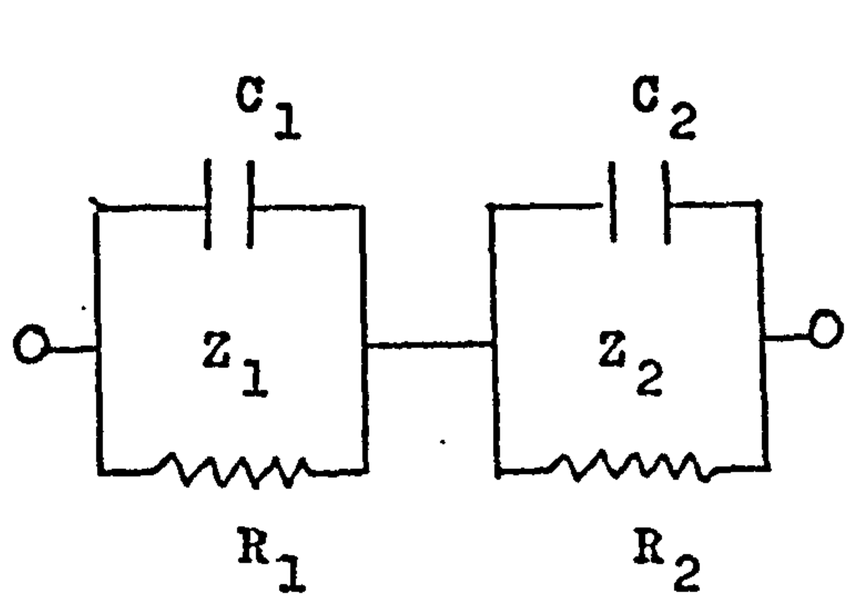

COMPLEX PLANE PLOT

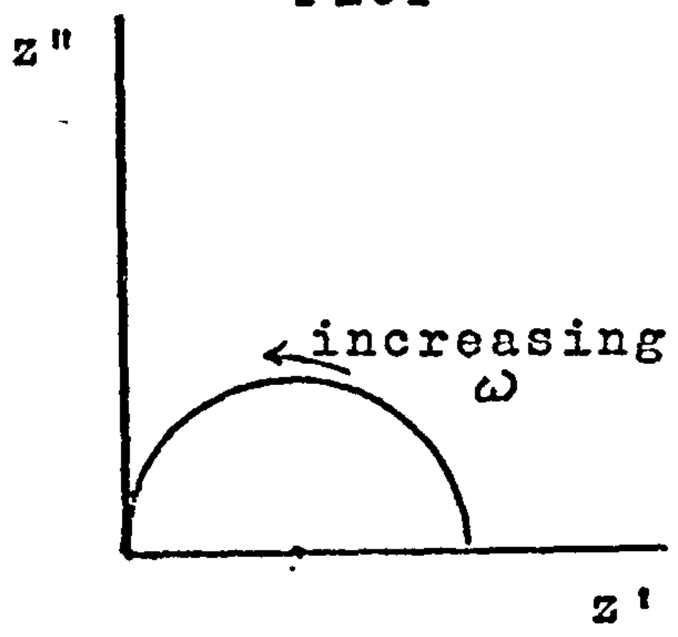

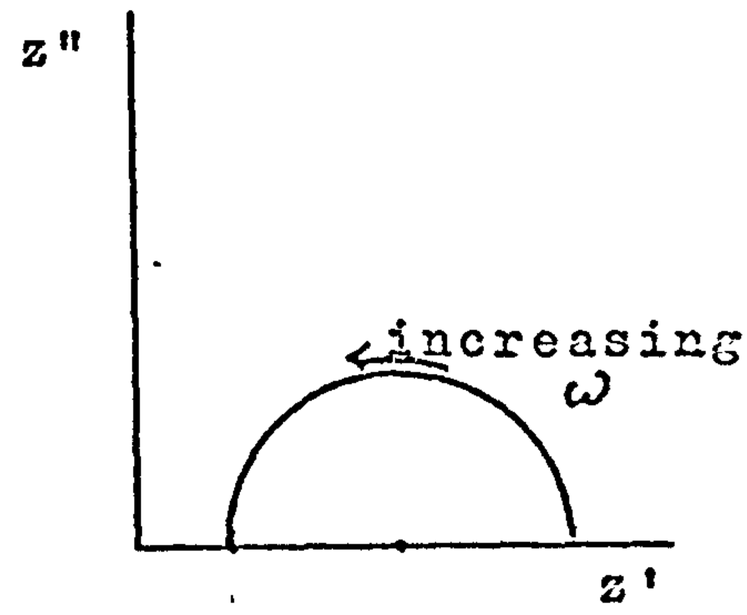

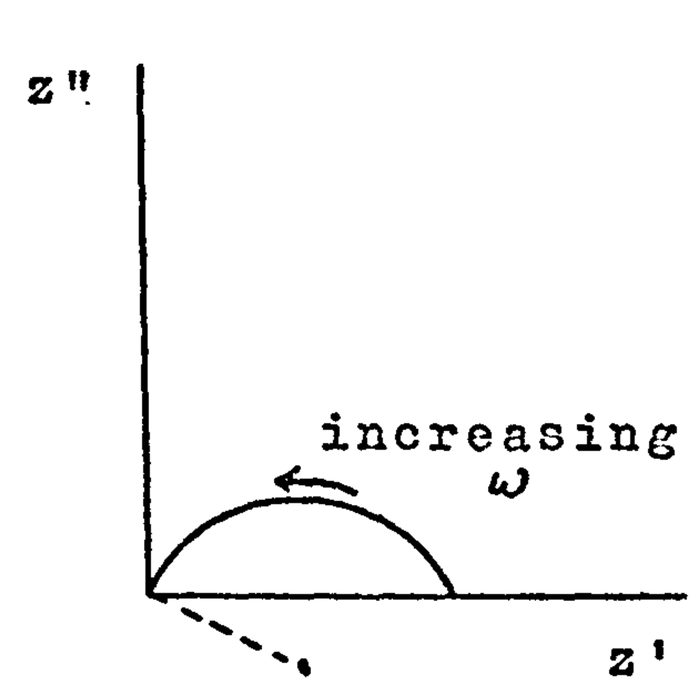

FIG.4.1. CIRCUITS USED IN THE CALCULATION OF THE COMPLEX PLANE PLOTS

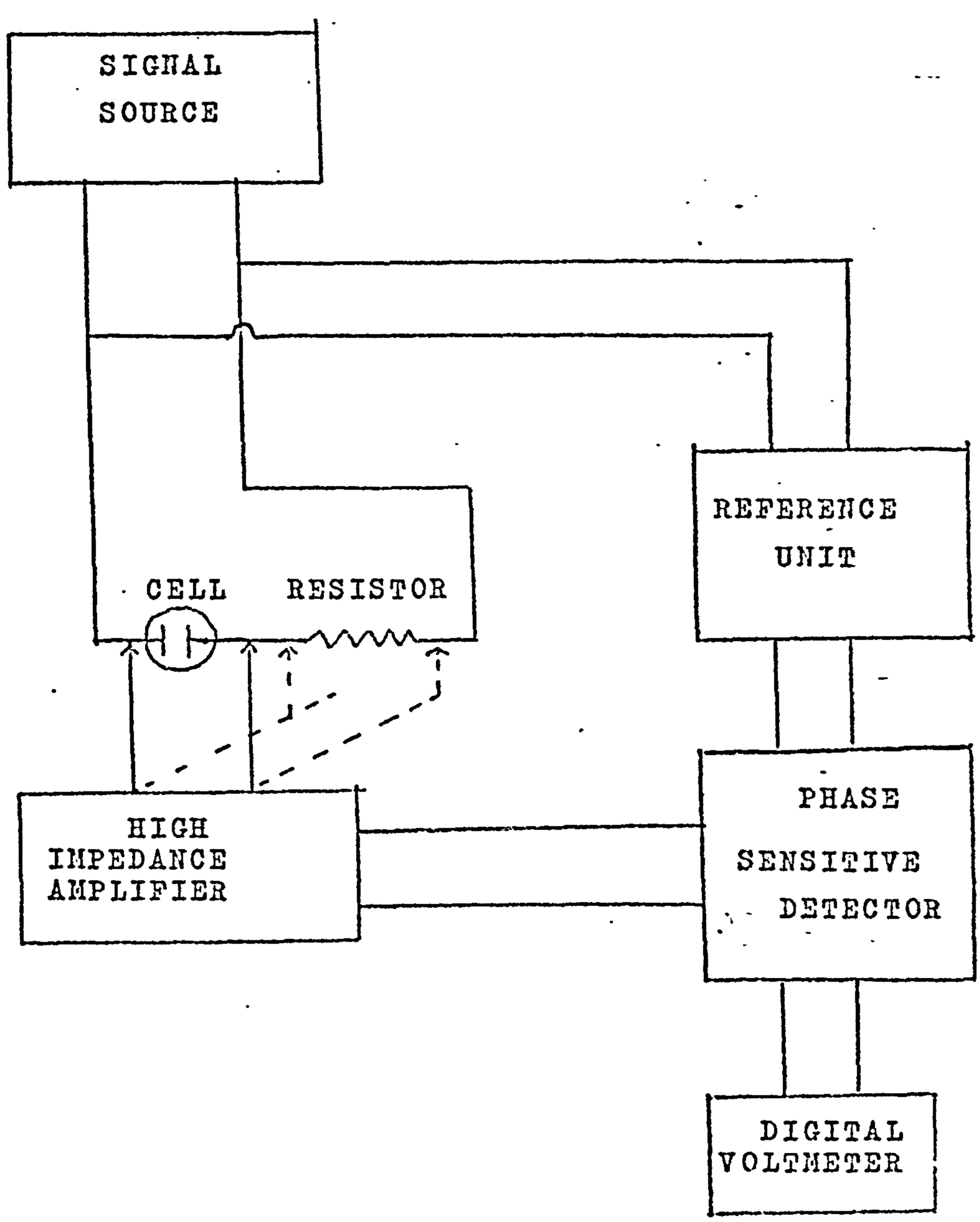

FIG. 4.2 SCHEMATIC DIAGRAM OF THE APPARATUS USED TO MEASURE THE IMPEDANCE

MASKING APPARATUS

a)

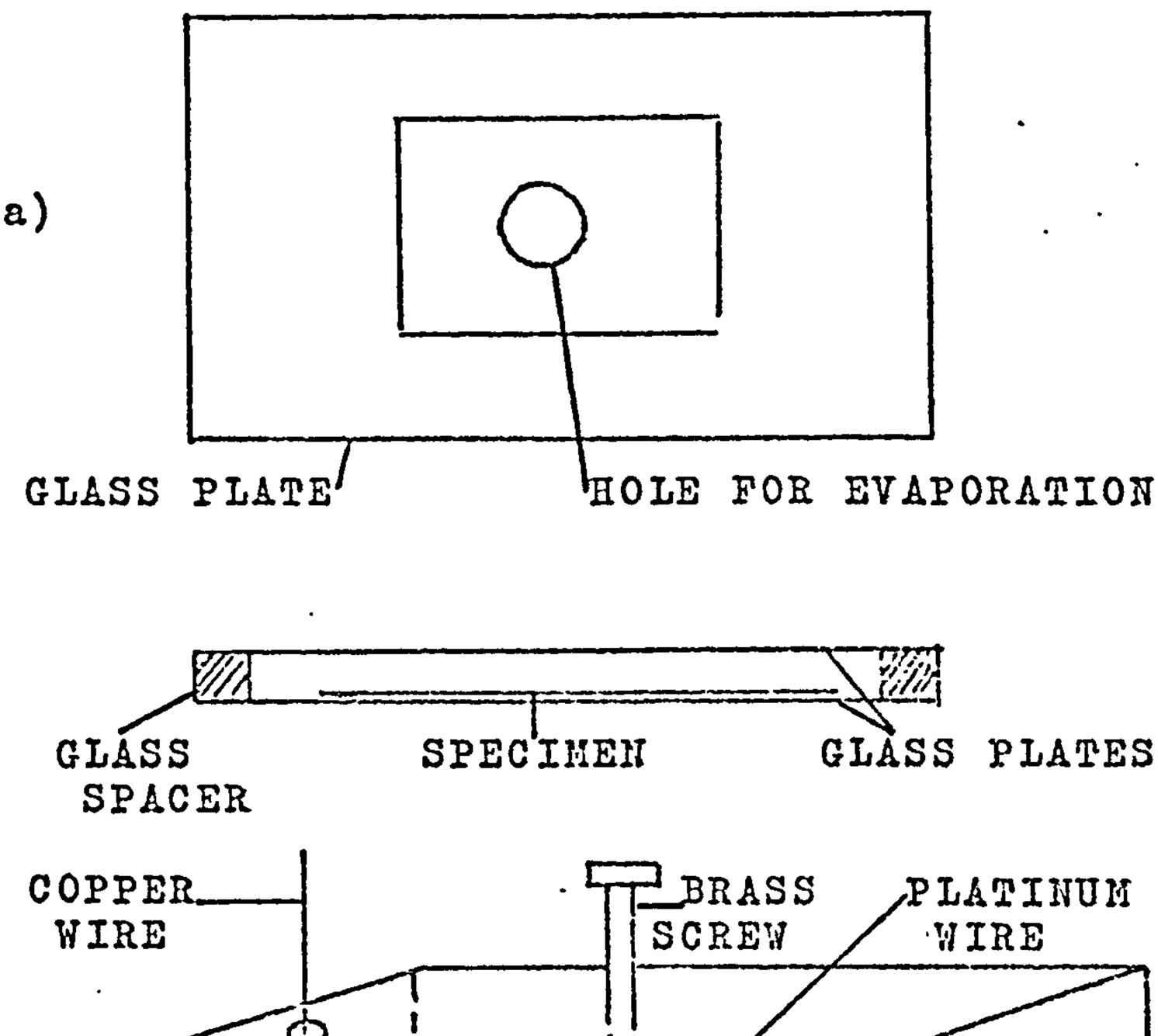

FIG. 4.3 a) MASKING APPARATUS

b) CELL USED FOR IMPEDANCE MEASUREMENTS

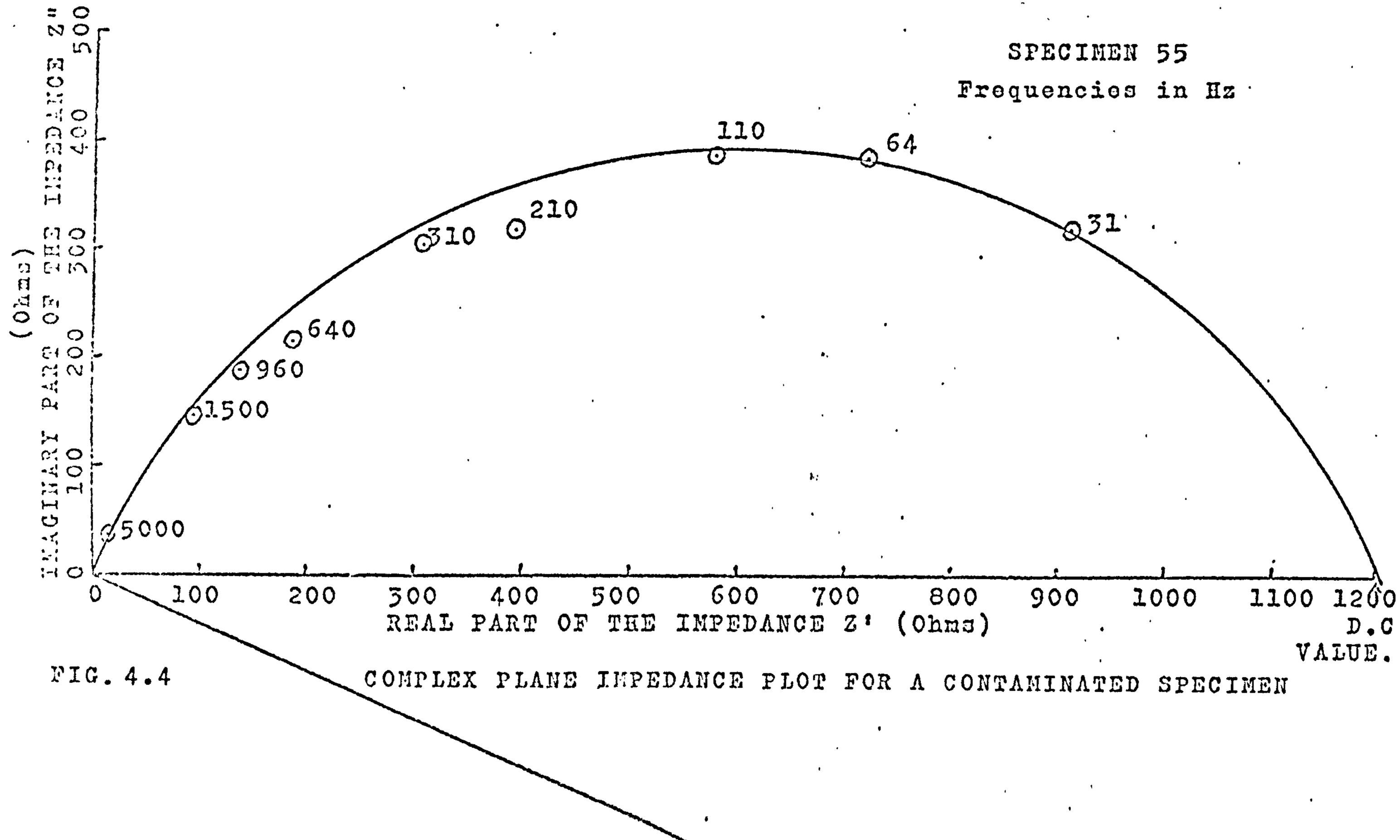

FIG. 4.4 COMPLEX PLANE IMPEDANCE PLOT FOR A CONTAMINATED SPECIMEN

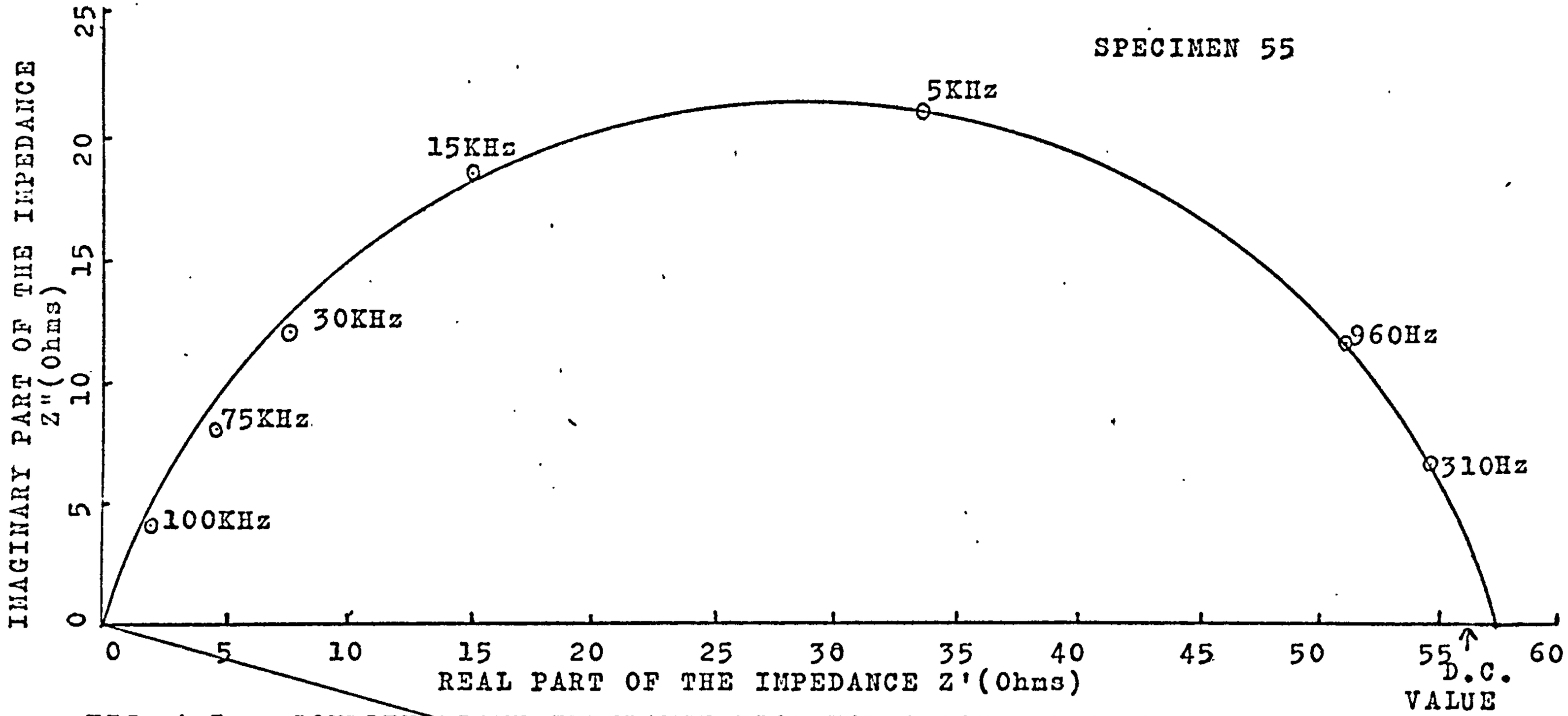

FIG. 4.5 COMPLEX PLANE IMPEDANCE PLOT FOR A CONTAMINATED SPECIMEN AFTER WASHING IN PETROLEUM ETHER

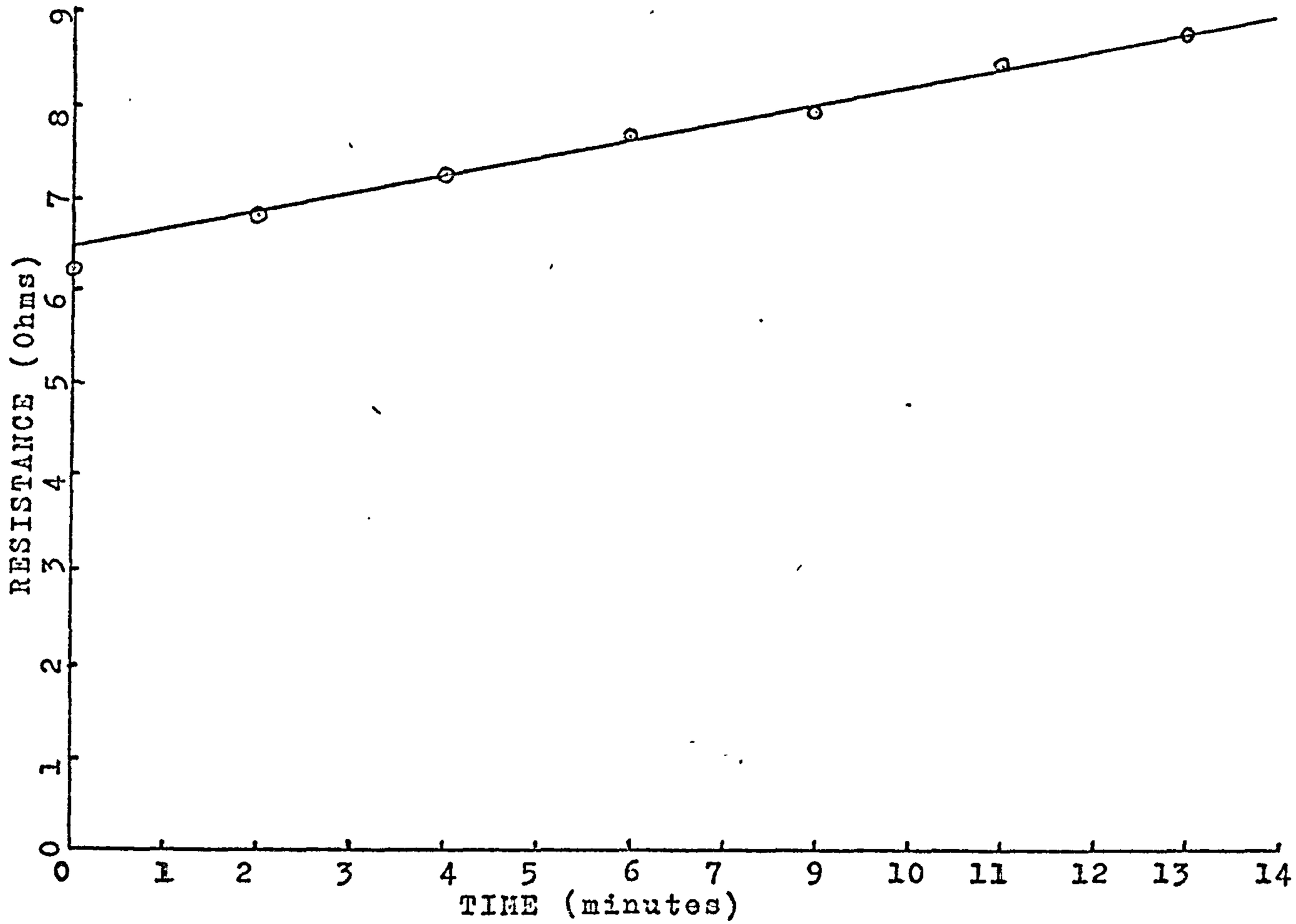

FIG. 4.6 VARIATION OF RESISTANCE WITH TIME

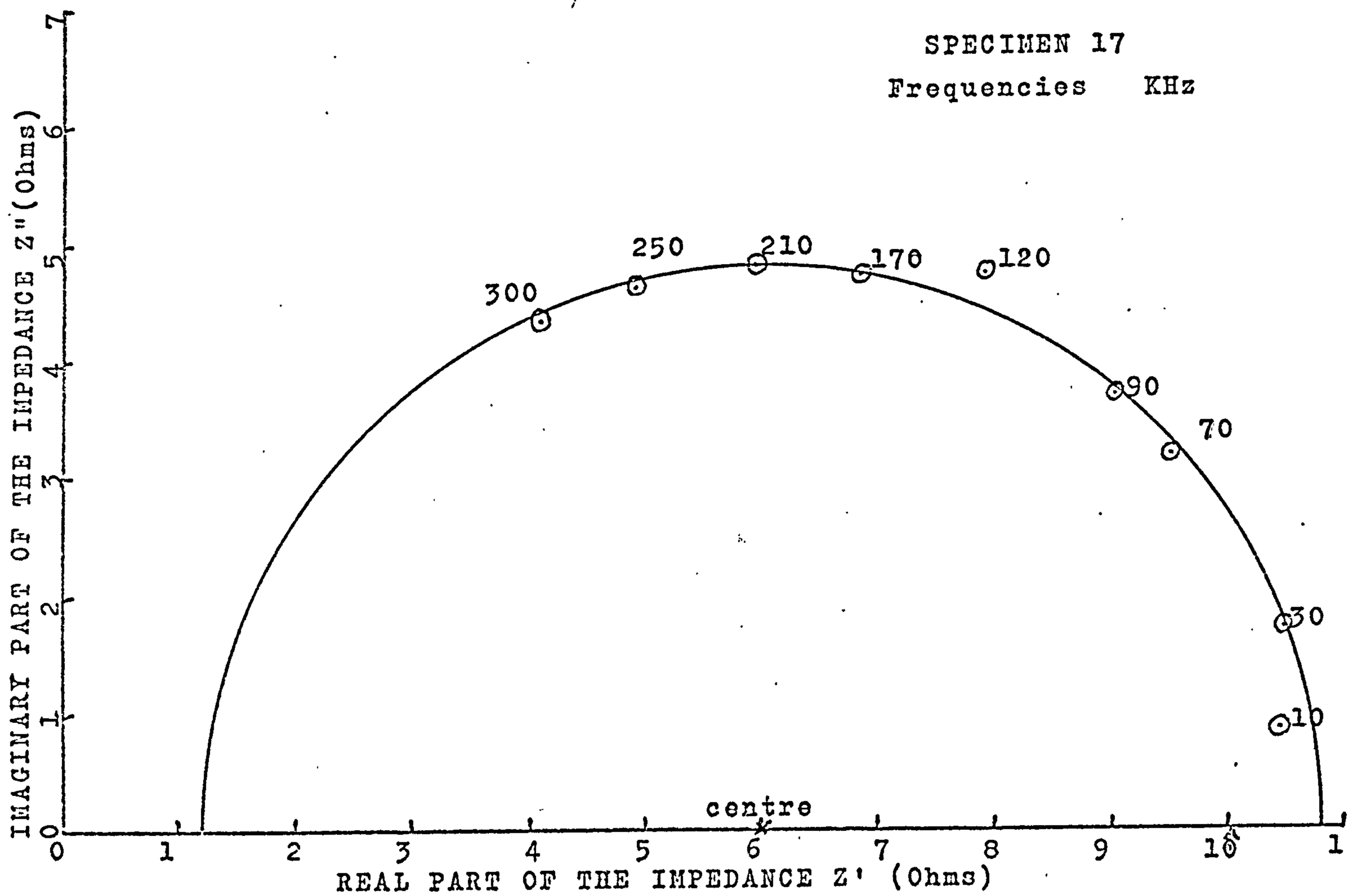

FIG. 4.7 COMPLEX PLANE IMPEDANCE FOR THE SECOND SERIES MEASUREMENTS (SEMI-CIRCLE WITH CENTRE ON THE REAL AXIS)

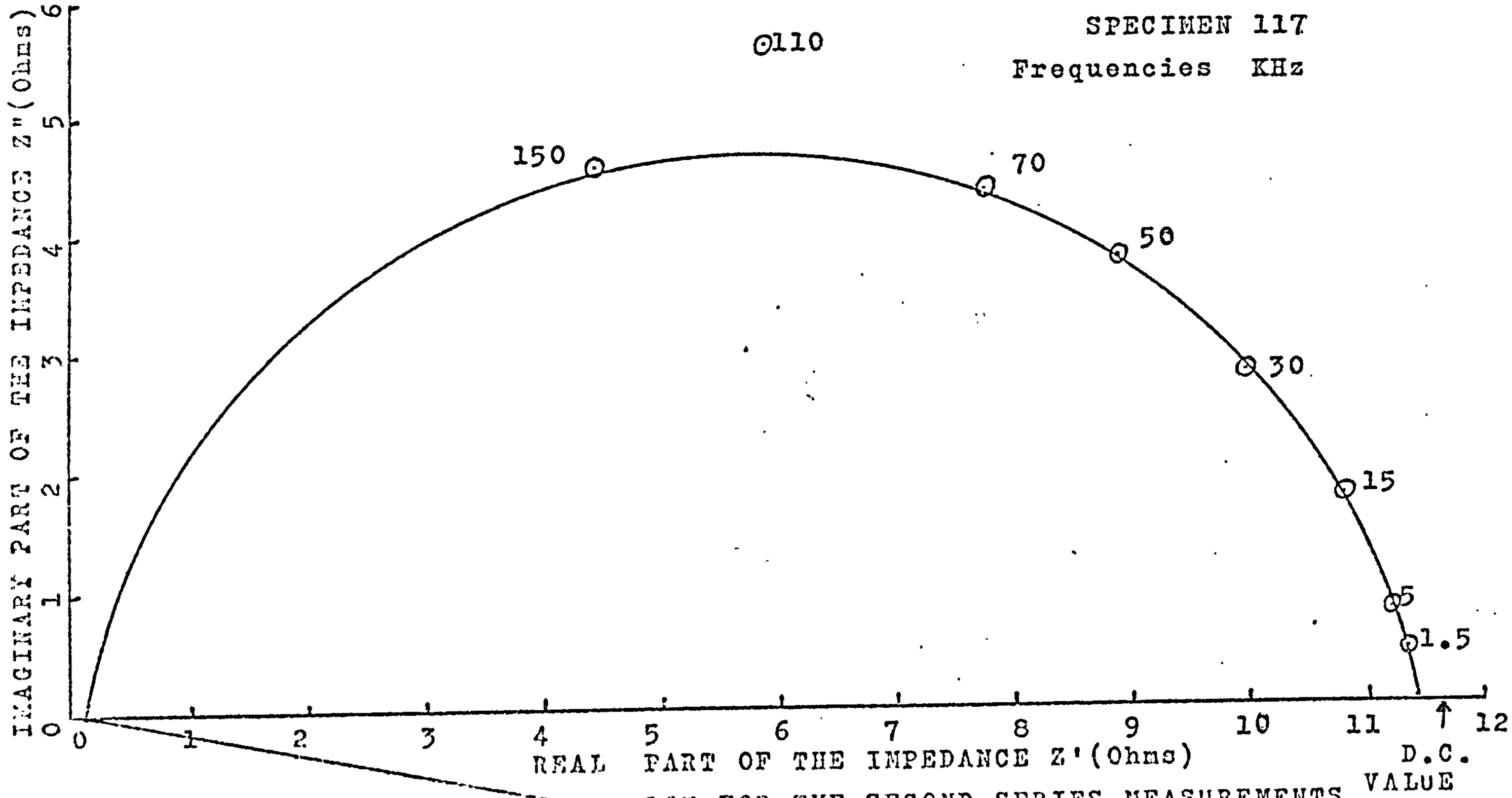

FIG. 4.8 COMPLEX PLANE IMPEDANCE PLOT FOR THE SECOND SERIES MEASUREMENTS (SEMI-CIRCLE WITH CENTRE BELOW REAL AXIS)

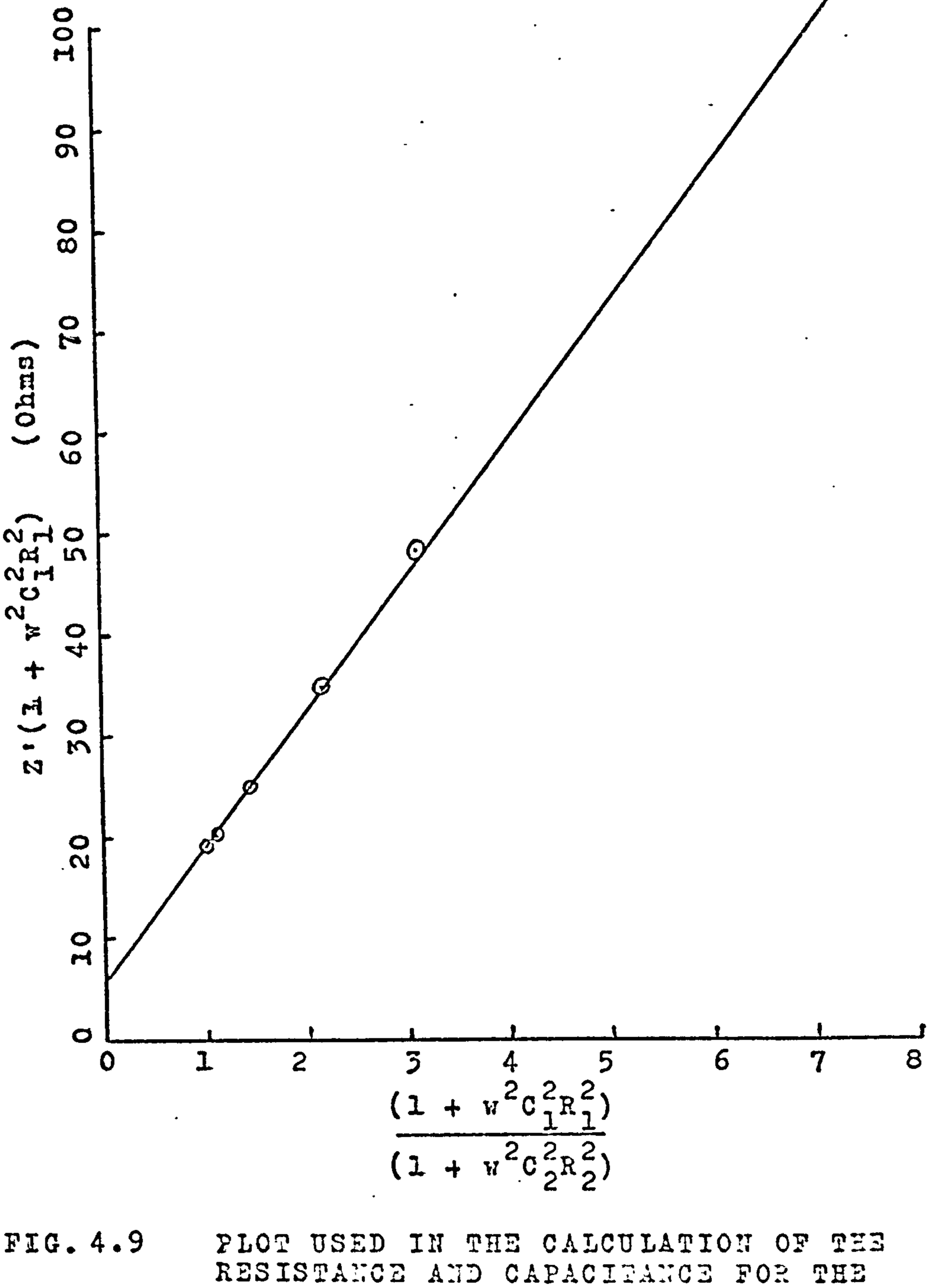

FIG. 4.9 PLOT USED IN THE CALCULATION OF THE RESISTANCE AND CAPACITANCE FOR THE CASE IN WHICH THE CENTRE OF THE SEMI-CIRCLE IS BELOW THE REAL AXIS

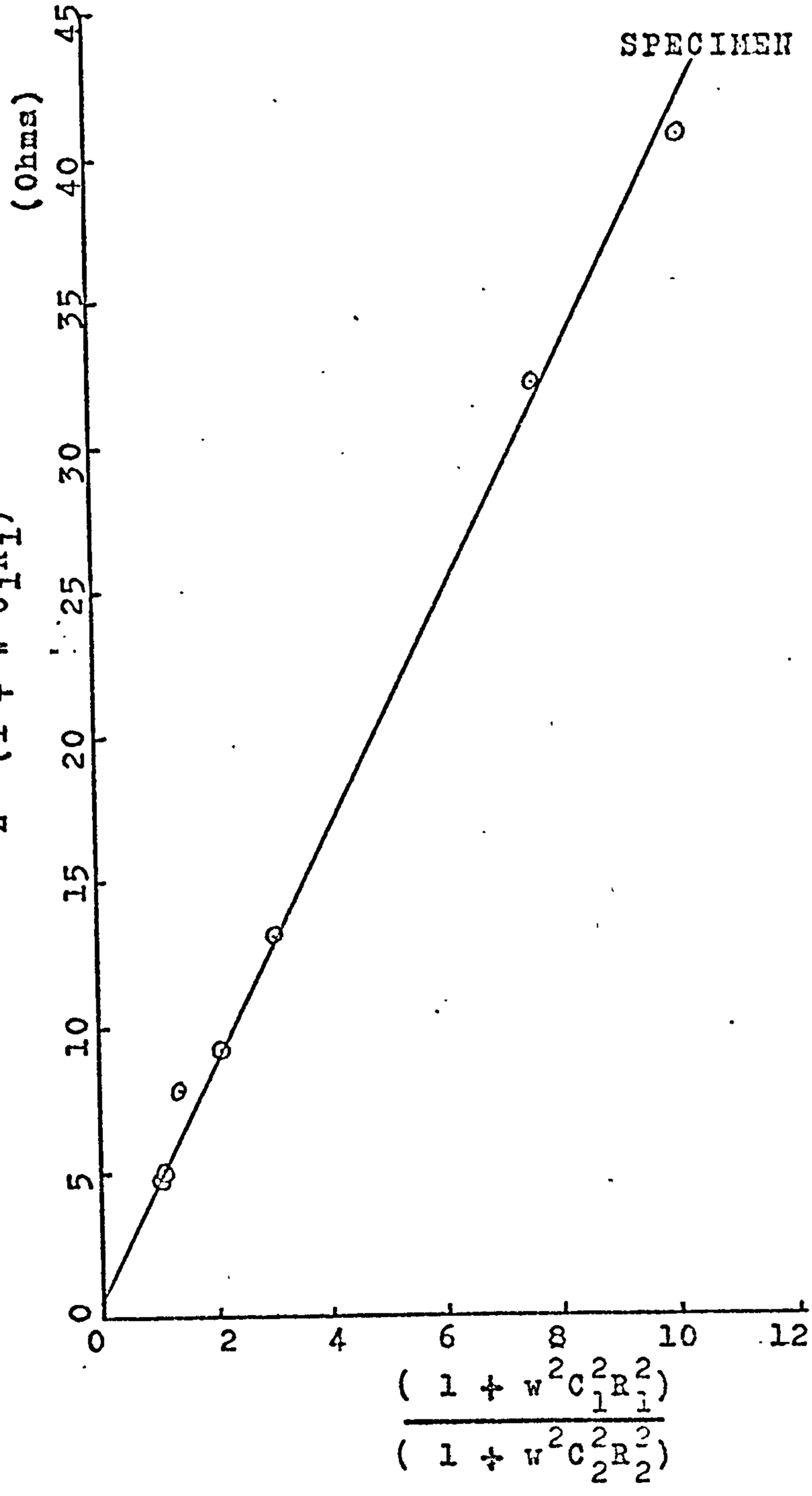

FIG. 4.10 PLOT USED IN THE CALCULATION OF THE RESISTANCE AND CAPACITANCE FOR THE CASE IN WHICH THE CENTRE OF THE SEMI-CIRCLE IS BELOW THE REAL AXIS

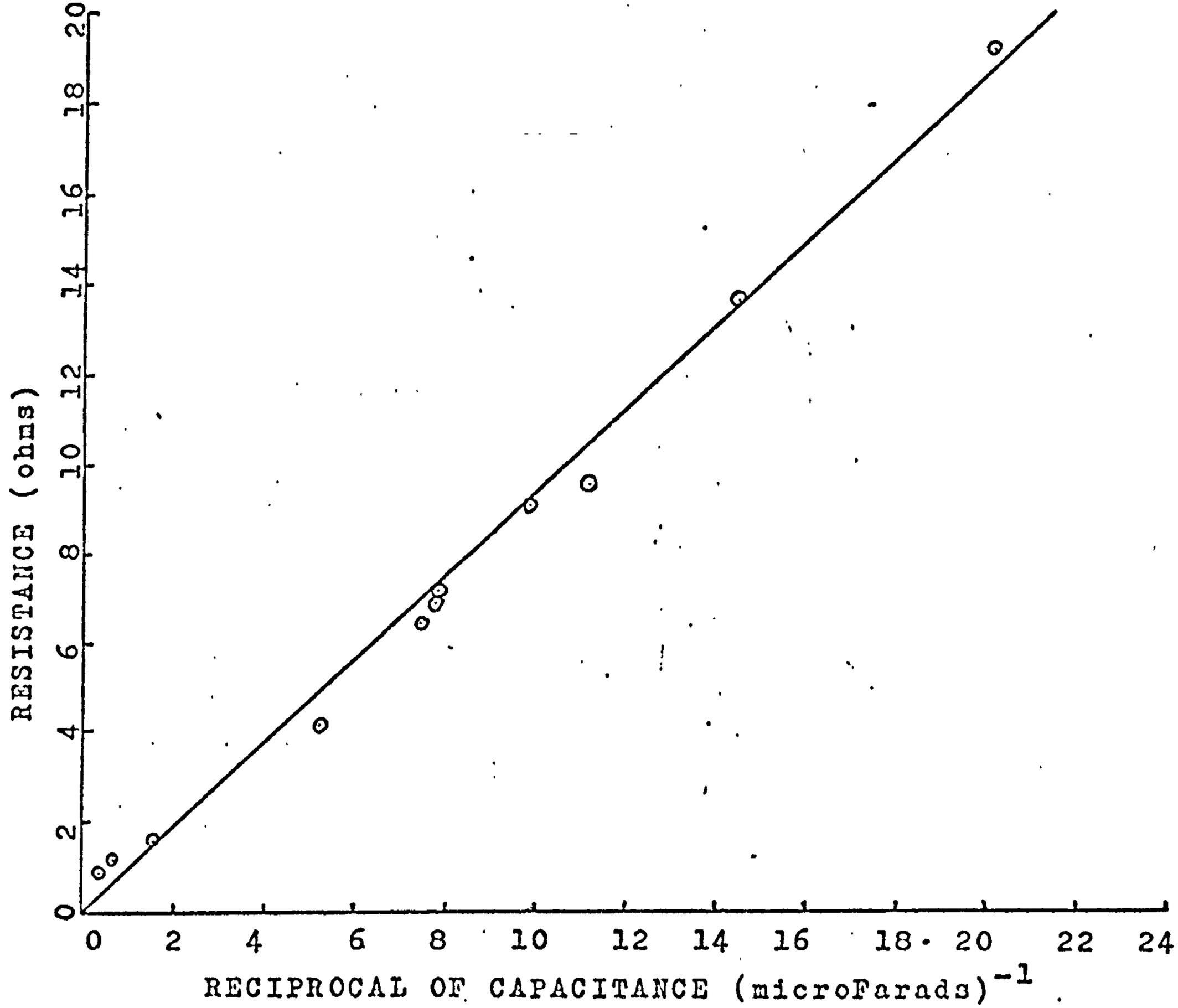

FIG.4.11. RESISTANCE AGAINST RECIPROCAL OF CAPACITANCE.

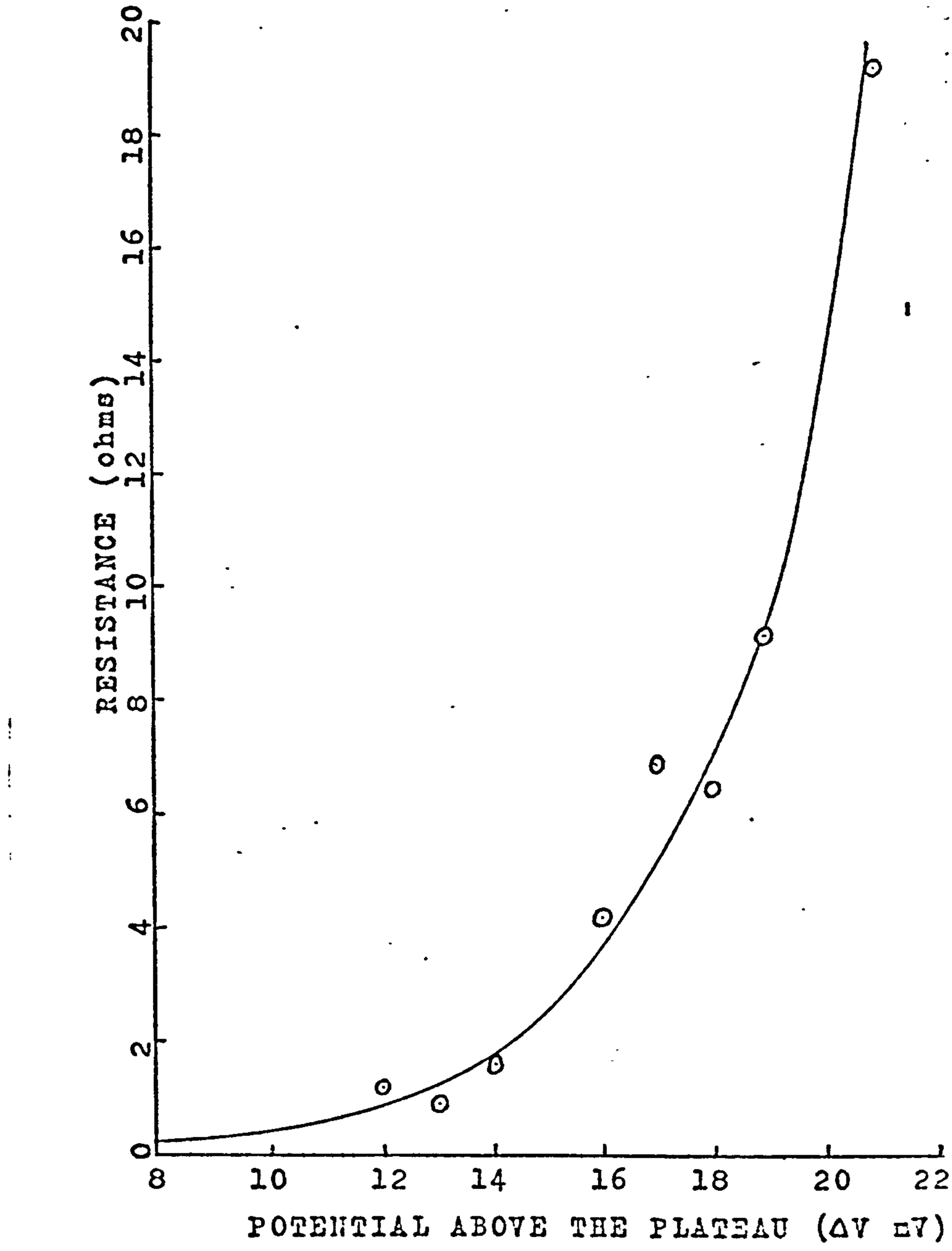

FIG.4.12. RESISTANCE AGAINST POTENTIAL ABOVE THE PLATEAU.

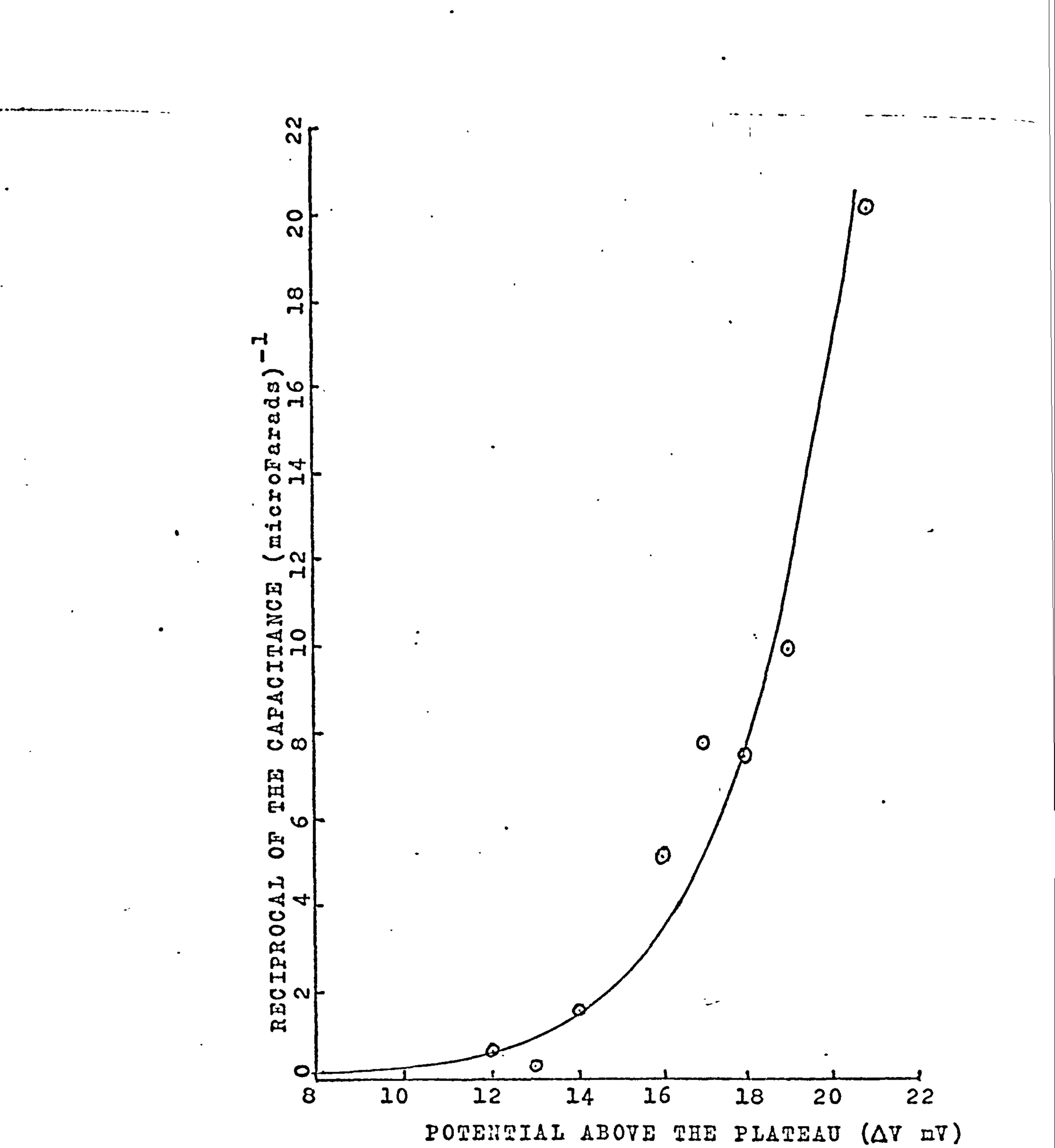

FIG.4.13. RECIPROCAL OF CAPACITANCE AGAINST POTENTIAL ABOVE THE PLATEAU.

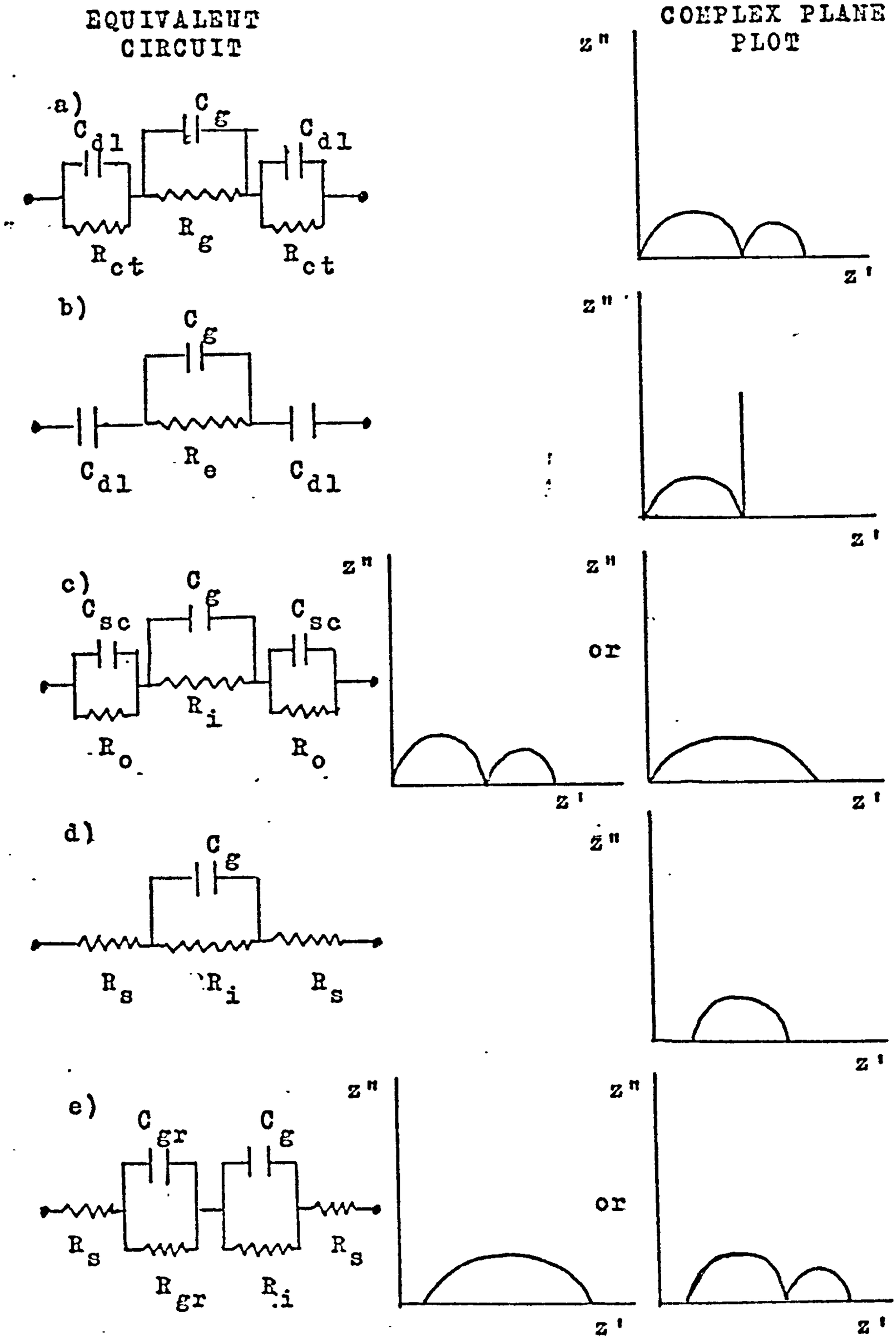

FIG.4.14. EQUIVALENT CIRCUITS AND COMPLEX PLANE PLOTS.

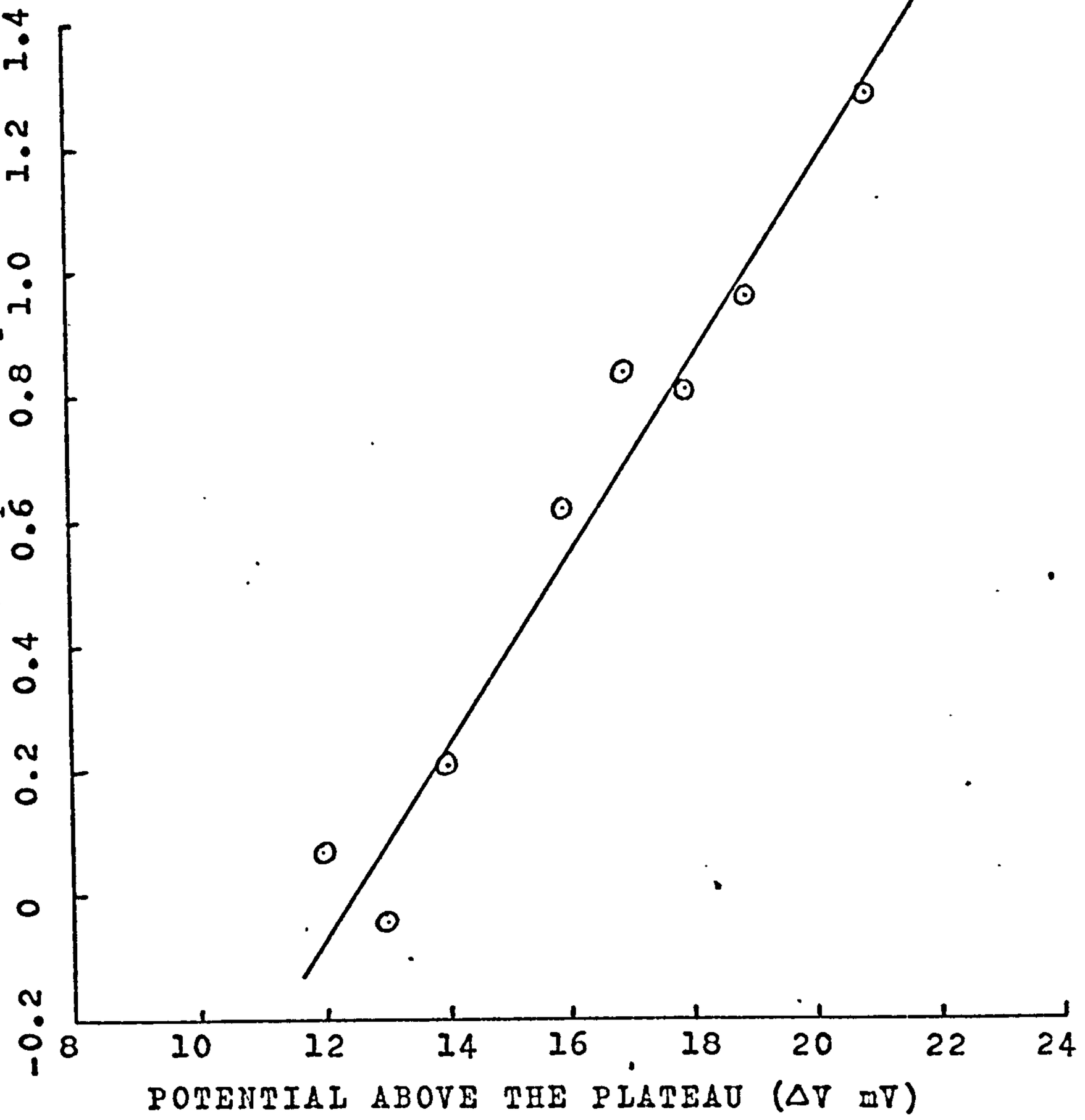

FIG.4.15. LOGARITHM OF THE RESISTANCE AGAINST POTENTIAL ABOVE THE PLATEAU.

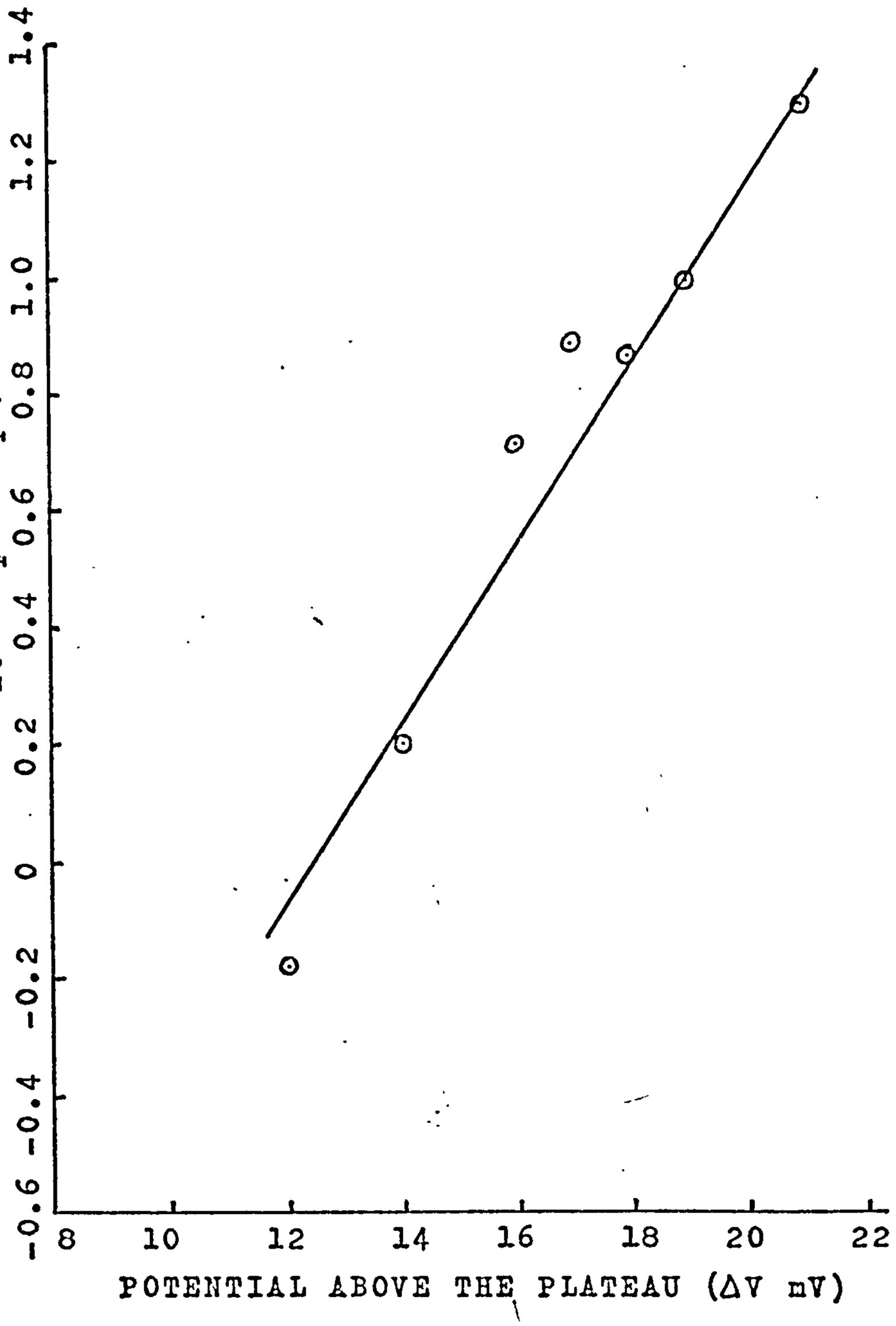

FIG.4.16. LOGARITHM OF THE RECIPROCAL OF THE CAPACITANCE AGAINST POTENTIAL ABOVE THE PLATEAU.

CHAPTER 5

ELECTROCHEMICAL THEORY

The basic electrochemical theory which must be involved in the colouring process will be discussed in this chapter. The application of transition state theory to electrochemical redox reactions will first be described followed by the extension of this theory to metal dissolution reactions. The rate equations obtained for electrochemical reactions and their application to corroding electrodes will then be considered.

5.1. THE APPLICATION OF TRANSITION STATE THEORY TO REDOX REACTIONS

If a redox reaction of the type

$$O^{z+} + ne \rightleftharpoons R^{(z-n)+}$$

is considered, the rate of consumption of the oxidised species O^{z+} will be given by Faraday's Law

$$-\frac{dn_o}{dt} = \frac{\vec{i}A}{nF} \qquad (1)$$

n_o = number of moles of the oxidised form

$\vec{i}$ = current density

F = Faraday constant

A = electrode area

t = time

Assuming the overall reaction to occur in one step and applying the Transition State theory, gives

$$-\frac{dn_o}{dt} = A.l.\frac{kT}{h}\ \frac{a_o}{\gamma_{\pm}}\ \exp\left(-\frac{\Delta G^{\#}}{RT}\right) \qquad (2)$$

l = thickness of the layer containing the ions to be discharged in their initial state

a_o = activity of O^{z+} in it's initial state

$\gamma_{\pm}$ = activity coefficient of the activated complex

$\Delta G^{\#}$ = standard free energy of activation

Combining equations (1) and (2) yields

$$\vec{i} = n.Fl\ \frac{kT}{h}\ \frac{a_o}{\gamma_{\pm}}\ \exp\left(-\frac{\Delta G^{\#}}{RT}\right) \qquad (3)$$

If initially the electrode and the ions to be discharged are at a potential φ_2 with respect to the solution, then a change in the electrode potential to a new potential φ_m will result in a change in the standard free energy of the initial state,given by

$$\Delta G^{o}_{initial} = -nF(\varphi_m - \varphi_2) = -nF\Delta\varphi \qquad (4)$$

If it is assumed that the free energy of the activated state is raised by an amount $-(1-\beta)nF\Delta\varphi$, the change in activation energy will be given by

$$\Delta G_2^{\#} - \Delta G_1^{\#} = -(1-\beta)nF\Delta\varphi - (-nF\Delta\varphi) = +\beta nF\Delta\varphi \qquad (5)$$

The activation energy of the process when the potential is φ_m is thus

$$\Delta G_2^{\#} = \Delta G_1^{\#} + \beta nF\Delta\varphi$$

$$\therefore \quad \vec{i} = nFl \frac{kT}{h} \frac{a_o}{\gamma_{\pm}} \exp - \frac{(\Delta G_1^{\#} + \beta nF\Delta\varphi)}{RT} \qquad (6)$$

Since all the terms on the right hand side of this equation apart from a_o and $\Delta\varphi$ are independent of $\Delta\varphi$ the expression may be rewritten

$$\vec{i} = nF\, k_1''\, a_o \exp\left(- \frac{\beta nF\Delta\varphi}{RT}\right) \qquad (7)$$

a_o is the activity of O^{z+} in the initial state at a potential φ_2. These ions are assumed to be in equilibrium with ions near the electrode but at the potential of the bulk solution (which is taken to be zero) thus,

$$\mu_o^I + zF\varphi_2 = \mu_o^s$$

$$\therefore \quad \mu_o^o + RT \log_e a_o + zF\varphi_2 = \mu_o^o + RT \log_e a_o^s$$

$$\therefore \quad a_o = a_o^s \exp\left(- \frac{zF\varphi_2}{RT}\right) \qquad (8)$$

(the superscript s denotes ions near the electrode but at the potential of the bulk solution).

The applied potential E between the working and reference electrode is $E = \varphi_m - \varphi_R$

$$\text{thus} \qquad \Delta\varphi = (\varphi_m - \varphi_2) = (E + \varphi_R - \varphi_2) \qquad (9)$$

Substituting for $\Delta\varphi$ from equation (9) and a_o from equation (8) in equation (7) gives

$$\vec{i} = nF\, k_1''\, a_o^s \exp\left(- \frac{zF\varphi_2}{RT}\right) \exp\left(- \frac{nF(E + \varphi_R - \varphi_2)}{RT}\right) \qquad (10)$$

The potential φ_R is constant with respect to the bulk of solution and φ_2 is independent of E if concentrated solutions are used or if an excess of inert electrolyte is present. In the latter case the activity coefficients will also be constant so that

$$\vec{i} = nF\, k_1\, c_o^s \exp(-\beta\, nfE) \qquad (11)$$

where $f = \frac{F}{RT}$

A similar derivation for the reverse reaction yields

$$\overleftarrow{i} = nF\, k_{-1}\, c_R^s \exp\{(1-\beta)\, nfE\} \qquad (12)$$

At the reversible potential E_R of the redox system, $\vec{i} = \overleftarrow{i}$.

There is no nett current flow and i_o the exchange current density is defined as $i_o = -\vec{i} = \overleftarrow{i}$

In the case of no nett current flow, the surface and bulk concentrations will be the same, so that

$$i_o = nF\, k_1\, c_o^b \exp(-\beta\, nfE_R)$$

$$= nF\, k_{-1}\, c_R^b \exp\{(1-\beta)\, nfE_R\} \qquad (13)$$

If it is assumed that $c_o^b = c_o^s$ and $c_R^b = c_R^s$ then equations (11) and (13) can be combined to give

$$\vec{i} = i_o \exp\{-\beta\, nf(E - E_R)\} \qquad (14)$$

$(E - E_R)$ is termed the overpotential and is denoted by η

$$\therefore \quad \vec{i} = i_o \exp(-\beta nf\eta) \tag{15}$$

Similarly combining equations (12) and (13) we obtain

$$\overleftarrow{i} = i_o \exp\{(1-\beta) nf\eta\} \tag{16}$$

The nett current flowing is given by

$$i = \vec{i} - \overleftarrow{i} = i_o \{\exp(-\beta nf\eta) - \exp(1-\beta) nf\eta\} \tag{17}$$

This equation relates the nett current flowing to the overpotential η and has two important limiting cases. When η is sufficiently negative ($nf\eta < -60$ mV), the second exponential term in equation (17) may be ignored so that

$$i = i_o \exp(-\beta nf\eta) \tag{18}$$

When η is sufficiently positive, the first exponential term in equation (17) may be ignored so that

$$i = i_o \exp\{(1-\beta) nf\eta\} \tag{19}$$

Plots of log i against η are thus linear in the cases where equations (18) and (19) apply and the slopes of these plots are called Tafel slopes.

5.2. THE EFFECT OF MASS TRANSPORT TO THE ELECTRODE SURFACE

In the treatment given above, it has been assumed that the bulk and surface concentrations of reactants and products are equal

$$c_o^s = c_o^b$$

$$c_R^s = c_R^b$$

Although this may be true in concentrated solutions or for very slow electrode reactions it is often not the case. Transport of material to the electrode surface may occur by, migration of charged species, convection due to stirring or thermal gradients and diffusion as a result of concentration gradients. In the presence of excess supporting electrolyte migration becomes unimportant. If controlled stirring of the solution is employed convection can be maintained. This is assumed to be the case and the contribution of diffusion is first discussed.

The flux of material passing through an imaginary plane of unit area in a solution where the concentration gradient is $\frac{\partial c}{\partial x}$ is given by

$$J = \frac{1}{A}\frac{dN}{dt} = D\frac{\partial c}{\partial x} \qquad (20)$$

if the current density i causes reduction of the oxidised form O^{z+} then

$$i = \frac{nF}{A}\frac{dN}{dt}$$

$$= nFD(\frac{\partial c}{\partial x})_{x=0} \qquad (21)$$

where $(\frac{\partial c}{\partial x})_{x=0}$ is the concentration gradient at the electrode surface. This quantity can be written in terms of the bulk and surface concentrations of O^{z+} and the effective thickness of the diffusion layer δ

$$(\frac{\partial c}{\partial x})_{x=0} = \frac{c_o^b - c_o^s}{\delta}$$

thus, $$i = nFD\frac{(c_o^b - c_o^s)}{\delta} \qquad (22)$$

The value of δ depends on the geometry of the electrode and is constant only when steady state conditions are attained. In studies of electrode kinetics forced convection, for example by stirring, is usually employed to aid the attainment of steady state conditions. The value of δ then depends on the geometry of the electrode and the nature of the stirring employed.

If the potential of the electrode is made more negative so that the current for the removal of O^{z+} is increased there will come a point at which $c_o^s \rightarrow 0$. The current will then be given by

$$\vec{i}_d = \frac{nFD}{\delta}(c_o^b) \qquad (23)$$

The current cannot increase with further increase in potential since it is now limited by diffusion to the electrode. Substituting for δ from equation (23) into equation (22) and rearranging gives

$$c_o^s = \left(\frac{\vec{i}_d - i}{\vec{i}_d}\right) c_o^b \qquad (24)$$

A similar derivation applied to the reverse reaction yields

$$c_R^s = \left(\frac{i_d - i}{\overleftarrow{i}_d}\right) c_R^b \qquad (25)$$

In the derivation of equation (17) it was assumed that the surface concentrations were equal to the bulk concentrations, that is mass transport effects were ignored. Equation (17) may now be corrected for mass transport effects using equations (24) and (25). If equation (24) is used in conjunction with equation (13) to obtain an expression for c_o^s this can be

substituted in equation (11) to yield the corrected version of equation (15)

$$i = i_o \left(\frac{\vec{i}_d - i}{\vec{i}_d}\right) \exp\left(-\beta nf\eta\right) \qquad (26)$$

Similarly the corrected version of equation (16) becomes

$$i = i_o \left(\frac{\overleftarrow{i}_d - i}{\overleftarrow{i}_d}\right) \exp\left[(1-\beta)\, nf\eta\right] \qquad (27)$$

so that the overall equation, corrected for diffusion is

$$i = i - i = i_o \left\{ \left(\frac{\vec{i}_d - i}{\vec{i}_d}\right) \exp\left(-\beta nf\eta\right) - \left(\frac{\overleftarrow{i}_d - i}{\overleftarrow{i}_d}\right) \exp\left[(1-\beta) nf\eta\right] \right\} \qquad (28)$$

If only the forward reaction is important

$$i = i_o \left(\frac{\vec{i}_d - i}{\vec{i}_d}\right) \exp\left(-\beta nf\eta\right) \qquad (29)$$

$$\text{so that} \quad \left(\frac{\vec{i}_d}{\vec{i}_d - i}\right) i = i_o \exp\left(-\beta nf\eta\right) \qquad (30)$$

if this is compared with equation (18) it can be seen that

$$\left(\frac{\vec{i}_d}{\vec{i}_d - i}\right) i = i_k \qquad (31)$$

corresponds to the current that would have been observed in the absence of mass transport effects. This current i_k is, thus, related to the observed current by

$$\frac{1}{i_k} = \frac{1}{i} - \frac{1}{\vec{i}_d} \qquad (32)$$

5.2.1. THE ROTATING DISC ELECTRODE

The importance of the diffusion layer thickness in determining mass transport to electrode surfaces was discussed above. One of the most convenient methods of stirring is to employ a rotating disc electrode. Levich[75] solved the Navier-Stokes equations for transport to an infinite horizontal lamina rotating about a perpendicular axis in an infinite volume of solution and was able to obtain the expression for the thickness of the Nernst diffusion layer for this system. While the exact equation has been derived, it is normally adquate to use the more simple, slightly approximate equation.

$$\delta = 1.61\, D^{\frac{1}{3}}\, \nu^{\frac{1}{6}} \omega^{-\frac{1}{2}} \qquad (33)$$

where D is the diffusion coefficient of the species ($cm^2\ s^{-1}$)

ν the kinematic viscosity of the solution ($cm^2\ s^{-1}$)

ω the angular velocity of the electrode (radian s^{-1})

The rotation speed dependence of the diffusion layer thickness can be used to correct the measured current for the effects of mass transport. For a reaction where the reverse reaction can be neglected, i_k the current density which would have been observed in the absence of diffusion is given by equation (32)

$$\frac{1}{i_k} = \frac{1}{i} - \frac{1}{\vec{i}_d}$$

but $$\vec{i}_d = \frac{nFD}{\delta}\, c_b^o$$

$$\therefore \quad \vec{i}_d = \frac{nFD\, c_b^o}{1.61\, D^{\frac{1}{3}}\, \nu^{\frac{1}{6}}\, \omega^{-\frac{1}{2}}} \qquad (34)$$

$$\therefore \quad \vec{i}_d = B_o \omega^{\frac{1}{2}} c_o^b \qquad \text{where} \qquad B_o = \frac{nFD^{\frac{2}{3}}}{1.61\, v^{\frac{1}{6}}}$$

$$\therefore \quad \frac{1}{i} = \frac{1}{i_k} + \frac{1}{B_o \omega^{\frac{1}{2}} c_o^b} \tag{35}$$

A plot of $\frac{1}{i}$ against $\omega^{-\frac{1}{2}}$ will have an intercept equal to $\frac{1}{i_k}$ so that the current density in the absence of mass transport effects may be calculated.

When the reverse reaction cannot be neglected, a similar treatment yields

$$\frac{1}{i} = \frac{1}{c_o^b k_f - c_R^b k_b} + \frac{(\frac{k_f}{B_o} + \frac{k_b}{B_R})}{c_o^b k_f - c_o^R k_b} \omega^{-\frac{1}{2}} \tag{36}$$

Thus, a plot of $\frac{1}{i}$ against $\omega^{-\frac{1}{2}}$ will have an intercept equal to $\frac{1}{c_o^b k_f - c_R^b k_b}$ which is the reciprocal of the current which would flow if mass transport effects were absent.

5.2.2. CONSIDERATIONS FOR THE DESIGN OF ROTATING DISC ELECTRODES

In order to fulfil the conditions necessary for the application of Levich's theory, certain practical features must be included in the design of the rotating disc electrode.

The diameter of the disc must be large compared with the thickness of the layer of solution dragged around with it. The thickness of this layer, the Prandtl layer, is given by $2.7 (\frac{v}{\omega})^{\frac{1}{2}}$. Moreover the thickness of the disc is considered to be zero so that no edges can cause turbulence in the solution. In order to satisfy these requirements the rotating disc electrode is generally imbedded in an inert insulator. It is also necessary to ensure that the disc surface is flat and that the electrode rotates accurately about it's axis of rotation (eccentric rotation will result in an erroneously, high current).

The distance between the electrode periphery and the cell walls must be at least 0.5 cm to prevent the walls affecting fluid flow in the solution. The Luggin capillary must be small and not too close to the electrode surface to prevent shielding of the electrode and interference to fluid flow.

The rotation speed must be such that laminar flow to the electrode surface occurs, if rotation speeds are too low then natural convection will affect the flow of solution to the electrode surface, if it is too high then turbulence will ensue. The limits of application of the theory are that the Reynolds number $Re = \frac{a^2\omega}{\nu}$ (a = disc radius/cm) must lie between 10^2 and 5×10^4.

5.3. METAL DISSOLUTION

The process of metal dissolution can be understood in terms of the theory developed above. The problem essentially reduces, as with that of the redox reaction discussed above to the effect of the applied potential on the activation energies for the anodic and cathodic processes. An equation for the current density at a given potential for the reaction

$$M \rightleftharpoons M^{z+} + ze$$

may be derived[76-78] which differs from that for redox reactions only in the charge transfer valency z

$$i = i_o \left\{ \exp\left(\frac{\alpha z F \eta}{RT}\right) - \exp\left(-(1-\alpha)\frac{zF}{RT}\eta\right)\right\} \qquad (37)$$

The dissolution of the metal may, however, be complicated by other factors;

a) In aqueous solutions metal dissolution reactions often involve the participation of an anion from solution, e.g.,

$$M + OH^- = MOH + e$$

$$MOH + OH^- = M^{2+} + 2OH^- + e$$

b) The rate determining step generally changes with potential, whilst the charge transfer process is rate determining at high overpotentials other processes such as nucleation and growth of holes in the metal surface can be rate determining at low overpotentials.

c) The dissolution reaction may be affected by the formation of surface films.

5.4. THE APPLICATION OF ELECTROCHEMICAL THEORY TO CORROSION

5.4.1. THE STERN-GEARY METHOD

This method of evaluating corrosion rates has often been applied to corroding systems. It is described here for two reasons. First it s derivation represents an attempt to relate the electrochemical theory described earlier to the corroding electrode and is consequently relevant to the application of this theory to the processes occurring during the colouring process. Second, the possibility of its use in determining the rate of metal dissolution during the colouring process.

As shown earlier an exponential dependence of the current density on electrode potential can be predicted theoretically for both redox reactions at inert electrodes and metal dissolution reactions. In Chapter 1 the qualitative treatment of corrosion by superposition of the current-

potential curves for the anodic and cathodic partial processes was described. A quantitative treatment of the corroding electrode was developed by Stern and Geary[79], who used the exponential dependence of the current on potential in conjunction with the principle of superposition.

Stern and Geary considered the two coexisting reactions that occur at the surface of the corroding metal; the oxidation-reduction system constituting the cathodic process

$$z^+ + e \rightleftharpoons z$$

and the dissolution-deposition reaction of the metal, the anodic process

$$M^+ + e \rightleftharpoons M$$

When the corrosion potential is sufficiently far from the equilibrium potentials of these reactions, the steady state potential will be attained when the rate of metal oxidation equals the rate of reduction of z

$$\vec{i}_z = \overleftarrow{i}_m \qquad (38)$$

The corrosion rate i_{corr} will be equal to the rate of metal oxidation so that

$$i_{corr} = \vec{i}_z = \overleftarrow{i}_m \qquad (39)$$

If the dependence of the current density for metal dissolution on potential is given by,

$$\overleftarrow{i}_m = i_{o,m} \exp\left(+\frac{\eta_m}{b_m}\right) \qquad (40)$$

and the dependence of current density on potential for reduction of z by,

$$\overrightarrow{i}_z = i_{o,z} \exp\left(-\frac{\eta_z}{b_z}\right) \qquad (41)$$

then since $\eta_m = E - E_R^m$ and $\eta_z = E - E_R^z$

$$\overleftarrow{i}_m = i_{o,m} \exp\left(\frac{E - E_R^m}{b_m}\right) \qquad (42)$$

and

$$\overrightarrow{i}_z = i_{o,z} \exp - \left(\frac{E - E_R^z}{b_z}\right) \qquad (43)$$

At the corrosion potential $E = E_c$

and

$$i_{corr} = \overleftarrow{i}_m = \overrightarrow{i}_z$$

$$\therefore \quad i_{corr} = i_{o,m} \exp\left(\frac{E_c - E_R^m}{b_m}\right)$$

$$= i_{o,z} \exp - \left(\frac{E_c - E_R^z}{b_z}\right) \qquad (44)$$

so that substituting for $i_{o,m}$ in equation (42) and $i_{o,z}$ in equation (43)

$$\overleftarrow{i}_m = i_{corr} \exp \frac{E - E_c}{b_m} \qquad (45)$$

$$\overrightarrow{i}_z = i_{corr} \exp - \left(\frac{E - E_c}{b_z}\right) \qquad (46)$$

The nett current flowing at a potential E is thus,

$$i = \overleftarrow{i}_m - \overrightarrow{i}_z = i_{corr} \left\{ \exp\left(\frac{E - E_c}{b_m}\right) - \exp - \left(\frac{E - E_c}{b_z}\right) \right\} \qquad (47)$$

Denoting $E - E_c$ as ε and linearising the exponential terms in equation (47) gives on rearranging,

$$i = i_{corr}\,\varepsilon\,\left(\frac{1}{b_m} + \frac{1}{b_z}\right) \qquad (48)$$

Stern and Geary thus predicted a linear relation between the current and applied potential when the latter is close to the corrosion potential E_c. The actual value of the corrosion current could be obtained from the slope of the current-potential curve at the corrosion potential

$$\left(\frac{d\varepsilon}{di}\right)_{\varepsilon\to 0} = \frac{b_z\, b_m}{i_{corr}\,(b_z + b_m)} \qquad (49)$$

The application of this method of determining corrosion rates, known as the linear polarisation method, or the polarisation resistance method, was discussed in more detail by Stern in a later paper[80].

The assumptions made in the derivation of the Stern-Geary equation were discussed by Oldham and Mansfeld[81]. The derivation assumes that:

1) The equations of electrochemical kinetics are valid.

2) Ohmic potential drops and concentration polarisation are absent.

3) The corrosion potential does not lie close to the reversible potentials of the metal/metal ion or redox couples.

4) The whole electrode functions simultaneously as a cathode and an anode rather than being a mosaic of separate anodic areas.

5) That there are no secondary electrochemical reactions.

6) That no thick film of corrosion products covers the electrode surface.

Oldham and Mansfeld[82] have also derived the Stern-Geary equation by a method which does not require linearisation of the exponential terms

in equation (10). This derivation also shows that the polarisation curve will be linear near the corrosion potential only under special circumstances.

Subsequently these authors presented[83] a more general treatment of corrosion processes, which did not require assumption 3 to apply. The equation they obtained reduces to the Stern-Geary equation when this assumption is introduced. An outline of the more general treatment is given below.

Making use of the current-potential relationships for both the forward and reverse reactions for metal dissolution and the oxidation-reduction reaction, an expression for the current in terms of the applied potential is obtained

$$i = i_{o,z} \exp\left(\frac{E - E_R^z}{b_a^z}\right) - i_{o,z} \exp\left(\frac{E_R^z - E}{b_c^z}\right) + i_{o,m} \exp\left(\frac{E - E_R^m}{b_a^m}\right) - i_{o,m} \exp\left(\frac{E_R^m - E}{b_c^m}\right) \quad (50)$$

This equation is rearranged using the relationships

$$\frac{1}{b_a^z} + \frac{1}{b_c^z} = \frac{n_1 F}{RT}$$

$$\frac{1}{b_a^m} + \frac{1}{b_c^m} = \frac{n_2 F}{RT}$$

to give an expression which is differentiated with respect to potential in order to obtain the slope $(\frac{\partial i}{\partial E})$. The value of this slope at the corrosion potential, obtained by the substitution of E_c for E is obtained as

$$\left(\frac{\partial i}{\partial E}\right)_{E_c} = i_c \left\{ \frac{1}{b_a^z} + \frac{1}{b_c^m} + \frac{n_1 F}{RT} \left(\exp\left(\frac{n_1 F \Delta E_1}{RT}\right) - 1 \right)^{-1} + \frac{n_2 F}{RT} \left(\exp\left(\frac{n_2 F \Delta E_2}{RT}\right) - 1 \right)^{-1} \right\} \quad (51)$$

where $\Delta E_1 = E_c - E_R^z$

$\Delta E_2 = E_R^m - E_c$

This equation reduces to the Stern-Geary equation in the case where the corrosion potential is far from the equilibrium potential of either the metal dissolution deposition or redox couples. Thus when

$$n_1 \Delta E_1 \gg \frac{RT}{F} \ll n_2 \Delta E_2$$

$$\left(\frac{\partial i}{\partial E}\right)_{E = E_c} = i_{corr} \left\{ \frac{1}{b_a^z} + \frac{1}{b_c^m} \right\} \qquad (52)$$

In cases where the corrosion potential is near the reversible potential of the redox couple i.e.

$$n_1 \Delta E_1 < \frac{RT}{F} \ll n_2 \Delta E_2$$

the general equation reduces to

$$\left(\frac{\partial i}{\partial E}\right)_{E = E_c} = i_{corr} \left\{ \frac{1}{b_a^z} + \frac{1}{b_c^m} + \frac{1}{\Delta E_1} - \frac{n_1 F}{2RT} \right\} \qquad (53)$$

In cases where the corrosion potential is near to that of metal dissolution, i.e.

$$n_2 \Delta E_2 < \frac{RT}{F} \ll n_1 \Delta E_1$$

we obtain $$\left(\frac{\partial i}{\partial E}\right)_{E = E_c} = i_{corr} \left\{ \frac{1}{b_a^z} + \frac{1}{b_c^m} + \frac{1}{\Delta E_2} - \frac{n_2 F}{2RT} \right\} \qquad (54)$$

Alternatively a more general approximation of equation (51) may be used

$$\left(\frac{\partial i}{\partial E}\right)_{E = E_c} = i_{corr}\left\{\frac{1}{b_a^z} + \frac{1}{b_c^m} + \frac{1}{\Delta E_1} + \frac{1}{\Delta E_2}\right\} \qquad (55)$$

These relationships can be used to calculate the corrosion current at potentials including those which are close to the reversible potentials of either the redox process or the metal dissolution process.

5.4.2. MEASUREMENT OF CORROSION RATES

Several methods of determining the corrosion current have been discussed by Oldham and Mansfeld. The original method of Stern and Geary may be applied, but this requires either the determination or more usually an assumption of the anodic and cathodic Tafel slopes. Alternatively, regions of the polarisation curve which exhibit Tafel behaviour can be extrapolated back to the corrosion potential to obtain the corrosion current, since for potentials sufficiently far from the corrosion potential,

$$i = i_{corr} \exp \frac{(E - E_c)}{b_m}$$

$$\log i = \log i_{corr} + \left(\frac{E - E_c}{b_m}\right)$$

$$\therefore \text{ at } \quad E = E_c, \log i = \log i_{corr}$$

This method has the disadvantage that the regions where Tafel behaviour is exhibited lie far from the corrosion potential and there is a strong possibility of changes in the nature of the electrode surface.

81

Oldham and Mansfeld propose a graphical method which allows the determination of the corrosion current from polarisation data obtained at potentials between those used for the Stern-Geary method and those used to obtain Tafel plots. This method does not require an assumption of Tafel

constants. In a later paper[84] Mansfeld also discusses a method of obtaining the Tafel slope and the polarisation resistance simultaneously, from the polarisation curve in the region of the corrosion potential which would allow the determination of the corrosion rate as a function of time. This method is based on the Stern-Geary equation. The Tafel coefficients are obtained by a curve fitting procedure which compares the data obtained from polarisation measurements with data calculated from assumed theoretical values of the Tafel coefficients. The Tafel coefficients obtained are then used to obtain an accurate value of the corrosion current.

5.4.3. CONCLUSION

During the formation of the film on the coloured stainless steel the potential rises quite rapidly initially ($\sim$100 mV minute^{-1}) followed by a region in which the potential rises reasonably slowly (1 mV minute^{-1}). It is clear therefore that if the potential of the stainless steel electrode is to be regarded as a corrosion potential, a treatment which allows for a variation in corrosion potential with time must be used. The method of Oldham would thus appear the most suitable, since it does not require an assumption of the Tafel slopes and can be used in situations where the corrosion potential varies with time. Although this method[84] has been applied by Mansfeld to determine the corrosion rate in a situation where the corrosion potential is time dependent the rate of potential variation with time was extremely slow compared with that during the colouring process.

The fundamental difficulty with the application of the Stern-Geary type of approach to the colouring process is, that it is assumed that changes of the potential near the corrosion potential affect only the rates of the metal dissolution deposition and oxidation reduction reactions. In

the case of the colouring process, however, even very small changes in potential (1 mV) produce changes in the nature of the film present on the surface of the steel (either changes in composition between the induction and colouring regions or changes in thickness in the colouring region).

CHAPTER 6

EXPERIMENTAL TECHNIQUES AND APPARATUS

6.1. ELECTROCHEMICAL CELLS

Two cells were used in this investigation; the first was used principally for the work on the reduction of dichromate at gold and platinum electrodes, the second was used for studies of the behaviour of stainless steel in 2.5M chromic acid, 5M sulphuric acid. Both cells were made from Pyrex glass.

The first cell (Fig. 6.1) consisted of three compartments, housing the working electrode, counter electrode and reference electrodes respectively. The first two compartments were separated by a sintered glass frit. The reference electrode chamber was connected to the working electrode compartment by a Luggin capillary which entered the cell through a Sovereil screw fitting. Diffusion between the reference electrode chamber and the working electrode compartment was minimised by a solution-sealed tap. Reflux condensers were mounted both on the working electrode compartment and the counter electrode compartment (in the positions shown in Fig. 6.1) to prevent evaporation of the solution. The counter electrode was introduced into the cell through the reflux condenser. The working electrode was inserted through a central socket, which fitted the Teflon cone on the bearing housing (Section 6.2). This cell was used in a thermostatically controlled oil bath. As a result of the unpleasant fumes from the oil, water (covered with polystyrene balls to reduce evaporation) replaced the oil in the experiments with cell two.

The second cell Fig. 6.2 consisted of four compartments to accommodate the working electrode, counter electrode and reference electrode

and provide a reservoir for solution. The reservoir was included so that the working electrode contained within its own almost empty compartment, could be rapidly immersed in the solution maintained at the temperature of the thermostatic bath. To do so solution from the reservoir was forced into the working electrode compartment using nitrogen. The counter and working electrode compartments were fitted with reflux condensers to prevent solution evaporation. Initially the reference electrode compartment was attached to the body of the cell using a Sovereil screw fitting and a Teflon seal, diffusion of cell solution to the reference compartment being prevented by a liquid-sealed tap. Although this arrangement proved satisfactory when used in an oil bath, it resulted in conduction from both the tap and the screw fitting via the water in the thermostatic bath to the bath itself. This caused instability in the potentiostat and erratic behaviour of the stainless steel electrode on open circuit. Satisfactory results were obtained when the Luggin capillary was sealed into the cell and a sintered glass frit replaced the solution-sealed tap.

6.2. ROTATING DISC ASSEMBLY

The rotating disc electrode was driven indirectly using two sets of bearings and nylon gear wheels (Fig. 6.3). The electrode was mounted on a shaft which passed through one set of bearings and a Teflon cone attached to the bearing housing. The cell was clamped onto the Teflon cone so that the electrode was seated centrally in the cell.

The servo motor (Section 6.4) bearings and clamp were all attached to an aluminium backplate which could be raised or lowered to allow easy installation of the cell into the thermostatic bath.

The electrode drivewas modified for experiments to determine the rotation speed dependence of the potential-time curve. It was thought that

heat losses from the electrode, through the drive shaft to the rest of the electrode drive assembly, would result in the electrode taking rather a long time to reach 70°C. Moreover the rate at which heat was supplied to the electrode, from the hot solution, would depend on its rotation speed. Thus the time required for the electrode to reach 70°C would have a rotation speed dependence and this could swamp any effects due to mass transport. To reduce the effects of heat loss, a tube was used as the electrode drive shaft and the end of this tube covered with Teflon (Fig.6.4) to act as a thermal insulation between the electrode holder section and the tube. Electrical contact was made to the electrode using an insulated wire which passed down the centre of the tube and made contact to the electrode tip at the bottom and the mercury pool at the top.

The electrode which was of the second type described below was attached to the shaft by three grub screws at 120° to each other. The electrode was positioned so that the grub screws screwed onto the Teflon covered part of the shaft to prevent heat losses from the electrode.

6.2.1. ELECTRODES

Three different rotating disc electrode designs were employed. The first (Fig. 6.5) consisted of a brass tube which was attached to drive shaft by three grub screws at 120° to each other. A ½" diameter brass rod was soldered onto the brass tube and the bottom of the rod was machined down and threaded. Stainless steel specimens (EN 58 AM) could be tapped and screwed onto the brass rod. The brass tube was covered with Teflon and a Teflon cap covered the top of the electrode holder. The brass rod, stainless steel specimen and the electrode drive shaft were covered with shrink wrap Teflon. (Pope Scientific Inc.).

The stainless steel specimen could be removed from the assembly,

by cutting the shrink wrap Teflon and unscrewing the specimen. Electrical contact was made to the electrode through a mercury contact in the top of the electrode drive shaft.

A second electrode holder was used to mount stainless steel sheet specimens. Instead of tapping the rod as described above the rod was left with a flat end. Stainless steel sheet (EN 58 E) was punched into discs and the discs were attached to the brass rod using conducting araldite and sealed by means of shrink wrap Teflon.

The use of shrink wrap Teflon to insulate the sides of the electrode and its holder was found to be reasonably successful although leakage of the electrolyte, around the sides of the electrode, sometimes occurred. In an attempt to overcome these leakage problems, and produce a readily re-usable electrode holder a third electrode design (Fig. 6.6) was used. The electrode tip and the hole in the bottom of the electrode holder were made in the form of truncated cones. A spring on the electrode drive shaft applied pressure to the electrode tip to ensure contact between it and the electrode holder and thus prevent solution creeping between them. The electrode holder was made out of Kel-F rather than Teflon because of its better mechanical properties. This design, however, was found particularly prone to leakage, partly because of the elevated temperature used in the experiments and partly because the stainless steel, is much harder than Kel-F (this design has been found suitable for soft metals such as tin, at room temperature).

The surface of electrodes prepared from steel rod were polished using successively finer grades of alumina (down to fine polishing alumina) (Griffin and George Ltd.) held on Selvyt cloth. They were then well washed with purified water (Section 6.3) degreased in acetone and again washed with purified water. Electrodes or specimens prepared from stainless steel sheet already had polished surfaces. They were cleaned by degreasing in acetone.

and washing with purified water.

6.3. REFERENCE ELECTRODES

The reference electrodes used in this work were a hydrogen reference electrode in 5M sulphuric acid at 70°C and a commercial saturated calomel electrode (E.I.L.) which was immersed in 5M sulphuric acid at 70°C. The hydrogen reference electrode was prepared by platinising a platinum electrode in accordance with the procedure described by Spiro[85]. The potentials in this thesis are all quoted with respect to the saturated calomel electrode.

PREPARATION OF SOLUTIONS

Sulphuric acid and chromic acid/sulphuric acid solutions were prepared from Aristar sulphuric acid (B.D.H.) and Analar chromic acid (B.D.H.). The water used in the preparation of solutions was purified by passing oxygen through distilled water at 98-99°C for 12 hours and then redistilling the water in an oxygen atmosphere. This procedure, described by Powers[86], produces high purity water with a very low conductivity.

6.4. ELECTRICAL APPARATUS

The potentiostat used for this work was a Chemical Electronics TR70/2A potentiostat. Current-potential curves were obtained using a linear sweep generator, built in this department, in conjunction with the potentiostat and were recorded on a Bryans 24000 X-Y recorder. A Servoscribe Y-t recorder was used to record the potential-time curves and the variation of current with time at fixed potentials.

A Tamson thermostatic bath was used to maintain the temperature of the cell constant to within $\pm$ 0.5°C.

The rotating disc electrodes were driven by a velodyne motor-generator unit. In this both the motor and generator are mounted on the same shaft. This allows the rotation speed of the motor to be controlled by a servo amplifier controlled from the output of the generator. Rotation speeds were measured using an Advance Tachoratiometer and a magnetic transducer. The pulses in the transducer were generated by a 60 toothed soft iron wheel mounted on the motor shaft and these were converted to a direct reading of the electrode rotation speed by the Tachoratiometer.

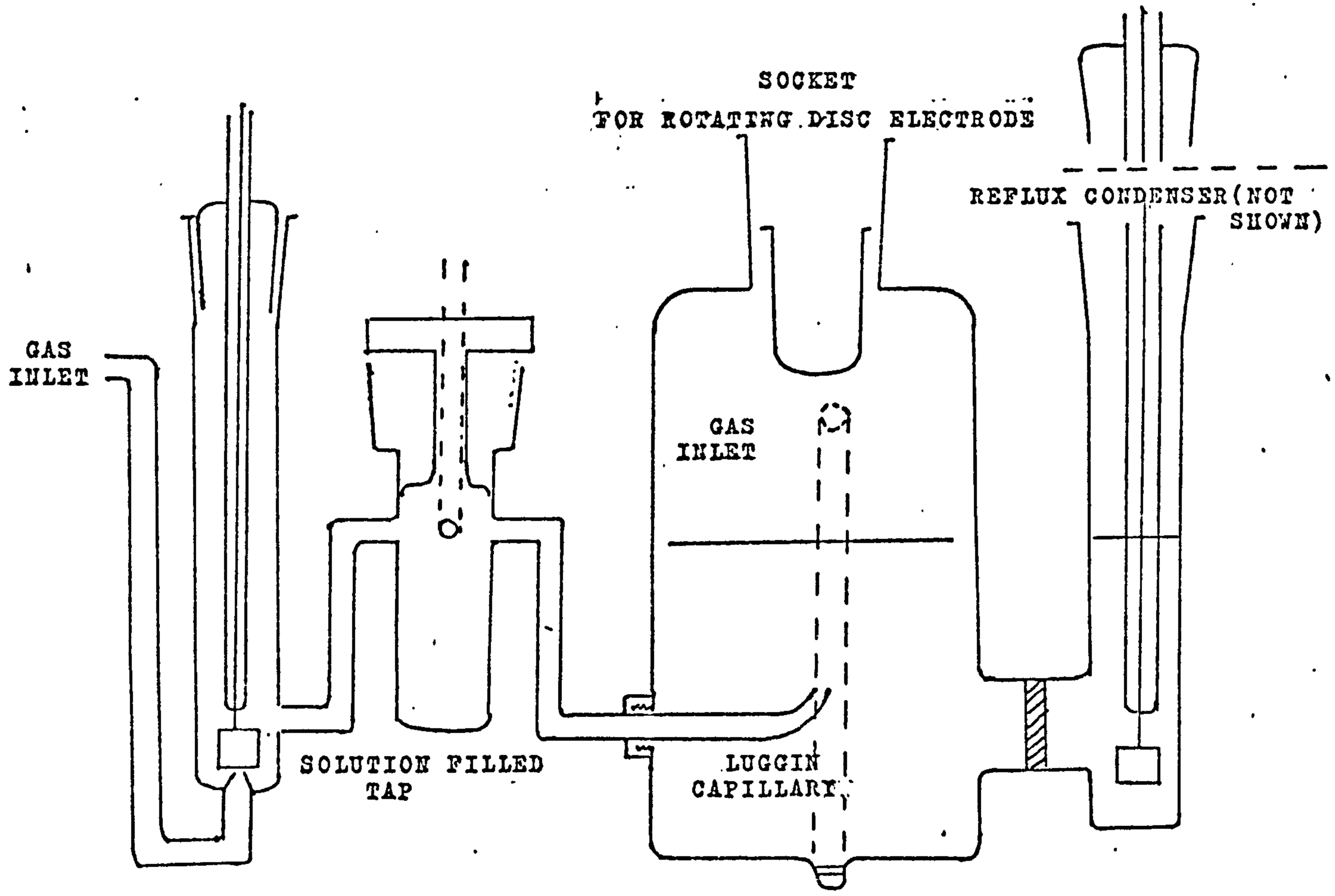

FIG. 6.1 ELECTROCHEMICAL CELL (CELL 1)

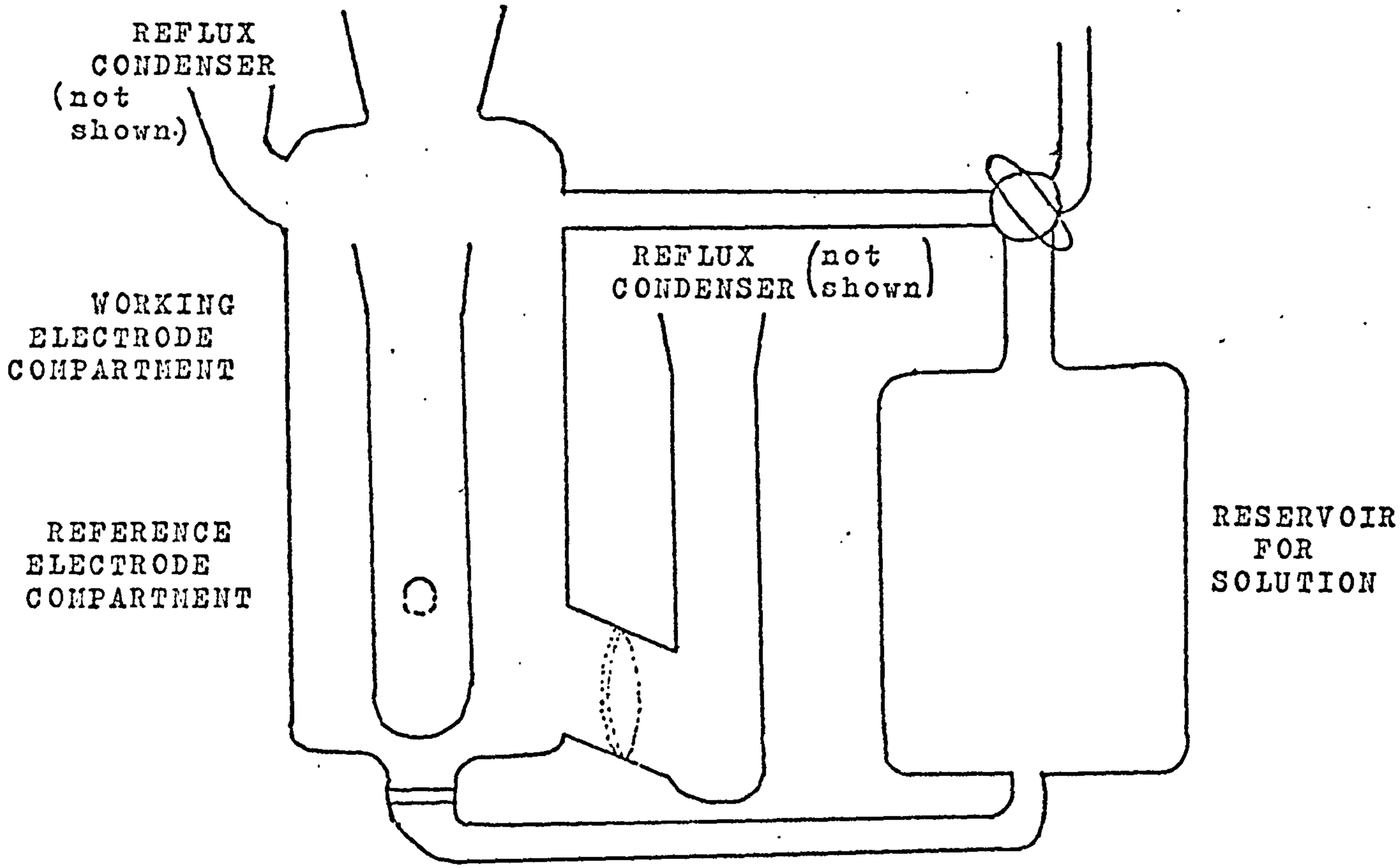

FIG. 6.2 ELECTROCHEMICAL CELL (CELL 2)

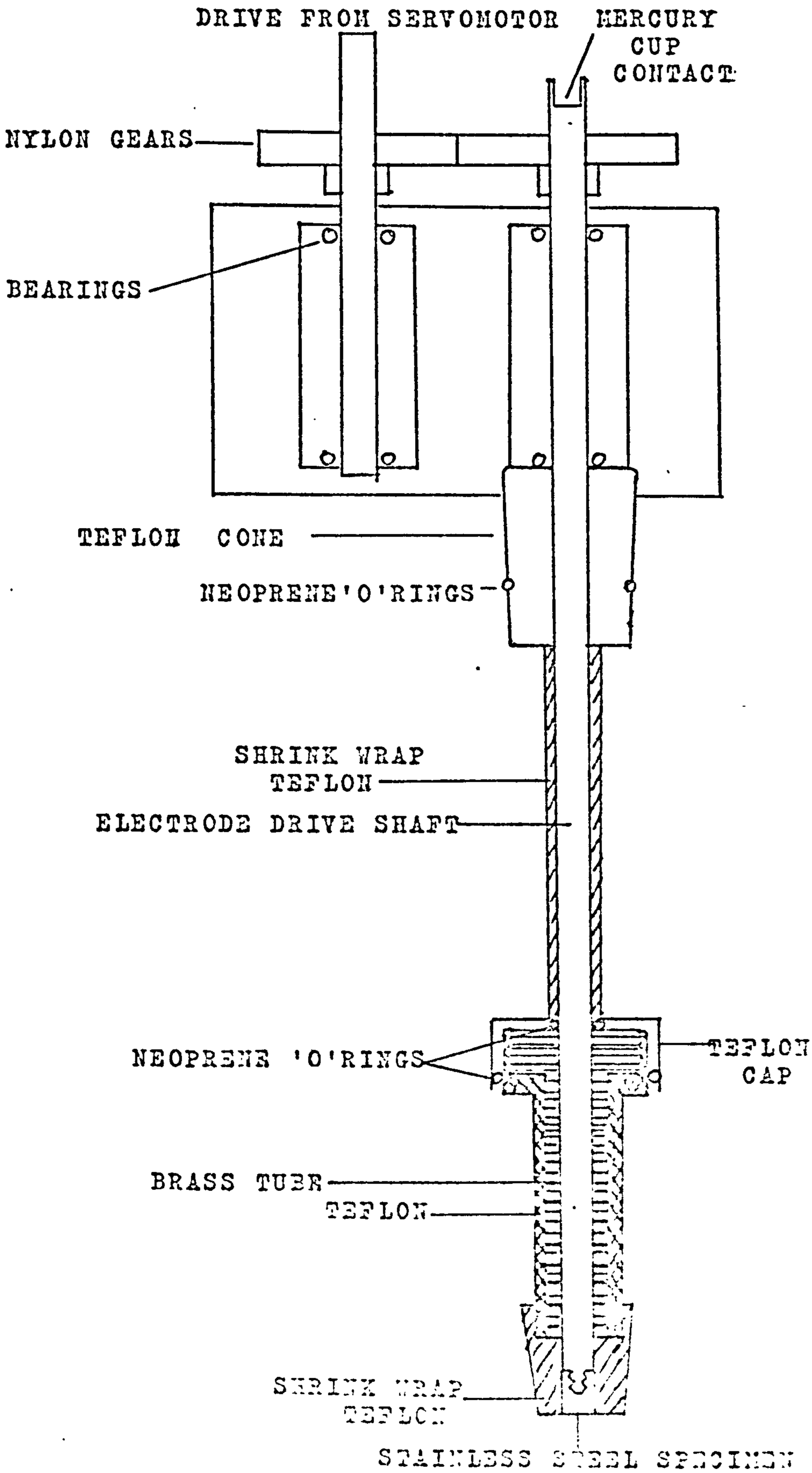

FIG. 6.3 ROTATING DISC ASSEMBLY

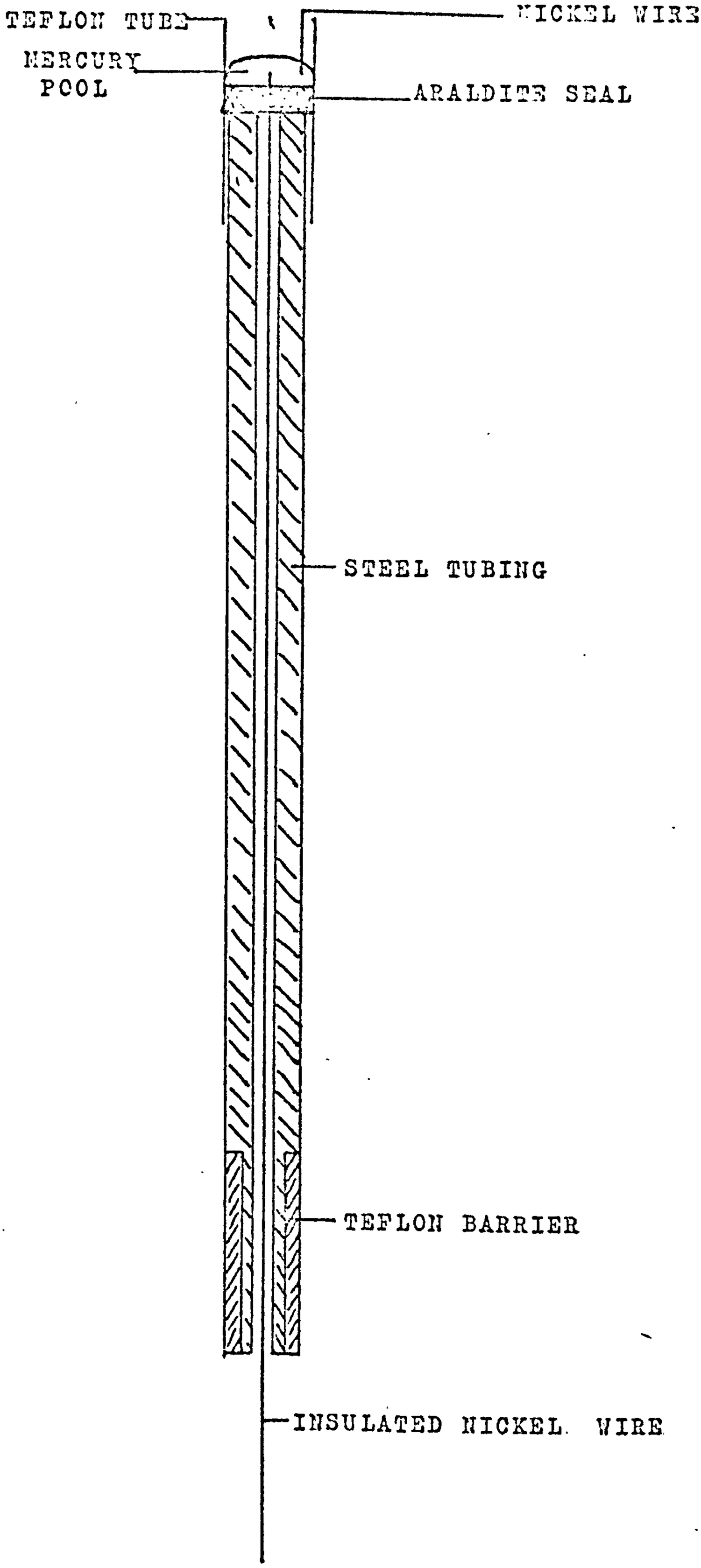

FIG. 6.4 ELECTRODE DRIVE SHAFT

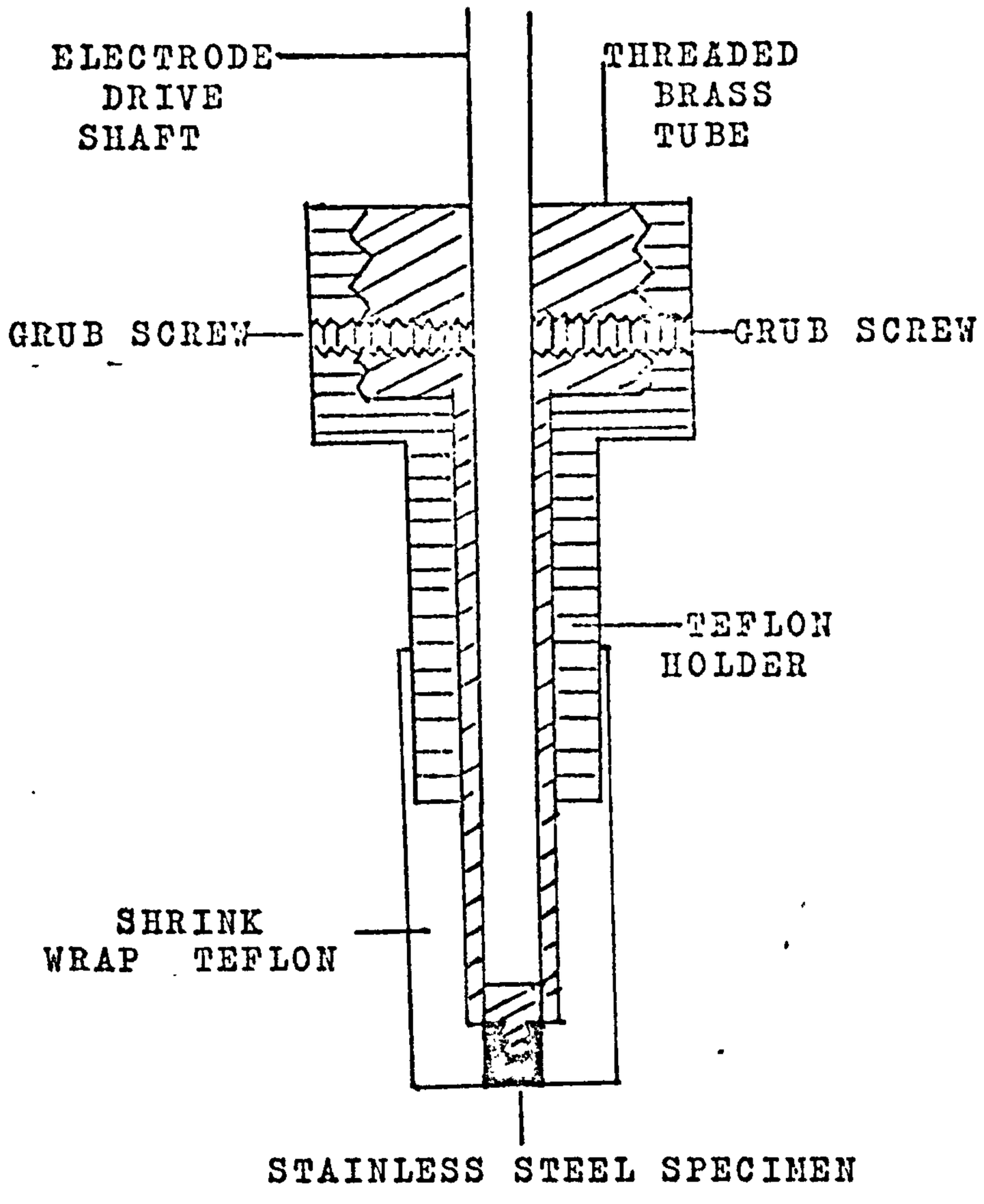

FIG.6.5 ROTATING DISC ELECTRODE.

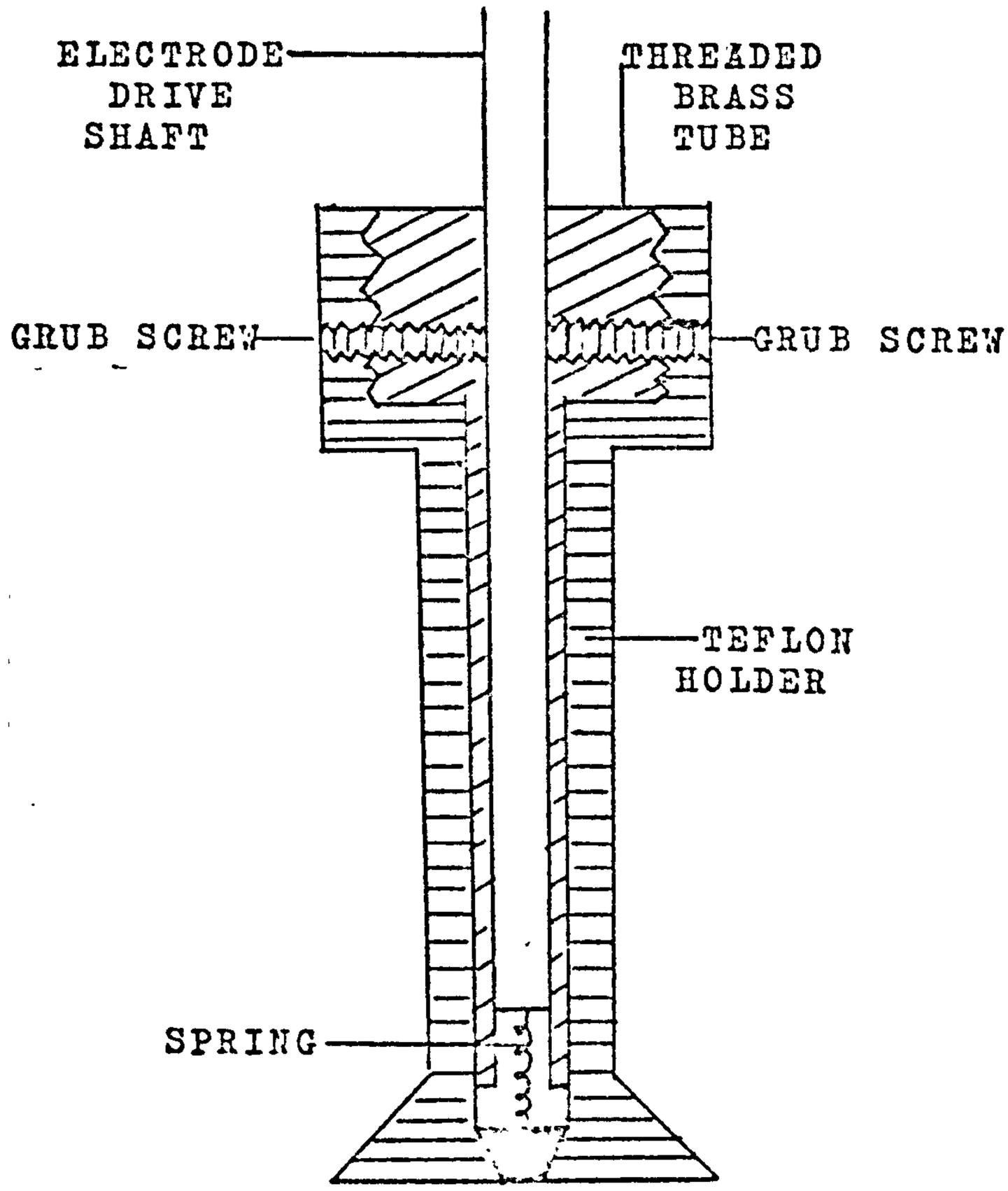

FIG.6.6 TRUNCATED CONE ELECTRODE DESIGN

CHAPTER 7

THE BEHAVIOUR OF STAINLESS STEEL AND COLOURED STAINLESS STEEL IN 5M SULPHURIC ACID AT 70°C

As discussed in Chapter 1 corrosion processes can be understood in terms of Evans diagrams, in which the polarisation curves for the anodic and cathodic reactions are used to predict the corrosion rate and corrosion potential of a metal in a corrosive environment. In the colouring process the stainless steel is placed in a corrosive environment, the anodic reaction being steel dissolution and the cathodic reaction being dichromate reduction. The behaviour of stainless steel in the absence of dichromate is consequently important to an understanding of the colouring process.

The situation in the colouring bath is, however, complicated by the presence of the film on the surface of the steel. It was thought that by studying the behaviour of the film covered stainless steel in sulphuric acid as well as that of the steel itself, the dissolution rate of the steel through the coloured film might be determined. As will be shown later, however, this did not appear to be possible.

7.1. STAINLESS STEEL IN SULPHURIC ACID

7.1.1. EXPERIMENTAL

The cell used for these measurements was the second cell described in Chapter 6. Stainless steel electrodes were cut from stainless steel foil (Goodfellows metals EN 58 E). The electrical apparatus was described in Chapter 6 Section 6.4. The electrodes were pretreated by holding at a potential of -384 mV (S.C.E.) for five minutes in 5M sulphuric acid at 70°C. The potential of the electrode was swept from -384 mV to 1200 mV (S.C.E.) and back at a sweep rate of 10 mV s^{-1}. Current-time

curves at fixed potentials were obtained by immersing the electrode in the sulphuric acid solution at the potential concerned, no pretreatment of the electrode was performed.

7.1.2. RESULTS AND DISCUSSION

A typical polarisation curve for stainless steel in 5M sulphuric acid at 70°C is shown in Fig. 7.1. The current time curves obtained at fixed potentials 5M sulphuric acid at 70°C are shown in Fig. 7.2. It was noted that these electrodes were covered with a light brown film on removal from solution.

The polarisation curve for the stainless steel electrode in the sulphuric acid solution shows the active-passive transition, the passive region and the region of transpassive dissolution. It can be seen that the potentials at which transpassive dissolution occurs correspond to those at which the film normally forms in the colouring solution (1090 to 1130 mV S.C.E.).

7.2. COLOURED STAINLESS STEEL IN SULPHURIC ACID SOLUTION

7.2.1. EXPERIMENTAL

The cell and electrical apparatus used were the same as those described in the last section. Stainless steel electrodes, which had been coloured by immersion in 5M sulphuric acid 2.5M chromic acid solution at 70°C were placed in a 5M sulphuric acid solution at 70°C at a potential of 1050 mV (S.C.E.). The potential of the electrode was then swept to -384 mV (S.C.E.) and back at a sweep rate of 10 mV s^{-1}.

Current-time curves at fixed potentials were obtained by holding coloured stainless steel electrodes in 5M sulphuric acid solution at 70°C, at potentials corresponding to those at which the colouring reaction

normally occurs in the colouring solution.

7.2.2. RESULTS AND DISCUSSION

The current-potential curve for the coloured stainless steel in sulphuric acid solution (Fig. 7.3) was of the same form as that for the uncoloured stainless steel (Fig. 7.1) but did show a higher cathodic current in the region 450 to -250 mV (S.C.E.). On removal of the electrode from solution, after the potential sweep, the coloured film had been removed from some areas of the specimen but not from others.

It was thought that the cathodic current obtained in the region 450 to -250 mV might correspond to the reduction of the film material. However, on holding the electrode at potentials between 450 and 100 mV no visible modification of the electrode surface occurred, nor was there any discontinuity in the current-time curve at these potentials. It appears, therefore, that the coloured film is removed as a consequence of the active dissolution of the steel.

The time dependence of the current at fixed potentials for the coloured stainless steel in 5M sulphuric acid at 70°C is shown in Fig. 7.4. It was found that, on holding the potential of the coloured stainless steel at values where colouring would normally occur in the colouring solution, the colour rapidly became less intense. Since no change in the film occurred when specimens were left in sulphuric acid on open circuit, the anodic current obtained was consequently not due only to dissolution of steel through the coloured film; some of the current must be used to modify the film. After prolonged treatment in this way, the film became brown in colour.

In order to clarify this situation various coloured films were produced and immersed in the sulphuric acid solution at a potential of

1121 mV (S.C.E.) in an attempt to correlate the current potential curves with the colour of the film. Whilst these curves exhibited the same general form (Fig. 7.5) there was some variation in the magnitude of the anodic current flowing in the early part of the curve. Assuming that the final anodic current, which was virtually independent of film thickness (see Table 7.1), represented the rate of metal dissolution at all stages of the process, the quantity of electricity in excess of that for metal dissolution was calculated, and is reported in Table 7.1. Apart from the precoloured film this quantity of electricity showed a decrease with increasing thickness of film material. This indicates that the quantity of electricity calculated does not correspond solely to film modification.

TABLE 7.1

Quantity of electricity in excess of that for metal dissolution

		Charge required to modify film mC cm^{-2}	Film current mA cm^{-2}
1	precoloured	18.7	4.9
2	blue	52.0	5.6
3	blue	38.6	5.5
4	blue/gold	32.4	6.4
5	gold	22.1	4.8
6	powder	11.2	5.6
1	precolour	35.2	5.6
2	blue	57.1	5.8
3	blue	67.6	5.3
4	blue	70.9	5.5
5	green/red	59.4	5.6

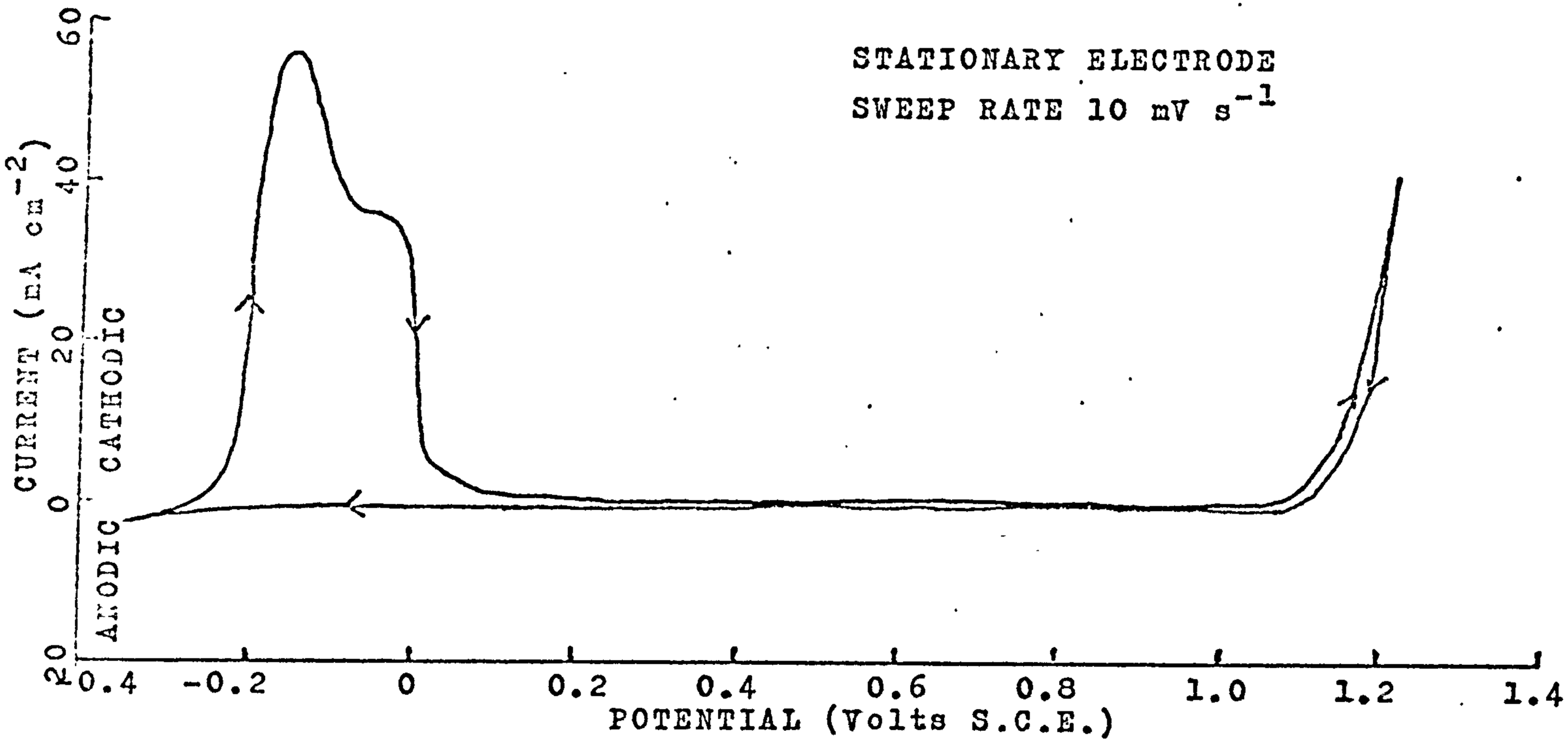

FIG.7.1 CURRENT-POTENTIAL CURVE FOR STAINLESS STEEL IN 5M SULPHURIC ACID

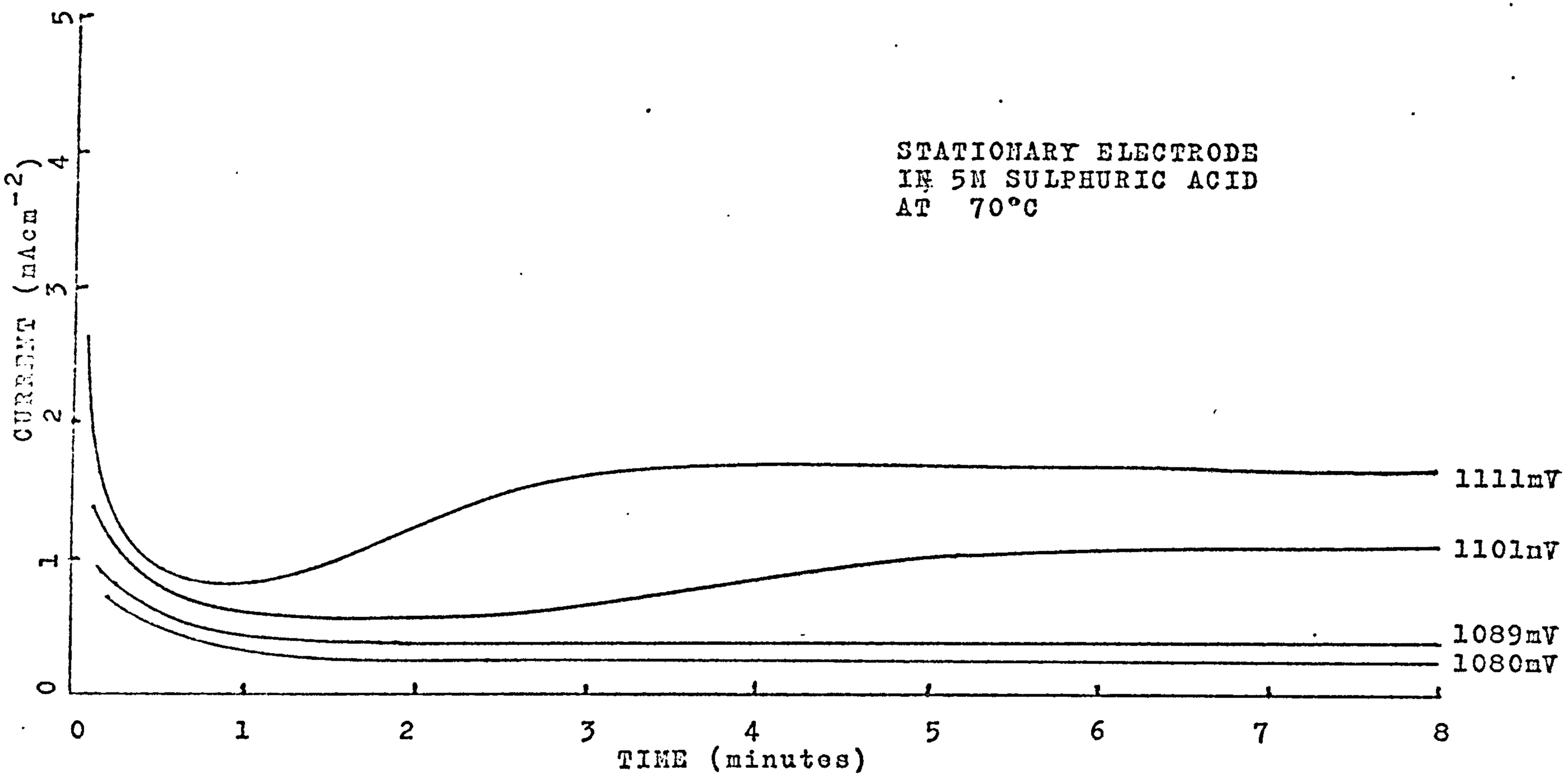

FIG. 7.2 CURRENT TIME CURVE FOR STAINLESS STEEL IN SULPHURIC ACID AT 70°C AS A FUNCTION OF POTENTIAL

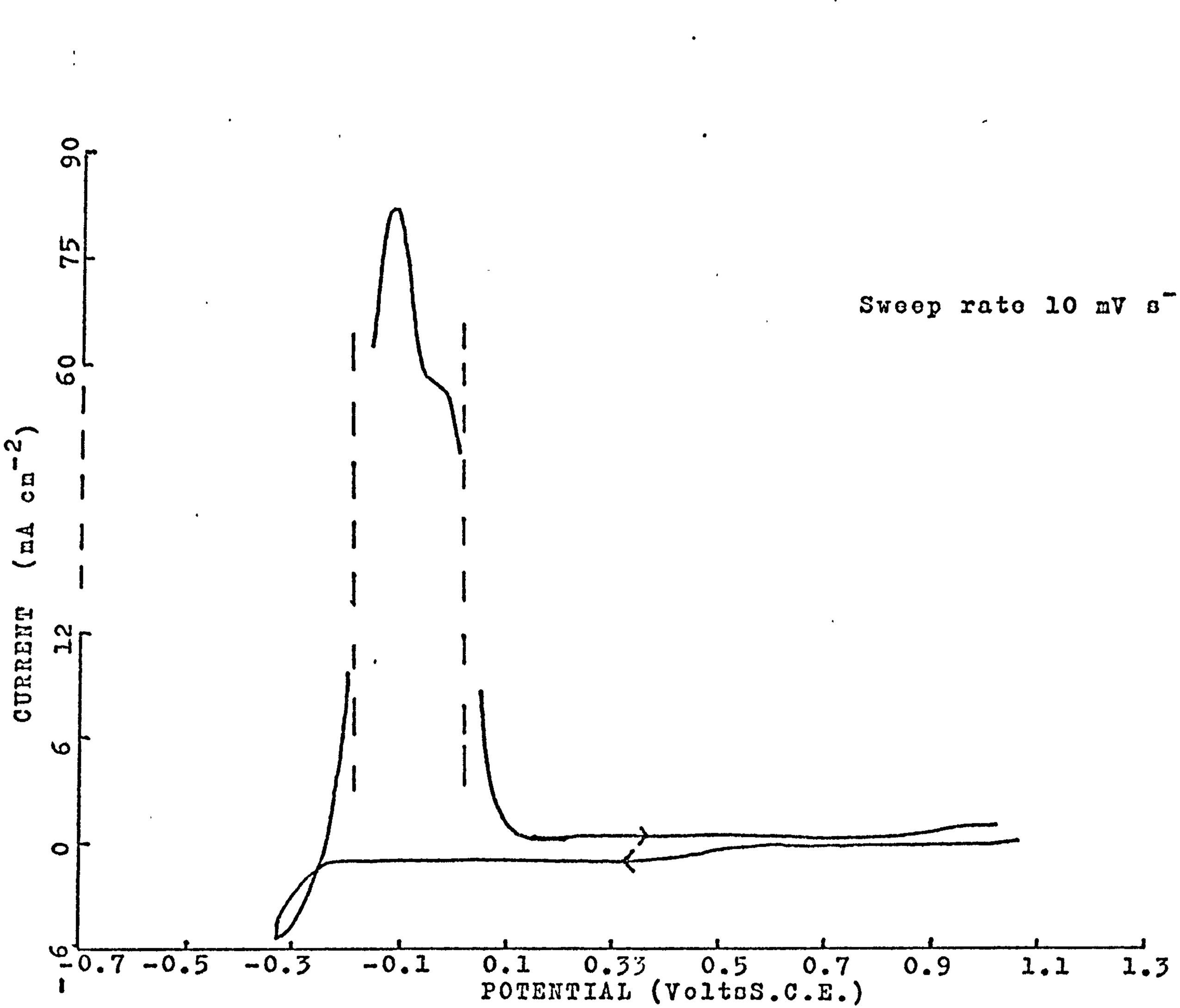

FIG. 7.3 CURRENT-POTENTIAL CURVE FOR COLOURED STAINLESS STEEL IN 5M SULPHURIC ACID

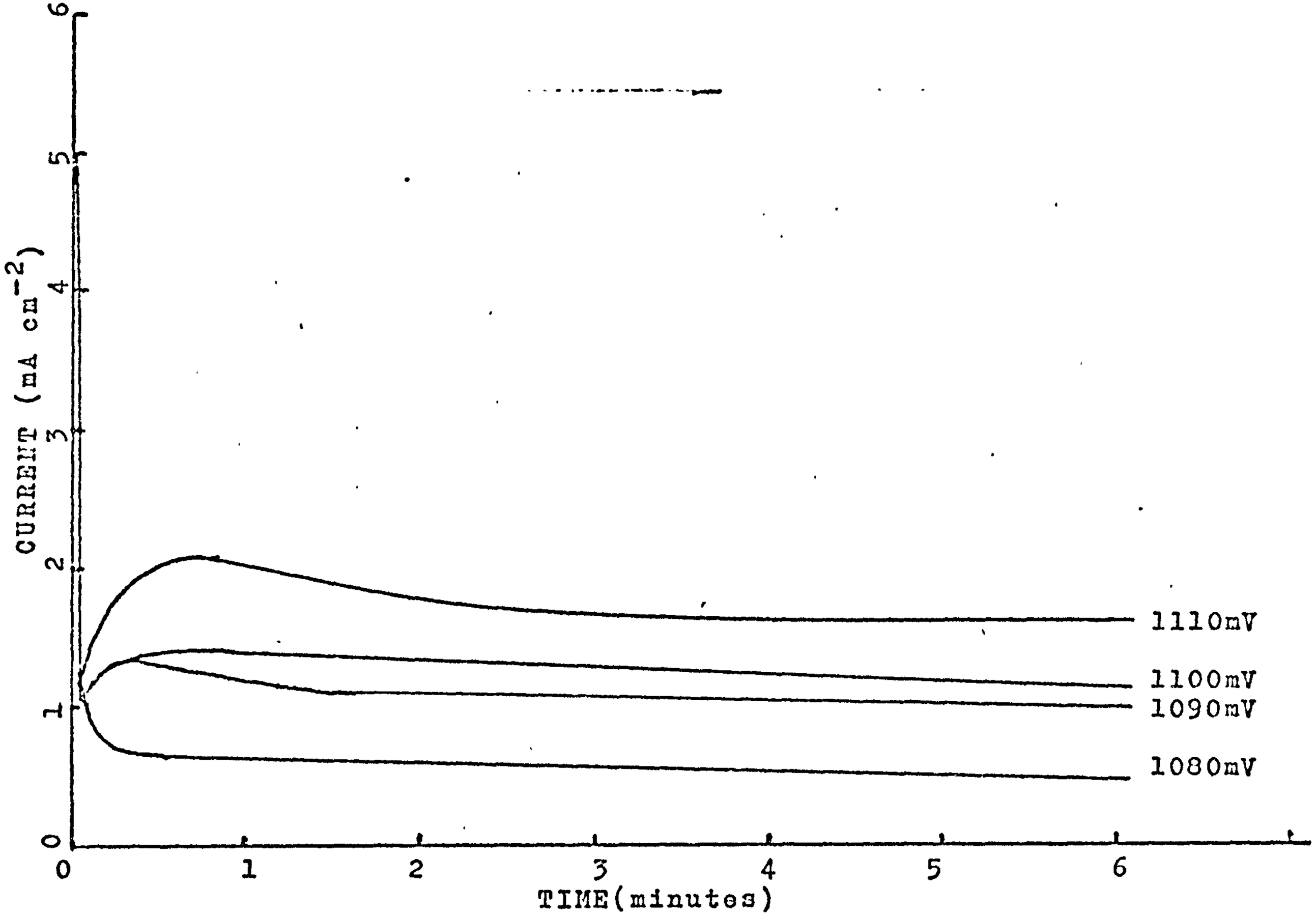

FIG. 7.4 CURRENT TIME CURVES FOR BLUE COLOURED STEEL HELD AT VARIOUS POTENTIALS IN 5M SULPHURIC ACID AT 70 C

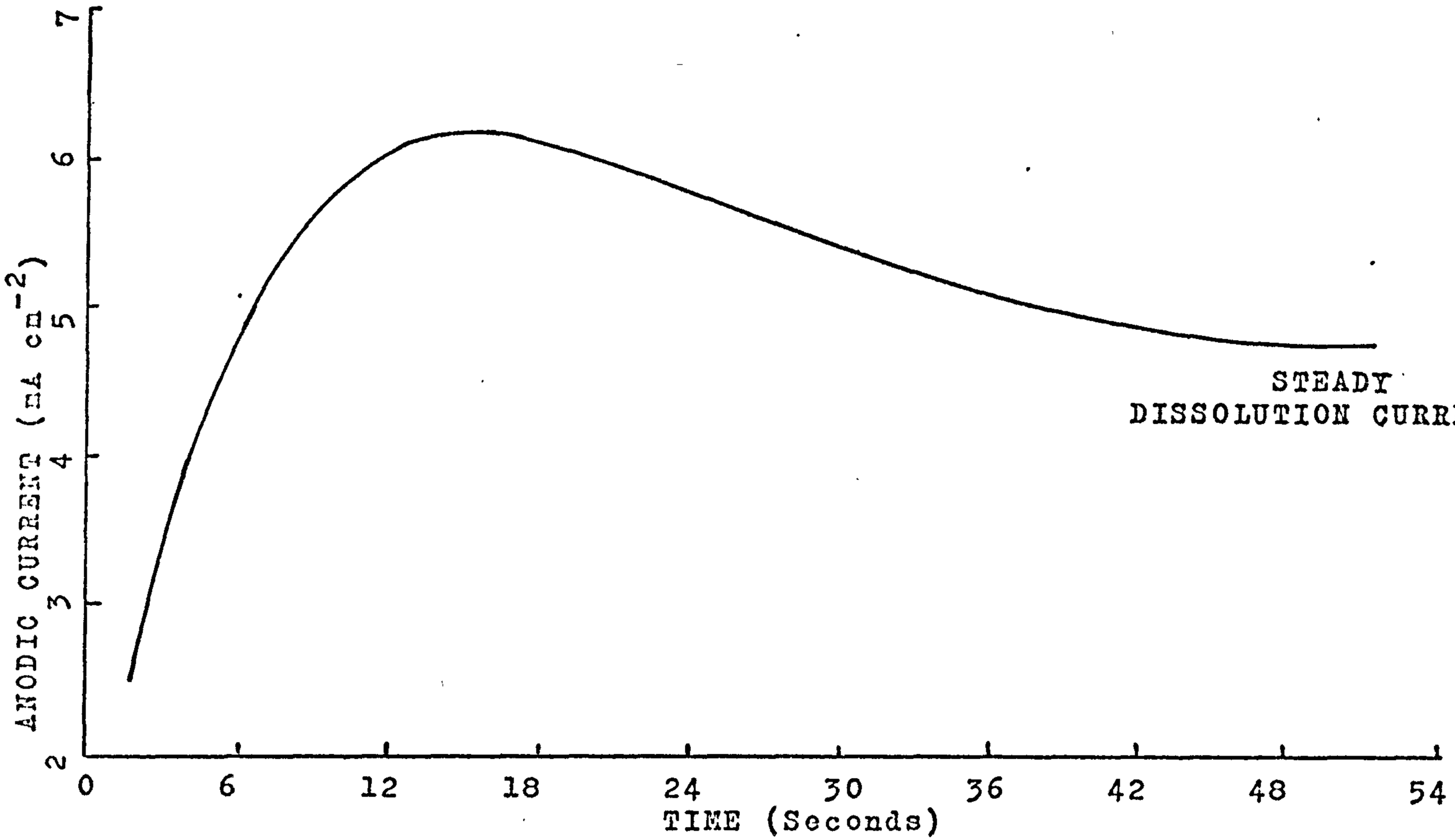

FIG. 7.5 TYPICAL CURRENT TIME CURVE OBTAINED DURING FILM MODIFICATION IN 5M SULPHURIC ACID AT 70 C.POTENTIAL 1121mV S.C.E.

CHAPTER 8

LINEAR POTENTIAL SWEEPS FOR THE STAINLESS STEEL ELECTRODE IN 2.5M CHROMIC ACID, 5M SULPHURIC ACID AT 70°C

8.1. INTRODUCTION

In many circumstances linear potential sweeps may be used to obtain qualitative information about processes occurring at electrode surfaces. In Chapter 7 the potential region in which active metal dissolution, passivation and transpassive dissolution occurred could be identified. This chapter describes the use of the linear potential sweep technique to obtain information about the behaviour of stainless steel in 2.5M chromic acid, 5M sulphuric acid at 70°C over a wide potential range. It was hoped that a potential region in which only one of the constituent processes occurred might be identified and that such a region might be used to obtain quantitative data about that process. Particular attention was paid to the cathodic process, since at potentials where the anodic process was likely to be the only process occurring high dissolution rates and resultant changes in surface structure would make quantitative interpretation of data difficult. Even in the case of the cathodic process it was, however, only possible to draw some qualitative conclusions.

8.2. EXPERIMENTAL

The second cell described in Section 6.1 was used for these measurements. The stainless steel rod electrode (Section 6.2.1.) was left on open circuit in 2.5M chromic acid, 5M sulphuric acid until it's potential had risen into the colouring region. Both single and repetitive sweeps were carried out at 30 mV s^{-1} between the colouring potential and -278 mV (S.C.E.) with the stationary film-covered electrode. Potential sweeps were

also recorded with a stationary electrode, allowing the potential of the electrode to reach progressively higher open circuit values between each subsequent sweep. A slow, 1 mV s^{-1}, potential sweep was also carried out with a stationary electrode from a potential of +1140 to +1080 mV (S.C.E.). Current-potential curves were also obtained with a rotated electrode (Section 6.2.1.) at a sweep rate of 10 mV s^{-1}.

8.3. RESULTS

The current-potential curves obtained with film-covered electrodes in 2.5M chromic acid, 5M sulphuric acid are shown in Figures 8.1 to 8.5. The current-potential curve for a single cathodic sweep, on a film-covered electrode, is reproduced in Fig. 8.1. The curve obtained on repetitive sweeping is shown in Fig. 8.2. The initial sweeps, obtained on electrodes which had been allowed to attain progressively higher potentials between successive sweeps, are given in Fig. 8.3. The short-range potential sweep is shown in Fig. 8.4, while Fig. 8.5 is the potential sweep obtained with a rotated electrode. No rotation speed dependence was observed in the region of either cathodic peak.

8.4. DISCUSSION

Although no detailed analysis of the current-potential curves can be performed, some general conclusions may be drawn.

The magnitude of the cathodic current is much too low for it to be a mass transport limited reduction of dichromate. This is most easily shown from the results obtained with the rotating disc electrode where the maximum current observed was about 6 mA cm^{-2}.

Since the mass transport limited current for a rotated electrode

(Section 5.2.1.) is

$$i_d = \frac{n\ F\ D^{\frac{2}{3}}\ C_b\ w^{\frac{1}{2}}}{1.61\ V}$$

then assuming reasonable values for D and V of 10^{-6} cm^2 s^{-1} and 10^{-2} cm^2 s^{-1} respectively, and that three electrons are involved, we have

$$i_d = \frac{3 \times 96{,}500 \times 10^{-4} \times 2.5 \times 10^{-3} \times 27.2^{\frac{1}{2}}}{1.61 \times 10^{-\frac{1}{3}}} = 0.51\ A\ cm^{-2}$$

A similar calculation makes it clear why no rotation speed dependence of the current was apparent. The appropriate equation (Sections 5.2 and 5.2.1.) is

$$i = \frac{n\ F\ D^{\frac{2}{3}}\ w^{\frac{1}{2}}}{1.61\ V}\ (C_b - C_s)$$

hence $$C_b - C_s = \frac{1.61 \times 10^{-\frac{1}{3}} \times 0.6 \times 10^{-3}}{3 \times 96{,}500 \times 10^{-4} \times 27.2^{\frac{1}{2}}} = 3 \times 10^{-5}\ mole\ cm^{-3}$$

That is, the difference between the bulk and surface concentrations is so small that the change resulting from changing the rotation speed would probably not result in a detectable change in the current.

The very low currents obtained in the return sweep, when the initial sweep extended to -278 mV, indicates that this treatment passivates the electrode. The higher anodic currents observed at more positive potentials on the return sweep presumably correspond to the breakdown of this passivity (transpassive dissolution). On continuous sweeping (Fig.8.2) the breakdown of passivity is not complete. Consequently the cathodic peak at more positive potentials is not observed, while that at less positive potentials is substantially decreased.

The increase in the cathodic currents, resulting from allowing the open circuit potential of the electrode to rise to progressively higher values (Fig. 8.3), strongly suggests that dichromate reduction can occur more rapidly the thicker the film present on the electrode. While it is true that the surface of the electrode is altered by the cathodic sweep, it seems logical to assume that during the time the electrode is on open circuit, the film is restored to the condition appropriate to the potential achieved. This view receives strong support from the fact that the shapes of the cathodic current-potential curves obtained in this experiment are closely similar to one another.

Because of; the marked hysteresis and hence lack of definition of the corrosion potention in the short range potential sweep, (Fig.8.4), the extreme sensitivity of the current to changes in the electrode surface, and the reasons given in Section 5.4.3., the Stern-Geary method was not applied to this curve.

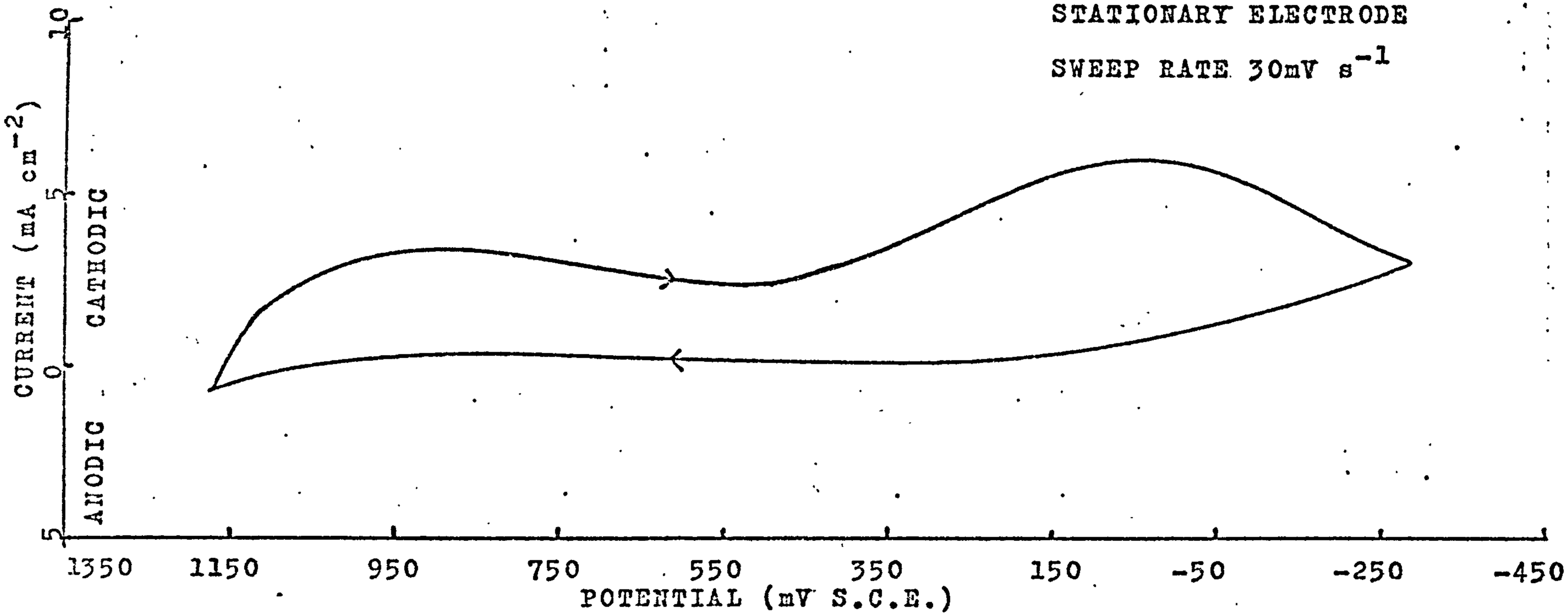

FIG. 8.1 CURRENT-POTENTIAL CURVE FOR A CATHODIC SWEEP ON A FILM COVERED ELECTRODE IN 2.5M CHROMIC ACID, 5M SULPHURIC ACID AT 70°C

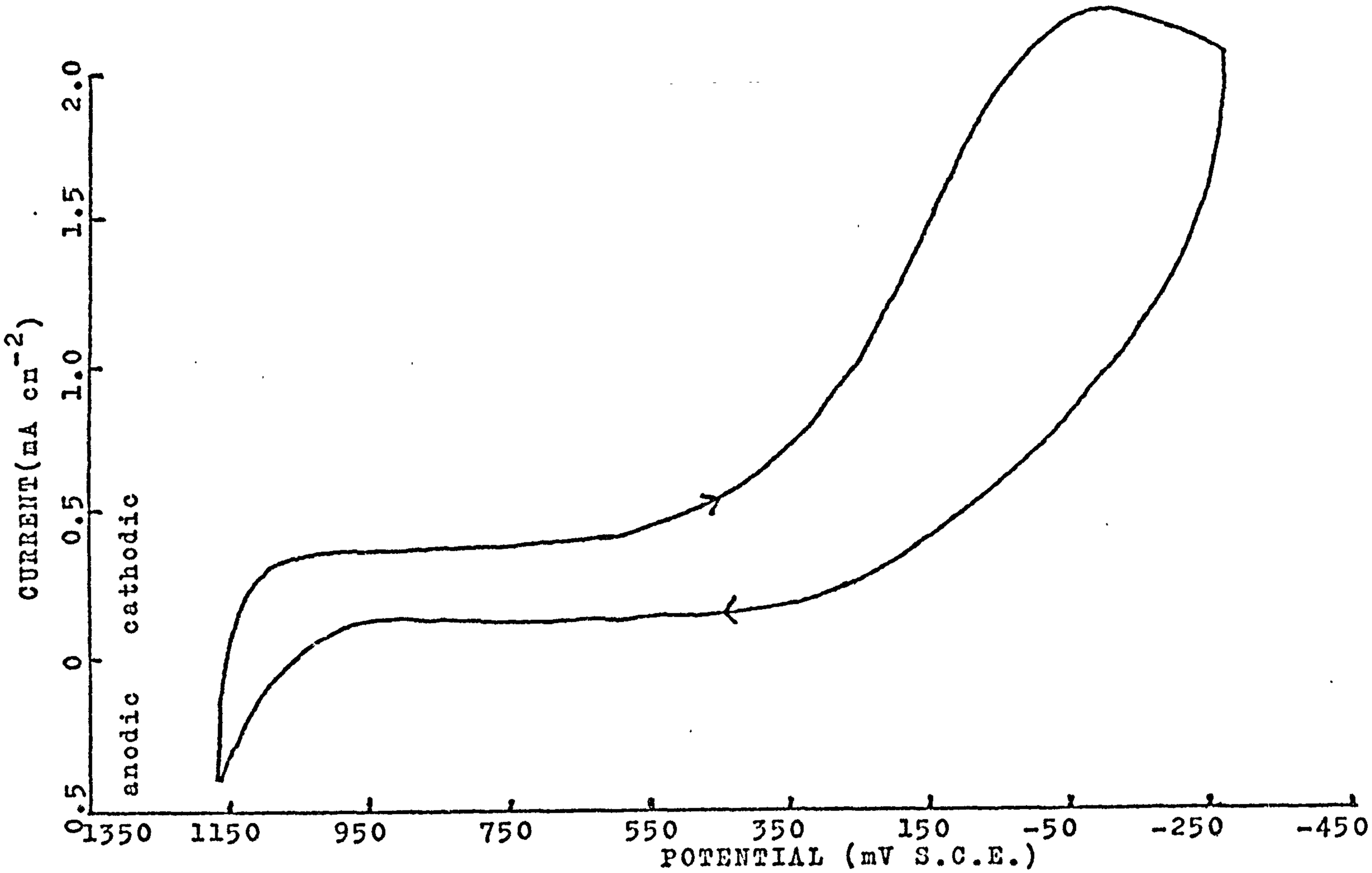

FIG.8.2 CURRENT-POTENTIAL CURVE OBTAINED ON CYCLING THE POTENTIAL OF A FILM COVERED ELECTRODE IN 2.5M CHROMIC ACID, 5M SULPHURIC ACID AT 70 C

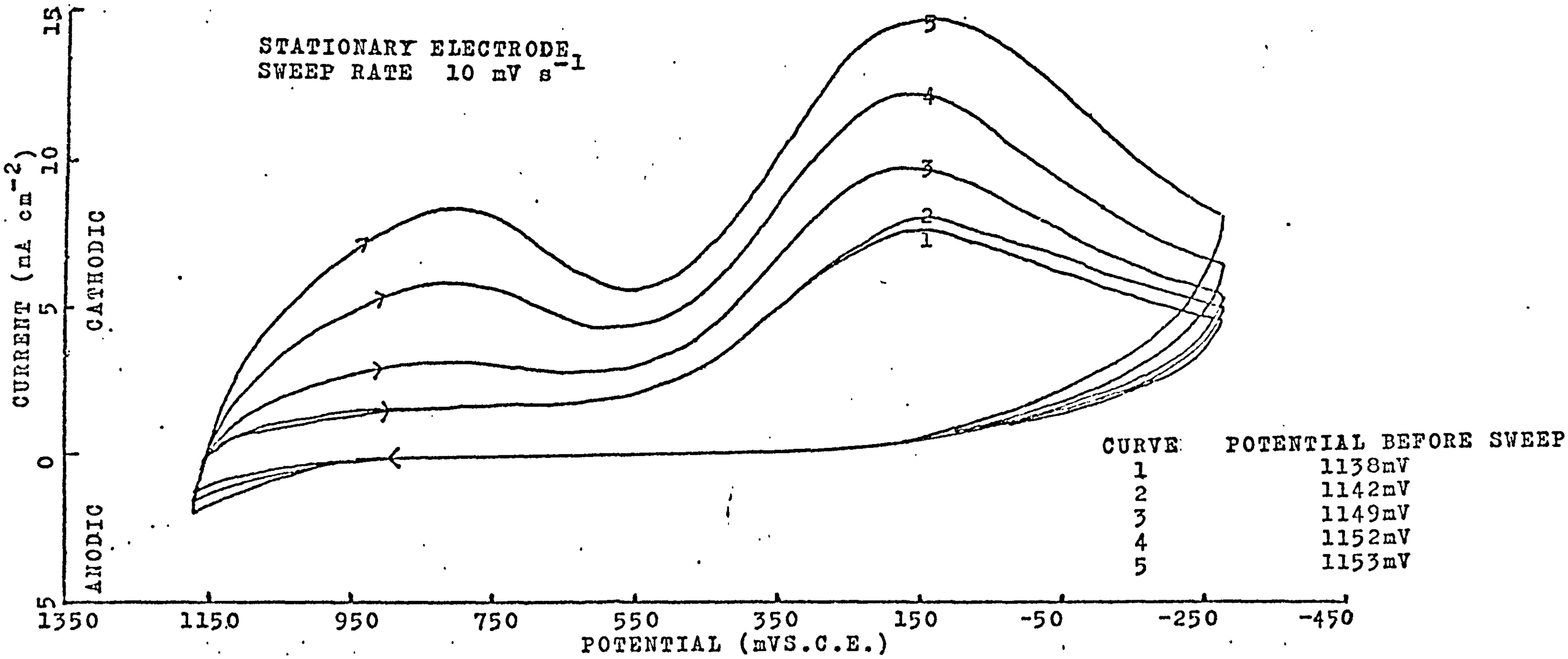

FIG. 8.3 CURRENT-POTENTIAL CURVE SHOWING THE EFFECT OF ALLOWING THE ELECTRODE TO ATTAIN PROGRESSIVELY HIGHER POTENTIALS BETWEEN SWEEPS.

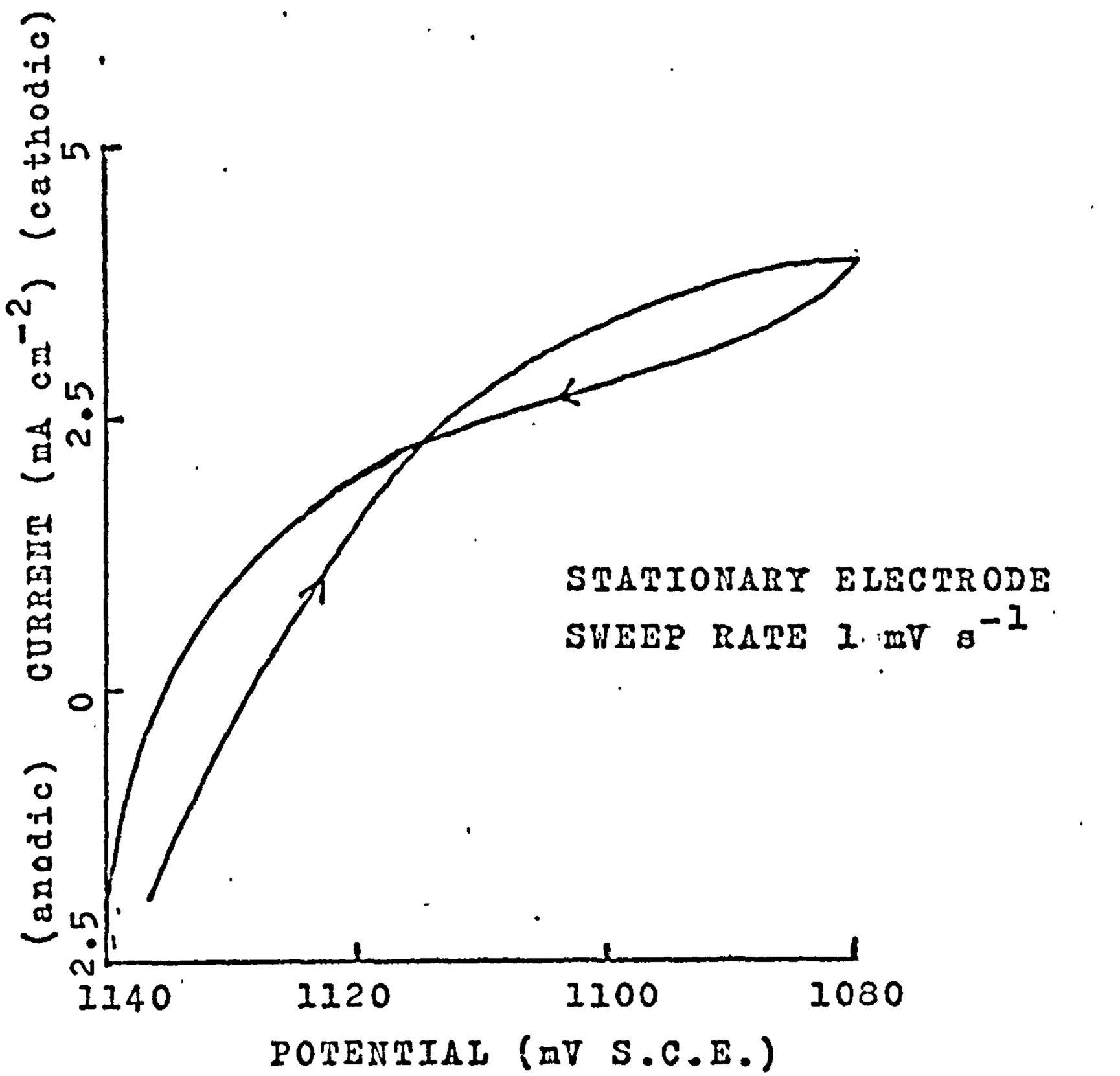

FIG. 8.4 CURRENT-POTENTIAL CURVE FOR SHORT RANGE POTENTIAL SWEEP ON STAINLESS STEEL IN 2.5M CHROMIC ACID, 5M SULPHURIC ACID.

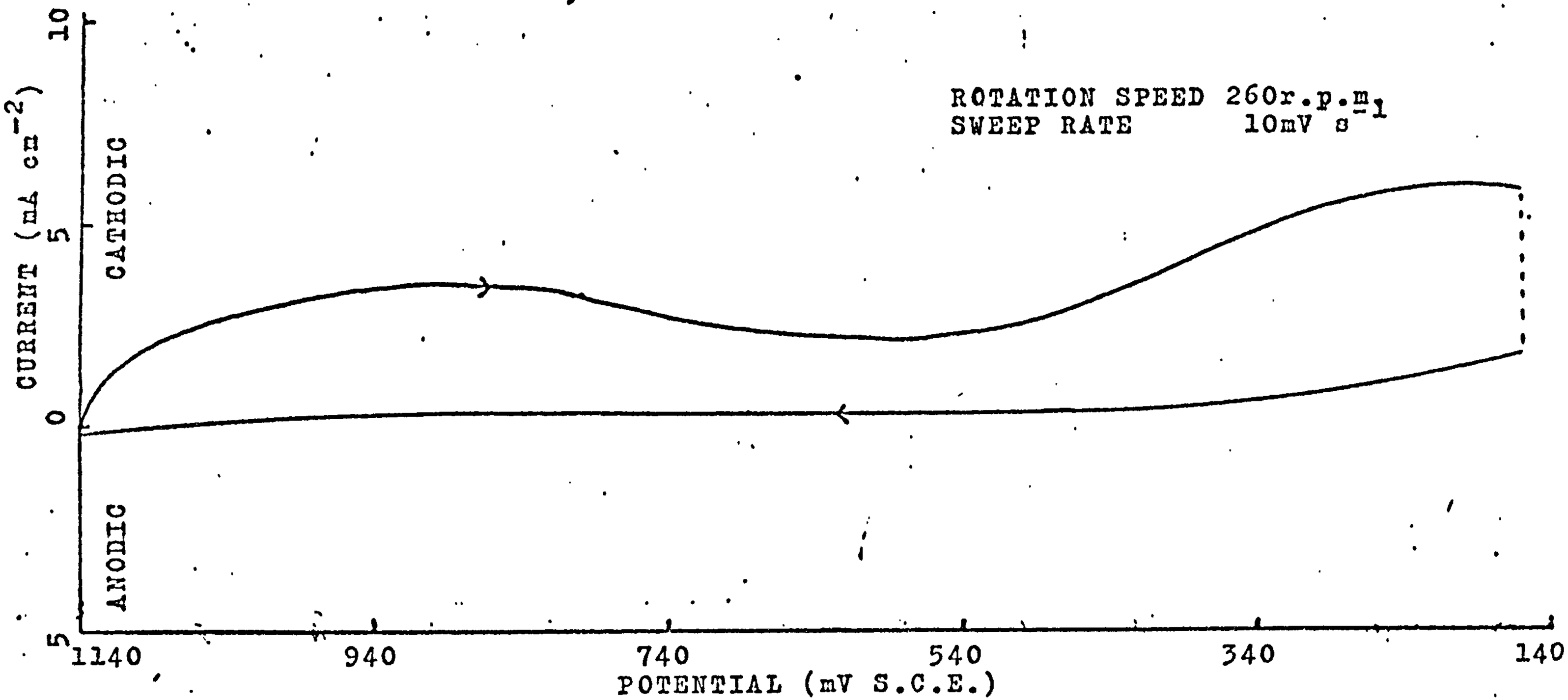

FIG. 8.5 CURRENT-POTENTIAL CURVE FOR A ROTATED STAINLESS STEEL ELECTRODE IN 2.5M CHROMIC ACID, 5M SULPHURIC ACID AT 70°C

CHAPTER 9

THE BEHAVIOUR OF STAINLESS STEEL IN 2.5M CHROMIC ACID 5M SULPHURIC ACID AT 70°C

In the previous chapters the properties of the coloured films formed on stainless steel have been considered. In this chapter the investigation of the processes which occur during the formation of the coloured film is described.

The most informative technique was the measurement of "in situ" weight losses during the formation of the coloured film. These weight losses were used to calculate the current for steel dissolution. This current, used in conjunction with the potential-time behaviour of the steel, allowed the determination of the relationship between current and potential during the formation of the film.

Atomic absorption analysis of the solution, in which coloured films had been formed, was carried out to determine the nature of the dissolution products of the steel. Measurements of current at fixed potential in the colouring region were also made although the results of these experiments can only be treated qualitatively.

It had been suggested that during the induction period, before visible film formation occurs, the solution near the steel surface was becoming saturated with dissolved film material which precipitated when the solubility product was exceeded. Measurements were made with a rotating disc electrode to test this view since, if it was correct, an increase in rotation speed would lead to an increase in the length of the induction period.

9.1. WEIGHT LOSS MEASUREMENTS

9.1.1. INTRODUCTION

If a metal specimen is placed in a solution in which anodic

dissolution and film formation can occur, then the weight of metal which has undergone anodic dissolution in a given time is given by Faraday's law as,

$$\text{weight of metal which has suffered dissolution} = \frac{M}{nF} \int i_{diss}\, dt$$

The metal will end up in solution and, depending on the mechanism of film formation, in the film. In the present case it seems very probable that the film formation reaction involves steel which has undergone anodic dissolution

$$\therefore \frac{M}{nF} \int i_{diss}\, dt = w_a + w_{sf} \qquad (1)$$

w_a = weight of metal in solution

w_{sf} = weight of metal in the film

M = average atomic weight of the steel

n = number of electrons per mole of steel dissolved

The weight of the metal specimen at a given time will be

$$w_t = w_i - w_a + w_o \qquad (2)$$

w_i = initial weight of specimen

w_a = weight of material in solution

w_o = weight of material other than metal incorporated into the film.

The weight loss the specimen is

$$\Delta w = w_i - w_t \qquad (3)$$

from 2 $$\Delta w = w_a - w_o \qquad (4)$$

Substituting w_a from equation (4) into equation (1)

$$\frac{M}{nF} \int i_{diss}\, dt = w_o + w_{sf} + \Delta w \qquad (5)$$

Workers at International Nickel Ltd.[3] have shown that during the colouring region the weight of film material represents at most only 10% of the weight of material lost from the steel. Consequently if equation (5) is modified to give

$$\frac{M}{nF} \int i_{diss}\, dt = \Delta w \qquad (6)$$

an error of less than 10% will be introduced.

The dissolution current at a given time can be found if the weight loss is measured as a function of time.

$$i_{diss} = \frac{nF}{M} \frac{d\Delta w}{dt} \qquad (7)$$

The accuracy with which this current may be determined is limited by the assumption that the film weight is negligible.

The weight change of the specimen with time could be followed by weighing the specimens, before and after different periods of immersion in the solution. However the length of time of immersion, to produce a particular potential, showed some variation. As a result of this, weight change data on different specimens might not show the correct time dependence. Moreover there is a possibility that material may be removed from the specimen surface as a result of washing.

An alternative to this method is to measure both the potential-time dependence and the weight change-time dependence during the formation

of the film on a specimen whilst it is immersed in the solution. This method makes it easier to obtain a complete weight loss-time curve without the possibility of irreproducibility from specimen to specimen which could occur with the previous method. There are, however, some experimental factors which may lead to errors, when using the in situ method of weighing.

As a result of metal dissolution the volume of the specimen decreases and consequently it displaces less solution, the weight loss of the specimen in solution would thus be less than the real weight loss. A correction for this effect must be applied.

When the specimen is immersed in the solution there is a period of expansion during which the specimen would apparently lose weight. Since the specimen is a metal this effect should be important only at short times. (The specimen took approximately 4 minutes to cool down from 70°C).

During a continuous weighing the position of the specimen in the solution varies, it is therefore essential that the specimen be totally immersed in the solution. The length of suspension wire immersed, however, decreases hence less liquid is displaced giving rise to an apparent weight loss.

A more serious effect, resulting from the change in position of the specimen in solution is due to the method of making electrical contact to the specimen. As described later this was done by having a nickel wire dipping into a mercury pool in a nickel crucible connected to the specimen suspension. As the specimen loses weight the balance pan and hence the mercury pool moves upwards. The amount of mercury displaced by the wire in the mercury pool therefore increases. This exerts an increasing force on the fixed nickel wire, as a result of which there is a force downward on the mercury pool and hence the balance pan. The apparent

weight loss of the specimen is thus not as great as its real weight loss.

Correction for the change in volume of the steel on dissolution, the effect of immersion of the suspension wire in solution and the effect of immersion of the contact wire can be made as shown below.

The initial weight of the specimen is given by,

$$M_1 = W_1 - (V_1 + L_1A)D_L + l_1a\,D_{Hg} \qquad (8)$$

where M_1 = measured initial weight of specimen

W_1 = actual initial weight of specimen

L_1 = length of suspension wire immersed in solution

A = area of cross section of suspension wire

l_1 = length of contact wire immersed in mercury

a = area of cross section of contact wire

V_1 = volume of stainless steel sample

D_L = density of colouring solution

D_{Hg} = density of mercury

The weight of the specimen after time t is similarly given by

$$M_2 = W_2 - \left\{V_1 - \Delta V + (L_1 - \Delta L)A\right\} D_L + (l_1 + \Delta L)a\,D_{Hg} \qquad (9)$$

where M_2 = measured weight of specimen after time t

W_2 = actual weight of specimen after time t

ΔV = volume of steel dissolved

ΔL = distance suspension wire moves upwards during time t

The difference between the initial measured weight and the weight at time t will be

$$M_2 - M_1 = W_2 - W_1 + \Delta V\ D_L + \Delta L\ A\ D_L + \Delta La\ D_{Hg}$$

Since the change in volume of the specimen is related to the change in its actual weight,

$$-\Delta V\ D_s = (W_2 - W_1)$$

where D_s is the density of the steel

$$M_2 - M_1 = (W_2 - W_1)(1 - \frac{D_L}{D_s}) + \Delta L(A\ D_L + aD_{Hg})$$

Since for the balance used

$$\Delta L = -k(M_2 - M_1)$$

$$M_2 - M_1 = (W_2 - W_1)(1 - \frac{D_L}{D_s}) - k(M_2 - M_1)(AD_L + aD_{Hg})$$

if $k' = k(AD_L + aD_{Hg})$

then $(M_2 - M_1)(1 + k') = (W_2 - W_1)(1 - \frac{D_L}{D_s})$

so that $W_2 - W_1 = \frac{(M_2 - M_1)(1 + k')}{(1 - D_L/D_s)}$ (10)

The measured weight loss values were corrected using the densities of the steel and the solution and the factor k' in the expression was minimised by using wires of small cross sectional area.

In addition to the effects for which corrections may be applied, there was the possibility of condensation on the suspension wire during the measurements. This would make the apparent loss of weight of the

specimen appear smaller than its real loss in weight. However the dry weight loss, measured between the beginning and end of each in situ experiment, was almost the same as the corresponding value of the in situ weight loss obtained using the corrections described above.

9.1.2. EXPERIMENTAL

An Oertling R20 balance, with an attachment for under balance weighing, was used to measure the weight changes in solution. The balance was placed on a bench in which a hole had been drilled to allow the suspension wire to pass through it, and situated above the thermostatic bath. The specimens were hung from the suspension wire using a short piece of stainless steel wire. This was hooked at each end, the lower hook passing through a small hole in the upper part of the stainless steel specimen (Fig. 9.1).

Electrical contact was made to the specimen, by means of a wire dipping into a pool of mercury contained in a small nickel crucible fixed to the cross bar of the under balance weighing attachment. A commercial saturated calomel reference electrode (E.I.L.) was immersed directly in the sulphuric-chromic acid solution. The potential change was monitored using a Solartron digital voltmeter.

The specimens were degreased in acetone, washed with distilled water, dried and then weighed. The specimen was then hung from the suspension wire so that it was totally immersed in the colouring bath. The balance was then set to within 100 mg of the weight of the specimen and the change in weight was followed on the milligram scale on the balance. The potential and weight change were measured at one minute intervals throughout the colouring process and the final weight of the specimen measured after it had been washed and dried.

In addition to the in situ weight loss measurements, a series of specimens were coloured in the 2.5M chromic acid, 5M sulphuric acid solution until various potentials above the plateau were attained. The specimens were weighed before and after immersion so that a series of "dry" weight loss measurements at a range of potentials in the colouring region were obtained.

9.1.3. RESULTS

It was found that the measured weight loss values, corrected in the manner described in Section 9.1.1. were exponential functions of the time of immersion of the specimen in the colouring solution. A typical plot of $\log \Delta w$ against time of immersion and the potential-time curve for this specimen are shown in Figs. 9.2 and 9.3. The cause of the change in the slope in the graphs of $\log \Delta w$ against time is considered later. Over the colouring region the potential-time curves were almost linear. Their slopes are reported in Table 9.1.

A plot of $\log \Delta w$ against potential above the plateau, derived from the dry weight loss measurements made on a series of specimens, is shown in Fig. 9.4. The dry weight losses and corresponding potentials are presented in Table 9.2.

9.1.4. DISCUSSION

Over the latter part of the colouring region, the graphs of $\log \Delta w$ against time were linear. Empirically, therefore, this section of the curve obeys the equation

$$\Delta w = k \exp[b\ (t - t_o)]$$

where Δw = corrected weight loss

t_o = time at which the linear potential increase began, while k and b are constants.

According to this equation, however, $\Delta w = k$ when $t = t_o$. In reality was zero at $t = t_o$ so that the true equation must be

$$\Delta w = k \{ \exp[b (t - t_o)] - 1 \} \quad (11)$$

The applicability of this equation can be tested in the following manner. Defining a further constant a) as

$$a = \exp(- bt_o) \quad (12)$$

gives $$\Delta w = k a \exp(bt) - k \quad (13)$$

Taking pairs of values of Δw obtained at times separated by a constant interval (Δt), we have

$$\Delta w_2 = k_1 a \exp[b (t_1 + \Delta t)] - k$$

$$\Delta w_1 = k_1 a \exp(b t_1) - k \quad \text{which on subtraction gives}$$

$$\Delta w_2 - \Delta w_1 = k a \exp(b t_1)\{\exp(b \Delta t) - 1\}$$

or $$\Delta w_2 - \Delta w_1 = k' \exp(bt_1) \quad (14)$$

where $$k' = ka\{\exp(b \Delta t) - 1\} \quad (15)$$

Consequently $\ln(\Delta w_2 - \Delta w_1) = \ln k' + bt_1$

and a graph of $\ln(\Delta w_2 - \Delta w_1)$ against t_1 should be linear.

Graphs such as this, based on differences, rely heavily on the accuracy of the experimental data. The values of b and k' obtained in this way are therefore to be regarded as somewhat approximate. Having obtained these values however, it is possible to calculate ka, from equation (15) and then use equation (13) by plotting Δw against ka exp bt.

This latter graph must have a slope of unity and from it an accurate value of k may be obtained. This allows a more accurate test of the initial equation by rearranging equation (13) to give

$$\ln \left(\frac{\Delta w}{k} + 1\right) = \ln a + bt \qquad (17)$$

and plotting $\ln \left(\frac{\Delta w}{k} + 1\right)$ against t. The data shown in Fig.9.2 are replotted in this fashion in Fig. 9.5. It is now seen that the graph is linear over the whole time scale at which reasonably accurate values of Δw could be measured. This was true of all the results obtained.

Differentiation of equation (11) with respect to time, yields

$$\frac{d\Delta w}{dt} = kb \exp b(t - t_o) \qquad (18)$$

Combining this with equation (7), Section 9.1.1., gives

$$i_{diss} = \frac{nF}{M} \frac{d\Delta w}{dt} = \frac{n\ F\ kb}{M} \exp b(t - t_o) \qquad (19)$$

Since the potential is a linear function of time after $t = t_o$, we may write

$$\Delta V = k_2 (t - t_o) \qquad (20)$$

where ΔV is the potential above the plateau, and k_2 is a constant.

Substituting equation (20) into (19), gives

$$i_{diss} = \frac{n\ F\ kb}{M} \exp \frac{b \Delta V}{k_2} \qquad (21)$$

Since atomic absorption analysis, Section 9.2., suggests that the predominant species dissolving during the colouring process is iron, a value of 56 for the molecular weight of the dissolving species would appear reasonable. In view of the highly oxidising nature of the solution and the potentials at which the process occurs the value of n in expression (21) is most probably 3. Combining these values with those of k and b determined as described earlier and k_2 determined from the potential-time plot, allows a quantitative expression for the dependence of current on potential to be evaluated.

Values of $\frac{n\ F\ kb}{M}$ and $\frac{b}{k_2}$ calculated in this manner are reported in Table 9.3. This table also includes values obtained from the series of dry weight-loss measurements. In this case the value of k_2 was assumed to be 1 mV $(minute)^{-1}$. This is an average value of the slopes of a number of potential-time curves. The assumption is necessary because of the irreproducibility of the potential-time curve from specimen to specimen, discussed in Section 1.1.

Using the mean values of nFkb/M and b/k_2 calculated from Table 9.3, the values of current at various potentials above the plateau may be calculated. A plot of the logarithm of this current against the potential with respect to the S.C.E. is included in Fig. 9.6 assuming the plateau potential to be 1.100V.

The slope of this curve (ca 34 mV/decade) is in reasonable agreement with the slope of a plot of log i against potential (Fig. 9.6) obtained from the data for stainless steel in sulphuric acid (Chapter 7).

It is also in reasonable agreement with that obtained by previous workers on the transpassive dissolution of chromium in sulphuric acid solutions who obtained slopes of 36 mV/decade[34] and 40 mV/decade[9]. A mechanism which predicts a Tafel slope of 34 mV is discussed in Appendix B.

The absolute magnitudes of the currents obtained from the weight loss data are lower, however, than those obtained in sulphuric acid.

9.2. SOLUTION ANALYSIS FOR IRON AND NICKEL BY ATOMIC ABSORPTION ANALYSIS

9.2.1. EXPERIMENTAL

Stainless steel specimens 7 cm x 7 cm x 0.1 cm were cut from the stainless steel sheet and the edges filed down so that they would sit on the bottom of a 1 litre beaker.

30 cm^3 of colouring solution was run onto the specimen from a burrette, so that the specimen was covered with colouring solution. A second 30 cm^3 of solution was run into a litre beaker. Both beakers were placed in the same thermostatic bath and the time from the immersion of the solution in the bath measured.

The beakers were removed from the bath. The stainless steel sheet was washed with distilled water and the washings collected in the litre beaker. The solution and the washings were transferred to a graduated flask and made up to 250 cm^3 with distilled water. These solutions were then analysed for their iron and nickel content, using atomic absorption analysis, with the solution that did not have steel immersed in it as a blank.

The results of this analysis are included in Table 9.4.

9.2.2. DISCUSSION

Although the atomic absorption analysis gives the iron and nickel content of the solution accurately if the blank is used, the small volume of solution used to colour the specimen leads to a lack of uniformity of colour on the specimen. As a result of this, comparisons of the analyses with the weight-loss measurements must be treated with some caution. However, the values are of the same order of magnitude as the weight-loss values and suggest that iron forms a major component of the steel dissolving in the colouring bath.

9.3. ROTATION SPEED DEPENDENCE OF THE POTENTIAL-TIME CURVE DURING THE FORMATION OF THE COLOURED FILM

9.3.1. EXPERIMENTAL

The potential-time behaviour of a stainless steel rotating disc electrode fabricated from stainless steel sheet (Chapter 6, Section 6.2.1.) immersed in 5M sulphuric acid 2.5M chromic acid at 70°C was measured. The cell used for these measurements was described in Chapter 6 Section 6.1 The electrode was initially polished using successive grades of alumina (Griffin and George Ltd.). After the potential-time curve at a particular rotation speed had been determined, the electrode was repolished to ensure that the coloured film produced on the surface had been completely removed and a reproducible surface obtained. The potential of the electrode was measured with respect to a saturated calomel electrode.

The construction of the electrode drive shaft for these experiments was modified, as described in Chapter 6 to minimise conduction of heat away from the electrode tip. This was necessary because the transport of heat to the electrode would depend on the rotation speed of the electrode in a similar manner to mass transport as described in Chapter 5.

Consequently the temperature of the electrode would depend on the rotation speed. Since the colouring process is temperature dependent, variations in the colouring behaviour of the steel could arise either from a variation in mass transport to the electrode or heating effects.

The potential-time curves obtained at various rotation speeds are shown in Fig. 9.7.

9.3.2. DISCUSSION

There was no marked change in the potential-time behaviour of the specimen or the colour which the electrode attained on increasing the rotation speed of the electrode. In particular the induction period, before the potential rise begins, was probably shorter with rotated than with stationary electrodes. This implies that the processes involved in the film formation reaction are not significantly affected by mass transport. Since the induction period was not increased, by rotating the electrode, it strongly suggests that the film is not formed by a dissolution-precipitation mechanism.

9.4. CURRENT-TIME CURVES AT CONSTANT POTENTIAL FOR A STAINLESS STEEL ELECTRODE IN 2.5M CHROMIC ACID 5M SULPHURIC ACID

9.4.1. EXPERIMENTAL

The cell used for these measurements was the second cell described in Chapter 6, Section 6.1. Stainless steel electrodes cut from stainless steel foil (Goodfellow Metals EN 58 E) were immersed in 5M sulphuric acid, 2.5M chromic acid at 70°C. The potential of the electrode, with respect to the saturated calomel reference electrode, was maintained using a Chemical Electronics TR70/2A potentiostat. Current-time curves were

recorded on a Bryans 2400 A4 XY recorder. The current-time curves obtained at various potentials are shown in Fig. 9.8.

9.4.2. DISCUSSION

The current-time curves obtained at constant potential always had a form similar to those shown in Fig. 9.8. Except at very positive potentials, they are characterised by an initial anodic current which rises to a maximum and then falls linearly to zero, followed by a linearly increasing cathodic current which usually became constant after periods of greater than 30 minutes. The magnitude of the current at a given time, was very sensitive to the potential difference between the plateau and the applied potential. Since it did not prove possible to reproduce the plateau potential accurately it was not possible to make a systematic study of these current-time curves. Attempts were made to overcome this irreproducibility by determining the plateau potential on a separate specimen immediately before conducting the fixed potential experiments. Although the currents obtained in this manner were not particularly reproducible it was possible to observe the change in nature of the stainless steel surface at a potential of nominally 7 mV above the plateau. At this potential no visible film was produced on the electrode surface until after the maximum in the current-time curve. When the nett current flow became zero a blue film was observed and after the current became cathodic the film progressively thickens until a powdery film is formed.

Had it proved possible to conduct weight-loss experiments under constant potential conditions, sufficient data may have been obtained to allow an explanation of the current-time curves. However with the limited data available only a few qualitative statements can be made. Thus the almost linear decrease of current with time, after the maximum, could be

due to:

a) the anodic current i_a being constant while the cathodic current i_c decreases linearly with time

b) i_c being constant while i_a decreases linearly with time

c) i_a increasing and i_c decreasing with time

d) i_a decreasing and i_c either increasing or decreasing with time.

It is of interest to note that the maximum value of the current depends logarithmically on potential (curve C Fig. 9.6). The slope of this line is again close to 30 mV/decade. Furthermore since in the particular experiment described, colouring was not observed at 1120 mV but occurred at 1130 mV the plateau could be assumed to be about 1125 mV. Plotting the logarithm of the current against ΔV causes these points to fall very close to those obtained from the weight loss measurements (Fig. 9.9).

TABLE 9.1

Slope of Potential time curve $k_2/V\ s^{-1}$
1.4215×10^{-5}
1.2590×10^{-5}
1.898×10^{-5}
1.3597×10^{-5}
2.2756×10^{-5}
1.9697×10^{-5}

TABLE 9.2

Dry weight losses

Colour	V	dry weight loss ($\mu g\ cm^{-2}$)	$\log \Delta w$
hardly visible brown	4	25.0	1.40
bronze/blue	6	56.5	1.752
blue	8	78.8	1.90
pale blue	10	95.9	1.98
gold blue	12	114.0	2.06
pale gold	14	150.1	2.18
gold	16	173.7	2.24
red	18	209.0	2.32
blue green	21	260.8	2.42
green	23	286.7	2.46

TABLE 9.3

Value of $\frac{nFkb}{M}$ and $\frac{b}{k_2}$ calculated from weight loss and potential time data

	$\frac{nFkb}{M}$ (mA cm^{-2})	$\frac{b}{k_2}$ (V^{-1})
	0.528	44.9
	0.317	75.4
	0.651	42.8
	0.272	96.8
	0.622	51.7
	0.437	66.5
dry*	0.302	96.7
mean	0.447	67.8

* calculated on basis of an assumption of $\frac{dV}{dt}$ = 1 mV $minute^{-1}$

TABLE 9.4

Solution analysis for iron and nickel by atomic absorption analysis

Specimen No.	Colour	immersion time minutes	Fe $\mu g\ cm^{-2}$	Ni $\mu g\ cm^{-2}$	Total $\mu g\ cm^{-2}$
1	blue/colourless	-	41.75	5.00	46.75
2	blue	-	51.25	5.25	56.50
3	green	-	145.50	19.00	174.50
4	blue	24	38.00	4.50	42.50
5	blue/gold	26	69.50	9.50	79.00
6	gold/blue	28	101.30	14.30	115.60
7	green/red/gold	30	176.80	26.00	202.80
8	green/red	34	707.50	89.50	747.00

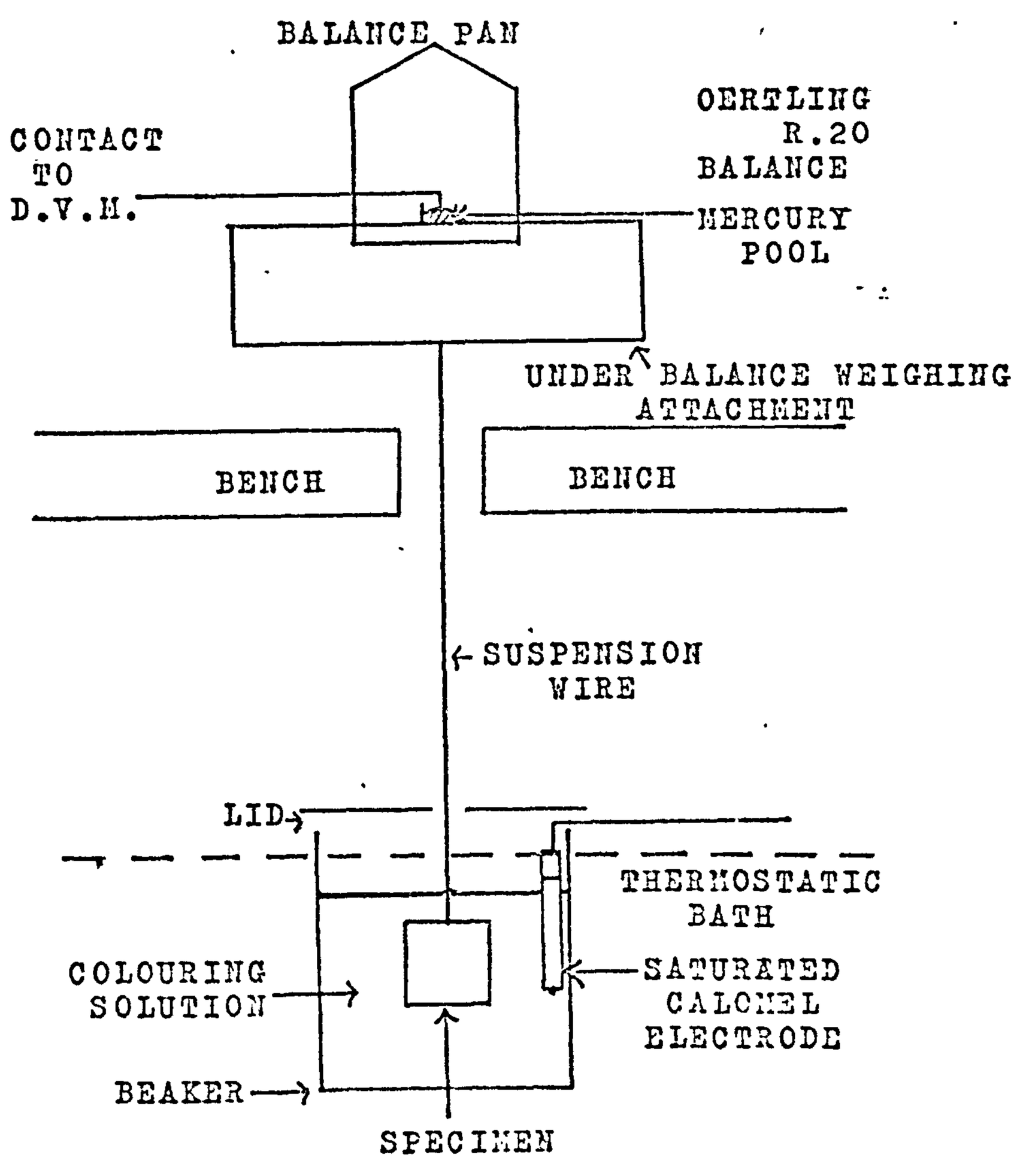

FIG. 9.1 SCHEMATIC DIAGRAM OF THE APPARATUS USED FOR WEIGHT-LOSS MEASUREMENTS

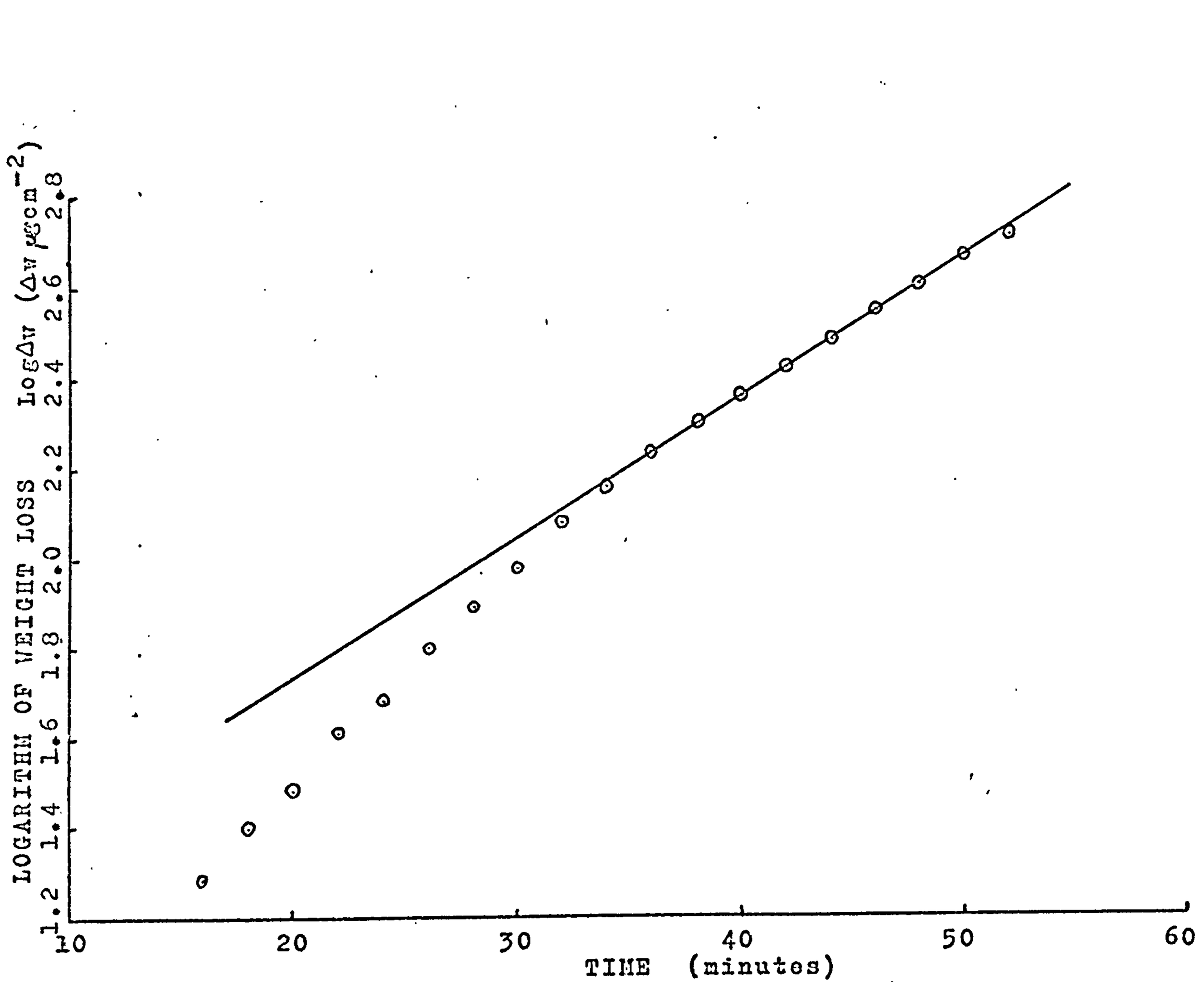

FIG.9.2 LOGARITHM OF WEIGHT LOSS AGAINST TIME

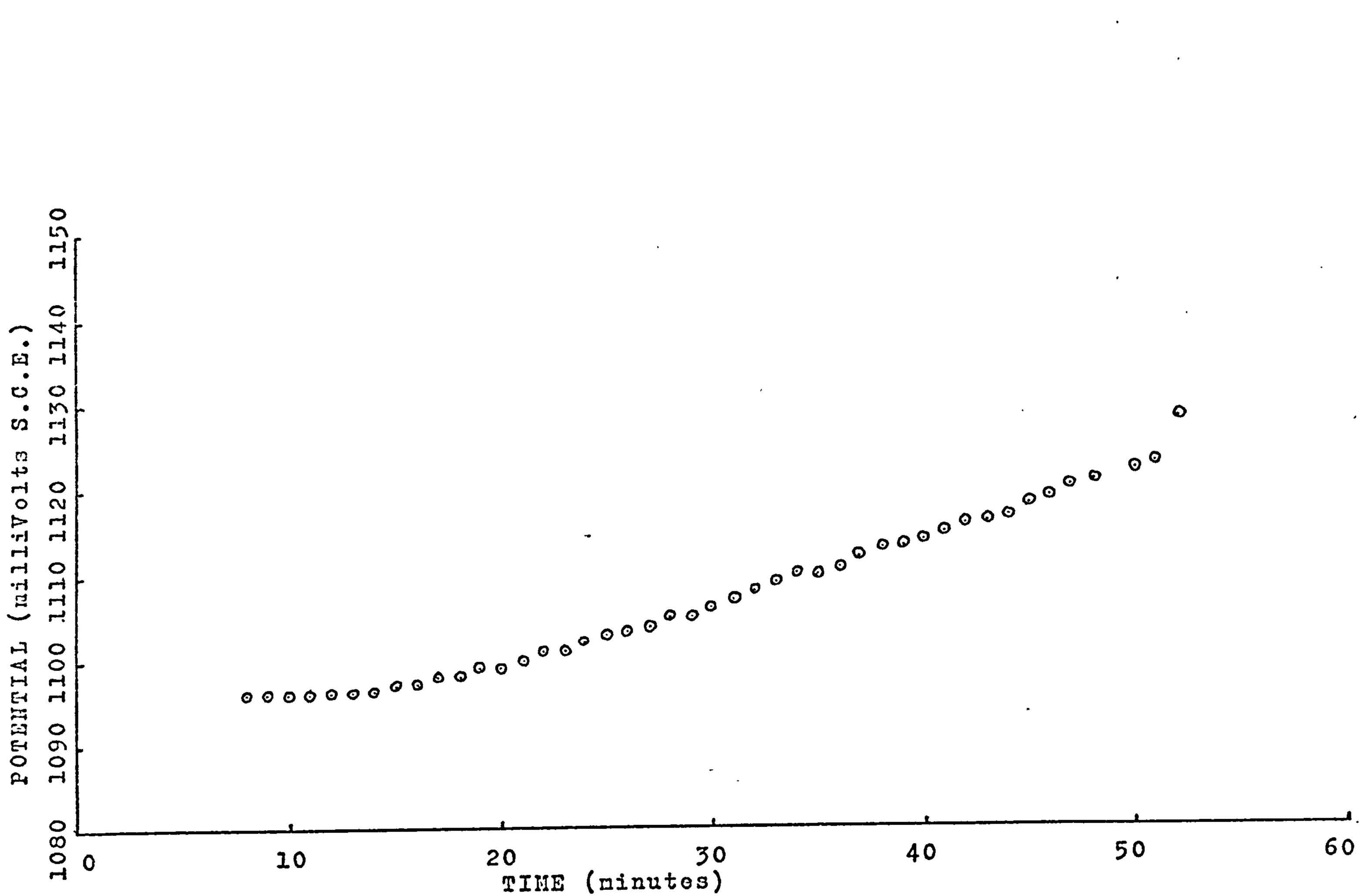

FIG. 9.3 POTENTIAL TIME CURVE

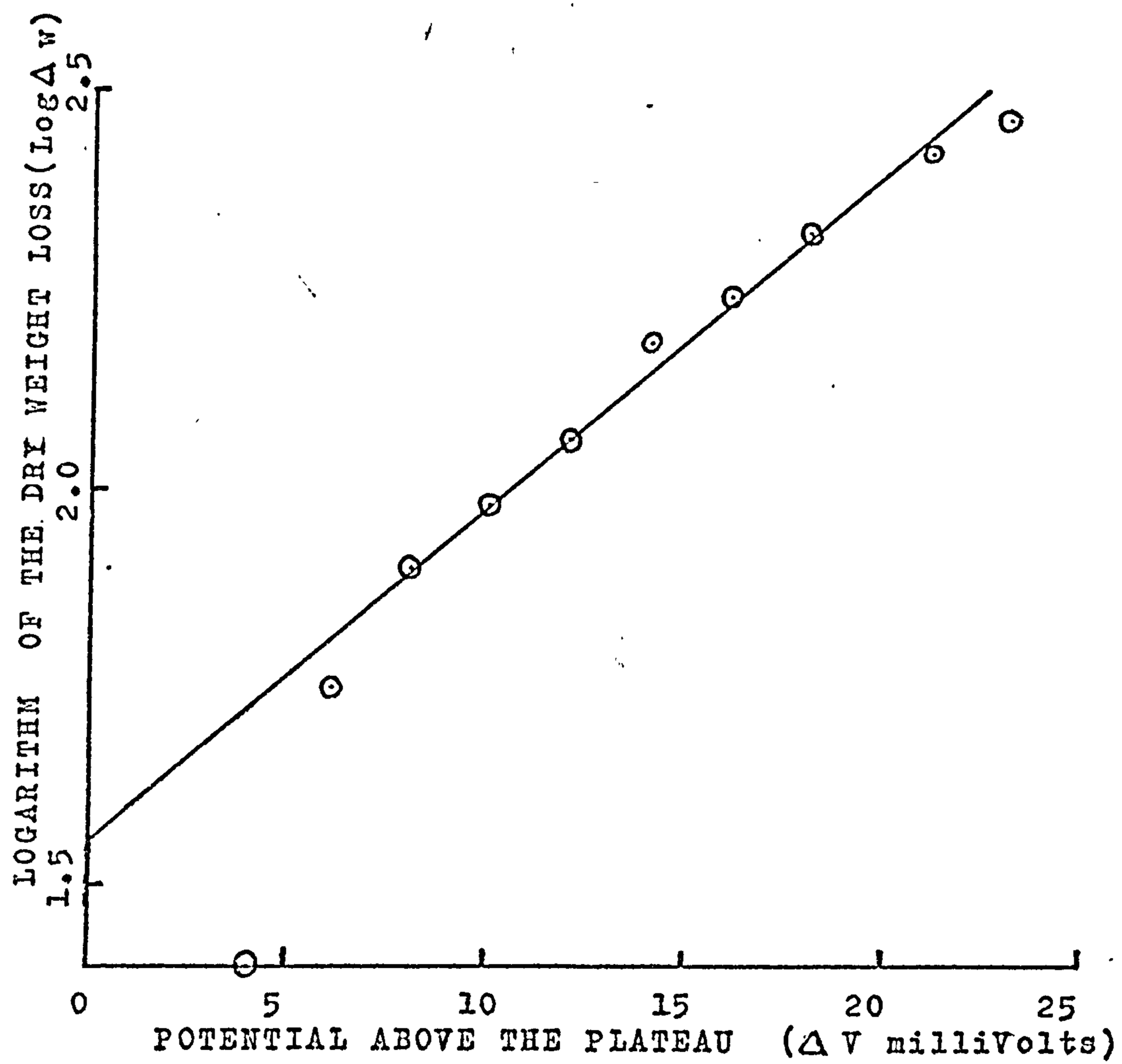

FIG. 9.4 LOGARITHM OF THE DRY WEIGHT LOSS PLOTTED AGAINST POTENTIAL ABOVE THE PLATEAU.

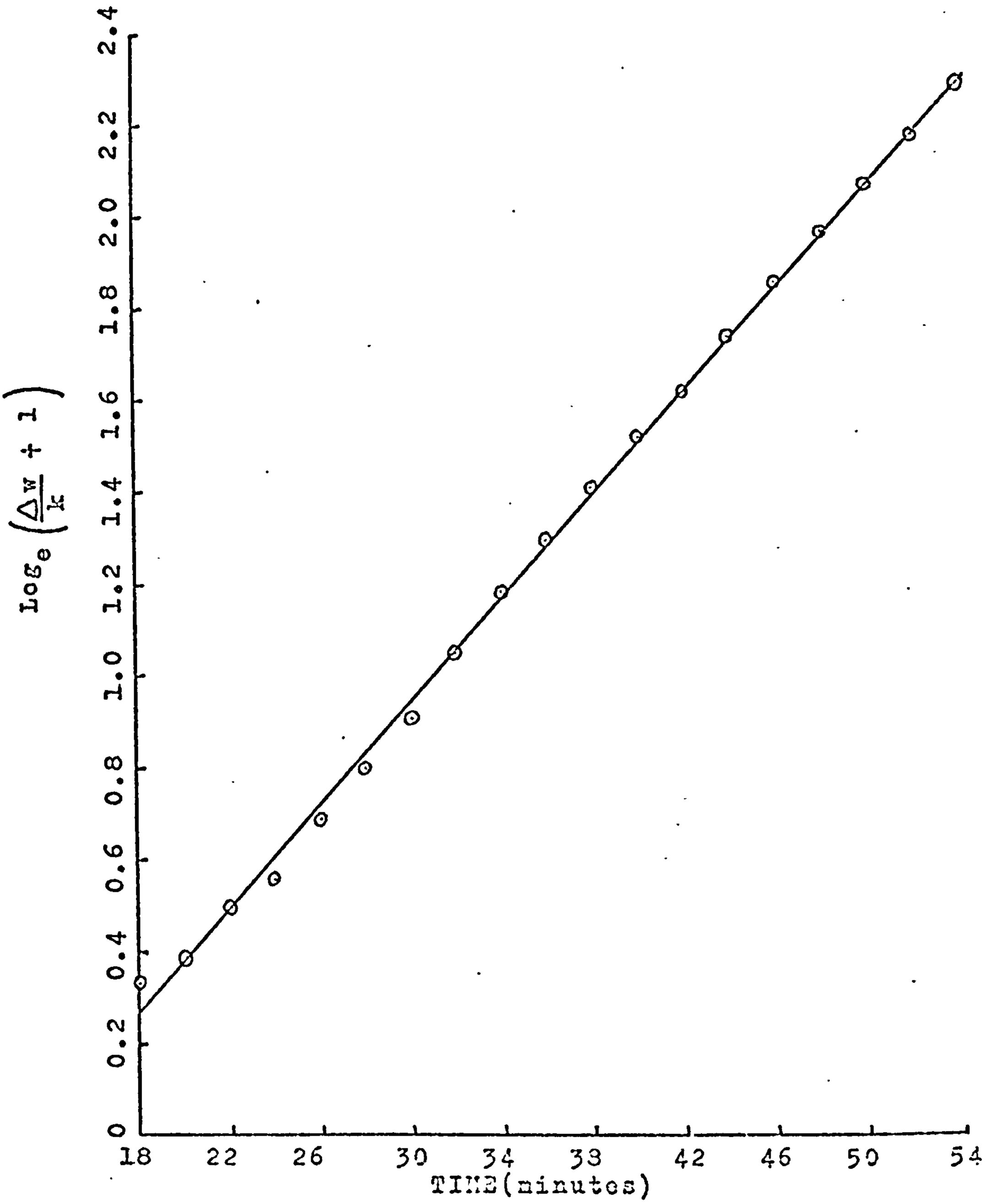

FIG.9.5 WEIGHT LOSS TIME DATA PLOTTED IN ACCORDANCE WITH EQUATION 17.

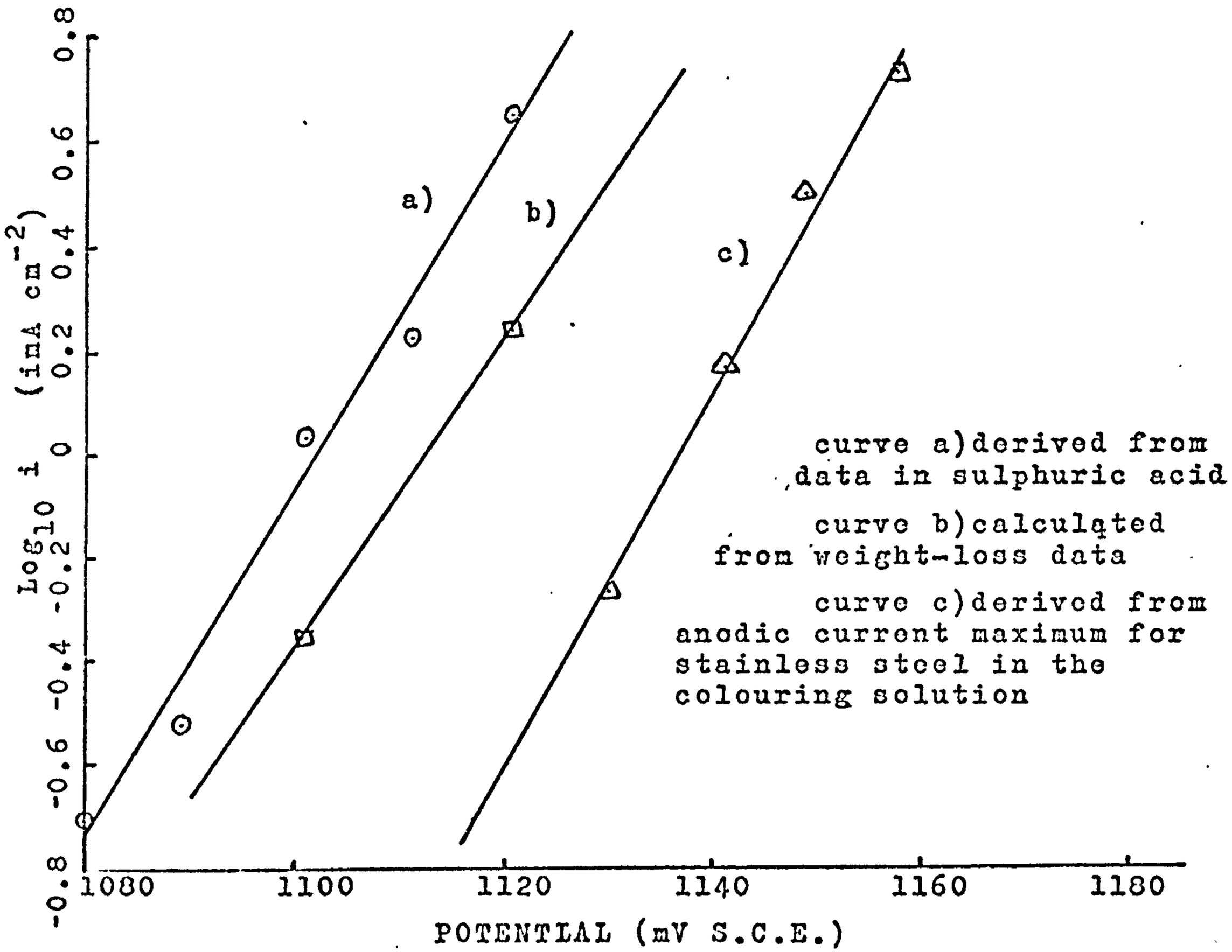

FIG.9.6 COMPARISON OF CURRENT POTENTIAL DATA FROM WEIGHT-LOSS MEASUREMENTS AND THAT FOR STAINLESS STEEL IN SULPHURIC ACID AND IN THE COLOURING SOLUTION.

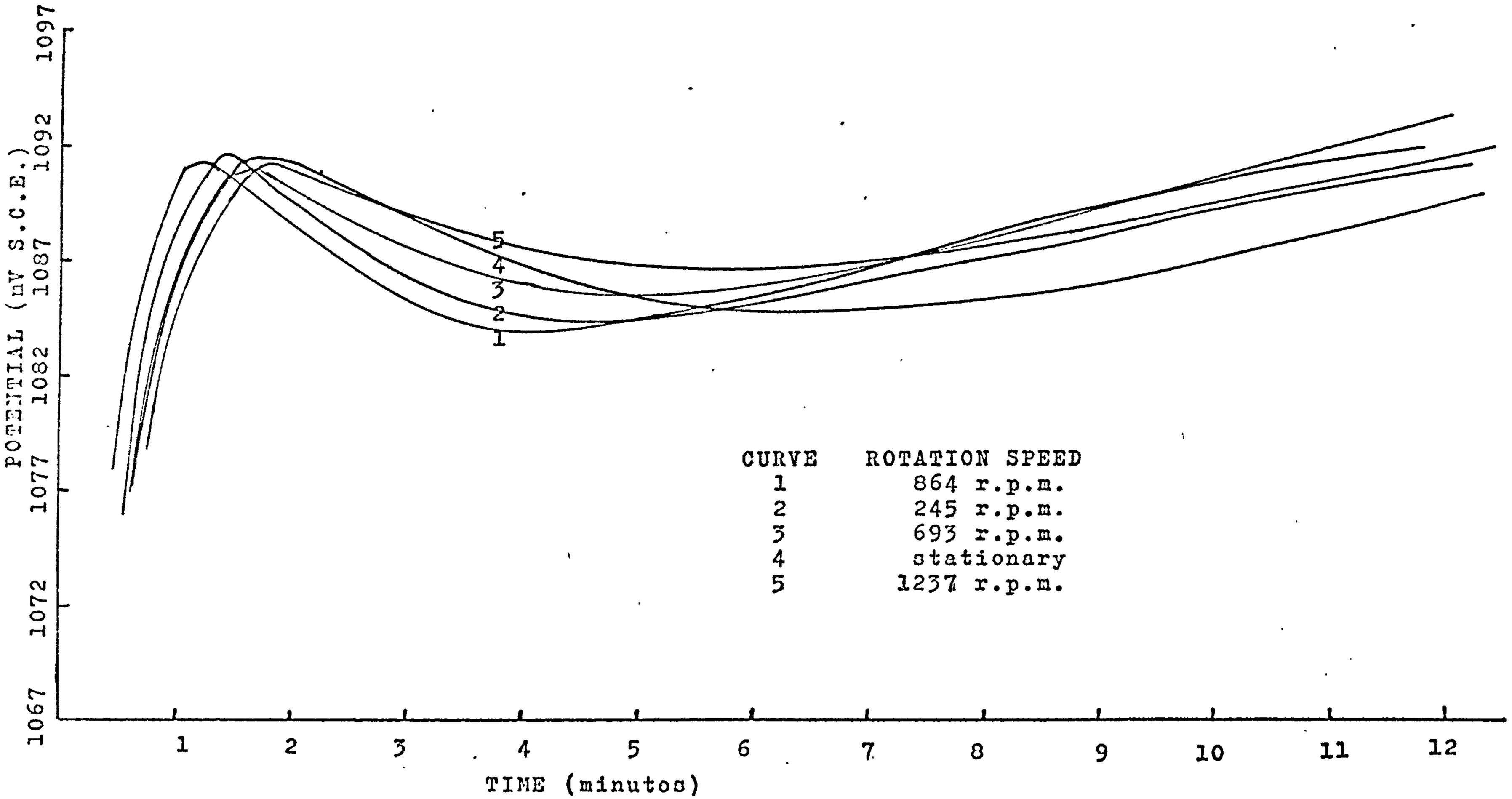

FIG.9.7 ROTATION SPEED DEPENDENCE OF THE POTENTIAL TIME CURVE

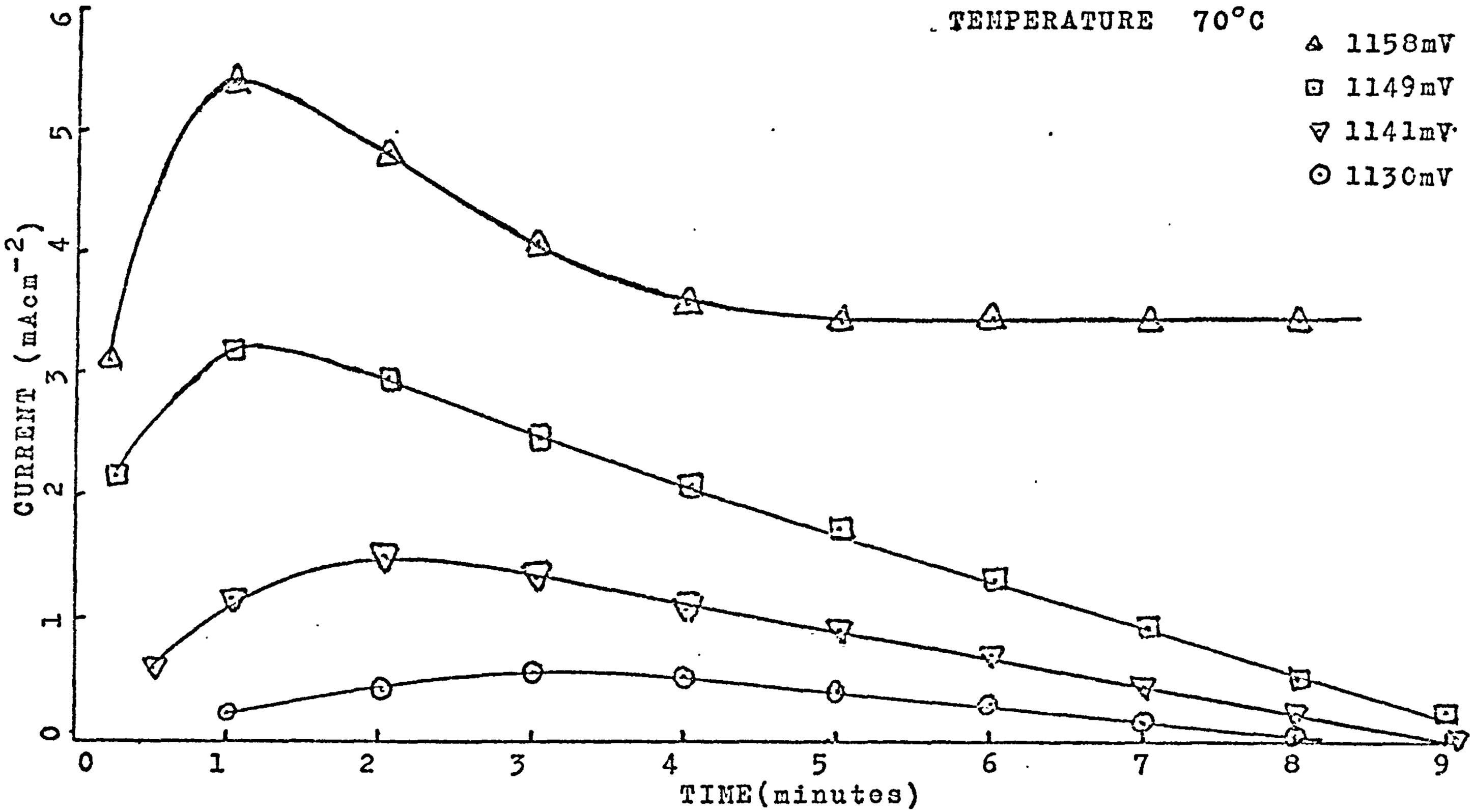

FIG. 9.8 CURRENT TIME CURVES FOR STAINLESS STEEL IN 2.5M CHROMIC ACID 5M SULPHURIC ACID AT VARIOUS POTENTIALS.

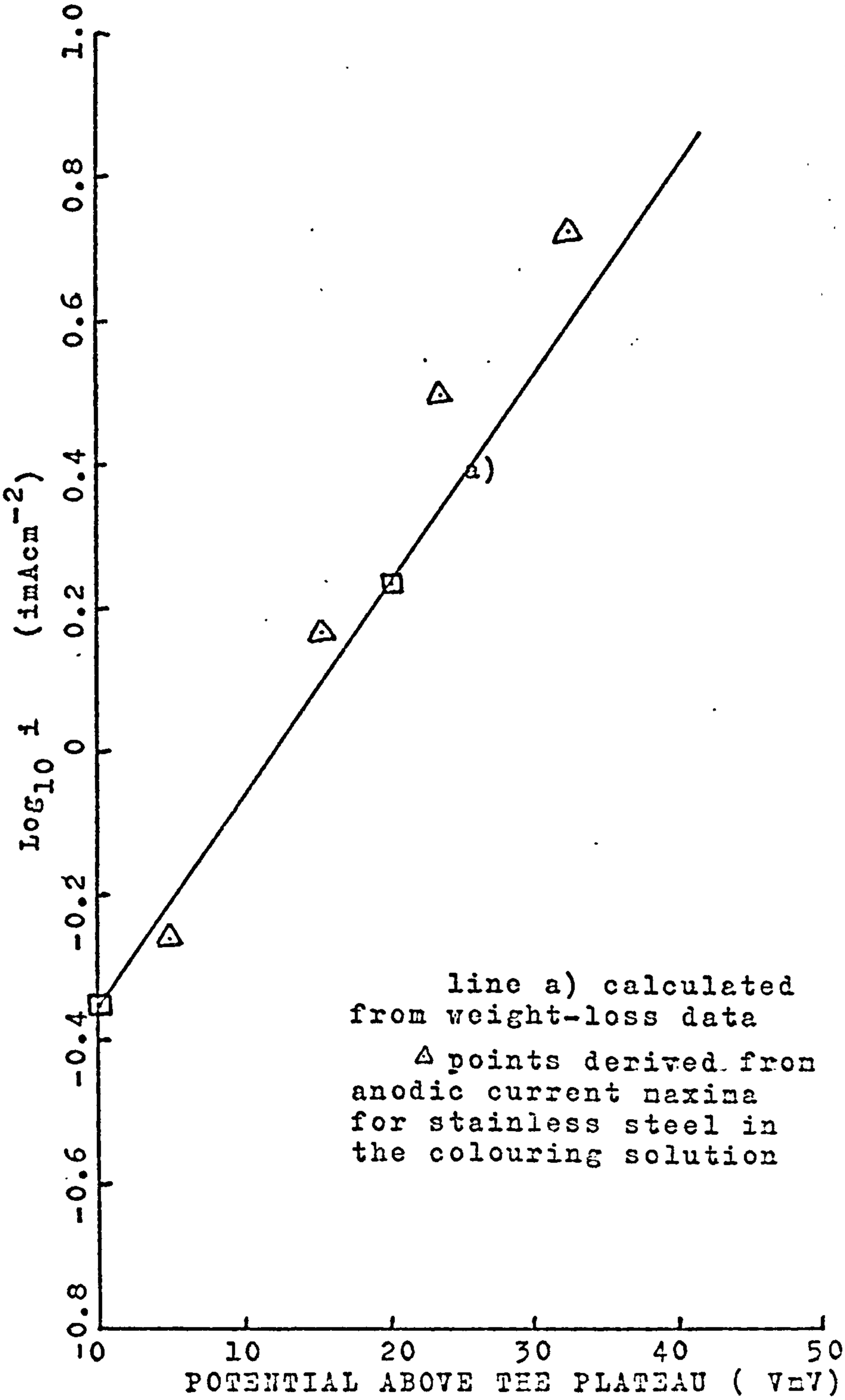

FIG. 9.9 PLOT OF CURRENTS CALCULATED FROM WEIGHT LOSS DATA AND THOSE DERIVED FROM THE ANODIC CURRENT MAXIMUM FOR STAINLESS STEEL IN THE COLOURING SOLUTION AGAINST POTENTIAL ABOVE THE PLATEAU.

CHAPTER 10

THE FORMATION OF THE FILM ON COLOURED STAINLESS STEEL

10.1. INTRODUCTION

As has been pointed out by Evans[88], there are a number of features associated with this process which are unusual; in particular the rate of increase of film thickness increases with time, whereas the rate of most film-forming processes either decrease or are constant with time. While it would be desirable to present a quantitative explanation of all the experimental observations, the complexity of the system and the lack of detailed understanding of both the transpassive behaviour of steel and the kinetics of dichromate reduction, make this a formidable task. The aim of this chapter, therefore, is the more limited one of attempting to correlate the experimental observations and propose a qualitative mechanism for the process.

10.2. SUMMARY OF OBSERVATIONS

For convenience, the facts established in this work are listed below.

1) On immersion in the colouring solution the potential of the steel increases with time as shown schematically in Fig. 10.1. The various stages indicated on this potential-time curve will be discussed separately later.

2) The film present at the end of stage I has a different composition to that originally present on the steel. Since it is also thinner than the original film, the change in composition must be associated with dissolution of the original film (Section 2.2.1.5.).

3) During stage II, the film thickens somewhat and undergoes further changes in composition (Section 2.2.1.5.). The potential is almost constant during this stage and is close to that for the onset of transpassive dissolution of steel in 5M H_2SO_4 at 70°C (Chapter 7).

4) The induction time (stages I and II) is not increased by rotating the steel specimen (Section 9.3).

5) The potential range corresponding to stages III and IV lies within the range at which transpassive dissolution of steel occurs in dichromate-free solutions.

6) Throughout stage III, the composition of the coloured film remains constant (Section 4.6.3. and Section 2.2.1.5.). During this stage the thickness of the film (1/cm) increases with potential above the plateau (ΔV/mV) according to the relation (Section 4.7)

$$1 = 3.1 \times 10^{-8} \exp 0.36 \Delta V \qquad (1)$$

7) The film produced during stage III is uniform in colour. Since the colour arises from interference effects, the film must be uniform in thickness over the surface of the specimen.

8) This coloured film has a spinel structure, is probably hydrated and contains a much greater proportion of chromium relative to iron than the substrate steel (Section 2.4).

9) The high chromium concentration in the film the presence of chromium in three valence states (III, IV/V and VI) and the presence of chromium in the film formed on Nilomag, indicate that incorporation of chromium from the dichromate in solution must occur (Section 2.4.).

10) No nickel could be detected in the surface or in the bulk of the film (Sections 2.3.2. and 2.2.1.5.). Analysis of stripped films gave the proportions of manganese iron and chromium as 14% (Mn), 41% (Fe), 45% (Cr).

Iron and nickel were present in the solution after it had been used to colour specimens (Section 9.2).

(11) Transmission electron microscopy of stripped films suggested that the films were composed of small crystallites and that the film may be porous (Section 2.3.3.).

(12) The coloured films showed no evidence of possessing significant ionic conductivity. Their electronic conductivity, however, was reasonably high at 1.67×10^{-6} ohm^{-1} cm^{-1} (Section 4.7).

(13) As the coloured film thickens, the rate at which dichromate can be reduced increases (Section 8.4).

(14) During stage III the film does not spall. In spite of this and the fact that the film thickens, the steel specimen loses weight (Section 9.1). This indicates that dissolution of the steel to give soluble products, occurs much more rapidly than film formation.

(15) By monitoring the weight loss and potential during the colouring process, it has been shown (Section 9.1) that the dissolution current during stages (I and II) is low. In stage III the dissolution current density (i_a/mA cm^{-2}) increases with the potential above the plateau (ΔV/mV) according to

$$i_a = 0.45 \exp 0.068 \Delta V \qquad (2)$$

While the values of i_a were somewhat smaller than those observed in the transpassive dissolution of steel, the potential dependence of these two currents was very similar (Section 9.1).

(16) Coloured films can also be produced by holding the potential of the steel, at a value within stage III, in the normal colouring solution. Under these circumstances the current was initially anodic, increased with

time, then after passing through a maximum fell almost linearly with time. A cathodic current, which initially continued the linear change with time was subsequently observed. Eventually this current became constant (Section 9.4, see also ref. 67).

(17) The maximum anodic current density observed in the constant potential experiments while somewhat lower than the corresponding value of i_a deduced from the weight-loss experiments, showed a similar dependence on potential (Section 9.4).

(18) The film produced at the end of stage III has a thickness of about 0.5 μm (Section 2.2.3.). That produced in stage IV is powdery and poorly adherent to the substrate (Section 1.1).

Observations which have been reported by workers at International Nickel[3] but which have either not been attempted or could not be substantiated in the present study are:

(19) The coloured film is porous, the pores having a diameter of 10-20 nm, the pore density is about 10^{11} cm^{-2} and pore fraction is 20-30%.

(20) The topography of the film reflects the underlying crystallographic orientation of the substrate. Features such as grain boundaries and twin boundaries in the substrate are clearly reproduced in the structure of the film.

10.3. POROSITY OF THE FILM

Although some evidence has already been presented to show that the ionic conductivity of the coloured film is very low, the importance of this, in establishing whether or not the film is porous, makes it worthy of further consideration. The results reported earlier indicate that the resistivity of the film is about 6×10^5 ohm cm, while the maximum anodic current flowing during the colouring process is approximately 3 mA cm^{-2}.

Assuming the resistivity of the dry film is not substantially smaller than that of the film immersed in the colouring solution, the field strength across the film during colouring cannot exceed E, where

$$E = 3 \times 10^{-3} \times 6 \times 10^{5} \text{ V cm}^{-1} = 1{,}800 \text{ V cm}^{-1}$$

'Low-field' conduction[25] occurs when $qaE/kT \ll 1$, where q is the charge on the mobile species (assumed to be M^{3+}) and a is the distance from the minimum to the maximum in the potential energy-distance relation (assumed to be 1 Å). Consequently, since in the present case

$$\frac{qaE}{kT} = \frac{3 \times 10^{-8} \times 1{,}800}{8.62 \times 10^{-5} \times 343} = 1.83 \times 10^{-3}$$

the low-field approximation seems justified. Under these conditions, the current density, due to ionic movement, is given approximately[25] by

$$i = \frac{4\, a^2\, n\, \nu\, q^2\, E}{kT} \exp -\frac{W}{kT} - 4\, a^2\, \nu\, q\, \frac{\partial n}{\partial x} \exp -\frac{W}{kT} \quad (3)$$

where n is the number of mobile ions in unit volume, ν is the number of chances per second that a given ion may jump the potential energy barrier if it has sufficient energy, W is the energy needed to jump the barrier and x is the distance.

In the steady state, Fick's first law gives

$$j = -D \frac{\partial n}{\partial x}$$

where j, the flux, is the number of ions diffusing through a plane of unit area in unit time and D is the diffusion coefficient of the mobile ion given by

$$D = D_o \exp -W/kT$$

Since the second term in equation (3) is the contribution to the current due to diffusion, it follows that

$$D_o = 4\, a^2 \nu$$

so that equation (3) may be rewritten as[87a]

$$i = \frac{n\, q^2\, E\, D}{kT} + D\, q\, \frac{\partial n}{\partial x}$$

While no value of the diffusion coefficient for any of the ions in the coloured film is available, a reasonable estimate may be made from data[87b] for Fe_3O_4. This material was chosen since it has a spinel structure and has as large a diffusion coefficient (for ferrous ion vacancies) as any comparable compound. At 343K, the value of D_{Fe} is about 5×10^{-35} cm^2 s^{-1}.

Assuming $\partial n/\partial x$ to be independent of x, its maximum value would arise when n = n at x = 0 and n = 0 at the surface of the film. The maximum value of n (in Fe_3O_4) would be that if all the iron ions were mobile. Since the molar volume of Fe_3O_4 is about 44.7 cm^3 the maximum value of n is about 4×10^{22} cm^{-3}. The maximum value of the current density obtainable by transport through such a film when it is 0.5 m thick is

$$i = \frac{4 \times 10^{22} \times (3 \times 1.602 \times 10^{-19})^2 \times 1{,}800 \times 5 \times 10^{-35}}{1.38 \times 10^{-23} \times 343}$$

$$+ \frac{5 \times 10^{-35} \times 3 \times 1.602 \times 10^{-19} \times 4 \times 10^{22}}{0.5 \times 10^{-4}}$$

hence $i = 1.76 \times 10^{-25} + 1.92 \times 10^{-26} = 1.95 \times 10^{-25}$ A cm^{-2}

This clearly indicates that dissolution cannot occur by transport of metal ions through the film (the dissolution current for the conditions employed here is approximately 3 mA cm^{-2}).

There is of course the possibility that in addition to metal ions passing out through the film, oxide ions move from the film surface to the metal. If this were to result in dissolution of the metal it would require the film to dissolve at the appropriate rate. The maximum additional current which could arise from oxide ion transport may be calculated (for Fe_3O_4) as above; in this case however $D_{ox} = 4.32 \times 10^{-15}$ and $n_{max} = 5.36 \times 10^{22}$ hence

$$i_{ox} = \frac{5.36 \times 10^{22} \times (2 \times 1.602 \times 10^{-19})^2 \times 1,800 \times 4.32 \times 10^{-15}}{1.38 \times 10^{-23} \times 343} +$$

$$\frac{4.32 \times 10^{-15} \times 2 \times 1.602 \times 10^{-19} \times 5.36 \times 10^{22}}{0.5 \times 10^{-4}}$$

$$= 9.04 \times 10^{-6} + 1.48 \times 10^{-6} = 1.05 \times 10^{-5} \text{ A cm}^{-2}$$

Again, however, the maximum possible current density is more than two orders of magnitude lower than the observed value. Clearly, therefore, the film must be porous and the anodic dissolution of the steel must occur through these pores.

Since as stated earlier (Section 9.1.) about 10% of the current is consumed in film formation it is apparent that the film formation reaction is also too rapid to occur by transport of ions through the film. This, of course, assumes that they must move through the whole thickness of the film. Since the film must be porous, it is conceivable that transport

of oxide ions and chromium ions into the film near the base of the pores could occur sufficiently rapidly to give the observed rate of film growth; fresh film being formed at the metal/film interface.

10.4. MECHANISM OF THE PROCESS

10.4.1. PREVIOUSLY SUGGESTED MECHANISMS

Only one attempt to produce a comprehensive explanation of the colouring process has been reported[88]. Some aspects of this theory are in accord with the results reported in this thesis and are similar to or identical with the suggestions presented later.

There are, however, two basic postulates which are difficult to accept. The first of these is that formation of the coloured film begins at the onset of stage II and that the film is formed by a dissolution-precipitation mechanism i.e. when the concentrations of anodically dissolved metal and cathodically produced Cr^{3+}, at the metal-solution interface, exceed the solubility of the chromium-rich spinel oxide precipitation of this oxide onto the metal occurs. The evidence obtained by X.P.S. (Section 2.2.1.5.), however, suggests that the composition of the film present during stage II is different from that of the coloured film. More important, if the coloured film were formed by a dissolution-precipitation process, the onset of film formation should be markedly delayed by rapid rotation of the electrode. In reality, however, whether film formation begins at the onset of stage II or III, rotating the electrode did not delay this process.

During stage III, it is suggested that the sites of the anodic and cathodic reactions are separated, the anodic reaction continuing at the base of the pores while the cathodic reaction occurs (only) at the surface of the film i.e. at the film/solution interface.

The second postulate which is questionable is that during stage III the rate of metal dissolution and film growth is determined by the rate of diffusion of the dissolution products through the pores of the film. There are two objections to this aspect of the theory. The first is that in deriving the desired equations, apparently conflicting assumptions are made. Thus it is argued that "since the (diffusion) process is a chemical, not an electrochemical one" the total flux of metal ions, due to both diffusion and migration is zero. If this were so, however, there would be no net movement of metal ions out of the pores, but the subsequent development of the theory is based on the rate of diffusion of metal ions along and out of the pores. A second criticism of the view that diffusion is the rate determining step is that this could only be true if the presence of metal ions at the bottom of the pores affected the rate of dissolution. This could be true if one of the following applied

a) The reverse process i.e. metal deposition could occur at a significant rate, or

b) The final stage in the dissolution process involved the chemical dissolution of a solid reaction product.

The potential at which film formation occurs is so very far from that at which metal deposition occurs, that the first of these conditions is certainly not satisfied. The second condition is explicitly ruled out by Evans and does not seem likely to produce the observed experimental rise of dissolution rate with potential.

10.4.2. SUGGESTED MECHANISM OF THE PROCESS OCCURRING ON OPEN CIRCUIT

Stage I

On immersion in the colouring bath the potential of the steel

rises because of the strongly oxidising nature of the dichromate solution. The surface of the steel becomes covered by a passivating film which is thinner than, and has a different composition to, that originally present on the steel. Dissolution of the initial film must therefore occur and the new film is probably produced by a combination of oxidation of the steel and reduction of dichromate. Little steel dissolution occurs during this stage since its surface is covered by a passivating layer.

Stage II

Throughout this stage the potential of the steel is almost constant and is close to that for the onset of transpassive dissolution. The film thickens somewhat and undergoes further changes in composition. In contrast to the mechanism proposed by Evans, it is proposed that these changes occur as a result of direct incorporation of material into the existing film. Some dissolution of the existing film may also occur.

The properties of the film are believed to change from those of a passive film to a transpassive film, as is to be expected from the potential at which the process occurs. The considerable time needed for completion of this change, suggests that either dichromate reduction or metal dissolution can occur only at a low rate on or through the film present during most of this stage. The weight loss measurements support this view since little change in weight is apparent during this stage.

Stage III

On the basis of the evidence cited earlier, it is believed that the composition of the film on the steel remains constant during this stage; its thickness, however, increases exponentially with potential whilst the potential rises linearly with time.

As argued earlier, the observed dissolution rates are possible only if the film is porous. The similarity of the Tafel slopes observed for this dissolution process and that of transpassive dissolution of steel in the absence of dichromate, strongly suggests that the mechanism of the dissolution process is the same in the two instances. The differences are that in the colouring process dissolution occurs because dichromate is being reduced and dissolution occurs through pores in a relatively thick film. In the normal transpassive dissolution the potential is maintained by a potentiostat and any film present is much thinner than the coloured film. A possible mechanism for the transpassive dissolution of steel is suggested in Appendix 2.

Because workers at International Nickel reported that the texture of the film reproduces crystallographic features of the underlying metal, Evans proposed that areas such as grain boundaries, twin boundaries and slip planes continue to act as anodic regions during the colouring process. He supports this proposal by the statement that "on the basis of the micrographic evidence (referred to above), these areas remain free of film". This is difficult to reconcile with the apparently uniform colouring of the steel surface.

Since "electron micrography also reveals the existence of small pores ---, distributed uniformly through the film" he suggests that these coincide with other sites for anodic dissolution. Whilst it would be difficult to contest this view, his further conclusion that "this evidence implies that the film,once nucleated on the metal surface, "freezes" the location of the sites for anodic dissolution" is open to question. Many passivating films are believed to be constantly undergoing disruption and repair. It seems logical therefore to accept the possibility that this also occurs with the coloured film.

Providing the area of metal undergoing anodic dissolution remains substantially constant, the observed relation between the rate of dissolution and potential is that to be expected from simple electrochemical principles.

The questions, posed by the observations concerning stage III, which need to be answered are;

a) Why does the potential rise with time,

b) Why is this rise so slow,

c) Why is it linear with time, and

d) Why does the film thickness increase exponentially with potential?

As stated in the introduction to this chapter, it is very difficult to give an accurate quantitative explanation of such a complex process. The following treatment, as will be shown later, is not exact but it indicates a possible answer to some of these questions.

Accepting, for the moment, the linear increase of potential with time then, as argued above an exponential increase in the dissolution rate with potential and hence with time is to be expected. Because the rates of the anodic and cathodic processes must always be equal, the rate of dichromate reduction must also increase exponentially with time and potential. Since the composition of the film remains constant during this stage and the increase in potential would normally decrease the rate of a reduction process the only factor which could allow the rate of dichromate reduction to increase would be an increase in the true area of the surface at which this process occurs. This surface is presumably the film/solution interface. In contrast to the view taken by Evans, if the film is not formed by a dissolution-precipitation mechanism and if the pores initially present do not have to persist, dichromate reduction can occur wherever the film and solution are in contact. Moreover as the film thickens, and if it is very

porous, a substantial increase in this area is to be expected. Experimental evidence that the rate of dichromate reduction is increased by increasing the thickness of the film was presented in Section 8.4.

Thus, assuming the rate of dichromate reduction is given by

$$i_c = k_c A \exp - \alpha_c f E \qquad (4)$$

where A is the total area of the film/solution interface. It is further assumed that

$$A = A_s + k_1 l \qquad (5)$$

where A_s is the area of the outside of the film which remains essentially constant, l is the thickness of the film and k_1 a proportionality factor converting the thickness into the internal accessible area of the film. As found experimentally, the dissolution rate obeys an equation of the form

$$i_a = k_a \exp \alpha_a f E \qquad (6)$$

and since $i_a = i_c$, then

$$k_a \exp \alpha_a f E = k_c (A_s + k_1 l) \exp - \alpha_c f E$$

consequently

$$l = \frac{k_a}{k_c k_1} \exp \left[(\alpha_a + \alpha_c) f E \right] - \frac{A_s}{k_1}$$

If it is assumed that $l = 0$ when $E = E_p$ (the plateau potential)

$$\frac{A_s}{k_1} = \frac{k_a}{k_c\ k_1} \exp\ (\alpha_a + \alpha_c)\ f\ E_p$$

hence $$1 = \frac{k_a}{k_c\ k_1} \left[\exp\ (\alpha_a + \alpha_c) f\ E - \exp\ (\alpha_a + \alpha_c) f\ E_p\right]$$

or $$1 = k_2 \left[\exp\ (\alpha_a + \alpha_c) f\ \Delta V - 1\right] \qquad (7)$$

where $\Delta V = E - E_p$

At first sight equation (7) does not appear to agree with the observed relationship (equation (1)). It should be noted, however, that according to equation (1), $k_2 = 3.1 \times 10^{-8}$ cm so that equation (7) may be rewritten as

$$1 + 3.1 \times 10^{-8} = 3.1 \times 10^{-8} \exp\ (\alpha_a + \alpha_c) f\ \Delta V \qquad (8)$$

Since the smallest value of 1 (or more strictly the resistance) which was used to obtain equation (1) was about 2.5×10^{-6} cm, the 3.1×10^{-8} on the L.H.S. of equation (8) can clearly be neglected.

Consequently on the basis of this model, which assumes that the potential increases linearly with time, the observed exponential dependence of the current on potential requires the film thickness to increase exponentially with potential as observed experimentally. Many of the equations used or derived above must, however, be erroneous for the following reasons.

1) No concentration term was included in equation (4), but the dichromate concentration will almost certainly vary through the film.

2) The expression for the current to a porous electrode is not that used in equation (4). A more correct expression for the current flowing into a cylindrical pore, which also takes account of mass transport within the

pores is[89]

$$i = \rho\, c\, \pi\, a^2\, n\, F\, D \tanh \rho\, l$$

where c is the concentration (of dichromate) at the mouth of the pore, a the pore radius, D the diffusion coefficient (of dichromate), l is the depth of the pore and

$$\rho = (2\, i_o / a\, n\, F\, c\, D)^{\frac{1}{2}} \exp - \frac{\alpha_c\, f\, E}{2}$$

where i_o is the exchange current density for the reaction being studied.

3) No account has been taken of the ohmic drop across the film. If during its formation the film has the same resistance as that measured experimentally, this ohmic drop cannot be neglected. Thus, e.g. when Δ V = 15 mV, the ohmic drop is about 4 mV while when Δ V = 20 mV the ohmic drop is 29 mV.

These considerations make it clear that any quantitative treatment of this model would be very complex. Qualitatively, however, the mechanism envisaged is that the dissolution reaction always occurs at the rate given by equation (6). The potential rises with time because the rate of dichromate reduction increases with time and this in turn is due to the thickness of the film increasing with time. The rate of increase in the potential is therefore determined, ultimately, by the rate of increase in film thickness.

At least two mechanisms of film formation can be envisaged. In the first, the reduction of dichromate results in incorporation of the reduction products and some Cr VI into the surface of the film. This changes its stoichiometry making it thermodynamically unstable. Restoration

of the initial stoichiometry is achieved by iron, manganese and oxygen being incorporated from the solution.

An alternative mechanism is that film formation occurs only at the metal/film interface. Diffusion of chromium ions and oxide/hydroxide ions from the solution at the base of the pores occurs. The driving force for this process being the introduction of excess iron and manganese ions into the film from the steel surface.

It should be noted, that the very different exponents in the equations relating the film thickness (equation (1)) and dissolution current (2) to the potential, imply that the film thickens more rapidly than the current rises with increase in potential.

Stage IV

During this stage, the film slowly changes in character and eventually becomes powdery. Since the potential remains almost constant with time the rates of dissolution and dichromate reduction probably also remain constant with time. This could be due to the film no longer thickening or if changes in thickness occur they may be compensated by changes in the properties of the film. The powdery state probably results, as Evans has suggested, from undermining of the film at the metal/film interface by excessive anodic dissolution.

10.4.3. CONSTANT POTENTIAL CONDITIONS

The foregoing model is also consistent with the current-time curve at constant potential in the colouring region (Section 9.4). Unlike the open circuit case, the rates of the anodic and cathodic reactions do not have to be equal. When the specimen is immersed in the solution the surface is passivated and dichromate reduction inhibited. As the nature

of the film changes the rate of dissolution increases more rapidly than the rate of reduction. This causes the observed rise in the (anodic) current. Subsequently as more film is produced the rate of reduction overtakes the rate of dissolution causing a progressive fall in the current. The (cathodic) current becomes constant when the rate of dichromate reduction reaches its maximum rate at that potential. Presumably no further film thickening occurs at this stage or if changes in thickness do take place they are compensated by changes in the properties of the film.

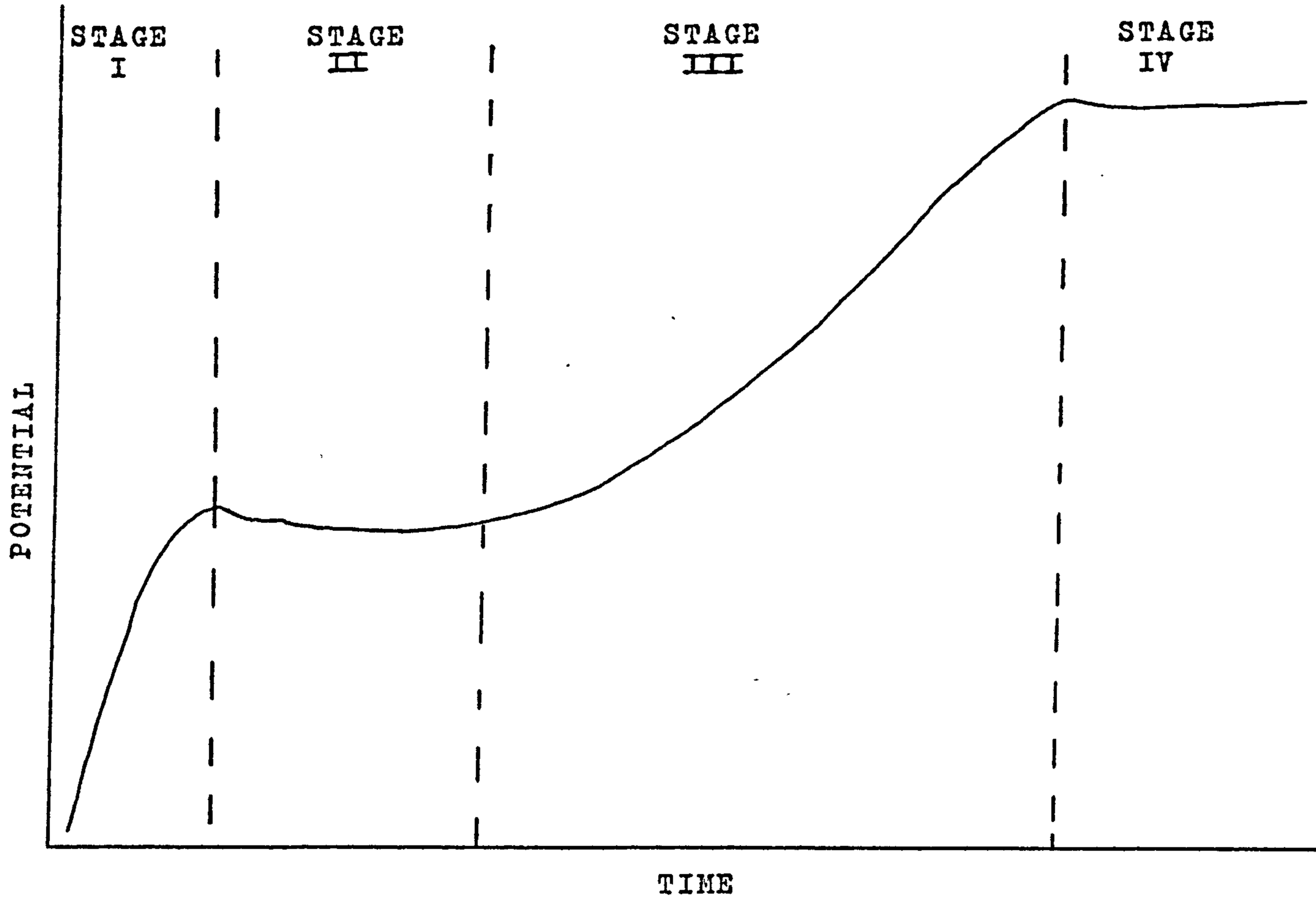

FIG 10.1 STAGES OF THE COLOURING PROCESS

APPENDIX

A.1. THE FEASIBILITY OF SEPARATING THE ANODIC AND CATHODIC PROCESSES USING A RING DISC TECHNIQUE

The ring-disc method has been reviewed by Albery and Hitchman[90]. It would provide a particularly suitable method of obtaining the anodic partial current if it were possible to detect the species dissolving during the colouring process, at the ring. Since the problems of fabricating a ring disc electrode are great, particularly for use at elevated temperatures, a preliminary study to determine a suitable ring material was undertaken.

On the basis of previous work on the reduction of dichromate[91], the most suitable ring material for use in the colouring solution appeared to be platinum. Consequently experiments to determine whether it would be possible to monitor the rate of dissolution of iron, which has been shown to be the major dissolving species (Section 9.2.), were carried out with a platinum rotating disc electrode.

A.1.1. EXPERIMENTAL

The cell employed was the first one described in Chapter 6. The electrode potentials quoted in this section are with respect to a hydrogen electrode in 5M sulphuric acid solution at 70°C. The most suitable method of making a platinum electrode for these studies was to seal a platinum wire into the end of a soda glass tube. The end of the tube was then cut at 90° to its axis to produce a flat surface containing the cross-section of the platinum wire as the electrode. The electrode was aligned on the drive shaft and secured using adhesive tape.

A preliminary linear potential sweep was carried out on the

platinum electrode in 5M sulphuric acid at 70°C to determine its behaviour in the background electrolyte. The reduction of ferric iron at the platinum electrode at 70°C was investigated in a solution which was 0.01M in ferric sulphate and 5M in sulphuric acid, using the rotated electrode and a sweep rate of 10 mV s^{-1}.

The behaviour of the platinum electrode in 2.5M chromic acid, 5M sulphuric acid at 70°C, over the potential range in which ferric iron reduction occurred in sulphuric acid was investigated by means of linear potential sweeps using a rotated electrode. The electrode was pretreated by either holding its potential at -0.2V or by leaving it on open circuit. In cases where the electrode was pretreated at -0.2V the potential was swept from this value. In cases where the electrode was held on open circuit the electrode potential was swept from +0.8V.

The dichromate solution was then made up to 0.01M in ferric iron by the addition of solid ferric sulphate and the current-potential curves recorded with the same methods of pretreatment described above. Subsequently the ferric iron concentration was made up to 0.02M and the same procedure repeated.

A.1.2. RESULTS

Typical current-potential curves are shown in Figs. A.1 to A.5. Fig. A.1 shows the background sweep on the platinum electrode in 5M sulphuric acid at 70°C. Fig. A.2 shows the current-potential curve for ferric iron reduction at the platinum electrode in a solution 0.01M in ferric iron and 5M in sulphuric acid at 70°C. Figs. A.3 and A.4 show the current-potential curves for the platinum electrode in a solution 2.5M in chromic acid and 5M in sulphuric acid at 70°C. Figs. A.5(a) and A.5(b) show the current-potential curves obtained after the addition of ferric sulphate to make the

solution 0.01M and 0.02M in ferric iron, respectively. These curves were obtained after pretreating the electrode by leaving it at its open circuit potential; no effect due to the addition of ferric iron was observed when the electrode had been pretreated at -0.2V.

A.1.3. DISCUSSION

In 5M H_2SO_4, the onset of ferric ion reduction at the platinum electrode occurred at a potential of 0.75V. The diffusion limited current at a rotation speed of 647 r.p.m. was 5.78 mA cm^{-2} for a 0.01M solution of ferric iron. When ferric sulphate was added to the dichromate solution, no effect on the potential sweep was observed when the electrode was pretreated at -0.2V. However when the electrode was pretreated by leaving it at its open circuit potential, a change in the current potential curve on the return sweep in the potential region 0.1 to 0.5V was observed. Although the current in this region increased with increase in ferric iron concentration (Fig. A.5) it was found to be rather irreproducible. An investigation of the rotation speed dependence of this current was not possible because of this irreproducibility.

Since the change in the current-potential curve is observed only on the return sweep and only after pretreating the electrode by allowing it to remain at its open circuit potential, it is unlikely that the observed change is due simply to the reduction of ferric iron. It seems more likely that the change in the current-potential curve, on addition of ferric iron, is due to the modification of an oxide film on the surface of the platinum. This would appear to be borne out by the irreproducibility of the currents and the absence of the effect after cathodic pretreatment.

The complicated processes which occur in dichromate solutions containing ferric ion and the irreproducibility of the current associated

with the presence of ferric iron, showed that platinum would not be a suitable material for a ring-disc study of iron dissolution during the colouring process.

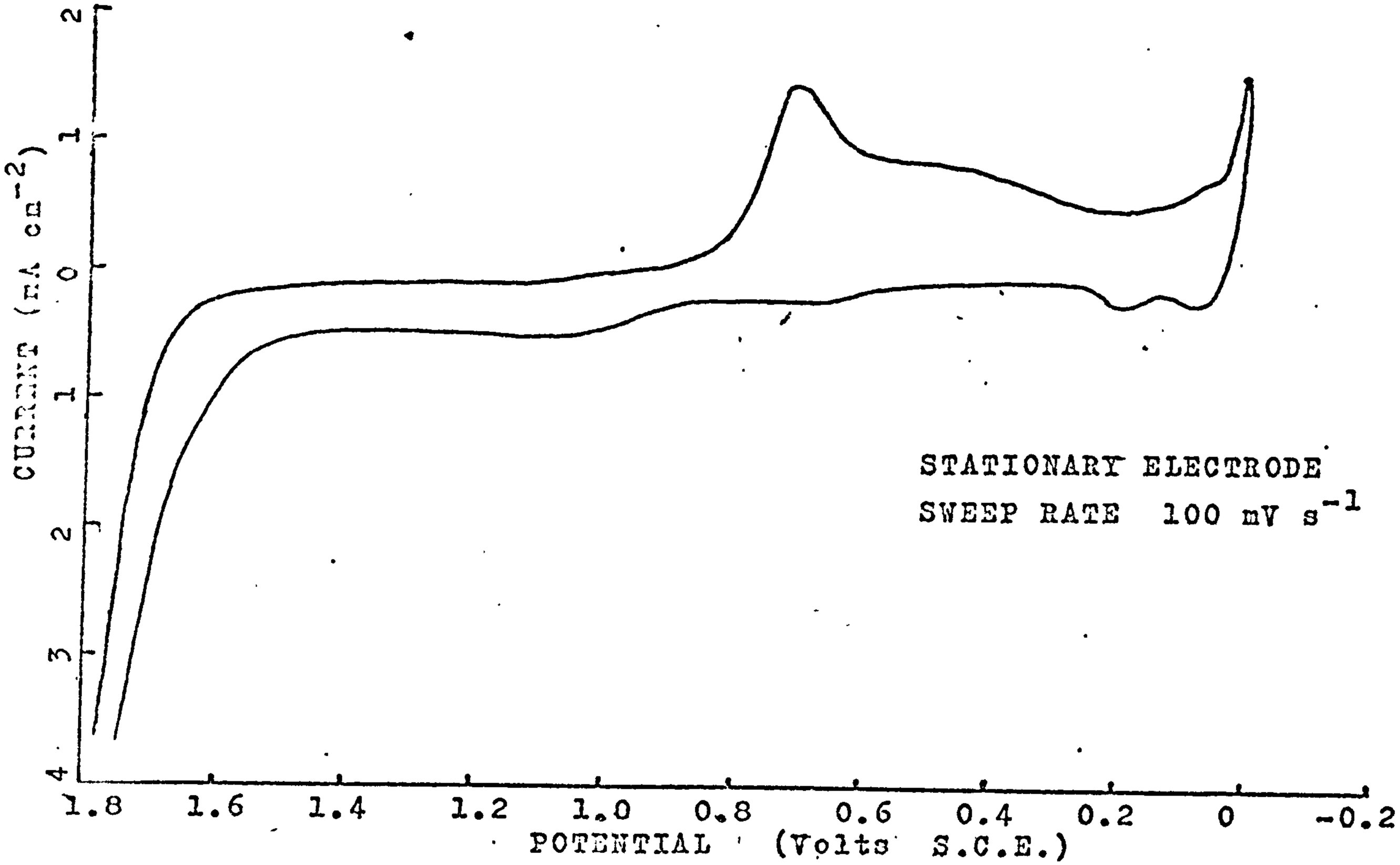

FIG. A.1 CURRENT-POTENTIAL CURVE FOR A PLATINUM ELECTRODE IN 5M SULPHURIC ACID AT 70°C

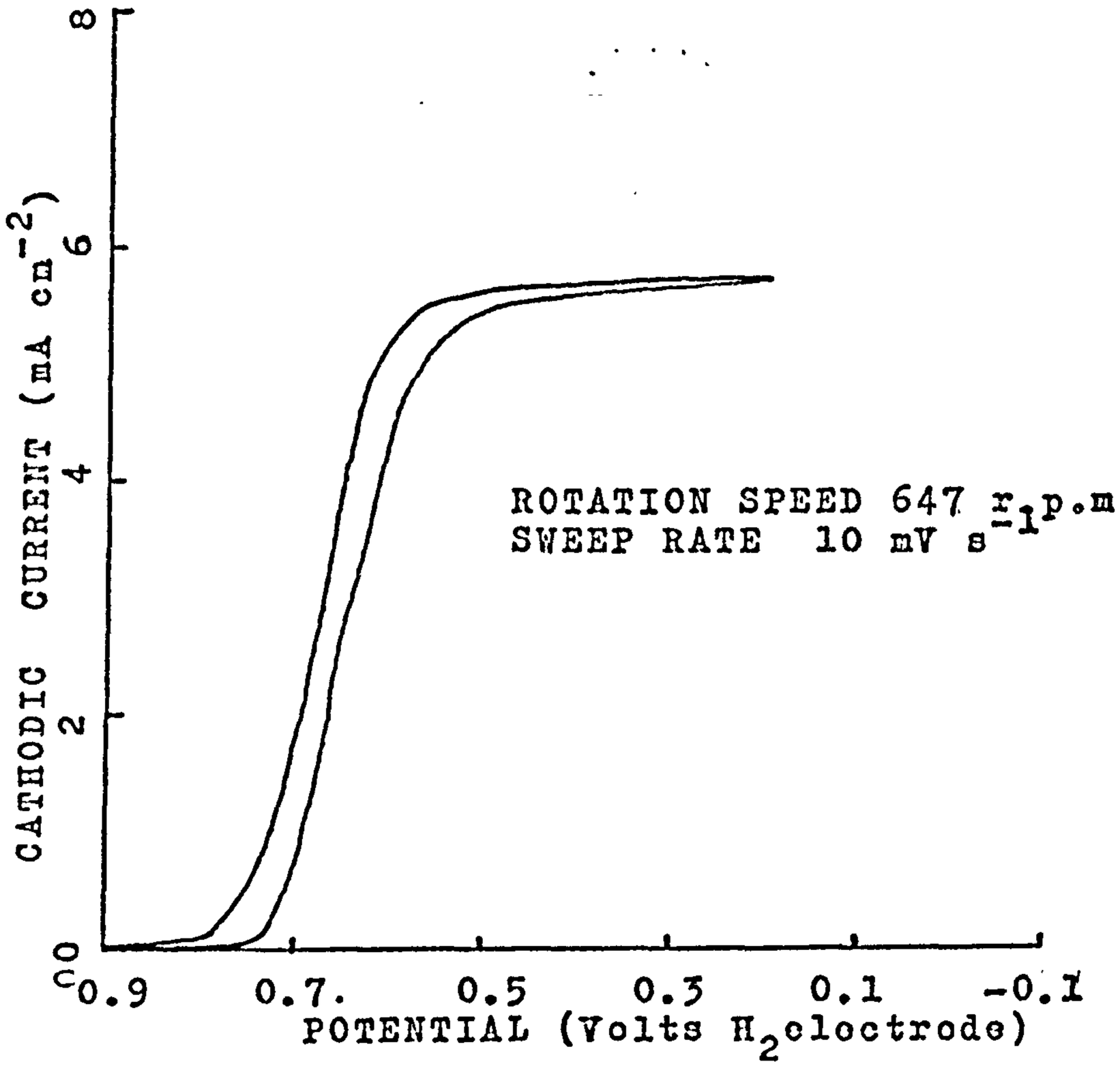

FIG. A.2 CURRENT-POTENTIAL CURVE FOR FERRIC ION REDUCTION AT A PLATINUM ELECTRODE IN 5M SULPHURIC ACID 0.01M FERRIC SULPHATE AT 70 C.

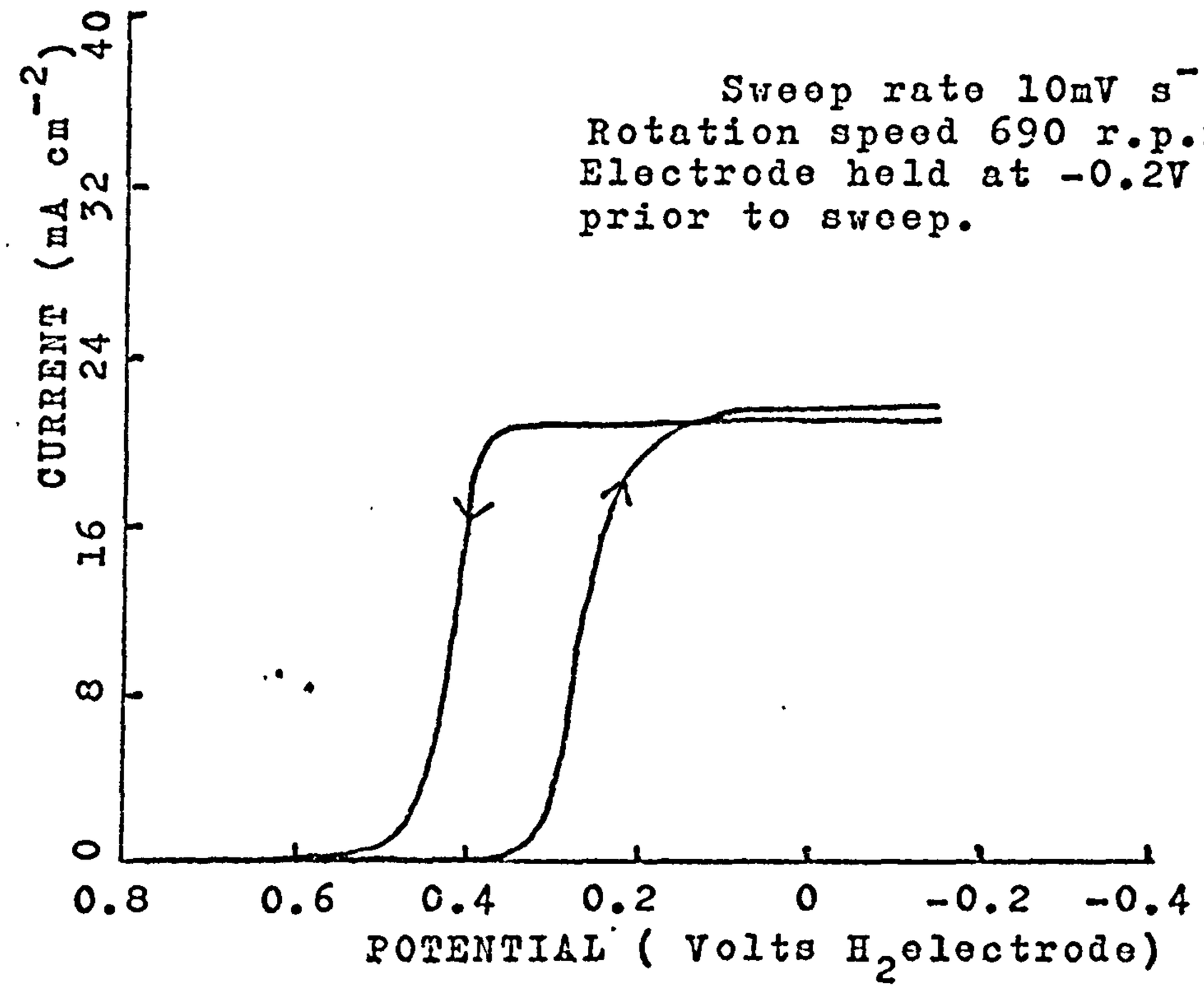

FIG.A.3 CURRENT-POTENTIAL CURVE FOR A PLATINUM ELECTRODE IN 5M SULPHURIC ACID 2.5M CHROMIC ACID AT 70°C

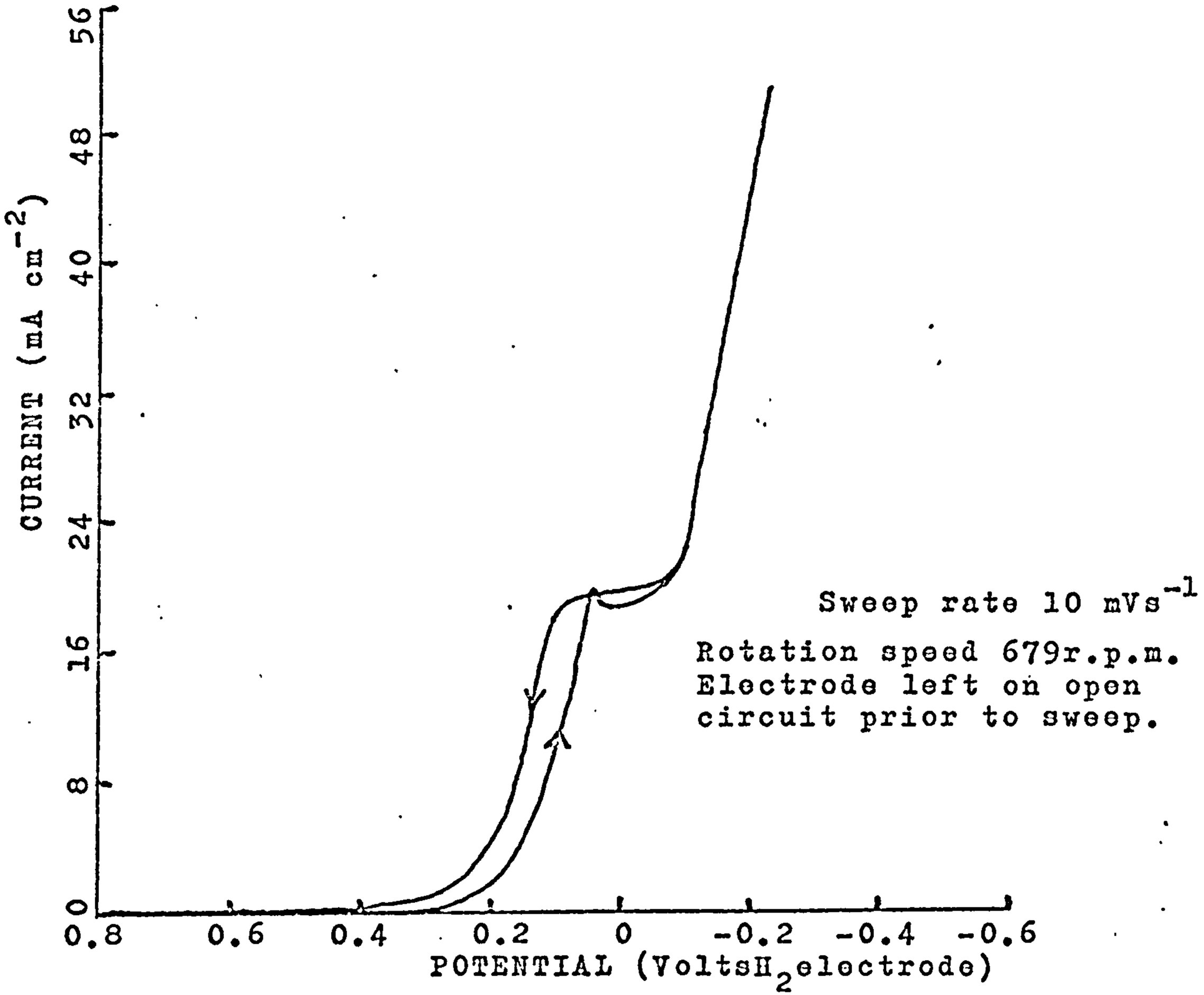

FIG.A.4 CURRENT-POTENTIAL CURVE FOR A PLATINUM ELECTRODE IN IN 5M SULPHURIC ACID 2.5M CHROMIC ACID.

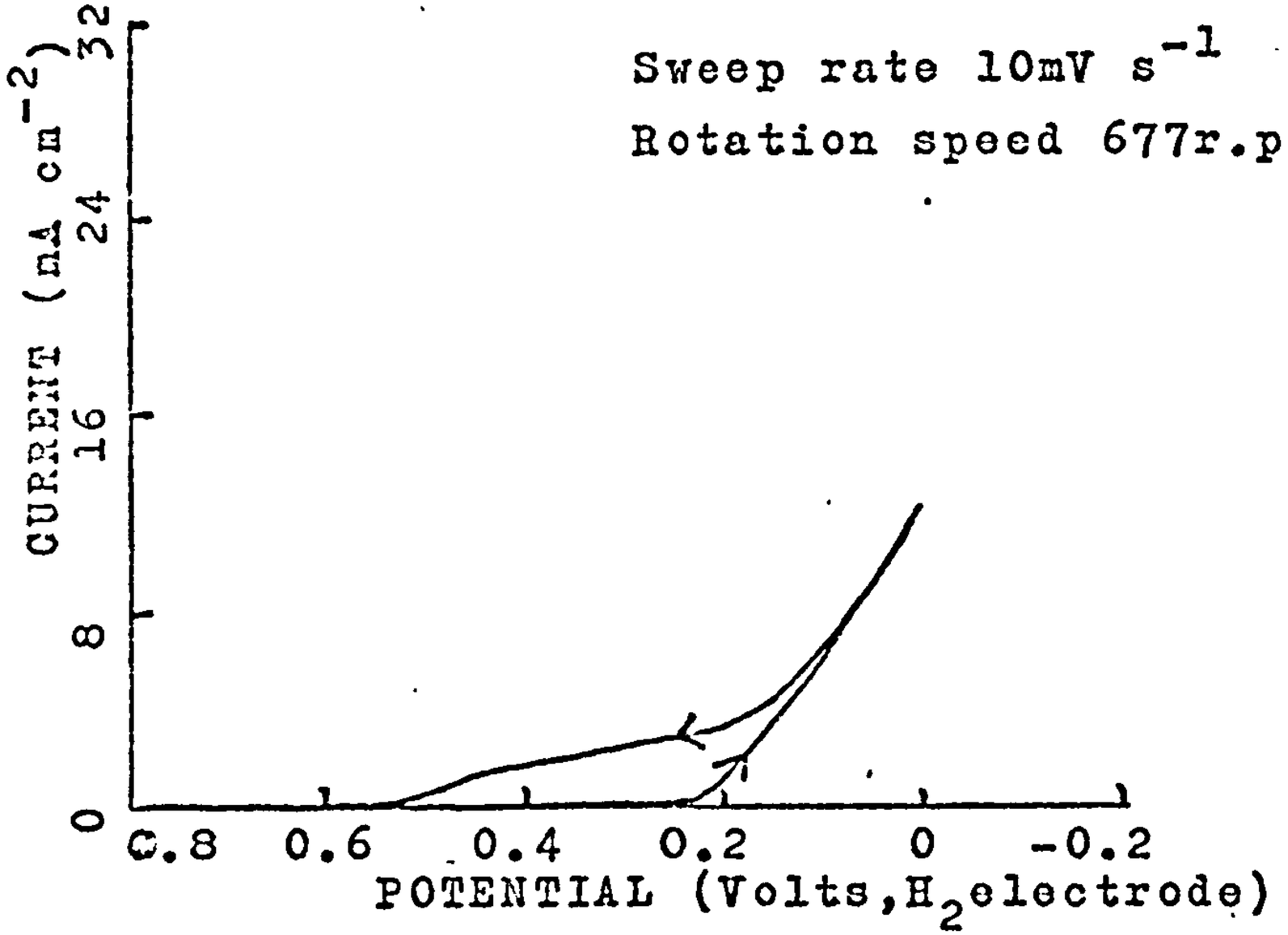

(a)

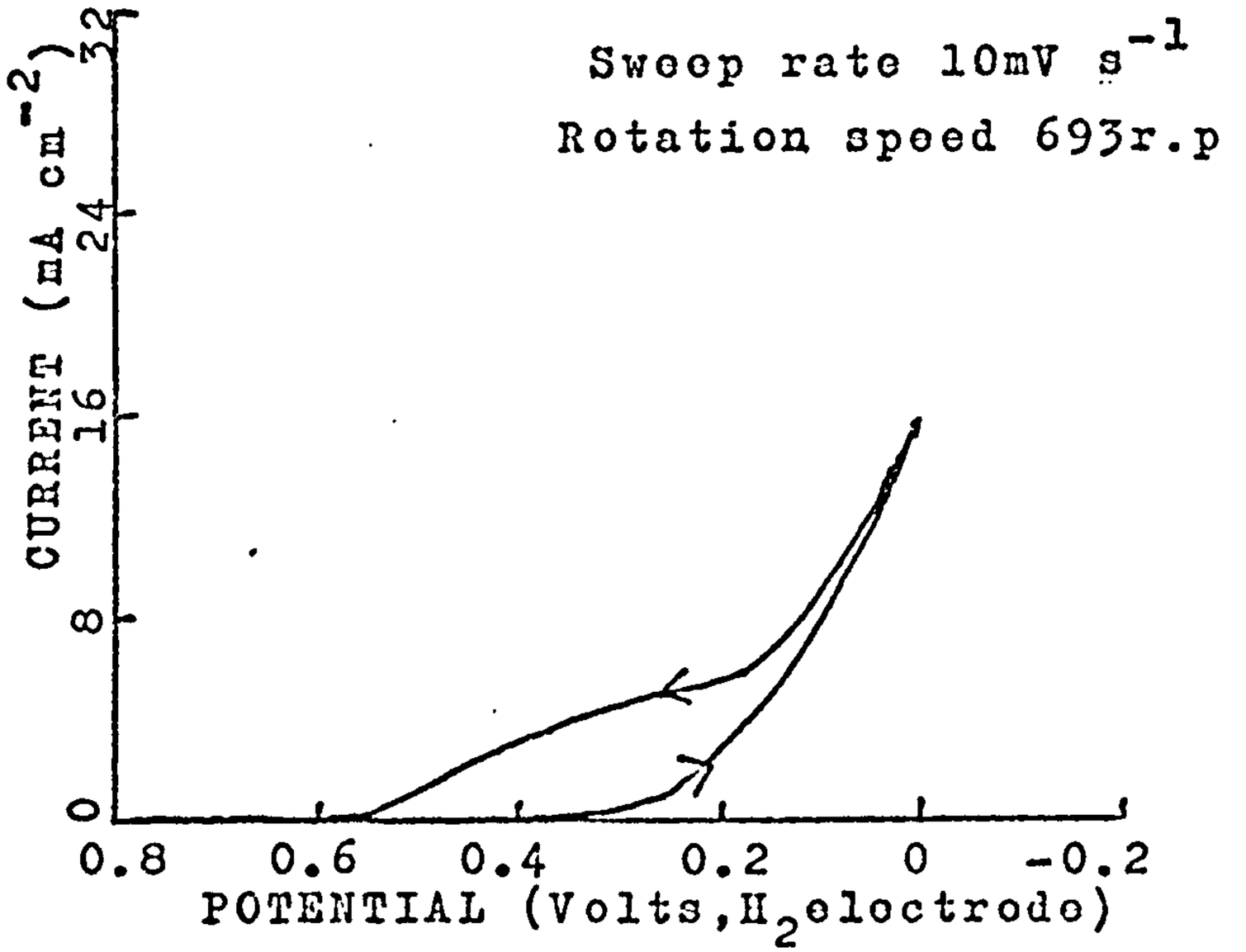

(b)

FIG. A.5 CURRENT-POTENTIAL CURVES FOR A PLATINUM ELECTRODE IN 2.5 M CHROMIC ACID 5M SULPHURIC ACID AT 70 C FOR SOLUTIONS

(a) 0.01M FERRIC SULPHATE

(b) 0.02M FERRIC SULPHATE

APPENDIX B

POSSIBLE EXPLANATION OF THE TAFEL SLOPE FOR STAINLESS STEEL DISSOLUTION

An explanation of the observed 34 mV Tafel slope can be given if the following reaction scheme involving adsorbed anion intermediates is considered and Temkin conditions assumed[92].

$$M + X^- \underset{k_{-1}}{\overset{k_1}{\rightleftharpoons}} MX + e \qquad (1)$$

$$MX + X^- \underset{k_{-2}}{\overset{k_2}{\rightleftharpoons}} MX_2 + e \qquad (2)$$

$$MX_2 + X^- \xrightarrow{k_3} MX_3(aq) + e \qquad (3)$$

The fraction of the surface covered by MX is denoted as θ_1, and that covered by MX_2 by θ_2 and the following assumptions are made.

1) Steps (1) and (2) are in quasi-equilibrium
2) Step (3) is the rate determining step
3) $\theta_1 > \theta_2$ and $\theta_1 = \theta_T$ (the total fractional coverage with adsorbed species)
4) The metal ion produced is trivalent
5) The standard free energy of adsorption of the adsorbed species may be written as[92]

$$\Delta G^o_{\theta,1} = \Delta G^o_o - g(\theta)$$

$$\Delta G^o_{\theta,2} = \Delta G^o_o - g(\theta)$$

The forward and reverse rates of reaction (1) are

$$V_1 = k_1 [X^-] \exp (1 - \beta_1) fE \exp[-(1 - \alpha)g(\theta)] \quad (4)$$

$$V_{-1} = k_{-1} \exp(-\beta_1 fE) \exp [\alpha g(\theta)] \quad (5)$$

consequently if this step is in quasi-equilibrium, then

$$V_1 = V_{-1}$$

$$k_1 [X^-] \exp(1 - \beta_1)fE \exp[-(1 - \alpha)g(\theta)] = k_{-1} \exp -\beta_1 fE \exp [\alpha g(\theta)]$$

hence $$\frac{k_1 [X^-]}{k_{-1}} \exp fE = \exp g(\theta)$$

or $$\exp g(\theta) = K_1 \exp fE \quad (6)$$

Since in the second step there is no increase in the number of sites covered with adsorbed species, then if it is in quasi-equilibrium

$$k_2 \theta_1 [X^-] \exp(1 - \beta_2)fE = k_{-2}\theta_2 \exp(-\beta_2 fE)$$

$$\therefore \quad \frac{\theta_2}{\theta_1} = \frac{k_2 [X^-]}{k_{-2}} \exp fE = K_2 \exp fE \quad (7)$$

The rate of reaction (3) is given by

$$V_3 = k_3 \theta_2 [X^-] \exp(1 - \beta_3)fE \exp \alpha_3 g(\theta) \quad (8)$$

It can be seen from equation (7) and the fact that $\theta_1 \simeq \theta_T$ that θ_2 cannot be ignored. However, substituting for θ_2 in equation (8) from equation (7) gives

$$V_3 = k_3\,\theta_1\,[X^-]\,K_2\,\exp\,fE\,\exp(1-\beta_3)fE\,\exp[\alpha_3\,g(\theta)] \qquad (9)$$

The term in θ_1 can now be ignored since the effect of this is much smaller than ignoring θ_2 in equation (8).

Leaving out the linear term in θ_1 and substituting for $\exp\alpha_3 g(\theta)$ from equation (6) in equation (9)

$$V_3 = k_3\,K_1^{\alpha}\,K_2\,[X^-]\,\exp\,fE\,\exp(1-\beta_3)fE\,\exp\,\alpha_3\,fE$$

Consequently if $\alpha_3 = \beta_3$ which is very probable since the symmetry factor for the effect of potential on the activation energy is likely to be the same as that for the effect of adsorption on the activation energy.

$$V_3 = k_3^1 \left\{\frac{k_1}{k_{-1}}\,[X^-]\right\}^{\alpha} \frac{k_2}{k_{-2}}\,[X^-]^2\,\exp\,2\,fE$$

$$i = k_3''\,[X^-]^{2+\alpha}\,\exp\,2\,fE$$

$\therefore$ Consequently since at 70°C

$$\frac{2.303\,RT}{F} = 0.068V$$

the Tafel slope $\frac{dE}{d\,\log\,i} = \frac{2.303\,RT}{F} = 34\ mV$

REFERENCES

1. T.E. Evans, A.C. Hart, H. James and V.A. Smith, Trans. I.M.F. 50, 77, (1972).

2. C.E. Naylor, Plating 37, 153, (1950).

3. T.E. Evans, A.C. Hart and A.N. Skedgell, Trans. I.M.F. 51, 108, (1973).

4. A.C. Hart, V.A. Smith and A.N. Skedgell, U.K. Patent Specification 1,341,220.

5. D.A. Vermilyea, page 211, "Advances in Electrochemistry and Electrochemical Engineering", Volume 3, Edited P. Delahay C.W. Tobias, Interscience (1963).

6. V. Brusic, page 1, "Oxides and Oxide films", Volume 1, Edited J.W. Diggle Marcel Dekker (1972).

7. T.P. Hoar, Corr. Sci. 7, 341, (1967).

8. J. O'M. Bockris, D. Drazik and A.R. Despic, Electrochim. Acta 4, 325, (1961).

9. Y.M. Kolotyrkin, Z. fur. Elektrochemie 62, 644, (1958).

10. H.H. Uhlig, page 25, Proceedings of 3rd International Congress on Metallic Corrosion, Mir, Moscow (1966).

11. L. Germer, A. Macrae, J. Appl. Physics 33, 2923, (1962).

12. K. Arnold, K. Vetter, Z. fur. Elektrochemie 62, 224, 407, (1960).

13. R.P. Frankenthal, Electrochim. Acta 16, 1845, (1971).

14. J. O'M. Bockris et al. ibid. 16, 1859, (1971).

15. M. Fleischmann and H.R. Thirsk, J. Electrochem Soc 110, 693, (1963).

16. R.D. Armstrong and H.R. Thirsk, Electrochim. Acta 17, 171, (1972).

17. R.D. Armstrong and J.A. Harrison, J. Electroanal. Chem. 36, 79, (1972).

18. K.J. Vetter, Electrochim. Acta 16, 1923, (1971).

19. K.J. Vetter, Z. fur. Elektrochemie 59, 67, (1955).

20. K.J. Vetter and F. Gorn, Electrochim. Acta 18, 321, (1973).

21. N. Cabrera, N.F. Mott, Repts. Prog. Physics 12, 163, (1948).

22. E.J.W. Verwey, Physica 2, 1059, (1935).

23. N. Sato and M. Cohen, J. Electrochem Soc. 111, 512, (1964).

24. A. Gunterschulze and H. Betz, Z. Phys. 92, 367, (1934).

25. L. Young, page 21, Anodic Oxide films, Academic Press (1961).

26. M. Prazak, V. Prazak and Vl.Cihal, Z. fur. Elektrochemie 62, 739, (1958).

27. A. Desestret, I. Epelboin, M. Froment, M. Keddam, and Ph. Morel, Electrochim. Acta 8, 433, (1963).

28. Th. Heumann, R. Schurmann Werkstaffe und Korrosion 9, 560, (1961).

29. V.V. Andreeva, page 535, Proceedings of 2nd International Congress on Metallic Corrosion, NACE New York (1966).

30. R. Olivier, page 314, Sixth Meeting C.I.T.C.E. Butterworths London 1955.

31. Vl. Cihal and M. Prazak, J. Iron Steel Institute 360, (1959).

32. I. Epelboin, M. Froment and Ph. Morel, Electrochim. Acta 6, 51, (1962).

33. R.H. Roberts and W.J. Shutt, Trans. Faraday Soc. 34, 1455, (1938).

34. R.D. Armstrong and M. Henderson, J. Electroanal. Chem. 32, 1, (1971).

35. Th. Heumann and W. Rosenev, Z. fur. Electrochmie 59, 722, (1955).

36. Th. Heumann and H.S. Panesar, J. Electrochem Soc. 110, 629, (1963).

37. W.J. Plieth and K.J. Vetter, Ber. Bunsenges. Phys. Chem. 73, 1077, (1969).

38. R. Knoedler and V.E. Heusler, Electrochim. Acta 17, 197, (1972).

39. R.D. Armstrong and M. Henderson, J. Electroanal. Chem. 40, 121, (1972).

40. C. Wagner and W. Traud, Z. fur. Elektrochemie 44, 391, (1938).

41. U.R. Evans, Metallic Corrosion Passivity and Protection, Edward Arnold London (1937).

42. T.P. Hoar "Modern Aspects of Electrochemistry" Volume 2, Edited J. O'M. Bockris, Butterworths, London, (1959).

43. K.J. Vetter, page 741 "Electrochemical Kinetics" Academic Press New York (1967).

44. M. Stern, J. Electrochem. Soc. 105, 638, (1958).

45. Y.M. Kolotyrkin, page 10 1st International Congress on Metallic Corrosion, Butterworths London (1962).

46. A. Piotrowski and R. Lebet, page 417, Proceedings of 3rd International Congress on Metallic Corrosion, Mir, Moscow, (1966).

47. M. Stern and A.C. Makrides, J. Electrochem. Soc. 107, 877, (1960).

48. G.H. Cartledge, J. Electrochem. Soc. 113, 328, (1966).

49. G.H. Cartledge, Brit. Corros. J. 1, 293, (1966).

50. N. Hackermann and R.A. Powers, J. Phys. Chem. 57, 139, (1953).

51. F.A. Posey and R.F. Sympson, J. Electrochem. Soc. 109, 716, (1962).

52. D.M. Brasher and A.D. Mercer, Trans. Faraday Soc. 61, 803, (1965).

53. D.M. Brasher et al. Br. Corros. J. 5, 264, (1970).

54. K.E. Heusler, Ber. Bunsenges Phys. Chem.72, 1197, (1968).

55. International Nickel Ltd. private communication.

56. K.S. Kim, A.F. Gossman and N. Winegrad, Analyt. Chem. 46, 197, (1974).

57. T. Dickinson, A.F. Povey and P.M.A.Sherwood,
J.C.A. Faraday 1 72, 298, (1975).

58. G.C. Allen, P.M. Tucker, A. Capon and R. Parsons,
J. Electroanal. Chem. 50, 335, (1974).

59. T. Dickinson, A.F. Povey and P.M.A. Sherwood,
J.C.S. Faraday 1 72, 686, (1977).

60. T. Dickinson, A.F. Povey and P.M.A. Sherwood,
J.C.S. Faraday 1 73, 327, (1977)

61. A.A. Metcalfe and A.F. Povey, J. Electroanal. Chem. submitted for publication.

62. A. Aoki, Jap. J. Appl. Phys. 15, 305, (1976).

63. U.R. Evans, J. Chem. Soc. 1020 (1927).

64. W.H.J. Vernon, J.F. Wormwell and T.J. Wurse, J. Chem. Soc. 621 (1939).

65. T.N. Rhodin, Ann. N.Y. Acad. Sci. 58, 855, (1954)

66. E.M. Mahla and N.A. Neilsen, Trans. Electrochem. Soc. 93, 1, (1948).

67. International Nickel Ltd. private communication.

68. A.C. Hart, U.K. Patent 1,305,636.

69. M. Sluyters-Rehbach and J.H. Sluyters, page 1, "Electroanalytical Chemistry" Volume 4, Edited, A.J. Bard, Marcel Dekker (1970).

70. R.D. Armstrong and K. Edmonson, Electrochimica Acta 18, 937, (1973).

71. R.D. Armstrong, T. Dickinson and P.M. Willis,
J. Electroanal. Chem. 53, 389, (1974).

72. J. Ross Macdonald, J. Chem. Phys. 61, 3977, (1974).

73. K.S. Cole and R.H. Cole, J. Chem. Phys. 19, 1484, (1951).

74. G. Okamoto and T. Shibata, Corr. Sci. 10, 371, (1970).

75. V.G. Levich, Acta Physicochimica U.R.S.S. 17, 257, (1942).

76. J.A.V. Butler, Trans. Faraday Soc. 19, 720, (1924).

77. T. Erdey Gruz and M. Volmer, Z. Physik. Chem. A 150, 203, (1930).

78. T. Erdey Gruz and M. Volmer, Z. Physik, Chem. A 157, 165, (1931).

79. M. Stern and A.L. Geary, J. Electrochem. Soc. 104, 56, (1957).

80. M. Stern, Corrosion 14, 440t, (1958).

81. K.B. Oldham and F. Mansfeld, Corr. Sci. 13, 813, (1973).

82. K.B. Oldham and F. Mansfeld, Corrosion 27, 434, (1971).

83. F. Mansfeld and K.B. Oldham, Corr. Sci. 11, 787, (1971).

84. F. Mansfeld, Corrosion 29, 397, (1973).

85. A.M. Feltham and M. Spiro, Chem. Rev. 71, 177, (1971).

86. R.W. Powers, General Electric Research Report No. 63-RL (3218) Jan.1963.

87a. Page 84 "Electrochemistry" J. Koryta, J. Dvorak and V. Bohackova, Methuen, (1970).

87b. Page 1144 "Physics of electrolytes" Volume 2 Edited by J. Hladik, Academic Press, (1972).

88. T.E. Evans, Corr. Sci. in the press.

89. R. de Levie, page 345 "Advances in Electrochemistry and Electrochemical Engineering" Volume 6. Edited by P. Delahay Interscience (1967).

90. W.J. Albery and M.L. Hitchman, "Ring disc Electrodes", Oxford University Science Research Papers O.U.P. (1971).

91. W. Makepeace, Ph.D. Thesis, University of Newcastle (1973).

92. E. Gileadi and B.E. Conway, page 368, Modern Aspects of Electrochemistry" No. 3. Edited J. O'M. Bockris and B.E. Conway, Butterworths London (1965).

ACKNOWLEDGEMENTS

I would like to thank Dr. T. Dickinson for the help and encouragement which he has given me during the course of this work. I would also like to thank Mr. T.E. Evans, Dr. W.H. Sutton and Mr. J.N. Wanklyn of International Nickel Ltd. for helpful discussions.

I would like to thank the Science Research Council and International Nickel Ltd. for financial support during this work.